CONSTRUCTION OF

THE INTENSITY-DURATION-FREQUENCY (IDF) CURVES

UNDER CLIMATE CHANGE

A Thesis

Submitted to the College of Graduate Research and Studies

In Partial Fulfilment of the Requirements

for the

Degree of Master of Science

in the

Department of Civil and Geological Engineering

University of Saskatchewan

Saskatoon, Saskatchewan, Canada.

By

Md. Shahabul Alam

PERMISSION TO USE

The author has agreed that the library, University of Saskatchewan, may make this thesis freely available for inspection. Moreover, the author has agreed that permission for extensive copying of this thesis for scholarly purposes may be granted by the professors who supervised the thesis work recorded herein or, in their absence, by the head of the Department or the Dean of the College in which the thesis work was done. It is understood that due recognition will be given to the author of this thesis and to the University of Saskatchewan in any use of the material in this thesis. Copying or publication or any other use of the thesis for financial gain without approval by the University of Saskatchewan and the author's written permission is prohibited.

Requests for permission to copy or to make any other use of material in this thesis in whole or part should be addresses to:

Head of the Department of Civil and Geological Engineering,

University of Saskatchewan,

57 Campus Drive,

Saskatoon, Saskatchewan,

Canada, S7N 5A9

ABSTRACT

Intensity-Duration-Frequency (IDF) curves are among the standard design tools for various engineering applications, such as storm water management systems. The current practice is to use IDF curves based on historical extreme precipitation quantiles. A warming climate, however, might change the extreme precipitation quantiles represented by the IDF curves, emphasizing the need for updating the IDF curves used for the design of urban storm water management systems in different parts of the world, including Canada.

This study attempts to construct the future IDF curves for Saskatoon, Canada, under possible climate change scenarios. For this purpose, LARS-WG, a stochastic weather generator, is used to spatially downscale the daily precipitation projected by Global Climate Models (GCMs) from coarse grid resolution to the local point scale. The stochastically downscaled daily precipitation realizations were further disaggregated into ensemble hourly and sub-hourly (as fine as 5-minute) precipitation series, using a disaggregation scheme developed using the K-nearest neighbor (K-NN) technique. This two-stage modeling framework (downscaling to daily, then disaggregating to finer resolutions) is applied to construct the future IDF curves in the city of Saskatoon. The sensitivity of the K-NN disaggregation model to the number of nearest neighbors (i.e. window size) is evaluated during the baseline period (1961-1990). The optimal window size is assigned based on the performance in reproducing the historical IDF curves by the K-NN disaggregation models. Two optimal window sizes are selected for the K-NN hourly and sub-hourly disaggregation models that would be appropriate for the hydrological system of Saskatoon. By using the simulated hourly and sub-hourly precipitation series and the Generalized Extreme Value (GEV) distribution, future changes in the IDF curves and associated uncertainties are quantified using a large ensemble of projections obtained for the Canadian and

British GCMs (CanESM2 and HadGEM2-ES) based on three Representative Concentration Pathways; RCP2.6, RCP4.5, and RCP8.5 available from CMIP5 – the most recent product of the Intergovernmental Panel on Climate Change (IPCC). The constructed IDF curves are then compared with the ones constructed using another method based on a genetic programming technique.

The results show that the sign and the magnitude of future variations in extreme precipitation quantiles are sensitive to the selection of GCMs and/or RCPs, and the variations seem to become intensified towards the end of the 21st century. Generally, the relative change in precipitation intensities with respect to the historical intensities for CMIP5 climate models (e.g., CanESM2: RCP4.5) is less than those for CMIP3 climate models (e.g., CGCM3.1: B1), which may be due to the inclusion of climate policies (i.e., adaptation and mitigation) in CMIP5 climate models. The two-stage downscaling-disaggregation method enables quantification of uncertainty due to natural internal variability of precipitation, various GCMs and RCPs, and downscaling methods. In general, uncertainty in the projections of future extreme precipitation quantiles increases for short durations and for long return periods. The two-stage method adopted in this study and the GP method reconstruct the historical IDF curves quite successfully during the baseline period (1961-1990); this suggests that these methods can be applied to efficiently construct IDF curves at the local scale under future climate scenarios. The most notable precipitation intensification in Saskatoon is projected to occur with shorter storm duration, up to one hour, and longer return periods of more than 25 years.

ACKNOWLEDGEMENTS

It is a great opportunity for me to thank those who made this thesis possible. First and foremost, I would like to express my sincere gratitude to the Almighty Allah, the most merciful and most beneficent, for giving me the opportunity and strength to learn and for His compassion throughout the study without which nothing could be accomplished.

I am grateful to my supervisor, Dr. Amin Elshorbagy, for his continuous guidance, support, tolerance and inspiration without which it would not be possible to finish this thesis. He is not only my supervisor but also like my guardian in Canada. His comments and suggestions throughout the study were meant to be invaluable for the research. I would like to take the chance to appreciate the generosity and patience he showed during the last two years, which helped me to study and work on my research in harmony.

I would also like to express my sincere gratitude to my advisory committee member, Dr. Naveed Khaliq and the committee chair Dr. Andrew Ireson for providing the valuable support, suggestions and feedbacks at different stages of my research work. I would like to thank Dr. Kerry Mazurek for her time to join and serve as a committee member. I also thank Dr. Chris Hawkes for his time to join as an acting chair and Dr. Kevin Shook for taking time to serve as my external examiner.

Financial support provided by the City of Saskatoon and Department of Civil and Geological Engineering to carry out this research is greatly acknowledged. I would like to express my gratitude to Al Pietroniro and Shannon Allen of Environment Canada for providing hourly rainfall data of Saskatoon. I highly appreciate Dr. Alireza Nazemi for his valuable support, insightful suggestions and comments on my research work throughout the program. My sincere thanks to Elmira, Jordan, Li, and Ming for their suggestions, company and friendship

over the years in the lab (CANSIM). Deep appreciation goes to Cristian Chadwick for his valuable tips on writing efficient codes in MATLAB.

I would like to convey my profound gratefulness to my parents (Md. Abdus Sobhan and late Sufia Khatun) and my parents in law (Akhand Md. Mukhlesur Rahman and Meherajun Nesa) for their supports. Special thanks to my loving wife, Ulfat Ara Khanam, for her continuous inspiration. Last but not the least, my sincere thanks to my sisters, brothers in law, nephews, nieces, and only sister in law for their encouragements.

TABLE OF CONTENTS

LIST OF TABLES

LIST OF FIGURES

LIST OF SYMBOLS AND ABBREVIATIONS

AAFC-WG	Agriculture and Agri-Food Canada Weather Generator
ACCESS1.0	Australian Community Climate and Earth-System Simulator 1.0
AMP	Annual Maximum Precipitation
ANN	Artificial Neural Network
AOGCM	Atmospheric Ocean General Circulation Model
AR4	Fourth Assessment Report
AR5	Fifth Assessment Report
BCCCSM1.1	Beijing Climate Center Climate System Model 1.1
CanESM2	Second generation Canadian Earth System Model
CCCMA	Canadian Centre for Climate Modelling and Analysis
CDCD	Canadian Daily Climate Data
CESM1-BGC	Community Earth System Model, version 1-Biogeochemistry
CGCM3	The third generation Coupled Global Climate Model
CHRM	Climate High Resolution Model
CMIP3	Coupled Model Intercomparison Project, phase 3
CMIP5	Coupled Model Intercomparison Project, phase 5
CO_2	Carbon dioxide
CRCM	Canadian Regional Climate Model
CSIRO-Mk3.6.0	Commonwealth Scientific and Industrial Research Organization, Mk3.6.0 version
ECDF	Empirical Cumulative Distribution Function
ESM	Earth System Model

GCM	Global Climate Model
GEV	Generalized Extreme Value
GLM	Generalized Linear Model
GLM-WG	Generalized Linear Model-based Weather Generator
GP	Genetic Programming
GSR	Genetic Symbolic Regression
HadCM3	Hadley Centre Coupled Model, version 3
HadGEM2-ES	The Earth System configuration of the Hadley Centre Global Environmental Model, version 2
HadRM	Hadley Center Regional Model
IAM	Integrated Assessment Model
IDF	Intensity-Duration-Frequency
INM-CM4	Institute of Numerical Mathematics Climate Model, version 4.0
IPCC	Intergovernmental Panel on Climate Change
K-NN	K-Nearest Neighbor
KS-test	Kolmogorov-Smirnov test
LARS-WG	Long Ashton Research Station Weather Generator
MARE	Mean Absolute Relative Error
MB	Mean Bias
MIROC-ESM	Model for Interdisciplinary Research on Climate-Earth System Model
MM5	Fifth Generation Pennsylvania State University/National Center for Atmospheric Research Mesoscale Model
MRI-CGCM3	Meteorological Research Institute-third generation Coupled Global Climate Model
PCMDI	Program for Climate Model Diagnosis and Intercomparison

R	Pearson’s correlation coefficient
RCF	Relative Change Factor
RCM	Regional Climate Model
RCP	Representative Concentration Pathway
RegCM	Regional Climate Model System
RMSE	Root Mean Squared Error
SDSM	Statistical Downscaling Method
SED	Semi-Empirical Distribution
SRES	Special Report on Emission Scenarios
WGEN	Weather Generator
WG-PCA	K-NN Weather Generator with Principal Component Analysis

CHAPTER 1: INTRODUCTION

1.1 Background

The use of Intensity-Duration-Frequency (IDF) curves, which incorporate the frequency and intensity of maximum precipitation events of various durations for the design of hydrosystems, is standard practice in many places. The amounts of maximum daily and sub-daily precipitation values, similar to those represented by IDF curves, have shown increasing trends in many locations of the world including Canada (Arnbjerg-Nielsen, 2012; Denault et al., 2002; Waters et al., 2003). The return period of a particular precipitation event (i.e., storm) is subject to change over time as a result of non-stationarity (Mailhot and Duchesne, 2010). The Intergovernmental Panel on Climate Change, IPCC (2012) concluded that the return period of a given Annual Maximum Precipitation (AMP) amount will decrease significantly by the end of the 21st century, with the occurrence of extreme precipitation events occurring more frequently. For example, if an urban storm water collection system was designed 30 years ago based on the 50-year 10-min precipitation storm, the design might only satisfy up to a 25-year design storm under non-stationary climatic conditions. Such conditions may significantly increase the vulnerability of urban storm water collection systems, which are associated with design-storm durations of less than a day and even less than an hour in many cases.

Understanding of the dynamics of hydrological processes and their impacts on urban storm water collection system requires a long record of fine resolution precipitation (Segond et al., 2006), but records of fine temporal and spatial resolution are often limited. Many regions have precipitation records at daily scale with limited hourly records in the world. Obtaining sub-hourly precipitation records has become an important issue as climate change has been shown to cause increased precipitation intensities in many parts of the world, including Canada (Waters et

al., 2003). Global Climate Models (GCMs) have the ability to represent weather variables at coarse grid scale (usually greater than 200 kilometers), which is too coarse for climate change impact studies (Mladjic et al., 2011; Nguyen et al., 2008), especially in urban hydrology where the required scale is usually less than a few kilometers. The GCMs' outputs are usually downscaled to the local scale using various downscaling methods; for instance, weather generators, such as Long Ashton Research Station Weather Generator (LARS-WG) (Racsko et al., 1991; Semenov and Barrow, 1997) to obtain required information for impact investigations.

LARS-WG is a semi-parametric, widely used and user-friendly weather generator, where precipitation and other outputs of GCMs can be downscaled to local scale (a scale of influence for hydrological processes and infrastructure) using the statistical properties of the observed weather at the local scale (Semenov and Barrow, 1997). In LARS-WG, the observed precipitation data are used to obtain the distribution of wet and dry spell lengths of the simulated series (King et al., 2012). Since the collection of fine resolution observations is not an easy option, transformation of the available data from one temporal and spatial scale to another is an important alternative (Sivakumar et al., 2001). The transformation of precipitation data from one scale to another can be achieved through the application of disaggregation models for transforming daily precipitation to hourly and to sub-hourly values.

The share of rainfall in the monthly precipitation showed significant increasing trends in a number of location in the Canadian prairies, when investigated using the historical data from the Historical Adjusted Database for Canada (HACDC) (Shook and Pomeroy, 2012). Several researchers have concluded that based on the simulation results of GCMs, a warmer climate is expected in Saskatchewan, Canada, on a regional scale (Lapp et al., 2008), which will ultimately intensify the hydrological cycle (Trenberth et al., 2003). In Saskatoon, the frequency and mean

value of daily precipitation quantities for late spring and summer seasons, specifically in June and July, show a significant increasing trend in the 21st century as revealed from the preliminary study based on Saskatoon's Airport historical precipitation data, five GCMs, and three emission scenarios (Nazemi et al., 2011). Depending on the GCMs and the emission scenarios, the amount of increase would vary; this suggests that uncertainty cannot be avoided in future climate projections and that uncertainty quantification measures should be associated with each projection so that the likelihood of future precipitation events might be quantified.

Saskatoon's storm water collection system consists of minor and major sub-systems (City of Saskatoon, 2012). The minor systems are designed to withstand storm events of either 2 or 5-year return periods, whereas the major systems must control peak runoff of a 100-year return period. The City of Saskatoon currently uses the IDF curves based only on historical data up to 1986, assuming that the future will behave like the past. Nevertheless, recent (2010) total spring and summer precipitation was record breaking, being almost 50% larger than the previous highest levels observed since the 1920s. Manitoba and Saskatchewan recorded the second highest losses of roads, houses, farms, and animals in Canadian history due to disasters caused by weather extremes after 2005 (Environment Canada, 2011). Evacuation and relocation of several communities had to be implemented as a result of higher water levels, as compared to the water levels in 2005 (Massie and Reed, 2012). The floods in the recent years were caused by the heavy spring precipitation, as a sum of rainfall and snow, when rivers are already in high flow situations (Environment Canada, 2011). This increase in precipitation and river water levels reveals that extreme events might not be following historical frequencies. The wet summers of recent years, supported by other regional studies of climate change, emphasizes the need to

investigate possible changes in the IDF curves and design storms in Saskatoon as a result of possible climate change.

1.2 Area of Interest

It is often necessary to downscale precipitation from the global coarse spatial scale to the local scale and to finer timescales for the study of climate change in urban areas. Hourly and even sub-hourly future precipitation scenarios are required for accurate modeling of hydrological response of urban drainage catchment (Watt et al., 2003), since urban drainage system involves a small catchment as compared to the natural catchments (Schilling, 1991). Therefore, disaggregation of precipitation to fine temporal and spatial resolutions is required to assess the vulnerability of storm water collection systems in urban areas. A stochastic weather generator (e.g., LARS-WG) is capable of producing an ensemble of future daily weather series at the local-scale based on the GCMs' predictions, which also provides the means for exploring uncertainty in climate change projections (Semenov and Stratonovitch, 2010). The stochastic weather generator can also be used to assess the effects of wet and dry spell lengths on the simulations, in addition to the effects of mean monthly precipitation amounts.

A method was sought to disaggregate the daily precipitation to finer temporal resolution, while maintaining the statistical properties of the observed precipitation. The K-nearest Neighbor (K-NN) method, based on the resampling algorithm from true observed data, so that statistical properties of the disaggregated precipitation series have a high probability of being preserved, was selected. The K-NN method can be used as a disaggregation model to generate long time-series of hourly and sub-hourly (5-minute) precipitation for the baseline (historical) period as well as the future climate projections. Afterwards, the long recorded data of hourly and sub-

hourly (5-minute) precipitation can be further analyzed to construct the IDF curves during the baseline and future periods (i.e., 2011-2100) for the City of Saskatoon.

The two-stage downscaling and disaggregation method can be applied to construct future IDF curves of all durations between 5 minutes and 24 hours; allowing the current IDF curves to be updated for the City of Saskatoon. Several previous studies related to IDF curves considered generation of annual maximum precipitation (Kuo et al., 2013; Hassanzadeh et al., 2013). Typically, the generation of continuous precipitation records has not been extensively considered in previous studies. However, long continuous precipitation time series (not only daily/annual maximum) of 5-minute resolution during the baseline and future periods might be important to represent high resolution extreme precipitation quantiles in the prairie region where precipitation during the summer months occurs mostly as convective precipitation (Shook and Pomeroy, 2012). Some previous studies used the K-NN method as a weather generator to produce daily precipitation by resampling from the observed daily precipitation data (Sharif and Burn, 2007) and as a disaggregation model to disaggregate daily to hourly precipitation values (Prodanovic and Simonovic, 2007) using a prescribed window size described by Yates et al. (2003). However, window size (number of nearest neighbors) needs to be examined for the hydrological system in Saskatoon for the K-NN hourly and sub-hourly disaggregation models; and two optimal windows can be selected separately for the two disaggregation models. The optimal window size for disaggregation models has not been thoroughly investigated in previous studies. Furthermore, the selection of nearest neighbors, either randomly or deterministically, needs verification when there are several neighbors showing the same minimum distance from the point of interest. A general and user-friendly method is needed, which can be applied to any location using precipitation output from any GCM.

Applying the above-mentioned two stage downscaling/disaggregation method, while identifying the optimal window size for the K-NN method and quantifying the various sources of uncertainties associated with developing the IDF curves for the City of Saskatoon, is the main area of interest in this thesis.

1.3 Knowledge Gap

Currently, there is no up-to-date study investigating the possible changes in the IDF curves and design storms in the City of Saskatoon under climate change or non-stationarity. The risk and rate of failure of systems designed using the historical design storms may increase in the face of non-stationary climatic conditions (Mailhot et al., 2007; Adamowski et al., 2009).

Characterization of the possible future changes in short-duration precipitation intensities faces several obstacles and appropriate methods need to be developed for this purpose. First, the short-duration precipitation events in the Canadian prairies, which includes Saskatoon, are mostly convective during the summer months (Shook and Pomeroy, 2012). Therefore GCM simulations might be insufficient to reproduce the precipitation for a small area (Olsson et al., 2009). Second, the outputs of GCMs for a given site and time period vary tremendously among various GCMs and representative concentration pathways (RCPs)/emission scenarios. However, no GCM can be preferred without a detailed study (Semenov and Startonovitch, 2010). Moreover, the outputs of GCMs are not available for durations shorter than a day in case of CMIP3 climate models, or several hours in case of CMIP5 climate models. The uncertainty due to the choice of GCMs requires multi-model ensembles of climate projections with several modeling alternatives for characterizing future precipitation events. Furthermore, hourly and even sub-hourly future precipitation scenarios are required for accurate modeling of the hydrological response of urban watersheds. Therefore, disaggregation of precipitation to fine

temporal resolutions should be performed to assess the vulnerability of storm water collection systems in the City of Saskatoon with an estimation of uncertainty associated with the constructed IDF curves and the subsequent hydrological risks. This study is part of a sole source project funded by the City of Saskatoon to fill the above-identified knowledge gap.

1.4 Objectives

The goal of this research project is to construct the Intensity-Duration-Frequency (IDF) curves/design storms for the City of Saskatoon under climate change scenarios. The specific objectives are the following:

(1) To generate representative long time series of hourly and sub-hourly precipitation for the City of Saskatoon, during the baseline period and under projections of climate change scenarios;

(2) To construct a set of potential future IDF curves for design purposes in Saskatoon; and

(3) To assess and quantify the uncertainties in the constructed IDF curves.

1.5 Scope of the Research

This research study aims to investigate the difference among GCMs available for AR5 (phase 5 of the Coupled Model Intercomparison Project: CMIP5 archive) based on representative concentration pathways (RCPs) and AR4 (phase 3 of the Coupled Model Intercomparison Project: CMIP3 archive) scenarios of CO_2 emissions on future hourly and sub-hourly precipitation in the City of Saskatoon. GCMs provide the basis for characterizing the effects of CO_2 emissions and management strategies on general circulation patterns in large temporal and spatial scales. As the outputs of GCMs are not directly applicable to small temporal and spatial scales, it is therefore necessary to downscale the future realizations of precipitation time series generated by GCMs using downscaling techniques. In this study, LARS-WG was used as one of

the available downscaling techniques to map the projections of GCMs from the coarse grid resolution to a local scale and to generate multiple realizations of future daily precipitation. Two GCMs, the Canadian CanESM2 and the British HadGEM2-ES were considered in this study. Then, a disaggregation technique was employed to further downscale the generated daily local precipitation data into hourly and sub-hourly values for the city. Figure 1.1 shows the framework of the research being conducted under this study. Other GCMs' and Regional Climate Models' (RCMs) simulations are not within the scope of this research study.

This research study uses a stochastic weather generator, LARS-WG, which uses historical daily precipitation data to estimate parameters of the empirical probability distributions of daily precipitation. The outputs of GCMs are used to update the parameters of the distributions and the updated parameters are then used to generate future daily precipitation series under climate change scenarios. An hourly disaggregation method disaggregates historical or future daily precipitation to the historical or future hourly precipitation data by sampling from the historical hourly precipitation time series. Similarly, a sub-hourly disaggregation method disaggregates historical or future hourly precipitation to historical or future sub-hourly precipitation data by sampling from the historical sub-hourly precipitation time series. The disaggregated precipitation time series, both historical and future, are then used to construct the historical and future IDF curves of fine resolutions. Genetic Programming is employed to find equations that expresses the relationship between the global scale daily precipitation quantiles, and local scale daily and sub-daily precipitation quantiles during the baseline period. These equations are then used to find local scale future precipitation quantiles and IDF curves using the global scale future quantiles. Changes in the future IDF curves are assessed relative to the historical IDF curves.

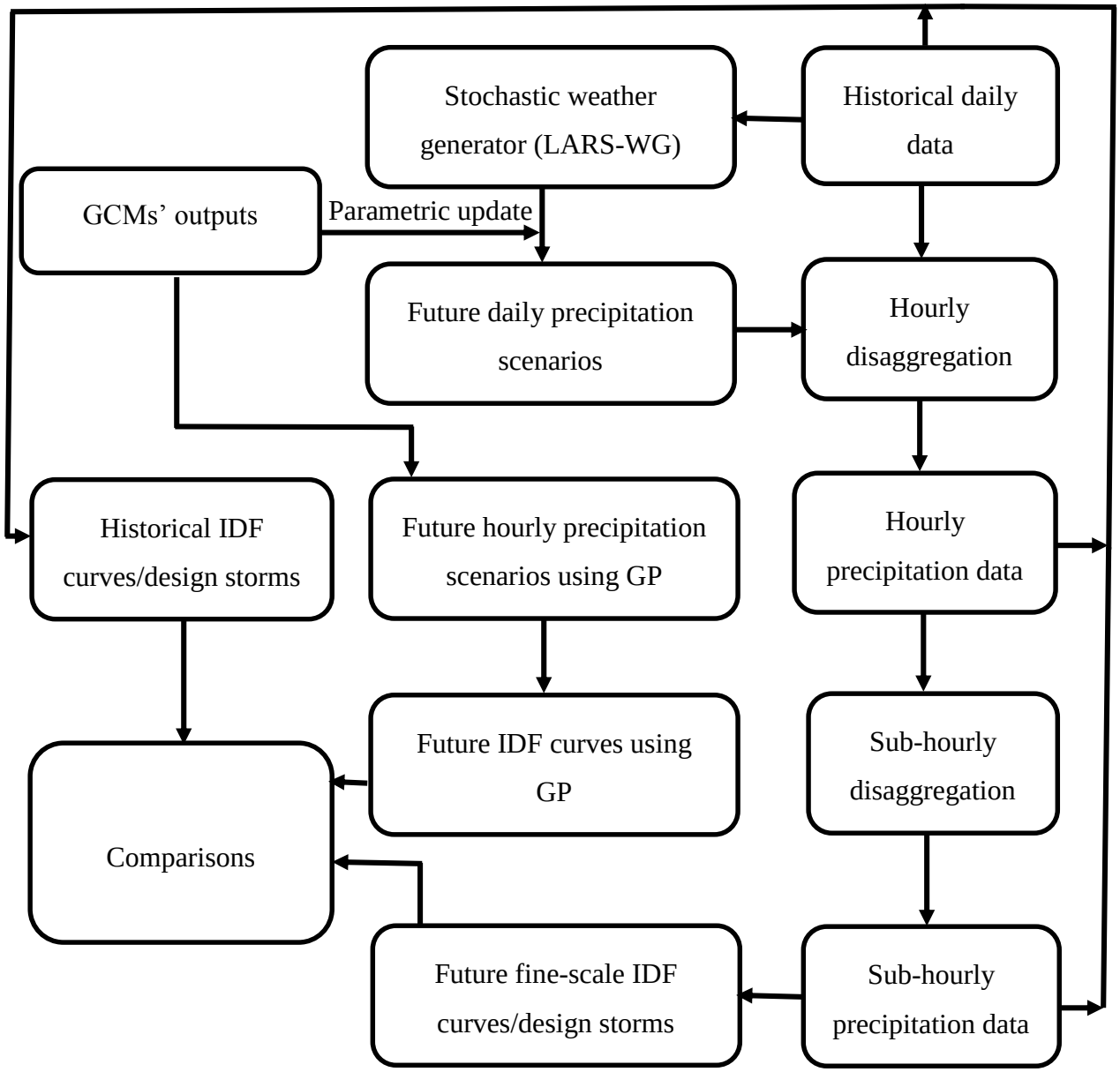

Figure 1.1: Framework of the research for constructing fine-resolution IDF curves

1.6 Synopsis of the Thesis

The rest of this thesis is organized in the following chapters. Chapter 2 provides a concise literature review on Global Climate Models (GCMs); various downscaling approaches; dynamic and statistical downscaling methods, including stochastic weather generators and LARS-WG;

IDF curves under the projections of climate change; generation of high resolution spatial and temporal precipitation time series; K-nearest Neighbor (K-NN) method; and Extreme Value statistical distributions. Chapter 3 presents the case study and data and methods used in this thesis. Chapter 3 also provides a description of the K-NN hourly and sub-hourly disaggregation models and the two-stage downscaling/disaggregation method. Chapter 4 presents results and analysis of LARS-WG, K-NN hourly and sub-hourly disaggregation models; analysis of variations in the IDF curves obtained using the proposed two-stage modeling method and another existing method; variations in the future fine-resolution IDF curves; different sources of uncertainty; and uncertainties in the construction of future IDF curves. Finally, chapter 5 presents a summary, conclusions, research contributions, limitations of the study, and recommendations for future studies.

CHAPTER 2: LITERATURE REVIEW

2. Overview

The research proposed for this thesis requires the development of a two-stage downscaling and disaggregation method to create IDF curves for the study area, Saskatoon, Canada, under the baseline period and under the projections of climate change scenarios using the precipitation output from selected Global Climate Models (GCMs). This chapter presents a literature review of the following important components of this study: (1) global climate models, (2) downscaling methods, (3) precipitation disaggregation methods, (4) extreme value distribution models, (5) construction of future fine-resolution IDF curves, and (6) uncertainty estimation related to the IDF curves.

2.1 Global Climate Models

Assessment of climate change is primarily based on General Circulation Models or Global Climate Models (GCMs). The GCMs are numerical models that can represent physical processes in the atmosphere, ocean, cryosphere and land surface. Currently, it is considered that the only scientifically sound way to predict the impact of increased greenhouse gas emissions on the global climate is through global scale simulation (Barrow, 2002). GCMs can simulate the responses of the global climate to increasing greenhouse gas concentrations (Taylor et al., 2012; Moss et al., 2010). GCMs can incorporate the three-dimensional nature of atmosphere and ocean, simulating as many processes as possible by coupling of atmosphere-ocean GCMs (AOGCMs) with the inclusion of changes in biomes, atmosphere, ocean, and even soil chemistry (McGuffie and Henderson-Sellers, 2014). AOGCMs are the physical climate models with high complexity, whereas the physical climate models with intermediate complexity, known as Earth System Models (ESM), can account for the major carbon fluxes among the ocean, atmosphere, land and

vegetation carbon reservoirs for long-term climate modeling (Moss et al., 2010; Taylor et al., 2012). In this study, the precipitation output from two ESMs (CanESM2 and HadGEM2-ES) was considered for the long term (2011-2100) impact assessment of climate change in Saskatoon.

Previously, the GCMs' simulations of climate variables based on three emission scenarios (SRES: A1B, A2, and B1) from the Coupled Model Intercomparison Project Phase 3 (CMIP3) were commonly used. The Fourth Assessment Report (AR4) of the Intergovernmental Panel on Climate Change (IPCC) was supported by CMIP3 and the outputs of climate models included in CMIP3 have been the basis of climate change impact studies conducted by the research community around the world since 2007 (IPCC, 2007; Taylor et al., 2012). The outputs of climate models from CMIP3 provided comprehensive multi-model impact assessment for climate change projections during the 21st century, based on the IPCC Special Report Emission Scenarios (SRES), i.e., A1B, A2, and B1. Scenarios describe plausible trajectories of the future climate conditions (Moss et al., 2010) and perform as an appropriate analytical tool to assess the influence of driving forces on future emission results and associated uncertainties (IPCC, 2007). A1B, A2 and B1 scenarios represented "a rich world", "a very heterogeneous world", and "a convergent world", respectively (for details please refer to Nakicenovic et al., 2000). The GCMs' outputs were contributed by some modeling centers and archived in the Program for Climate Model Diagnosis and Intercomparison (PCMDI) (http://www-pcmdi.llnl.gov/).

With the release of the Fifth Assessment Report (AR5) of IPCC based on Phase 5 (CMIP5), a new set of GCM simulations was made freely available to the research community. CMIP5 climate models produce a comprehensive set of outputs with the inclusion of new emission scenarios, known as Representative Concentration Pathways (RCPs) (Moss et al., 2010; Taylor et al., 2012). With the introduction in September 2013 of AR5 based on CMIP5, updating

the previous simulations of projected climate change based on CMIP3 climate models became a requirement. Generally, CMIP5 includes more than 50 sophisticated climate models (GCMs) from more than 20 modeling groups and a set of new forcing scenarios (Taylor et al., 2012). Examples of these GCMs include: ACCESS1.0, BCC-CSM1.1, CanESM2, CESM1-BGC, CSIRO-Mk3.6.0, HadGEM2-ES, INM-CM4, MIROC-ESM and MRI-CGCM3 (CMIP5, 2013). The new scenarios used in the simulations of climate models (GCMs) in CMIP5 are known as Representative Concentration Pathways (RCPs). The policy actions to achieve a wide range of mitigation were included in the RCPs aiming to have different radiative forcing targets by the end of the 21st century. The RCPs are denoted by the approximate radiative forcing they might reach by the end of the 21st century, as compared to the year 1750: i.e., RCP2.6, RCP4.5, RCP6.0, and RCP8.5 denote the target radiative forcings of 2.6, 4.5, 6.0 and 8.5 Wm^{-2}, respectively (IPCC, 2013). The values of radiative forcing represented by each RCP are indicative of the targets only by the end of year 2100. However, a range of 21st century climate policies can be represented by the RCPs as compared with the no-policy AR4 emission scenarios. The relative projections due to AR4 and AR5 emission scenarios/RCPs are shown in Appendix A (Figures A.1 and A.2).

The Integrated Assessment Models (IAMs) were used by the Integrated Assessment Modeling Consortium (IAMC) to produce the RCPs by considering various components such as demographics, economics, energy, and climate (IPCC, 2013). Generally, IAMs combine a number of component models, which mathematically represent findings from different contributing sectors. IAMs are broadly of two categories: policy optimization models and policy evaluation models (Weyant et al., 1996). Policy alternatives for the control of climate change can be evaluated by combining technical, economic and social aspects of climate change in an IAM

(Kelly and Kolstad, 1998). In this study, the precipitation output from two GCMs (CanESM2 and HadGEM2-ES) and the corresponding three RCPs (RCP2.6, RCP4.5, and RCP8.5) were considered.

2.2 Downscaling Methods

Assessment of climate change is primarily based on outputs from GCMs, although the climate variables at the local scale – scale of influence for hydrological processes and infrastructure – show large differences when compared with those at the coarse scale of GCMs (Zhang et al., 2011; Hashmi et al., 2011). To overcome this problem, various downscaling approaches are usually used, and they are broadly in two categories: dynamical and statistical downscaling methods (Hashmi et al., 2011; Franczyk and Chang, 2009). A brief description of these downscaling methods is provided in the following sections.

2.2.1 Dynamical Downscaling

Dynamical downscaling is performed by running Regional Climate Models (RCMs) at fine scales using the outputs of GCMs (Xue et al., 2014; Sharma et al., 2011) as boundary conditions. Originally, RCMs were developed as physically based downscaling tools; currently, however, their use for simulating physical processes has been increased (Giorgi and Mearns, 1999; Frei et al., 1998). Examples of RCMs include the Canadian regional climate model (CRCM), climate high-resolution model (CHRM), Hadley Center regional model (HadRM), regional climate model system (RegCM), and the Fifth Generation Pennsylvania State University/National Center for Atmospheric Research mesoscale model (MM5). Typically, high-resolution (10-50 km) RCMs are nested within the coarse resolution (typically greater than 200 km) GCMs for the purpose of dynamical downscaling, although the use of RCMs as a downscaling tool is computationally expensive.

Downscaling RCM outputs employs bias correction as biases in the GCMs' and RCMs' simulations restrict their direct use in climate change impact studies, which need what is known in the literature as "bias correction". In the simulations of RCMs, the biases could be due to the improper boundary conditions provided by the GCMs, lack of consistency in the representation of physics between GCMs and RCMs, and parameterizations of RCMs (Ehret et al., 2012). Out of many bias-correction methods available in the literature, the following list only provides a glimpse of them: correction of monthly mean (Fowler and Kilsby, 2007), delta change method (Hay et al., 2000; Olsson et al., 2012a), and quantile-based method (Kuo et al., 2014; Sun et al., 2011).

Biases in the output of RCMs may be overcome and/or reduced to some extent, if not fully, through improving the model predictability, use of multi-model ensembles of GCMs and/or RCMs (to estimate uncertainty bounds), and by processing the model output afterwards (Ehret et al., 2012). Fowler and Kilsby (2007) applied a simple monthly mean correction to the mean monthly precipitation from RCM (HadRM3H) and found it an effective method to estimate observed precipitation variability during the baseline period. They preferred this simple correction method to a complex quantile-based method (used by Wood et al., 2004) as a reasonable estimate of the observed climate variability was provided by the simple method with slight underestimation of the variability due to simplification of the method. Their method used probability distributions for correcting model bias and assumed that they will remain stable over time, which may not be the case in reality.

Olsson et al. (2012a) demonstrated how precipitation from RCM projections can be further downscaled using the delta change approach to fine resolutions in time and space suitable for the impact assessment of climate change on urban hydrology. The delta change approach

(also known as change factor) has been widely used and applied in climate change impact studies in many different ways, one of which is the multiplicative change factor. The multiplicative change factor (also called relative change factor) is the ratio between the future and the baseline simulations obtained from GCMs, which is then multiplied by the observed data (e.g., precipitation) to generate climate change scenarios of precipitation at the local scale (Anandhi et al., 2011). Kuo et al. (2014) concluded that the IDF curves constructed with bias corrected MM5 precipitation data using a quantile-based method were consistent with the IDF curves at the rain-gauges in Edmonton. Sharma et al. (2011) used statistical downscaling method (SDSM) and a data-driven technique for downscaling the RCM data; they found that the further downscaled data were closer to the observed data than the raw RCM data.

2.2.2 Statistical Downscaling

Statistical downscaling is based on the statistical relationship between the GCMs' outputs and the local scale observed data (e.g., precipitation) (Wilby et al., 1998). Statistical downscaling may be classified into three sub-types: weather typing approaches, regression-based methods and stochastic weather generators (Wilby and Wigley, 1997).

(i) Weather Typing Approaches

Local meteorological data are categorized by weather type according to the patterns prevailing in the atmospheric circulation. Mean precipitation, or the entire precipitation distribution, is associated with a particular weather type of large-scale variables provided by GCMs. The downscaling method is founded on the relationships between the large-scale climate variables (predictor) and local scale observed weather variables (predictand). However, instead of creating a continuous relationship between the variables, local scale climate variables (e.g., precipitation) are generated either by resampling from the observed data distribution conditioned

on the atmospheric circulation patterns given by GCMs, or by producing sequences of local scale weather patterns by the Monte Carlo simulation method and then resampling from the observed data (Wilby and Dawson, 2004). To downscale a future daily precipitation event produced by a GCM, an analogous condition is searched in the observed data of climatic variables, and the local scale observed precipitation for the same event is selected as downscaled future precipitation. Generally, pressure fields produced by GCMs are used as predictors, so weather types are classified using a classification scheme based on the pressure fields.

The weather typing downscaling method prevents the selection of an extreme future precipitation event beyond the most extreme events in the historical records, only allowing the modification of the sequence and frequency of historical precipitation. However, this limitation can be overcome if changes in the atmospheric circulation are considered along with changes in other atmospheric predictors (e.g., temperature, humidity) (Willems et al., 2012; Wilby and Dawson, 2004). Willems and Vrac (2011) compared the performance of a weather typing downscaling method with that of a quantile-perturbation based method (based on quantiles) in terms of changes in the IDF curves in Belgium. The changes in short-duration precipitation extremes were produced similarly by the two methods with the weather typing method using temperature as a large-scale predictor (in addition to atmospheric circulation).

(ii) Regression-based Methods

Regression-based methods are also known as transfer function methods; they involve developing relationships between the local scale (i.e., point station) variables (i.e., precipitation) and global scale (i.e., GCM) variables. Several studies have used regression-based downscaling techniques, such as multiple linear regression (Wilby et al., 2002; Jeong et al., 2012), generalized linear models (GLM) (Chun et al., 2013; Yang et al., 2005; Chandler and Wheater, 2002),

canonical correlation analysis (Busuioc et al., 2008; Von Storch et al., 1993), artificial neural networks (Schoof and Pryor, 2001; Hewitson and Crane, 1996), and the genetic programming-based method (Hassanzadeh et al., 2014).

Artlert et al. (2013) used the SDSM, a multiple regression-based statistical downscaling model (Wilby et al., 2002), to establish a relationship between the GCM-scale climate simulations and local scale precipitation characteristics. They analyzed future precipitation characteristics based on projected trends from the British GCM (HadCM3) and the Canadian CGCM3, which showed huge differences between the future precipitation projections by the two GCMs. The differences in future precipitation projections indicate a high uncertainty in the GCM-based climate simulations. The precipitation data obtained through downscaling are also uncertain, depending on the GCMs and downscaling methods used (Willems et al., 2012). Jeong et al. (2012) used a hybrid downscaling approach as a combination of regression-based (multiple linear regression) and stochastic weather generation techniques to simulate precipitation at multiple sites in southern Quebec, Canada. They found that the addition of a stochastic generation approach to the multivariate multiple linear regression method improved the performance of downscaling daily precipitation from the Canadian CGCM3. The use of a hybrid downscaling approach can overcome the shortcomings of multivariate multiple linear regression and stochastic generation approaches when they are used separately. Yang et al. (2005), and Chandler and Wheater (2002) used the GLM framework for generating daily precipitation sequences conditioned upon several external predictors; this offers superiority in simulating non-stationary sequences, since the external predictors may have spatial and temporal variations.

Hewitson and Crane (1996) applied Artificial Neural Networks (ANNs) for learning the linkage between the atmospheric circulation produced by GCMs and the local scale precipitation.

The ANNs were trained for each rain gauge station to predict daily precipitation values using the linkage learned by the ANNs. However, ANNs end up in generalized relationships, which always predict the same precipitation for a given circulation. Chadwick et al. (2011) used ANNs to reproduce temperature and precipitation dynamically downscaled by nested RCM within a GCM in Europe and concluded that ANNs were capable of reproducing the corresponding climate variables but missed high precipitation values over some mountain areas. The ANNs trained with only 1960-1980 data were not able to reproduce temperature or precipitation well for the 1980-2000 or 2080-2100 periods, although their performance was improved by training the ANNs using different time periods. The GP-based quantile downscaling (Hassanzadeh et al., 2014) is a novel type of statistical downscaling method because it maps the relationship between extreme precipitation (quantiles) at both the global and local scale without having to generate a continuous precipitation record. GP has the advantage of producing explicit mathematical equations for the downscaling relationship.

(iii) Stochastic Weather Generators and LARS-WG

Quantification of the uncertainty due to internal natural weather variability based on stochastic weather generators has a number of applications in design and/or operation of many systems, such as water resources systems, urban drainage systems and land management changes (Srikanthan and McMahon, 2001). Historically, efforts were made to describe precipitation processes in constructing weather generators, since precipitation is the most critical climate variable for many applications, and very often its value is precisely zero (Wilks and Wilby, 1999). The process of precipitation occurrence describes two states, wet and dry, which forces many weather generators to model separately the occurrence and intensity of precipitation.

The first statistical model for simulating the occurrence of daily precipitation was developed by Gabriel and Neumann (1962) using a first-order Markov Chain model. They assumed that the probability of precipitation occurrence is conditioned only on the weather condition of the previous day, i.e., wet or dry. Later, the first-order Markov Chain model of daily precipitation occurrence was combined with a statistical model (i.e., exponential distribution) of daily precipitation (with nonzero value) amounts by Todorovic and Woolhiser (1975). These initial models were constructed for the simulation of a single climate variable, generally daily precipitation for hydrological analysis. The simulation of other climate variables (e.g., daily precipitation, temperature and solar radiation) became reasonable using stochastic weather generators in the early 1980s, which were developed by Richardson (1981) and Racsko et al. (1991). Climate change has increased interest in stochastic weather generators for stochastic simulation of local weather (Semenov and Barrow, 1997).

A stochastic weather generator is used to simulate a daily time series of weather variables having statistical characteristics similar to observed weather variables (Wilks and Wilby, 1999). Various tools (Semenov and Barrow, 1997; Wilks, 1999; Wilks and Wilby, 1999; Wilby and Dawson, 2007; Sharif and Burn, 2007; Hundecha and Bardossy, 2008; King et al, 2014) have been proposed as weather generators. Multiple regression models and stochastic weather generators are examples of the statistical downscaling techniques that are widely used (Wilks, 1992, 1999), since they are less computation intensive than other downscaling methods, easy to use, and efficient (Semenov et al., 1998; Dibike and Coulibaly, 2005). Hashmi et al. (2011) conducted a comparison between a multiple regression-based model (i.e., SDSM) (Wilby et al., 2002) and a weather generator (i.e., LARS-WG), which showed their (SDSM and LARS-WG)

acceptability with reasonable confidence as downscaling tools in climate change impact assessment studies.

Two weather generators, LARS-WG and the Agriculture and Agri-Food Canada weather generator (AAFC-WG), were used by Qian et al. (2008) to reproduce daily extremes (maximum daily precipitation, the highest daily maximum temperature and the lowest daily minimum temperature) over the period 1971-2000. Both weather generators were found to reproduce extreme daily precipitation values quite satisfactorily, while LARS-WG was found to perform better in preserving the historical statistics (e.g., absolute maximum and minimum temperature, mean and standard deviation of precipitation) (Irwin et al., 2012). Chun et al. (2013) compared the downscaling abilities of LARS-WG and GLM-based weather generator (GLM-WG) (Chandler and Wheater, 2002) using the climate variables during the baseline (1961-1990) and future (2071-2100) periods. GLM-WG, a stochastic precipitation model, was developed based on the GLM structure and two-stage precipitation model (first, modeling the sequence of wet/dry days using logistic regression and second, modeling the precipitation amount using gamma distributions) (Coe and Stern, 1982). LARS-WG uses observed daily precipitation to generate synthetic daily precipitation series at a specific site (Semenov and Barrow, 2002), while GLM-WG simulates daily precipitation based on large-scale climate information at a particular time and location (Chandler and Wheater, 2002). In that particular study by Chun et al. (2013), both weather generators showed equal performance in simulating monthly and annual precipitation totals, while GLM-WG showed superiority in simulating annual daily maximum precipitations due to the large-scale climate information used in GLM-WG.

Qian et al. (2004) and King et al. (2012) concluded that LARS-WG performed better in simulating daily precipitation, but its performance in simulating temperature related statistics

(e.g., absolute maximum and minimum temperature) was not adequate when compared to the corresponding performances of AAFC-WG, SDSM, and K-NN weather generators with Principal Component Analysis (WG-PCA). However, LARS-WG was found to perform well in simulating climatic extremes across Europe (Semenov and Barrow, 1997). The IPCC's Fourth Assessment Report (AR4) (Solomon et al., 2007) used a multi-model ensemble, out of which 15 climate models have been incorporated in the new version (Version 5) of LARS-WG for climate projections. The model ensemble allows estimation of uncertainties associated with the impacts of climate change originating from uncertainty in climate predictions (Semenov and Stratonovitch, 2010).

Several studies using LARS-WG for climate change impact assessment (Semenov and Barrow, 1997) suggested that LARS-WG can be used as a downscaling model with substantial confidence to conduct climate change impact assessment by extracting site-specific climatic characteristics (Hashmi et al., 2011; Semenov and Stratonovitch, 2010; Qian et al., 2008; Semenov and Barrow, 1997). LARS-WG can be used to generate synthetic daily precipitation data by calculating site-specific weather parameters from observed daily data of at least 20 years (Semenov and Barrow, 1997). The LARS-WG is capable of producing daily climate scenarios for the future at the local scale based on the GCMs' predictions and emission scenarios, thus providing the means for exploring the uncertainty in climate change impact assessment (Semenov and Stratonovitch, 2010).

LARS-WG was adopted for this research as a stochastic weather generator tool to simulate climate data (e.g., temperature, precipitation) in Saskatoon, Canada, during the baseline period and under future climatic conditions. LARS-WG was employed in this research for generating multiple realizations of daily precipitation at the local scale in Saskatoon. LARS-WG

provides a computationally inexpensive platform for generating daily future climate data (e.g., temperature, precipitation) for many years under the projections of climate change scenarios, which are of spatial and temporal resolution suitable for local scale climate change impact studies. LARS-WG can reproduce changes in the mean climate, and in the climate variability at the local scale. The first version of LARS-WG was developed in 1990; the latest version was developed in 2002, incorporating a series approach (Racsko et al., 1991), which in this context means that the weather generation begins with the simulation of wet/dry spell length and then the precipitation amount is modelled (Semenov and Barrow, 2002). The performance of LARS-WG was compared with the performance of another popular stochastic weather generator, WGEN (Richardson, 1981), over several sites with diverse climates and was found to perform as well as WGEN (Semenov et al., 1998).

The weather generation process in LARS-WG is based on semi-empirical distribution (SED), which is defined as the cumulative probability distribution function describing the probability that a random variable X, with a given probability distribution, takes on a value less than or equal to x. The semi-empirical distribution is represented by a histogram with 23 semi-closed intervals, $[a_{i-1},ai)$, where a_{i-1}, a_i indicates the number of events in the observed data in the i-th interval and i=1,2,……..,23. The values of the events are selected randomly from the semi-empirical distributions, where an interval is selected first using the fraction of events in every interval as the probability of choice; subsequently, a value is chosen from that interval using a uniform distribution. SED provides a flexible distribution with a possibility to approximate a wide range of shapes through adjustment of the intervals, $[a_{i-1},a_i)$. The choice of the intervals, $[a_{i-1},a_i)$ is dependent on the weather variable type; for example, the intervals are evenly spaced in case of solar radiation, while the interval size is increased with the increase in "i" for the wet/dry

spell lengths and for precipitation in order to restrict the use of very coarse resolution intervals for extremely small values (Semenov and Stratonovitch, 2010; Semenov and Barrow, 2002). More explanation of the steps for generating daily precipitation time-series using LARS-WG is provided in Appendix B (Section B.1).

2.3 Precipitation Disaggregation Methods

To overcome the lack of high-resolution temporal and spatial precipitation data crucial for hydrological, meteorological and agricultural applications, disaggregation of available data from one temporal and spatial scale to another seems to be the most efficient alternative (Sivakumar et al., 2001). Several disaggregation techniques exist in water resources literature enabled the generation of high-resolution temporal and spatial precipitation data using the widely available daily precipitation data. Disaggregation techniques include the Bartlett-Lewis Rectangular Pulse model (Rodriguez-Iturbe et al., 1987, 1988; Khaliq and Cunnane, 1996; Bo et al., 1994), the Generalized linear models (GLMs) (Chandler and Wheater, 2002; Segond et al., 2006), the Multifractal cascade process (Shook and Pomeroy, 2010; Lavellee, 1991), the Chaotic approach (Sivakumar et al., 2001) and non-parametric methods such as, Artificial Neural Networks (Burian et al., 2000), and the K-nearest neighbor (K-NN) technique (Lall and Sharma, 1996; Yates et al., 2003; Sharif and Burn, 2007; Buishand and Brandsma, 2001). In this thesis, "downscaling" refers to the generation of daily precipitation time series at the local scale using the daily precipitation series at the global scale, while "disaggregation" refers to the generation of precipitation series from the coarse temporal scale to the fine temporal scale (e.g., transforming daily precipitation to hourly and to sub-hourly).

Yusop et al. (2013) and Abdellatif et al. (2013) used the Bartlett Lewis Rectangular Pulse (Rodriguez-Iturbe et al., 1987, 1988) model to disaggregate daily to hourly precipitation. Segond

et al. (2007, 2006) and Wheater et al. (2005) used GLMs to simulate daily precipitation while the Poisson cluster process was used as a temporal disaggregation method to generate precipitation at finer resolutions (i.e., hourly). Lu and Qin (2014) used an integrated spatial-temporal downscaling-disaggregation approach based on GLM, K-NN (Sharif and Burn, 2007), and MudRain (Koutsoyiannis et al., 2003) methods to evaluate future hourly precipitation patterns in Singapore. Olsson (1998) and Rupp et al. (2009) used a cascade model for disaggregation of daily to hourly precipitation. Burian et al. (2000) implemented a disaggregation model in ANNs for the disaggregation of hourly precipitation to sub-hourly (15 minutes). The ANN disaggregation model performed better in obtaining the maximum depth and time of 15-minute precipitation, when compared with two empirical precipitation disaggregation models developed by Ormsbee (1989). It was not clear whether the ANN disaggregation model was able to preserve the variance of the historical precipitation.

Yates et al. (2003) developed and applied a non-parametric weather generator based on K-NN for the simulation of regional scale climate scenarios. Sharif and Burn (2007) made an improvement to the K-NN based weather generator developed by Yates et al. (2003) by adding a random component in order to obtain precipitation data beyond the range of historical observations; this component is important in simulating hydrologic extremes (Irwin et al., 2012). Prodanovic and Simonovic (2007) used the improved K-NN based weather generator developed by Sharif and Burn (2007) to simulate daily precipitation and the same approach was used to disaggregate daily precipitation to hourly precipitation. The K-NN technique is a non-parametric method and easy to implement. Resampling from observed data forms the foundation of the method, enabling the disaggregated precipitation data to preserve the statistical characteristics of the observed data with high likelihood (Prodanovic and Simonovic, 2007). The ability to

preserve statistical characteristics of the observed data makes it a feasible approach for adopting in this thesis to disaggregate precipitation data from daily scale to hourly and sub-hourly scales.

The K-NN technique is a form of nearest neighbor (NN) search, which is also known as closest-point, similarity, or proximity search; the aim is to identify the most similar or closest points to the point of interest. The similarity or closeness is measured by Euclidean, Mahalanobis, or other distance metrics (Elshorbagy et al., 2000). The more similar the points, the closer they are to the point of interest. The K-NN technique can be defined as follows: If a space S contains a set P of points and a point of interest k is $k \in S$, the K-NN technique finds the closest points (measured by the distance metrics) to k in P (Liu, 2006).

The days in the historical time series for which the observed weather variable is similar to the simulated weather variable of a given day are known as nearest neighbors. The K-NN technique involves finding K similar or closest points to the point of interest. K-NN was originally used for pattern recognition, which was later demonstrated as a resampling (i.e., bootstrap) method by Lall and Sharma (1996). The resampling approach based on K-NN was extended to a stochastic weather generator for single (Rajagopalan and Lall, 1999) and multiple sites (Yates et al., 2003; Buishand and Brandsma, 2001); it was further improved by Sharif and Burn (2007) as perturbation of historical data enabled the extrapolation of weather data beyond historical records. The method developed by Sharif and Burn (2007) was further adopted by Prodanovic and Simonovic (2007) for the disaggregation of precipitation from a daily to hourly time scale. The K-NN technique was adopted in this study for the temporal disaggregation of daily precipitation to hourly and sub-hourly scales.

2.4 Extreme Value Distribution Models

The IDF curves are constructed by Environment Canada by fitting Gumbel the extreme value distribution to annual extremes of precipitation (i.e., annual maximum values), although quantiles of long return periods might be underestimated (Solaiman and Simonovic, 2011) due to its inability to describe the tail behavior appropriately. The Generalized Extreme Value (GEV) distribution can also be used for this purpose, although it is computationally intensive due to the use of three parameters (location, scale, and shape) instead of the two (location and scale) in the Gumbel distribution. However, the GEV distribution provides better description of the upper tail behavior of the distribution by introducing an additional parameter (Overeem et al., 2008). When shape parameter of the GEV distribution approaches to zero, the GEV distribution converges to the Gumbel distribution. Prodanovic and Simonovic (2007) used Gumbel's distribution in constructing IDF curves in two different studies, whereas Overeem et al. (2008) and Hassanzadeh et al. (2014) used the GEV distribution to construct IDF curves due to the superiority of the distribution in describing upper tail behavior.

2.5 Construction of Future IDF Curves from Fine-Resolution Precipitation

Intensity-Duration-Frequency (IDF) curves represent relationships among the return period of a storm event, the precipitation intensity and the storm duration to characterize the properties of extreme precipitation needed for hydrological analysis and design in an urban area. Generally, the steps involved in the construction of IDF curves are the following: (a) generation of precipitation series of various durations; (b) extraction of annual maximum precipitation intensities of these durations; and (c) fitting probability distributions (e.g. Gumbel's distribution, GEV distribution) to the annual maximum precipitation values to estimate precipitation quantiles corresponding to specified return periods. Recent studies show that the precipitation data needed

for IDF curves can be obtained by various approaches. RCMs with grid scales of 25 km or 50 km were utilized by Olsson et al. (2012b) and Liew et al. (2014). Olsson et al. (2012b) applied a stochastic scheme to obtain short duration precipitation events (up to 30 minutes) for the construction of local scale IDF curves in Stockholm, Sweden from RCM grid scale (typically 50 km by 50 km) simulations by performing spatial and temporal downscaling. Liew et al. (2014) derived IDF curves for 6-, 12-, 18-, and 24-hour duration precipitation events in Jakarta, Indonesia using simulations of RCMs (Weather Research and Forecasting Model, WRF with 30 km by 30 km resolution) during baseline and future periods. Rodriguez et al. (2014) used relative change factors and scaling properties of precipitation approaches to construct future IDF curves (1- to 24-hour durations) from GCM-based statistically downscaled precipitation series for Barcelona, Spain. The mean extreme precipitation was found to increase, which is dependent on the choice of GCMs and location of the station.

Mailhot et al. (2007) used maximum precipitation depths during the period from May to October for 2-, 6-, 12-, and 24-hour events to investigate future changes in the IDF curves using the simulations downscaled by the CRCM from Canadian GCM (CGCM2). They showed that the frequencies of the 2- and 6-hour events will be approximately doubled in the southern Quebec region in the future, compared to the baseline period. Kuo et al. (2013) used scaling properties of precipitation data in Edmonton, Alberta to develop regional IDF curves. They considered annual maximum precipitation intensity of 5-minute duration and applied a moving window approach to obtain the annual maximum precipitation intensity for other storm durations to develop the IDF curves during 1984-2009, which were found useful to estimate intensities of storms. Peck et al. (2012) provided daily maximum precipitation datasets of different durations, e.g. 5-, 10-, 15-, 30-minute, 1-, 2-, 6-, 12-, and 24-hour as input to the K-nearest neighbor (K-

NN) weather generator, originally developed by Sharif and Burn (2007). Peck et al. (2012) adopted shuffling and perturbation methods to generate future synthetic precipitation series of nine short durations for the construction of regional IDF curves in the City of London, Ontario. Peck et al. (2012) also used observed precipitation data with the K-NN weather generator to create a lower bound of climate change, and they used modified observed precipitation, using change fields according to the GCM, to create the upper bound of climate change. Burn and Taleghani (2013) investigated the changes in precipitation magnitudes of 51 stations in Canada, including the Prairie Provinces and observed more increasing than decreasing trends of precipitation magnitudes. The results of trends in the observed precipitation indicated that the IDF curves need to be updated with recent data, since outdated data may lead to inappropriate conclusions. In the Canadian prairies, Kuo et al. (2014) constructed grid-based IDF curves for Edmonton using a regional climate model, MM5, after bias correction by comparing with the IDF curves based on rain gauges of Edmonton for 15-minute to 24-hour durations during 1984-2010. Srivastav et al. (2014) used equidistant quantile matching methods for updating the IDF curves at four precipitation stations in Canada for nine durations based on the GCM (CanESM2) output from the CMIP5 and their Representative Concentration Pathways (RCP2.6, RCP4.5, and RCP8.5). All RCPs were found to show increased precipitation intensity during the period from 2006 to 2100.

Hassanzadeh et al. (2013) used Genetic Programming (GP) to develop equations for downscaling GCM-based daily extreme precipitation quantiles to the corresponding local scale daily and sub-daily (down to hourly) quantiles. They used daily and sub-daily quantiles for the baseline period and future projections derived from CGCM3.1 based on A1B, A2 and B1 emission scenarios to construct a set of IDF curves for the City of Saskatoon. The GP-based

downscaling approach was found to be efficient in constructing IDF curves, which showed a range of changes in the future IDF curves that depend on the mapping equations, the return period, the storm duration and the emission scenario. However, the climate change impact assessment in Saskatoon using the constructed IDF curves was based on extreme precipitation quantiles only; the GP method cannot produce continuous precipitation records for Saskatoon. The GP method considered in this study was used for the construction of IDF curves up to a 1-hour duration only, but sub-hourly precipitation data are needed for urban hydrology.

2.6 Uncertainty Estimation Related to the IDF Curves

IDF curves used for the design of urban drainage systems require the generation of extreme precipitation quantiles; which involve uncertainty, causing risks to any subsequent hydrological design (Xu et al., 2010). The projections of future climate variables (e.g., precipitation) under climate change scenarios may involve uncertainty originating from sources, including the data and models used. Xu et al. (2010) classified the sources of uncertainty into two categories: data uncertainty and model uncertainty. Precipitation may cause uncertainty in the construction of IDF curves due to a lack of data (i.e., short data series) and inaccurate measurements of data. In addition to the data uncertainty, uncertainties due to GCMs and the downscaling approaches need to be estimated to build confidence in the design of urban storm water collection systems under the projections of climate change.

In climate change impact assessment, the uncertainty due to the choice of GCM can be reduced by using several GCMs and emission scenarios (Prudhomme et al., 2003). The uncertainties in the construction of IDF curves can be quantified using various methods, such as Monte Carlo simulations, Bayesian estimations, Kernel estimations, and Fuzzy logic. Monte Carlo simulation methods of uncertainty estimation is a stochastic method where random

variables are sampled repeatedly from a given probability distribution of data and thus response of the corresponding stochastic system is measured (Landau and Binder, 2009; Mooney, 1997). Prudhomme et al. (2003) used Monte Carlo simulations for estimating the uncertainty due to the effects of climate change on flood regimes in the UK. Monte Carlo simulations are used to construct confidence intervals based on some assumptions about the distribution of data which are not always valid (Lu and Stedinger, 1992). Alzahrani (2013) used a weather generator and Monte Carlo simulations to quantify uncertainty in the future IDF curves for an urban area in Canada and found that the uncertainty in the IDF curves slightly increased with the increase in duration and return periods. Several approximate methods mentioned by Hu (1987) have been developed to serve the purpose of constructing confidence intervals, however these methods are not always able to construct the desired confidence intervals. With advanced computational ability, resampling methods (i.e., bootstrap) which do not consider such assumptions for the distribution of data are becoming more common in practice (Prudhomme et al., 2003).

Solaiman and Simonovic (2011) used parametric (Bayesian) and non-parametric (Kernel estimations) methods of uncertainty estimation in order to estimate uncertainties in extreme precipitation under climate change. The difference between the two methods lies in the fact that (a) uncertainties from various GCMs based on the mean bias are combined in the Bayesian method, therefore a single weight is used for all of the GCMs, and (b) Kernel estimations assign weights for each time step in evaluating the performance of various GCMs. The Bayesian method may be used alternative to the Kernel estimations; except when uncertainties due to extreme daily precipitation events are considered as weights are based on the mean (Solaiman, 2011). The Kernel estimations can also be challenging for selecting appropriate bandwidth (a parameter), which may lead to wrong conclusions about the shape of the distribution function.

In this study, the Monte Carlo simulations technique (1000 realizations for both baseline and future periods) included in LARS-WG was used to quantify uncertainty due to two GCMs, the corresponding six RCPs, and two downscaling methods during the three time periods of the 21st century.

CHAPTER 3: MATERIALS AND METHODS

3. Overview

This chapter provides a description of the study area, the precipitation data used for developing a two-stage downscaling-disaggregation method, and the methodology followed for conducting the modeling and analysis needed to achieve the study objectives. The model development and analysis consist of two steps: (1) downscaling daily precipitation from the coarse GCM scales (i.e., gridded precipitation) to the local scale (i.e., point/gauged precipitation); and (2) disaggregation of daily precipitation to hourly and 5-minute precipitation at the local scale. LARS-WG, the stochastic weather generator, was the downscaling method used in this study. In this chapter, a method based on the K-nearest neighbor (K-NN) technique, previously used to disaggregate daily precipitation to an hourly time scale (and adopted in this study with few modifications for the disaggregation of precipitation from daily to hourly and sub-hourly durations), is presented. Also included is a description of the Generalized Extreme Value (GEV) distribution used for the construction of IDF curves in the study area.

3.1 Case Study and Data

The Canadian Prairies are characterized by the grassland, numerous lakes, and relatively flat landscape. Relatively wet summer months and dry winter months are not uncommon in the region based on seasonal precipitation totals during 1961-2003 from four sites at Calgary, Banff, Saskatoon, and Winnipeg (Chun et al., 2013). The amount of annual precipitation is generally less than 500 mm, since these provinces are too far away to receive cyclonic precipitation originating from either the west or east coasts (Gan, 2000). Approximately 30% of annual total precipitation occurs as snowfall in the Canadian prairies, including Saskatchewan. Saskatoon (106.70 W, 52.20 N, and approximately 218 km^2) is the largest city in Saskatchewan and is

located on the banks of South Saskatchewan River (SSR). Its mean annual precipitation amount during 1961-2003 was 352 mm according to daily precipitation records available through the Canadian Daily Climate Data (CDCD) portal (www.climate.weatheroffice.gc.ca) and 421 mm according to the adjusted precipitation data available through the Adjusted and Homogenized Canadian Climate Data (AHCCD) data portal (http://www.ec.gc.ca/dccha-ahccd/). The SSR basin may be expected to observe extreme precipitation events more frequently under climate change (Martz et al., 2007). A study of daily precipitation during 1950-2009 showed an increasing trend in the annual maximum precipitation (AMP) in Saskatoon (Nazemi et al., 2011). However, only data up to 1986 were included in the construction of IDF curves currently being used for the design of storm water collection systems in Saskatoon. The study region selected for this research, the City of Saskatoon, is shown in Figure 3.1.

Figure 3.1: Location of the study area (Source: Natural Resources Canada).

The observed daily precipitation data at Saskatoon's Diefenbaker Airport station during the baseline period (1961-1990) measured by Environment Canada were considered for the calibration and validation of the employed weather generator (LARS-WG). These data are freely available through Environment Canada's official website (climate.weather.gc.ca) for the entire baseline period after the data have been reviewed through quality control; this is done for the majority of Environment Canada observed data. Daily precipitation data, in combination with observed hourly precipitation data (also obtained from Environment Canada) for the months of April-September (1961-1990), were used in developing a model for the disaggregation of

precipitation from a daily to hourly time scale. The City of Saskatoon operates tipping bucket rain gauges (Figure 3.2) in the city to measure sub-hourly rainfall (termed as precipitation in this thesis) to capture the spatial variability of the fine temporal resolution rainfall. The sub-hourly data from the rain gauges in Saskatoon between April-September were pre-processed and aggregated to obtain 5-minute rainfall. In this study, the 5-minute rainfall data were analyzed for consistency and length of records. The analysis showed that the sub-hourly precipitation recorded at the Acadia Reservoir (shown as Acadia in Figure 3.2) rain gauge has the longest record (1992-2009) and is more consistent with the Environment Canada daily precipitation; however, there are missing data during the period of 2002-2004. As the historical daily and hourly precipitation data were obtained from Environment Canada, and the sub-hourly rainfall data were obtained from the City of Saskatoon, a rain-gauge in the city was identified showing more consistency with the Environment Canada station. Although precipitation includes both rainfall and snow, and rainfall occurs only in the liquid form, the term precipitation was used both for Environment Canada daily and hourly precipitation data, and the City of Saskatoon 5-minute rainfall data in this thesis.

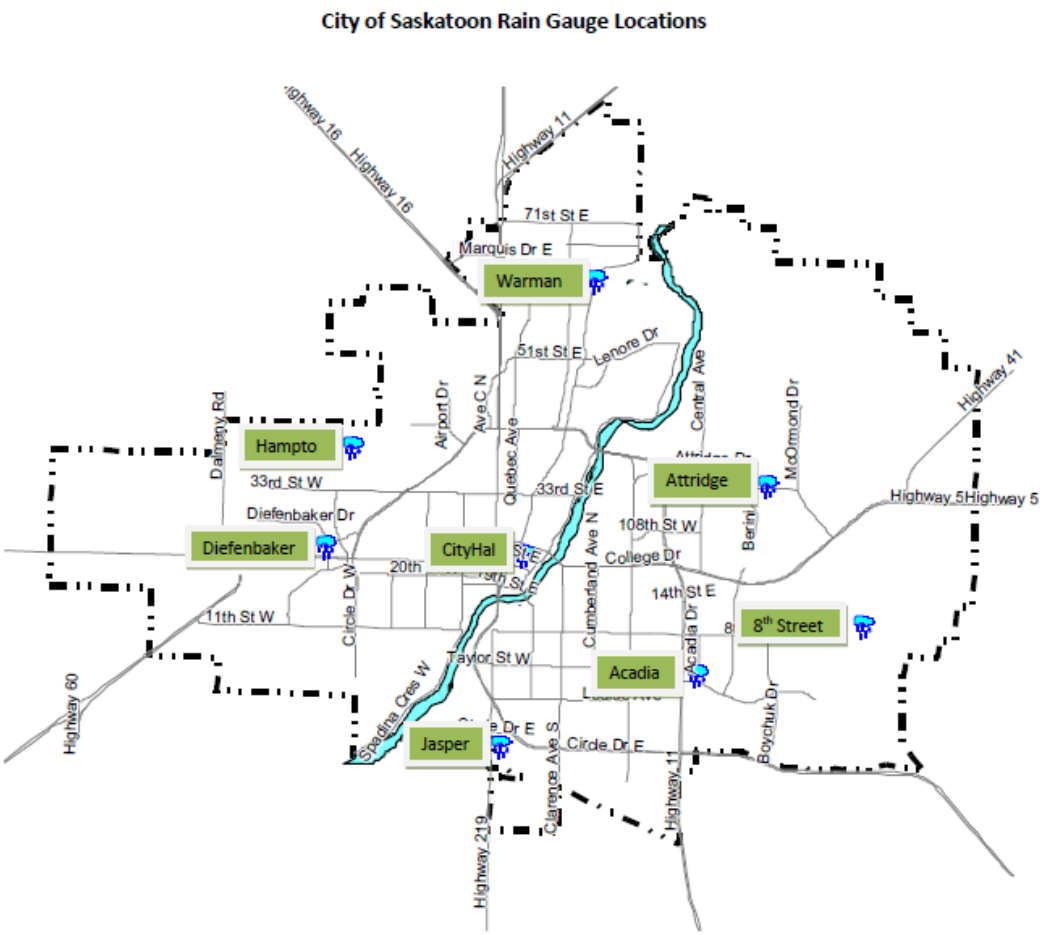

Figure 3.2: Location of rain gauges in Saskatoon (Source: City of Saskatoon).

The 5-min precipitation data recorded at the Acadia Reservoir rain gauge were used in developing a model for the disaggregation of precipitation from an hourly to sub-hourly time scale in this study. Details of the precipitation consistency analysis are included in Appendix C.

The observed daily and hourly precipitation records at the Saskatoon Diefenbaker Airport station during 1961-1990 are plotted in Figure 3.3. The observed daily and hourly records contain precipitation data from January to December (12 months); however, only the observed daily and hourly precipitation data from April to September (6 months) in each year were considered for this study.

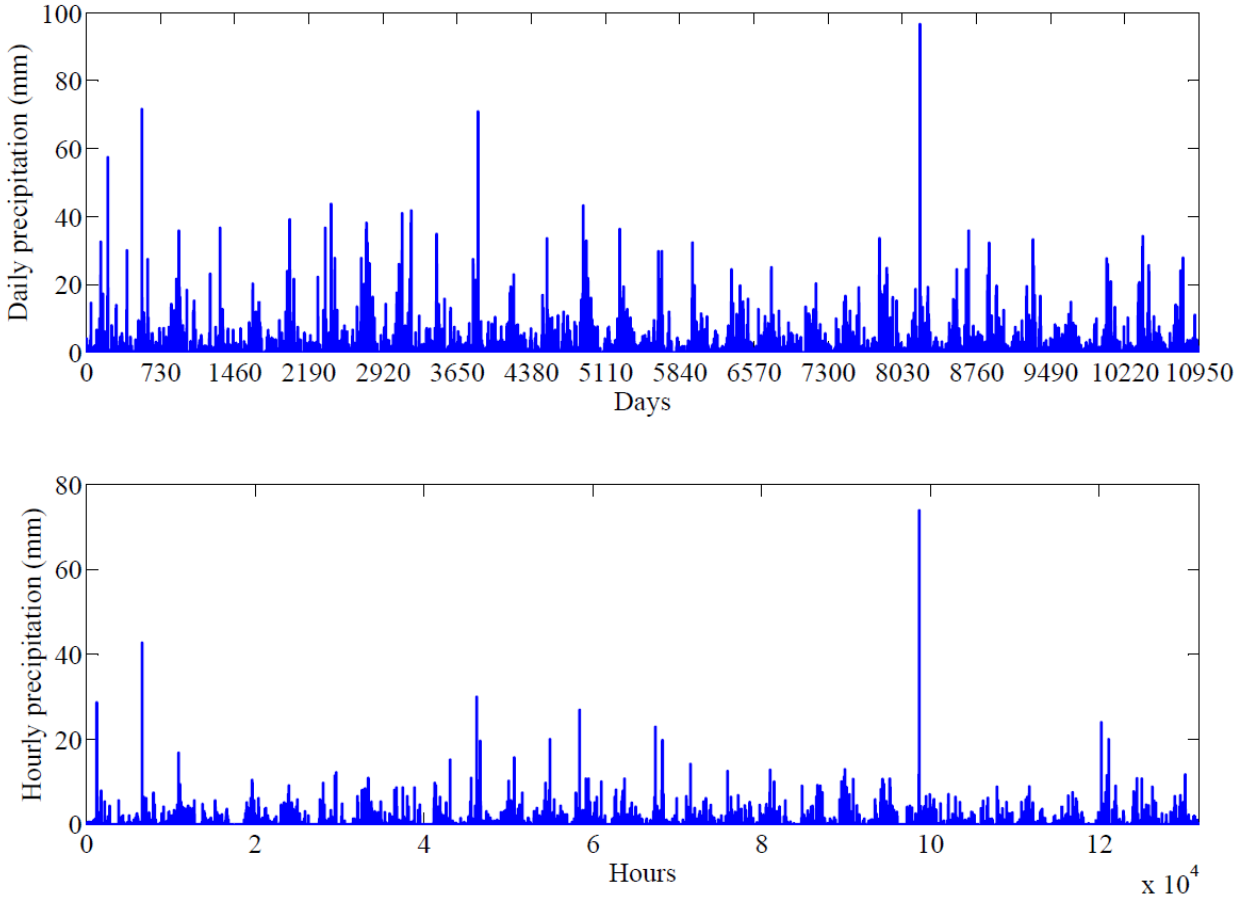

Figure 3.3: Observed daily (upper panel) and hourly (bottom panel) precipitation at Saskatoon's Diefenbaker Airport station during 1961-1990 (Source: Environment Canada)

The observed daily and hourly precipitation record at the Saskatoon Diefenbaker Airport station during 1961-1990 are described by the statistics presented in Table 3.1. The annual mean precipitation amount is consistent with the precipitation characteristics in the prairie region, typically less than 500 mm.

Table 3.1: Statistics of observed daily and hourly precipitation at Saskatoon Diefenbaker Airport station during 1961-1990

Statistic	Daily (Jan-Dec)	Hourly (Apr-Sep)
Mean (mm)	0.95	0.05
Standard deviation (mm)	3.35	0.51
Coefficient of variation	3.53	9.98
Skewness	8.99	42.47
Annual mean (mm)	346.61	224.92
Maximum (mm)	96.60	73.90

3.2 Methodology

3.2.1 Global Climate Models

In section 2.1, Global Climate Models (GCMs) and Representative Concentration Pathways (RCPs) were described. In this study, the Canadian climate model CanESM2 and the British climate model HadGEM2-ES (the Second Generation Earth System Model) daily precipitation outputs were obtained from the CMIP5 data portal (http://pcmdi9.llnl.gov/) for the baseline period (1961-1990) and for the projection period (2011-2100). The precipitation simulations were downloaded from the data portal for each of the selected GCMs based on three RCPs (RCP2.6, RCP4.5, and RCP8.5) and the first ensemble (run) out of five ensembles available. It is advisable to use several GCMs/RCPs for assessing broader representations of possible future precipitation and for better assessment of possible future changes in precipitation intensities with reasonable confidence through the estimation of uncertainties. For the purpose of this study, the six scenarios (three RCPs based on two GCMs) with multiple realizations (through the stochastic weather generator) cover a wide range of variability that is assumed to be sufficient for the investigation of the adopted two-stage modeling approach. Eight daily

precipitation time series were extracted; two for the baseline period from the two GCMs, and six representing future precipitation based on three RCPs and two GCMs.

3.2.2 Stochastic Weather Generator

In this study, the stochastic weather generator LARS-WG (Racsko et al., 1991; Semenov and Barrow, 1997), which was developed based on the series approach (Racsko et al., 1991), was used. Using the series approach, the sequence of wet or dry series length was modelled first and then the precipitation amount was modelled for each wet spell. LARS-WG computed a set of parameters for probability distributions of observed daily precipitation in Saskatoon. A synthetic precipitation time-series of arbitrary length (30 years in this study) was generated using the computed set of parameters by randomly sampling values from the probability distributions (Semenov and Startonovitch, 2010).

LARS-WG uses relative change factors (RCFs) for each month to estimate the local scale future daily precipitation scenarios produced from the GCM (Semenov and Barrow, 2002). RCFs are the ratios of future values to baseline period values. For example, RCF for the month of June is the ratio of future average precipitation in the month of June to that of the baseline period. LARS-WG (Version 5.0) contains RCFs for CMIP3' GCMs and IPCC AR4 emission scenarios. For verification of the calculated RCFs, the RCFs for mean monthly precipitation were calculated using the daily precipitation from CGCM3.1 (http://www.cccma.ec.gc.ca) based on three emission scenarios (A1B, A2, and B1) during the baseline period and under the projections of climate change, then compared with the RCFs embedded by the developers in LARS-WG. This verification step was needed because embedded RCFs are not available for CMIP5' GCMs, so these were calculated in this study.

The above-mentioned RCFs do not incorporate variability in future projections of precipitation due to wet and dry spell lengths. Therefore, average wet and dry spell lengths for each month were calculated during the baseline and future periods. Monthly ratio of the average length of wet or dry spell during the future period to the same length during the baseline period represent the RCFs related to wet or dry spell length. Changes in the average wet and dry spell lengths for any month alter the mean monthly precipitation of that month and this is expected to incorporate more variability in the future daily precipitation. However, LARS-WG does not incorporate the RCFs for wet and dry spell lengths in its archive since it considers only monthly output from GCMs. Because of the availability of daily precipitation for CMIP5, RCFs for wet and dry spell lengths were calculated. The RCFs for mean monthly precipitation amounts, and wet and dry spell lengths, were calculated, using two GCMs' (CanESM2 and HadGEM2-ES) precipitation available through CMIP5. The lengths of wet/dry spells were selected randomly from the probability distributions, constructed by LARS-WG, of wet/dry spells for the month in which the wet/dry spells begin.

The future realizations of climate data for Saskatoon were produced using LARS-WG in conjunction with GCMs. First, LARS-WG was calibrated based on Saskatoon's historical precipitation, which in this context means constructing probability distributions for the city's precipitation data based on the observed record and generating multiple (1000) realizations of the daily precipitation record during the baseline period. The constructed probability distributions were modified using the RCFs and perturbed to generate multiple (1000) realizations of future daily precipitation series in Saskatoon for each GCM/RCP combination. Accordingly, 6,000 realizations of future daily precipitation in Saskatoon were generated. The use of LARS-WG to produce future projections was considered as a "downscaling" method in this thesis.

In the cases of dynamic and regression-based downscaling, actual "downscaling" occurs as models (RCMs or regression relationships) link data/variables at coarse spatial and temporal (global) scale to those at a finer spatial and temporal (local) scale. The relationships developed from the baseline period is used to downscale future projections. However, the weather generator employs the statistical properties of observed variables at the local scale to generate multiple realizations at the same scale. Once future projections are produced by GCMs, a factor (called delta or relative change factor, RCF) is computed to quantify the shift in the data/variables from the baseline to the future periods. The same delta is used to shift the variables/data generated at the local scale to produce future projections. This argument is depicted in Figure 3.4. Figure 3.4 (1) shows that a relationship is established between the global scale variable and the local scale variable during the baseline period, the relationship is then used to generate the local scale future variable from the global scale future variable. In case of weather generator as shown in Figure 3.4 (2), RCFs are calculated for each month using global scale future and baseline scenarios, and these RCFs are applied to the local scale observed variable to generate local scale future variable.

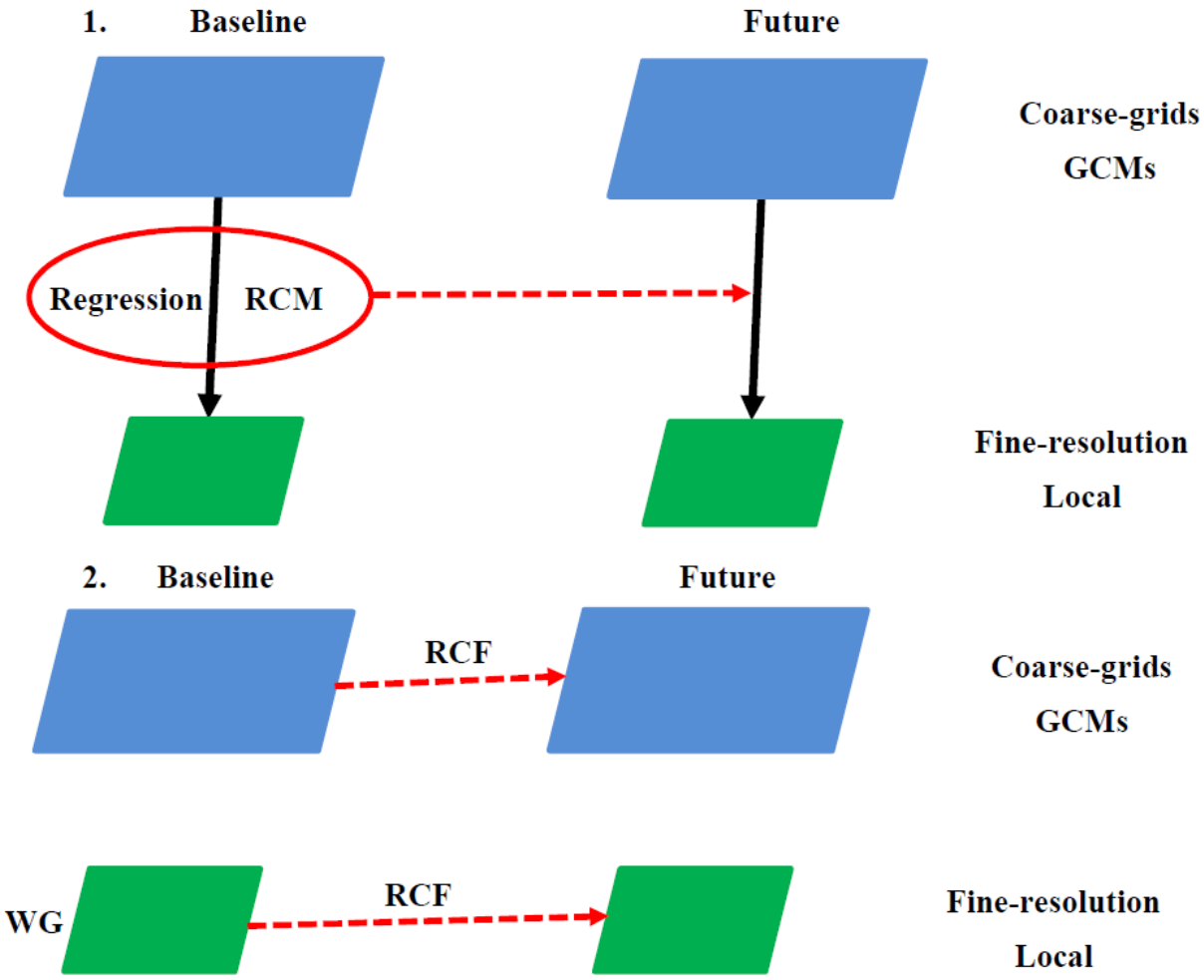

Figure 3.4: Generation techniques of future climate change scenarios at the fine resolution (local) scale from the coarse-grid GCMs' scale using (1) downscaling methods and (2) weather generators.

3.2.3 K-NN Hourly Disaggregation Model

The K-nearest neighbor (K-NN) method (Lall and Sharma, 1996; Yates et al., 2003; Sharif and Burn, 2007) was used for disaggregating precipitation data from daily to hourly scale. The hourly K-NN disaggregation model was conducted for precipitation from a single precipitation station for disaggregating both baseline and future daily precipitation of n years to hourly precipitation. Development of the disaggregation method is explained below.

Let X_t be the vector of daily precipitation values x_t, where t=1,……,365n (it excludes February 29 of a leap year); n is the total number of years in the daily precipitation time series. The steps of the algorithm as shown schematically in Figure 3.5 are as follows:

1. Let, Y_t^i be the vector of 24 hourly precipitation values y_t for day t of year i.

2. A window of w_d daily precipitation values in Figure 3.5 that includes x_t is identified to include the nearest neighbors to the selected daily precipitation x_t of a particular year i. If there is no rainy day within the window for the current year except x_t, the window size is increased each time by one day until it contains at least one rainy day. Accordingly, the corresponding hourly data block L from the time series Y_t of all years is identified. This way, the size of the hourly data block will be:

$$L_d = [(n*w_d)-1]*24 \quad [3.1]$$

3. In the work of Sharif and Burn (2007), w_d (i.e. optimal window size) was chosen to be 15, including x_t. So, if the current day of simulation is July 15, then all corresponding hourly profiles between July 8 and July 22 are selected from all n years of hourly record, excluding the corresponding hourly values for July 15 for the current year (to prevent the possibility of generating the same hourly profile as that corresponding to the current day). In this study, however, rather than using an arbitrary window size, the optimal window size was investigated and selected for the City of Saskatoon based on the simulated and observed annual maximum precipitation (AMPs) of various durations during the baseline period. Although w_d is allowed to change dynamically whenever at least one rainy day is not available in the window, a fixed size of w_d is used for the rest of the cases (containing at least one rainy day). The size of the fixed window is mentioned for easy understanding afterwards.

4. The daily precipitation amount (x_t) is compared with the set of neighboring hourly totals. The square of differences between x_t and each of the [(n*w_d)-1] segments in the L_d block is calculated and the segment showing the minimum squared difference is considered as the disaggregated hourly precipitation values for the current day. During the selection of optimal window size, more than one candidate among the nearest neighbors may be detected with the same minimum difference from the daily precipitation of the current day. So in addition to Sharif and Burn (2007), the performance of the model can be assessed using both random (selection of a segment randomly from a number of candidate segments) and deterministic (selection of the first segment from a number of candidate segments) sampling approaches during the baseline period based on simulated and observed AMPs of various durations. The hourly disaggregated precipitation sequences can be selected either randomly or deterministically from the hourly precipitation sequences of the nearest neighbors having equal minimum difference. The K-NN hourly disaggregation model was used to simulate the observed hourly precipitation sequences both randomly and deterministically using the optimal window size. The observed and simulated precipitation time series are accumulated to 24 different durations (1 to 24 hrs.) and the corresponding AMPs are identified. AMPs obtained from both simulations (random/deterministic) can be compared with the observed AMPs of 24 durations to assess the effect of both selection approaches.

5. In the case of climate change, when the future projected daily precipitation value is greater than the historical daily precipitation value, the hourly precipitation values may be increased by the same ratio as for the daily scale. The steps (1-5) of the hourly disaggregation model are illustrated in Figure 3.5.

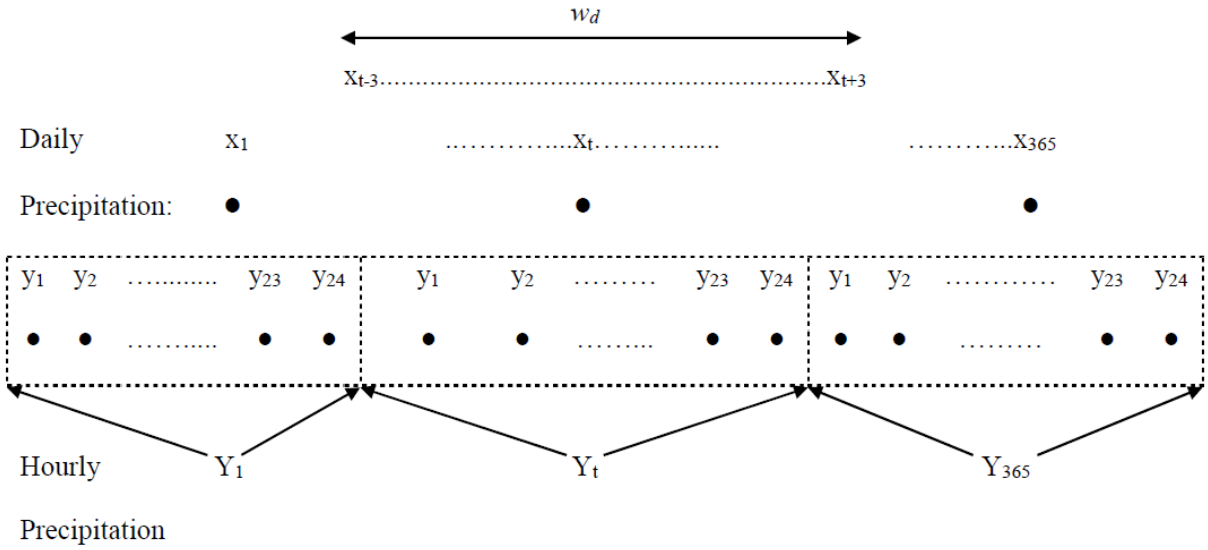

Figure 3.5: K-NN hourly precipitation disaggregation model for a typical year.

The hourly disaggregation model was repeated for all days of all of the years in the daily precipitation time series. A set of 1000 realizations of the daily precipitation was generated using LARS-WG, allowing the creation of ensembles of hourly disaggregated precipitation values by the K-NN method.

3.2.4 K-NN Sub-hourly Disaggregation Model

The K-NN method was also used to disaggregate precipitation from hourly to 5-minute values in the City of Saskatoon using the approach described in Section 3.2.3. The algorithm starts with the reading of each hourly precipitation value from the Y_t vector and it continues for the entire time series. The steps of the algorithm (as described schematically in Figure 3.6) are similar to the K-NN hourly disaggregation model. Let, S_t^j be the vector of 12 sub-hourly (5-minute) precipitation values s_t for hour t of day j; where t denotes specific hour of the day in a given year. Thus, the size of the 5-minute data block is:

$$L_h = [(n*w_h)*24-1]*12 \qquad [3.2]$$

Where w_h is the window size and n is the number of years in the hourly precipitation time series, the hourly precipitation amount (y_t) is compared with the set of neighboring totals of 5-minute precipitation values. The square of differences between y_t and each of the [(n*w_h)*24-1] segments in the L_h block were calculated; the segment showing the minimum square difference from the hourly precipitation is the disaggregated 5-minute precipitation values corresponding to the current hour. The extension of window size in the absence of rainy hours; selection of optimal window size for Saskatoon; random/deterministic sampling; and scaling of future sub-hourly precipitation values, were considered for the K-NN sub-hourly disaggregation model in a similar way to that of the hourly model. Steps of the sub-hourly disaggregation model are illustrated in Figure 3.6. In Figure 3.6, t denotes a specific day of a specific year in selecting hourly and sub-hourly data blocks, and h denotes hours in a day in a specific year; where h=1,2,…….,24.

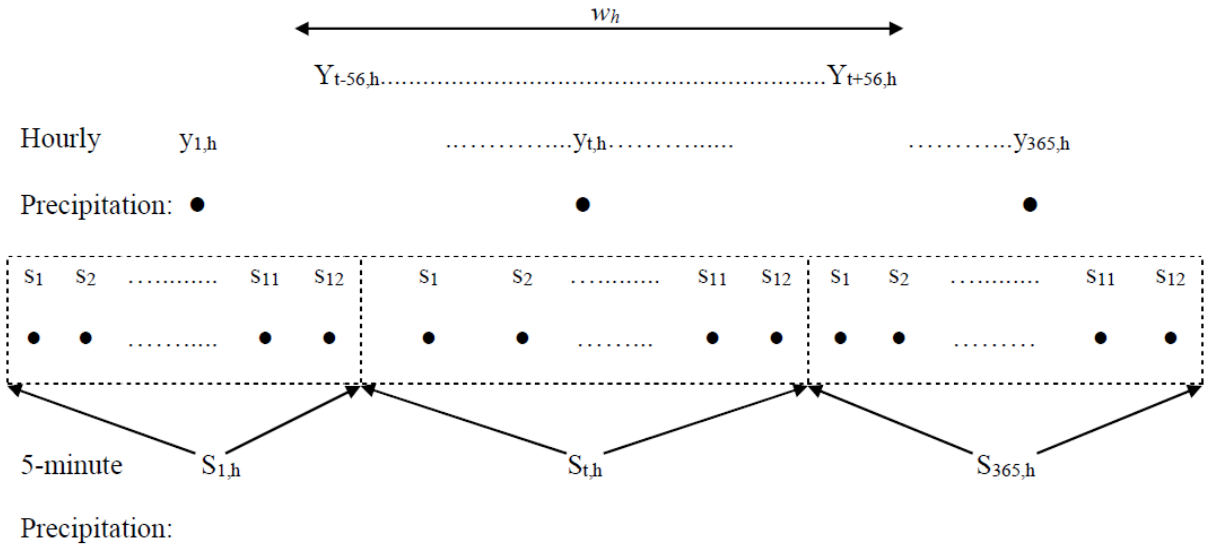

Figure 3.6: K-NN sub-hourly precipitation disaggregation model for a typical year.

3.2.5 Genetic Programming (GP)

The concept of biological evolution led to the development of Genetic programming (GP), which was introduced by Koza (1992) as an extension of genetic algorithms, which are optimization methods for searching for the global optimal of a function. GP, a data driven technique, was developed to solve problems by intelligent and adaptive searching. Depending on the search problem, GP takes on a special form called genetic symbolic regression (GSR) for establishing relationships as equations between the predictor and the predictand. The equations are optimized through an adaptive random search, providing insight into the functional (structural) form of the regression relationships between the input and the output; this is not the case for other regression methods. The GP technique was utilized in this study for obtaining equations that express mapping relationships between the global scale daily AMP quantiles and the local scale sub-daily (1 to 24 hours) AMP quantiles.

Babovic and Keijzer (2000), Savic et al. (1999), and Koza (1992) provide detailed explanations of GP and GSR methods. For an explanation of how GP can be applied to find relationships between local scale and global scale AMP quantiles, refer to Hassanzadeh et al. (2014). This study used GPLAB 3 package (Silva, 2007) for conducting experiments involving the local scale and global scale data.

Briefly, the GP search started with the creation of initial population of models (equations) in the form of parse trees without using prior information. The individual equations were assessed based on a goodness-of-fit measure; individuals with better fitness survive to create new individuals. Some operators originating from the concept of genetic evolution, specifically mutation and crossover, were considered for forming new parse trees using randomly selected parents during mating, thus creating the next generation. A threshold for the number of total

function evaluations and the convergence criterion were predefined as criteria for stopping the GP search. Because the GP-based method for producing future IDF curves for the City of Saskatoon was developed and published by Hassanzadeh et al. (2014), it was considered in this research to be a viable reference method for comparison with the developed two-stage modeling approach.

In this study, four statistical error measures were used to evaluate the performance of the mapping equations: the root mean squared error (RMSE), Pearson's correlation coefficient (R), mean absolute relative error (MARE), and mean bias (MB). These were calculated as follows:

$$RMSE = \sqrt{\frac{\sum_{i=1}^{N}(O_i - P_i)^2}{N}} \quad [3.3]$$

$$R = \frac{\sum_{i=1}^{N}(O_i - \bar{O})(P_i - \bar{P})}{\left[\sum_{i=1}^{N}(O_i - \bar{O})^2\right]^{0.5}\left[(P_i - \bar{P})^2\right]^{0.5}} \quad [3.4]$$

$$MARE = \frac{1}{N}\sum_{i=1}^{N}\left|\frac{O_i - P_i}{O_i}\right| \quad [3.5]$$

$$MB = \frac{1}{N}\sum_{i=1}^{N}(O_i - P_i) \quad [3.6]$$

Where O_i, P_i, $\overline{O}$, and $\bar{P}$ are observed values, simulated values, mean of observed, and mean of simulated values, respectively. N is the number of points in the dataset.

Strong relationships were observed between the global scale's (using the daily output of CGCM3.1) AMP quantiles and the corresponding daily and sub-daily local values by Hassanzadeh et al. (2014). Therefore, the relationships between the global-scale (using the output of CanESM2 and HadGEM2-ES) and the corresponding daily and sub-daily local values were investigated in order to map GCM quantiles to the corresponding local daily and sub-daily quantiles. Figure 3.7 is a visual verification of the hypothesis of this GP-based downscaling method; it compares the global scale (using CanESM2) AMP quantiles and the corresponding

daily and sub-daily local scale quantiles for the baseline period. Simlarly the output of HadGEM2-ES and CGCM3.1 are plotted in Appendix D (Figures D.1 and D.2).

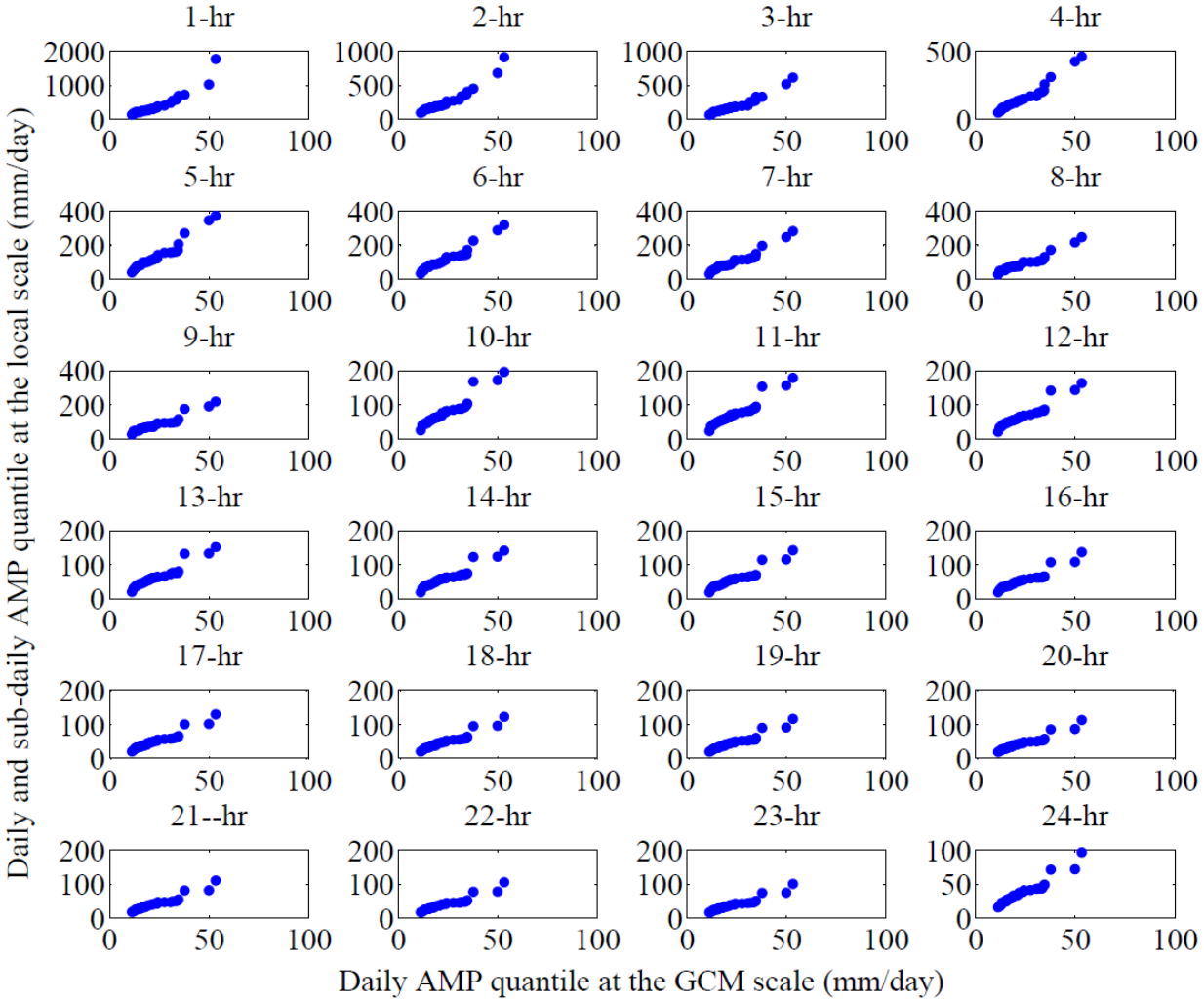

Figure 3.7. Quantile-Quantile plots of the GCM-scale (using output of CanESM2) daily AMP and the local-scale daily and sub-daily AMP during the baseline (1961-1990) period in Saskatoon.

The daily AMP data were extracted from the 30-year record of the baseline period. However, longer records of data are required for modeling purposes using the data-driven GP, which includes data for training and validation. GEV distributions were fitted to the observed 30 AMPs. A set of 10,000 uniform random numbers was generated to represent non-exceedance

probability, P ∈ [0 1] and then the corresponding AMP quantiles were sampled from the GEV distributions at the GCM-scale daily precipitation, and the local-scale daily and sub-daily precipitation data. The first 6000 data pairs (i.e., the GCM-scale daily AMP quantiles, and the local-scale daily and sub-daily AMP quantiles) were chosen as the training dataset from the randomly selected 10,000 data pairs for extracting each of the mapping equations using GP. A total of 24 mapping equations were extracted. The GCM-scale daily AMPs were used as the inputs, while the outputs were the local-scale AMPs of a specified duration. The remaining 4000 data pairs were used as the validation dataset. In addition, the original 30 AMPs for the GCM-scale daily precipitation and the local-scale daily and sub-daily precipitation were used as a completely unseen testing dataset to verify the developed equations. For a detailed explanation of the GP method implementation with setting internal parameters of the model, refer to Appendix D (Tables D.1 to D.5).

3.2.6 Generalized Extreme Value Distribution and the Construction of IDF Curves

Once the precipitation data were collected/generated, annual maximum precipitation (AMP) values at various durations were extracted. The Generalized Extreme Value (GEV) distribution, which is a family of parametric probability distributions, was used to estimate the frequency of the AMP as a random variable. Gumbel, Fréchet, and Weibull probability distributions are combined in the GEV distribution, which takes the following form (Katz, 2012):

$$F(x, \mu, \sigma, \xi) = exp\left\{-\left[1 + \xi\left(\frac{x-\mu}{\sigma}\right)\right]^{-1/\xi}\right\} \quad [3.7]$$

where $1 + \xi\left(\frac{x-\mu}{\sigma}\right) > 0$, $F \in [0\ 1]$ denotes the non-exceedance probability of the random variable x, $\mu \in R$ is the location parameter, $\sigma > 0$ is the scale parameter, and $\xi \in R$ is the shape parameter. The shape parameter ξ controls the tail behavior of the distribution. The GEV

distribution converges to Gumbel, Fréchet, and Weibull distributions when $\xi = 0$, $\xi > 0$, and $\xi < 0$, respectively. The GEV distribution with maximum likelihood method for parameter estimation was used in this study for the construction of IDF curves in the City of Saskatoon during the baseline period and the future projection period, as it was used successfully in previous studies (Beniston et al., 2007; Cameron et al., 2001, Hashmi et al., 2011; Hassanzadeh et al., 2014; Kharin and Zweris, 2005; Yilmaz and Perera, 2014). The GEV distribution was used for the construction of IDF curves, although it increases the computation intensity due to the involvement of three parameters (shape, scale, and location) instead of the two parameters in Gumbel distribution. However, the GEV distribution provides better description of the upper tail behavior of the data by introducing an additional parameter (Overeem et al., 2008). Figure 3.8 shows the ability of GEV distribution to fit empirical cumulative distribution functions (ECDF) of daily and sub-daily AMPs in Saskatoon. The goodness of GEV fit to the AMPs was confirmed by the Kolmogorov-Smirnov test with 95% significance level.

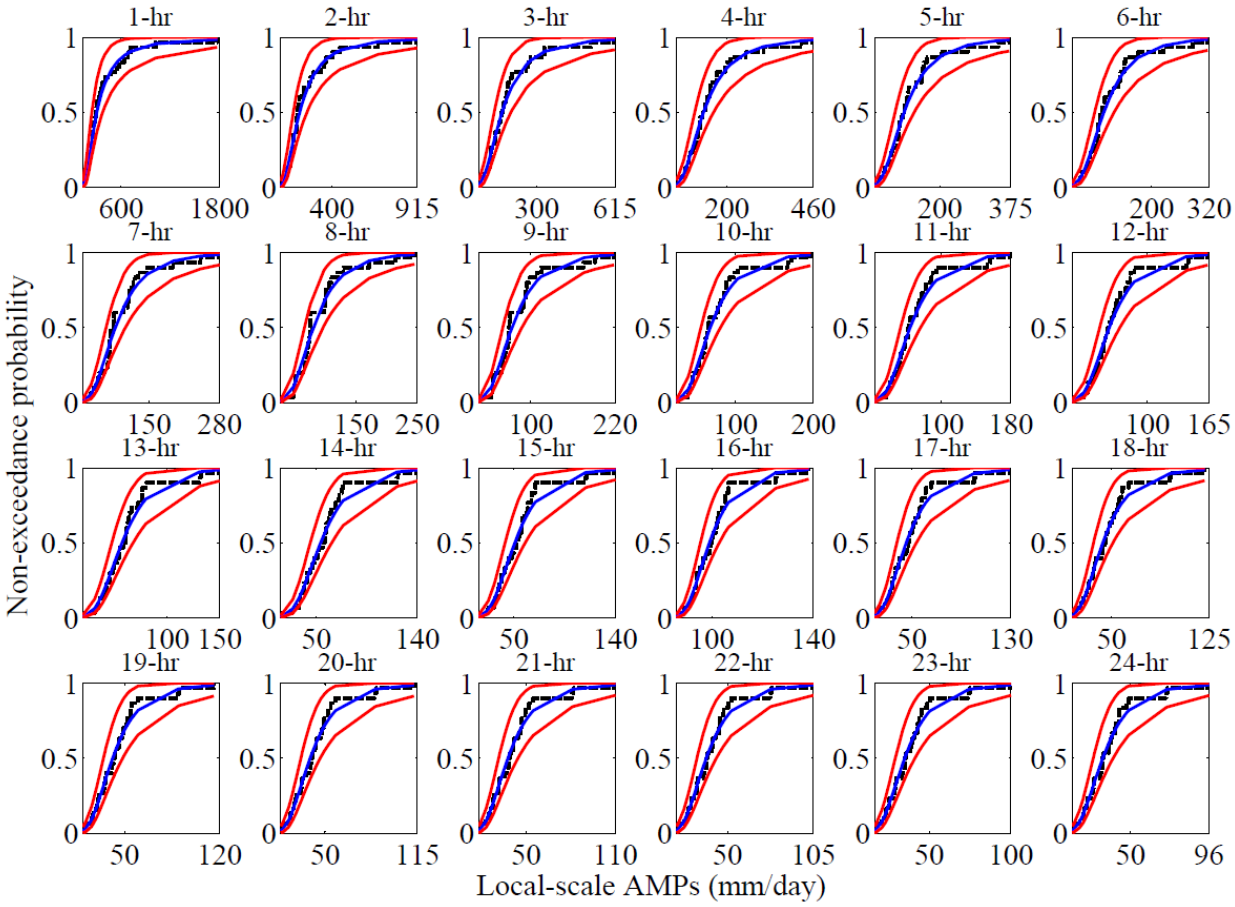

Figure 3.8: Comparison between the GEV (blue line) and empirical fit (black dots) for the local AMPs in Saskatoon with 95% confidence intervals of GEV fit shown by the red lines.

IDF curves can be constructed by using the inverse of the fitted GEV distributions, given the return period (T) and precipitation quantiles (Q_x), as follows:

$$Q_x = GEV_x^{-1}\left(1 - \frac{1}{T}\right) \quad [3.8]$$

Eventually, the hourly and sub-hourly disaggregation models, based on the K-NN method, were used to generate long time-series of hourly and sub-hourly precipitation values for both baseline and future periods (2011-2100). The AMPs of the disaggregated hourly and sub-hourly precipitation time series were used to construct two different sets of IDF curves based on quantiles obtained from the GEV distribution: (a) the IDF curves derived from historical data

(observations), which currently form the basis of the design and evaluation of Saskatoon's storm water collection system; and (b) the IDF curves based on the models developed in this study. A third set of IDF curves was constructed using the Genetic Programming (GP) method, which was introduced by Hassanzadeh et al. (2014) and was re-implemented in this study with new data based on CMIP5 simulations. The GP method employs a fundamentally different route for constructing the IDF curves because it generates AMPs at the local scale directly without having to generate the time series of continuous precipitation values. Accordingly, the GP method provides a reference for comparison with the two-stage modeling method developed in this study, and also helps show variability in IDF curves due to the adoption of different downscaling methods. The analyses of the results took into consideration the GCMs, RCPs, and the downscaling/disaggregation methods.

CHAPTER 4: RESULTS AND ANALYSIS

4. Overview

Results of the stochastic weather generation, the disaggregation technique, and GP method are presented in this chapter. Sections 4.1 and 4.2 show results related to the generated long time series of site-specific daily precipitation during the baseline period and under the projections of climate change scenarios for Saskatoon using LARS-WG. The hourly disaggregation model developed using the K-nearest neighbors (K-NN) technique is presented, analyzed, and compared with the GP method in Sections 4.3 and 4.4.2. The sub-hourly disaggregation model developed using the same K-NN technique is also presented and analyzed in Section 4.3. In Section 4.4, variations in future IDF curves as compared to the baseline IDF curves are presented and analyzed based on two GCMs and three RCPs during the 21st century. The two hourly disaggregation methods (i.e., K-NN and GP) were compared in terms of their ability to reproduce historical as well as future IDF curves for the City of Saskatoon. Sources of uncertainties and their relative contributions to the total uncertainty and uncertainties associated with the prediction of future IDF curves are included in Section 4.5.

4.1 Calibration and Validation of LARS-WG

Saskatoon's observed daily precipitation data during the baseline period (1961-1990) was used by LARS-WG to obtain parameters of the probability distributions of the local station's precipitation. This set of parameters was used to generate 1000 realizations of the observed precipitation series. The performance of the calibrated model is shown in Figure 4.1. The weather generator was calibrated based on the p-value calculated for all statistics (e.g., KS-, t-, and f-statistics shown in Appendix B: Table B.1) concerning the hypothesis test (e.g., Kolmogorov–Smirnov test) to determine if the observed and simulated precipitation series

belong to the same distribution. The model was then validated using Saskatoon's observed daily precipitation during the period of 1991-2009 (Figure 4.2).

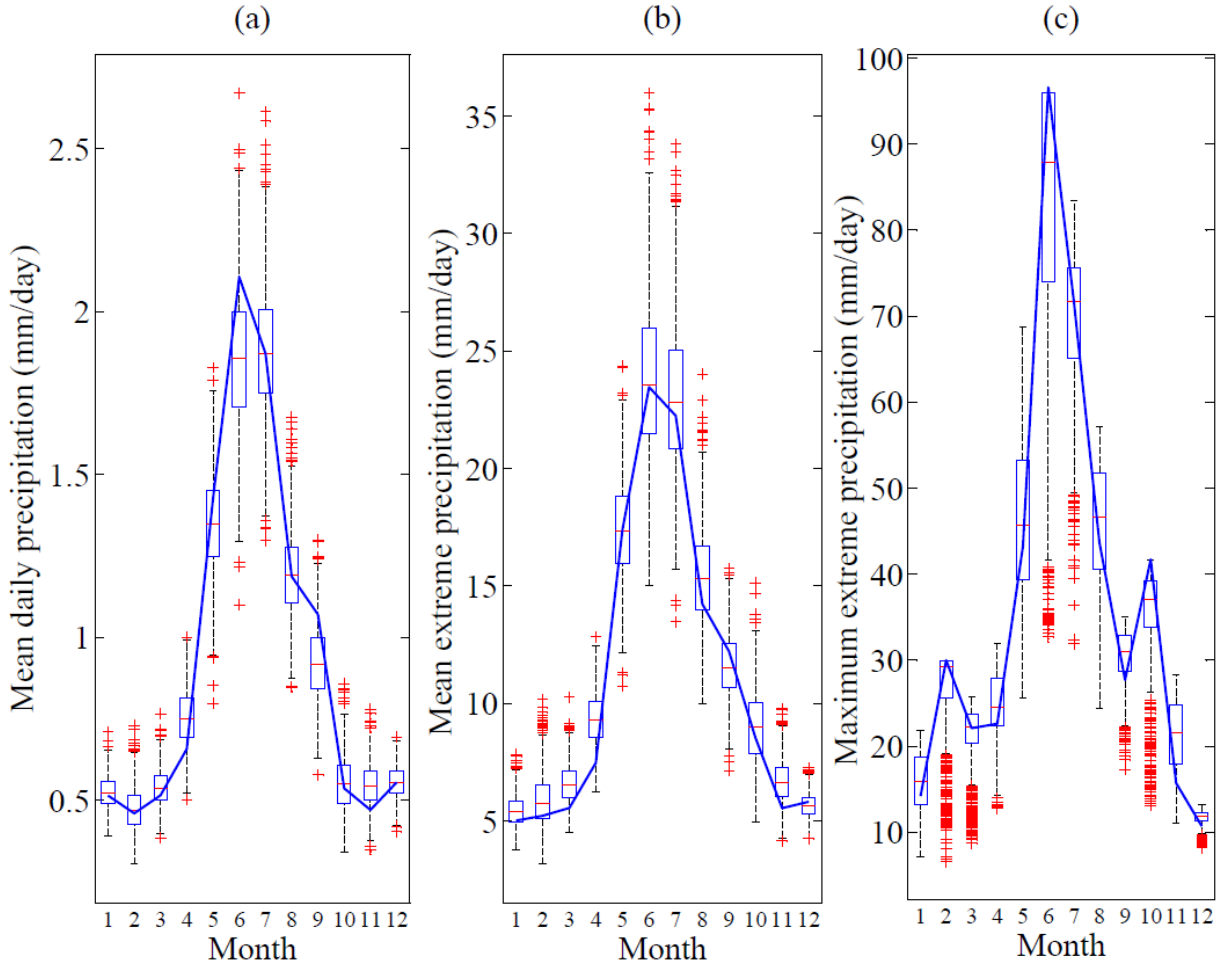

Figure 4.1: Performance of LARS-WG based on the observed monthly properties (solid lines) and 1000 realizations of synthetic (box plots) precipitation time-series during the baseline period (1961-1990) in Saskatoon.

Figure 4.1 plots the observed mean daily precipitation (4.1a) and mean maximum daily precipitation (4.1b) in each month and the corresponding ones of the synthetic daily precipitation in each month shown as boxplots, based on 1000 realizations obtained from LARS-WG during the baseline period. The mean daily precipitation was calculated as the mean of daily precipitation in each month over a period of 30 years (1961-1990), the 30 years have 30 AMPs

and the mean of 30 AMPs in each month was termed as mean extreme precipitation, while the maximum of the 30 AMPs in each month was denoted as maximum extreme precipitation in Figure 4.1. The figures show that LARS-WG generated the mean and mean of the extreme precipitation properties quite well during the baseline period. However, LARS-WG seems to slightly underestimate the maximum of the extreme precipitation in the month of June (Figure 4.1c) due to failure of the weather generator in reproducing maximum of the extreme precipitation values, which might contribute to some uncertainty in simulating future maximum extreme precipitation. The months outside the summer are not considered to be important for this study. Figure 4.2 shows that LARS-WG generated the mean and mean of the extreme precipitation properties quite well during the validation period. As per the validation results, LARS-WG seems to marginally underestimate the maximum extreme precipitation for the months of August and September, in addition to that for June (Figure 4.2c).

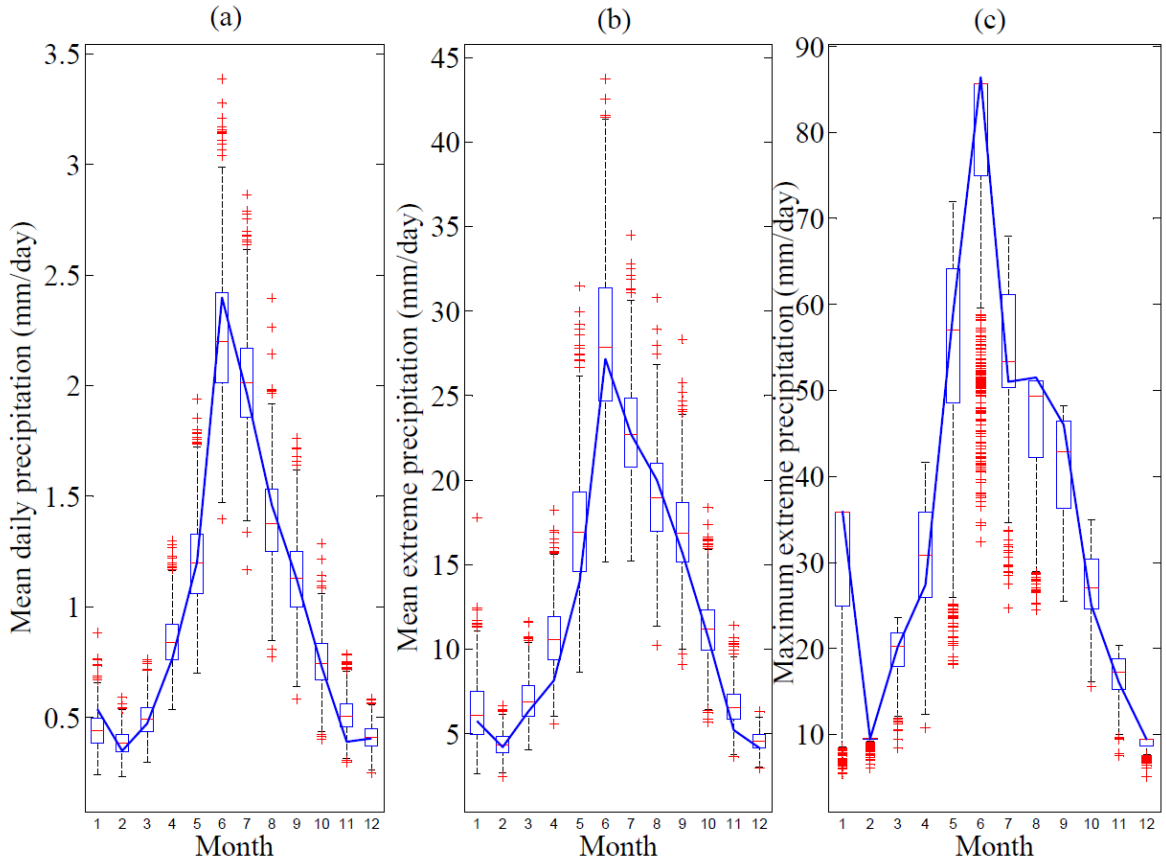

Figure 4.2: Performance of LARS-WG based on the observed monthly properties (solid lines) and 1000 realizations of synthetic (box plots) precipitation time-series during the validation period (1991-2009).

4.2 Effect of Wet and Dry Spell Lengths

Generation of daily precipitation series using LARS-WG requires the calculation of relative change factors (RCFs) related to the precipitation amounts, wet spell lengths, and dry spell lengths for each month. The relative change factors (RCFs) of monthly precipitation amounts for 15 GCMs from CMIP3 are embedded in the current version of LARS-WG. However, the RCFs for the GCMs from CMIP5 are not included in LARS-WG's archive; these need to be calculated using the GCMs' output. For verification, the output of CGCM3.1 (a

CMIP3 model) was used to calculate the RCFs related to the monthly precipitation amounts and compared with the corresponding values embedded in LARS-WG.

Table 4.1 shows a comparison between the relative change factors (RCFs), for each month, based on the embedded and GCMs simulated precipitation values. The comparison shows that the sign and magnitude of change in mean monthly precipitation amounts, as presented by the calculated RCFs, are not very different from those embedded in LARS-WG.

Table 4.1: Relative changes in monthly precipitation amounts between baseline and future (2020s, 2050s, and 2080s) climate as calculated from CGCM3.1 output (ratio of A1B future scenario to baseline scenario) as compared to the RCFs embedded in LARS-WG.

	(2011-2040)		(2041-2070)		(2071-2100)	
Month	LARS-WG	Calculated	LARS-WG	Calculated	LARS-WG	Calculated
Jan	1.17	1.20	1.18	1.16	1.21	1.15
Feb	1.15	1.20	1.21	1.20	1.26	1.16
Mar	1.15	1.12	1.25	1.14	1.47	1.22
Apr	1.17	1.20	1.36	1.44	1.63	2.02
May	1.14	1.16	1.41	1.74	1.43	1.58
Jun	1.03	1.10	1.24	1.28	1.10	1.14
Jul	0.98	0.97	1.06	0.95	0.96	0.91
Aug	0.96	0.97	1.01	1.23	0.95	0.86
Sep	1.00	0.96	1.01	0.90	1.07	0.97
Oct	1.08	1.07	1.11	1.16	1.24	1.27
Nov	1.11	0.99	1.17	1.12	1.27	1.20
Dec	1.15	1.23	1.15	1.10	1.24	1.32

The calculated RCFs for the mean monthly precipitation totals, and wet, and dry spell lengths are shown in Table 4.2, which were used in LARS-WG to generate realizations of future daily precipitation scenarios using CanESM2 (shown in Table 4.2) and HadGEM2-ES (shown in Appendix B: Tables B.4, B.5, and B.6) based on three RCPs (i.e. RCP2.6, RCP4.5, and RCP8.5).

Table 4.2: Relative change factors for CanESM2 during 2011-2040 (RCFs during other periods are shown in Appendix B: Tables B.2 and B.3).

	Mean monthly precipitation			Wet spell length			Dry spell length		
Month	RCP2.6	RCP4.5	RCP8.5	RCP2.6	RCP4.5	RCP8.5	RCP2.6	RCP4.5	RCP8.5
Jan	0.88	1.15	1.16	0.93	1.01	1.20	0.96	0.93	1.00
Feb	1.03	1.00	0.91	0.96	0.94	0.97	0.93	0.97	1.12
Mar	1.61	1.11	1.29	1.37	1.39	1.19	0.94	1.11	0.92
Apr	1.33	1.49	1.80	0.88	1.15	1.05	0.91	0.88	0.76
May	1.07	1.16	0.96	0.92	0.90	0.93	0.87	1.08	0.98
Jun	0.91	0.72	0.81	0.88	0.75	0.93	0.83	1.20	1.06
Jul	1.08	1.10	1.03	1.09	1.25	0.97	1.34	1.27	1.11
Aug	0.98	0.88	0.88	0.98	0.88	0.88	0.87	0.76	1.04
Sep	0.85	0.87	1.19	1.01	1.07	1.08	0.95	0.97	1.00
Oct	1.24	1.19	1.41	1.01	1.05	1.22	1.00	0.92	0.81
Nov	1.05	1.05	1.06	1.14	1.13	1.09	1.06	1.09	1.05
Dec	1.25	1.42	1.41	1.08	1.05	1.33	0.86	0.88	0.90

Two sets of relative change factors were calculated for each GCM of the CMIP5 based on all RCPs, one including wet and dry spell lengths and the mean monthly precipitation, and another by using only changes in mean monthly precipitation totals. The 1000 realizations of future daily precipitation time series for the GCMs/RCPs were generated using each of the two sets of relative change factors were used to differentiate between the contributions of changes in the mean monthly precipitation amounts and changes in wet/dry spell durations.

The annual maximum precipitation (AMPs) of the realizations of future daily precipitation projections, obtained from the simulations based on CanESM2 with and without using RCFs related to wet/dry spell lengths, were used to estimate the expected values and 95% confidence intervals using the Generalized Extreme Value (GEV) as shown in Figure 4.3. Although the RCFs of mean monthly precipitation amounts are the greater contributors to

changes in the future daily precipitation values, the RCFs of wet/dry spell lengths can affect the expected values and 95% confidence intervals, particularly in longer return periods.

The uncertainty in determining the sign and magnitude of change in future extreme precipitation seem to be more dependent on the RCPs and time periods. For the CanESM2 and a 100-year return period, the future expected precipitation intensities during 2041-2070 – using the RCFs related to wet/dry spell lengths for RCP2.6, RCP4.5, and RCP8.5, compared to the observed expected precipitation intensity of 115 mm/day during the baseline period – are 115, 96, and 123 mm/day, respectively. The corresponding future expected precipitation intensities, without using RCFs related to wet/dry spell lengths for RCP2.6, RCP4.5, and RCP8.5 are; 114, 84, and 107 mm/day, respectively. Future expected precipitation intensities, using RCFs related to wet/dry spell lengths during the time slices 2011-2040, 2041-2070, and 2071-2100, are 118, 95, and 96, respectively, using the RCP4.5 of CanESM2 and a 100-year return period. The corresponding future expected precipitation intensities without using RCFs related to wet/dry spell lengths into consideration for 2011-2040, 2041-2070, and 2071-2100 are 105, 84, and 96 mm/day, respectively, when the RCP4.5 of CanESM2 and a 100-year return period are considered. The results for HadGEM2-ES are shown in Appendix B (Figure B.3). Similar results were also obtained for CGCM3.1 (CMIP3 climate model), shown in Appendix F (Figure F.1).

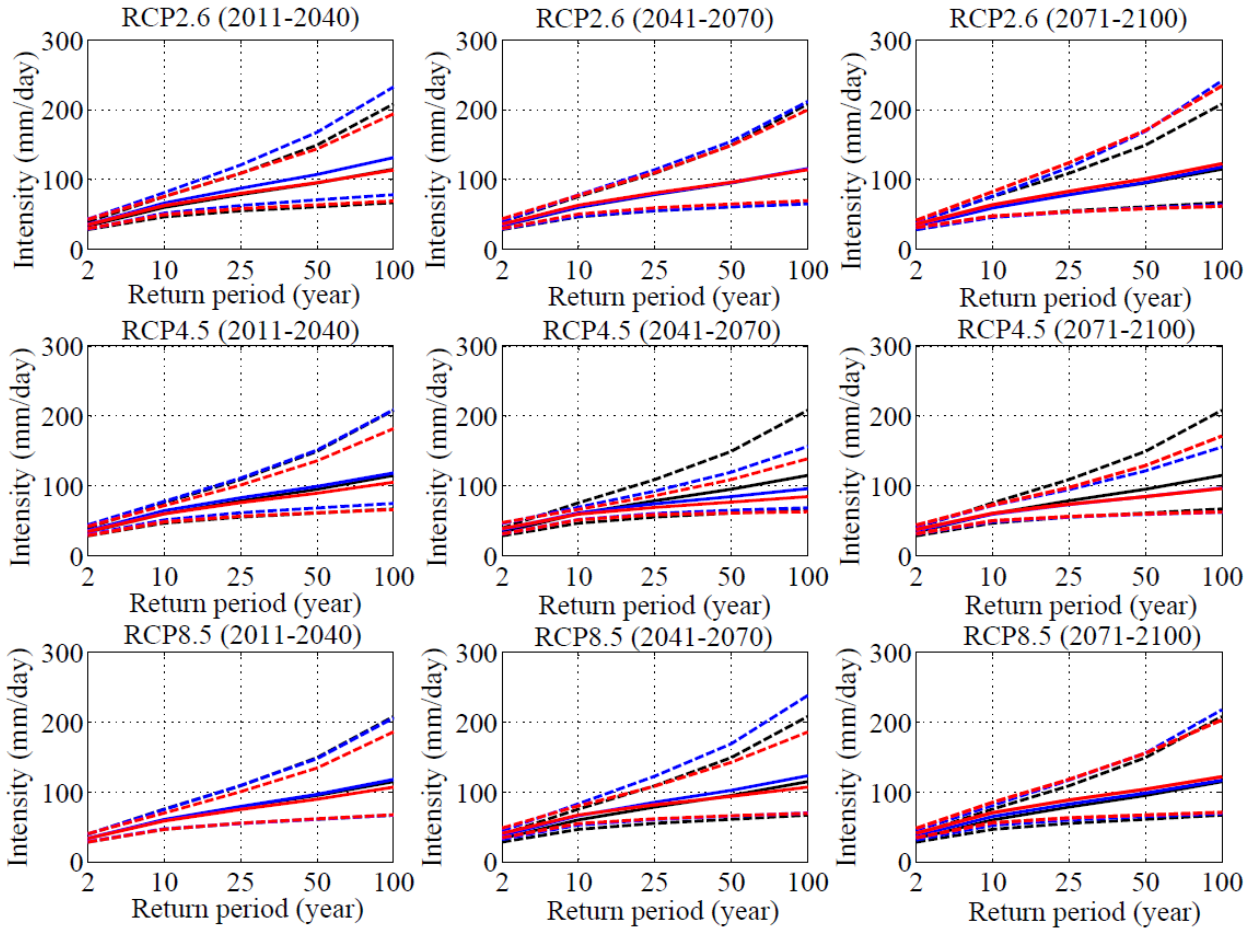

Figure 4.3: Variations in the future projections of daily AMP quantiles in the City of Saskatoon according to CanESM2 forced with three RCPs using two sets of change factors: with wet/dry spell (blue) and without wet/dry spell (red) effects. The expected quantiles (solid lines) and their 95% confidence intervals (dashed lines) are shown with the corresponding quantiles during the baseline period (black).

The AMP quantiles of 1000 realizations of daily precipitation obtained from LARS-WG based on CanESM2 and HadGEM2-ES, forced with three RCPs using both sets of RCFs, were calculated. Figure 4.4 shows the variability of the 2-year storm value (shown as quantiles in the boxplots). The quantiles were estimated by fitting GEV distributions to the daily AMPs from LARS-WG. The plot for the 100-year return period is presented in Appendix B (Figure B.4) and plots for CGCM3.1 are shown in Appendix F (Figures F.2 and F.3). In the case of both GCMs and all three RCPs, the extreme daily precipitation quantiles vary depending on whether wet/dry

spell effects were considered or not. Figure 4.4 also reveals that in most cases, the variabilities in the future IDF curves due to the choice of GCMs can be larger than those due to the inclusion/exclusion of wet and dry spells. Including the wet/dry spell effects in a 100-year return period, the future expected precipitation intensity is 131 mm/day for CanESM2 and RCP2.6 during 2011-2040, compared to the observed expected precipitation intensity of 115 mm/day during the baseline period, which is 100 mm/day for HadGEM2-ES and RCP2.6 during 2011-2040. Considering a 2-year return period, the future expected precipitation intensity is 35 mm/day for CanESM2 and RCP2.6 during 2011-2040, compared to the observed expected precipitation intensity of 33 mm/day during the baseline period, which is 37 mm/day for HadGEM2-ES and RCP2.6 during 2011-2040. The variations due to the choice of GCMs seem to increase with an increase in the return period.

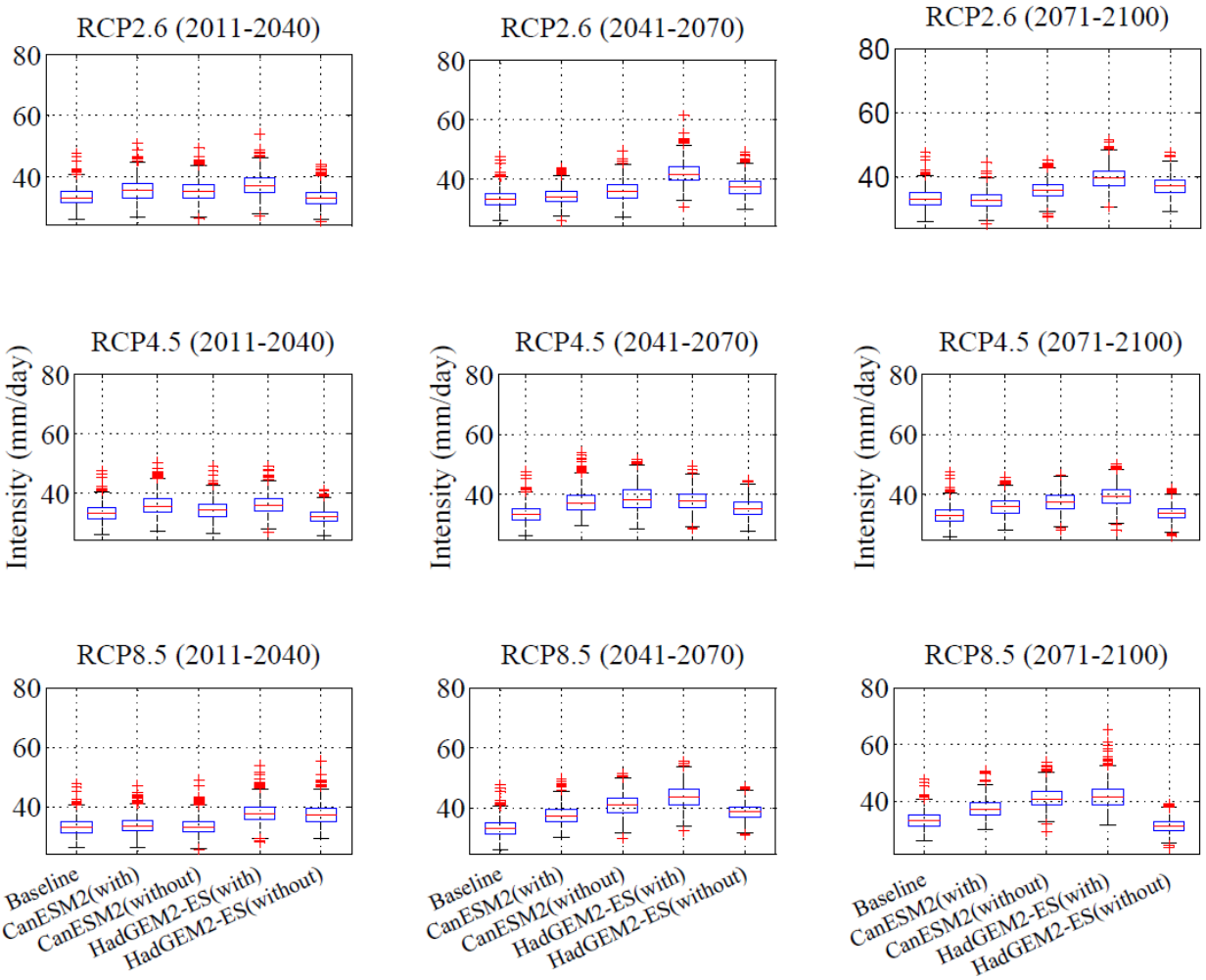

Figure 4.4: Boxplots of future projections of daily expected quantiles for 2-year return period precipitation in the City of Saskatoon according to CanESM2 and HadGEM2-ES forced with three RCPs using two sets of change factors, i.e. with wet/dry spell and without wet/dry spell effects along with the corresponding daily expected quantiles during the baseline.

4.3 K-NN Disaggregation Model

4.3.1 Selection of Optimal Window Size

In order to develop the most appropriate K-NN hourly disaggregation model, the optimal window size (i.e. number of nearest neighbors to the current day of disaggregation) was selected using the observed daily and hourly precipitation data during the baseline period (1961-1990). The K-NN hourly disaggregation model was used to disaggregate the observed daily

precipitation to hourly precipitation sequences using 30 different window sizes from 3 days to 61 days to identify the most appropriate memory length of the hydrological system for the City of Saskatoon. Each window size was used to generate the hourly precipitation sequences from daily precipitation values, from which the AMPs were identified for various durations (i.e., 1-hour to 24-hour). The simulated AMPs were then compared with the corresponding observed AMPs, and the performance of each window size was evaluated based on the Root Mean Squared Error (RMSE) in Equation 4.1, where X= normalized AMPs and i=1, 2, 3,……,n (total number of years in the time series).

$$X = \frac{(AMP_i - Minimum\ value)}{(Maximum\ value - Minimum\ value)} \quad [4.1]$$

The RMSE values from 30 window sizes, as shown in Figure 4.5, were evaluated to determine the optimal window size for the K-NN hourly disaggregation model. The window with 3 days (half window) on both sides of the current disaggregation day (i.e., a window of 7 days) provided the lowest RMSE of 0.12. Therefore, the optimal window size of 7 days was chosen for the K-NN hourly disaggregation model. As extreme precipitation values would influence the value of RMSE, the performance of each window was evaluated based on the RMSE calculated from the observed and simulated AMPs. However, other error measures, for instance, MARE, R, and MB may also be used depending on the objective of the investigation for the selection of an optimal window size.

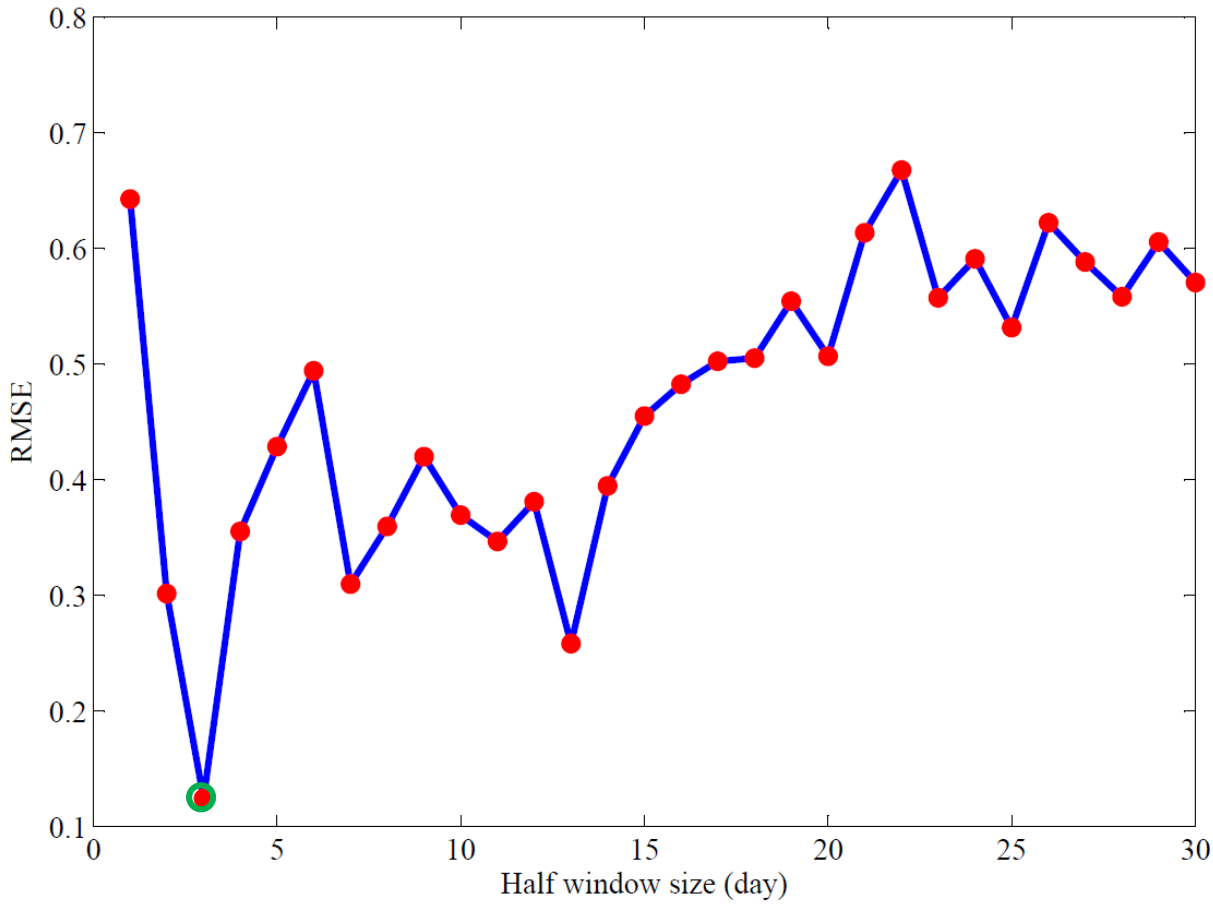

Figure 4.5: The performance of various windows obtained for selecting optimal (green circle) window size for the K-NN hourly disaggregation model.

The K-NN hourly disaggregation model was used to simulate the observed hourly precipitation sequences both randomly and deterministically using the optimal window size. A random selection of hourly precipitation sequences had no significant effect on the hourly disaggregation simulations of the extreme precipitation. Both deterministic and random sampling approaches produced the same optimal window size based on the RMSE measure. Random sampling results in a wider range of possible hourly disaggregated precipitation sequences than the deterministic sampling. Hence, the sampling in K-NN hourly disaggregation model using a random selection approach of one sequence can be adopted using a single random realization,

which reduces the modeling complexity and computational time tremendously without compromising the efficiency of the model.

The calculation of optimal window size was repeated with sub-hourly precipitation data. The RMSE values resulted from investigating 120 different window sizes (shown in Figure 4.6) were evaluated to determine the optimal window size for the K-NN sub-hourly disaggregation model. The window of 110 hours on both sides (half window) of the disaggregation hour, i.e., 221 hours in total has the minimum RMSE of 0.165. However, a window size of this size would be too large for a sub-hourly disaggregation model because it increases the model complexity and the computational time. A smaller window with reasonably good performance (with reasonable RMSE) can be more acceptable choice for the K-NN sub-hourly disaggregation model. The half window size of 56 hours, i.e., a window of 113 hours, has an RMSE of 0.219. This window size is almost half of the optimal window size and has a very similar RMSE. Therefore, the window of 113 hours was chosen for the K-NN sub-hourly disaggregation model. The K-NN sub-hourly disaggregation model was used to simulate the observed sub-hourly precipitation sequences randomly and deterministically. Simulations revealed that the random selection of sub-hourly precipitation sequences had no significant effect on the sub-hourly disaggregation simulations, when compared with the deterministic selection.

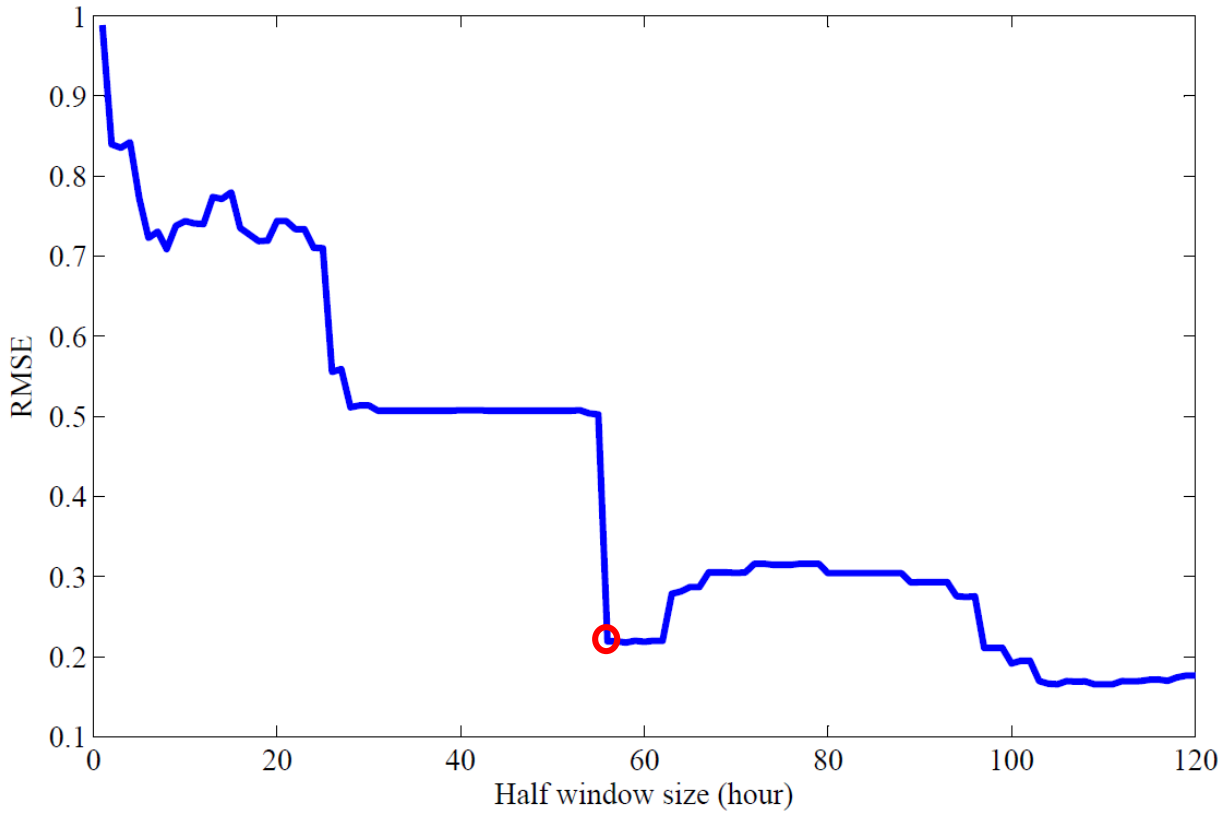

Figure 4.6: The performance of various windows obtained in selecting optimal (red circle) window size for the K-NN sub-hourly disaggregation model.

4.3.2 Performance of the Disaggregation Models

The K-NN hourly disaggregation model was run using 1000 realizations of daily precipitation from LARS-WG and the Saskatoon's observed hourly precipitation data during the baseline period (1961-1990) to obtain 1000 realizations of hourly precipitation. The disaggregation model used the optimal window size to generate 1000 realizations of observed hourly precipitation series. The performance of the calibrated model is shown in Figure 4.7 during the spring and summer months (April-September). The K-NN hourly disaggregation model appears to simulate the observed mean hourly precipitation, the mean of maximum hourly precipitation, and the maximum extreme precipitation quite well, except in June.

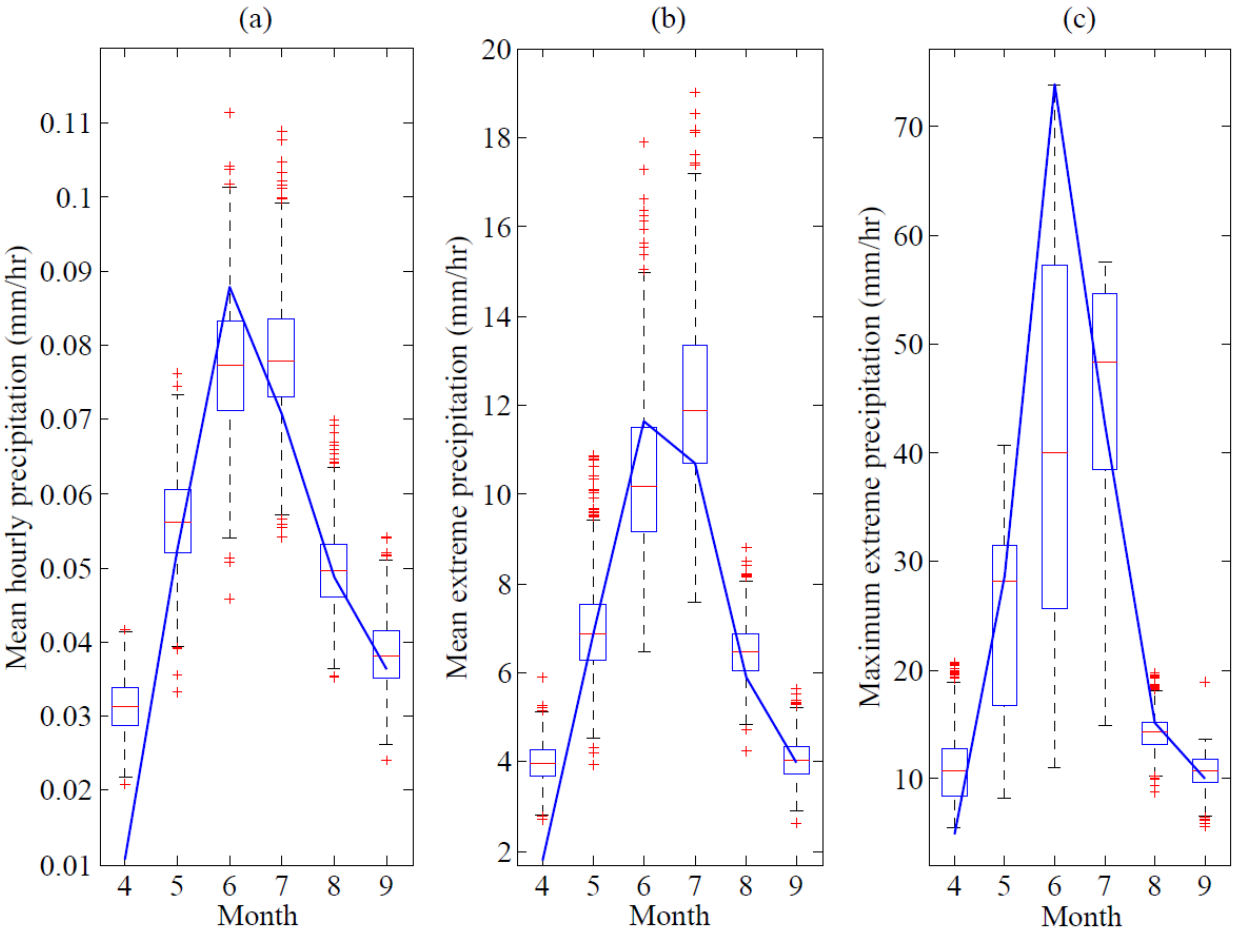

Figure 4.7: Performance of K-NN hourly disaggregation model based on the observed monthly properties (solid lines) and 1000 realizations of disaggregated (box plots) hourly precipitation time-series during the baseline period (1961-1990).

The K-NN sub-hourly disaggregation model was run using 1000 realizations of hourly precipitation obtained from the K-NN hourly disaggregation model and the Saskatoon's observed 5-minute precipitation data during the period 1992-2009 (May-September) to obtain 1000 realizations of 5-minute precipitation values during the same period. The disaggregation model used the selected optimal window size to generate 1000 realizations of the 5-minute precipitation series. The performance of LARS-WG and the K-NN hourly and sub-hourly disaggregation models are shown in Figure 4.8, Figure 4.9, and Figure 4.10, respectively, during

the period 1992-2009 (May-September). The 5-minute precipitation data from Acadia Reservoir rain gauge were aggregated to daily and hourly precipitation to conduct this part of the study.

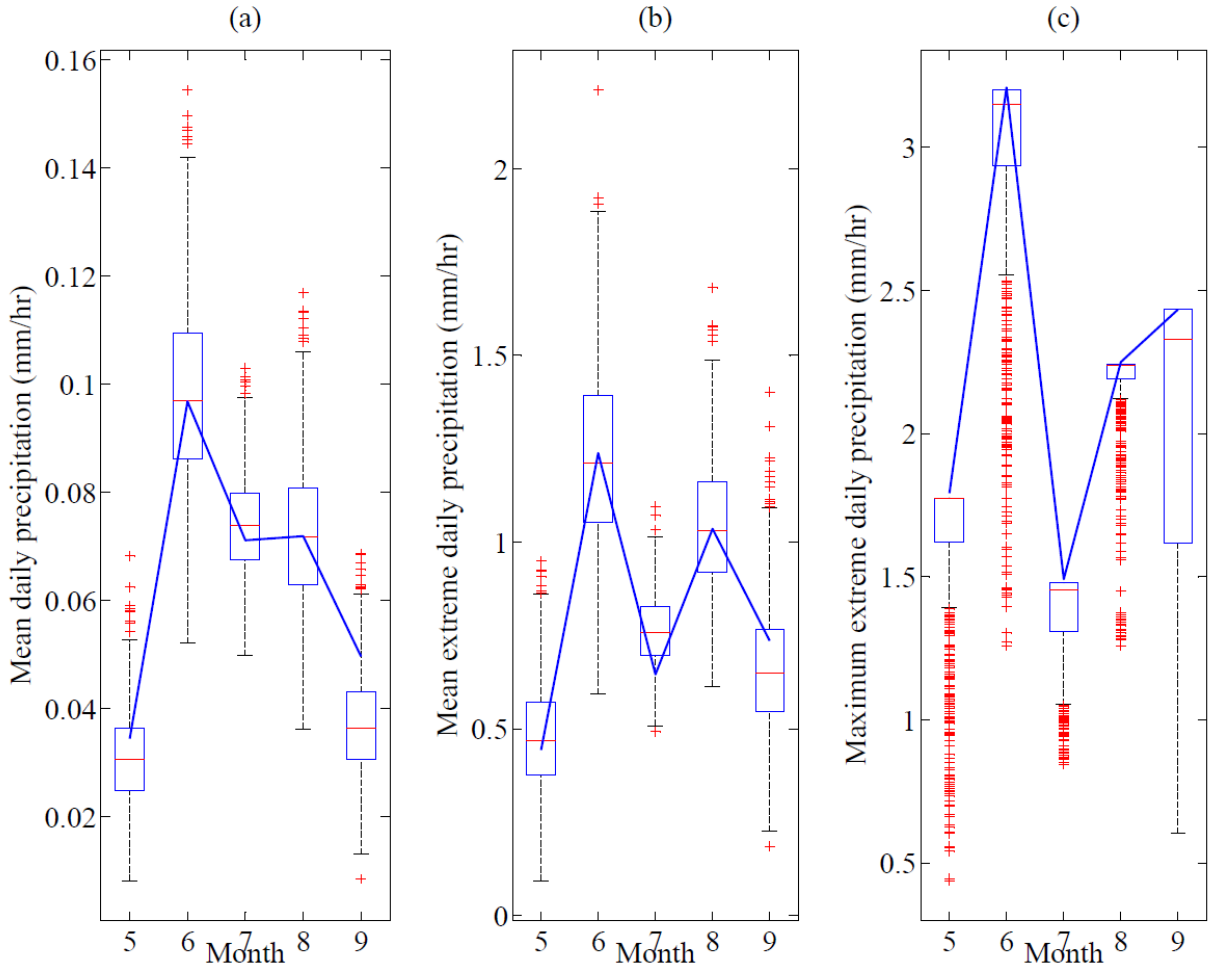

Figure 4.8: Performance of LARS-WG based on the observed monthly properties (solid lines) and 1000 realizations of downscaled (box plots) daily precipitation time-series during 1992-2009.

Figures 4.8 and 4.9, respectively, in addition to a comparison between the observed and simulated 5-minute precipitation in each of the five months based on 1000 realizations obtained from K-NN sub-hourly disaggregation model during the period 1992-2009 (Figure 4.10). These figures show that LARS-WG, K-NN hourly, and K-NN sub-hourly disaggregation models generated mean, mean extreme, and maximum extreme precipitation properties reasonably well

during the period 1992-2009, except in Figure 4.8(c), where LARS-WG appears to underestimate the maximum extreme precipitation in most months, which might contribute to the uncertainty in simulating future maximum extreme precipitation. Only 14 years of 5-minute precipitation data were available for conducting this part of the study; however, 20-30 years of daily precipitation data are generally required in order to simulate synthetic daily precipitation series in LARS-WG and capture the climate properties of the precipitation station (Semenov and Barrow, 2002). Since the baseline period used in this study is 30 years (1961-1990), this issue of underestimation can be minimized during the baseline period as shown in Figure 4.1(c).

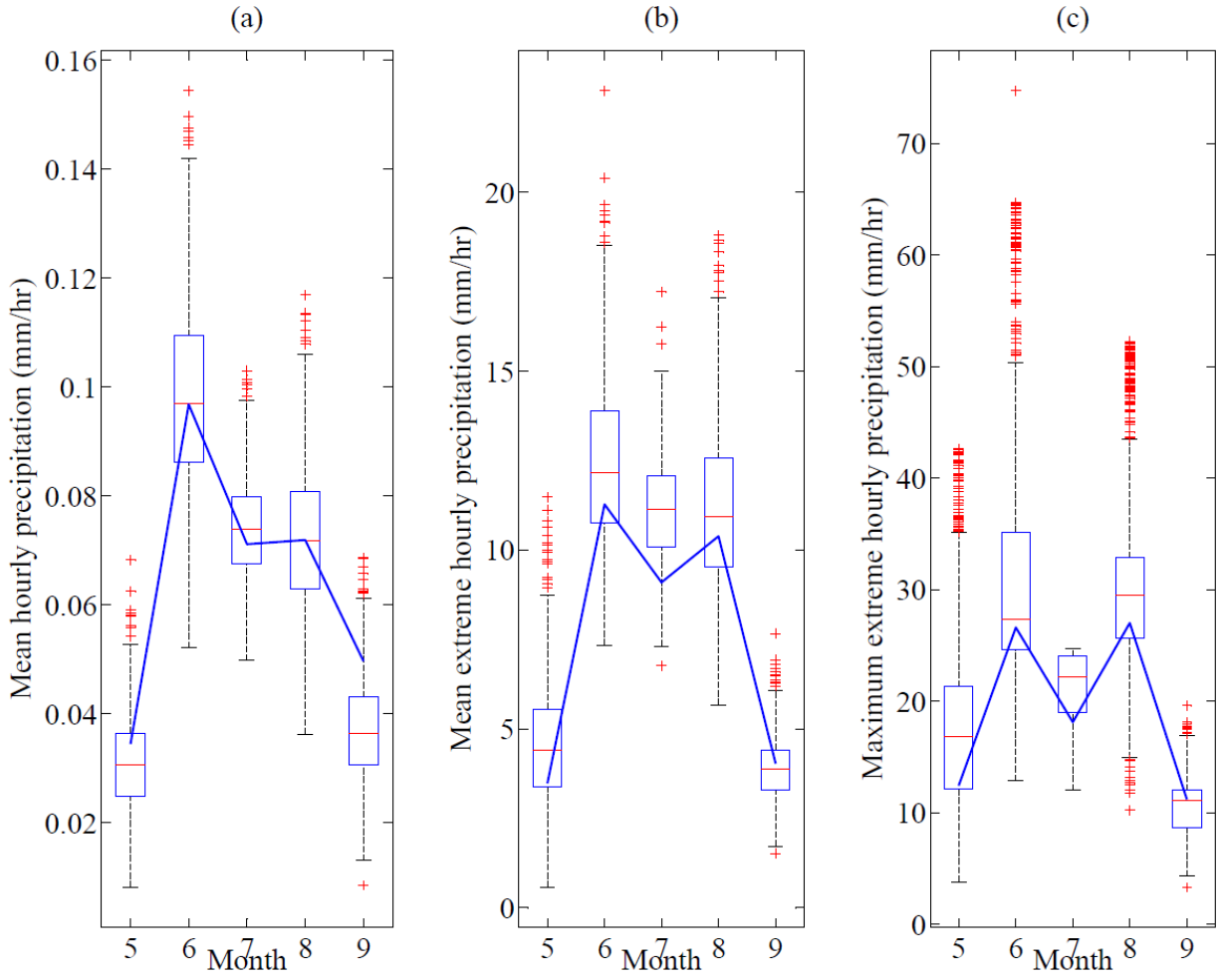

Figure 4.9: Performance of K-NN hourly disaggregation model based on the observed monthly properties (solid lines) and 1000 realizations of disaggregated (box plots) hourly precipitation time-series during 1992-2009.

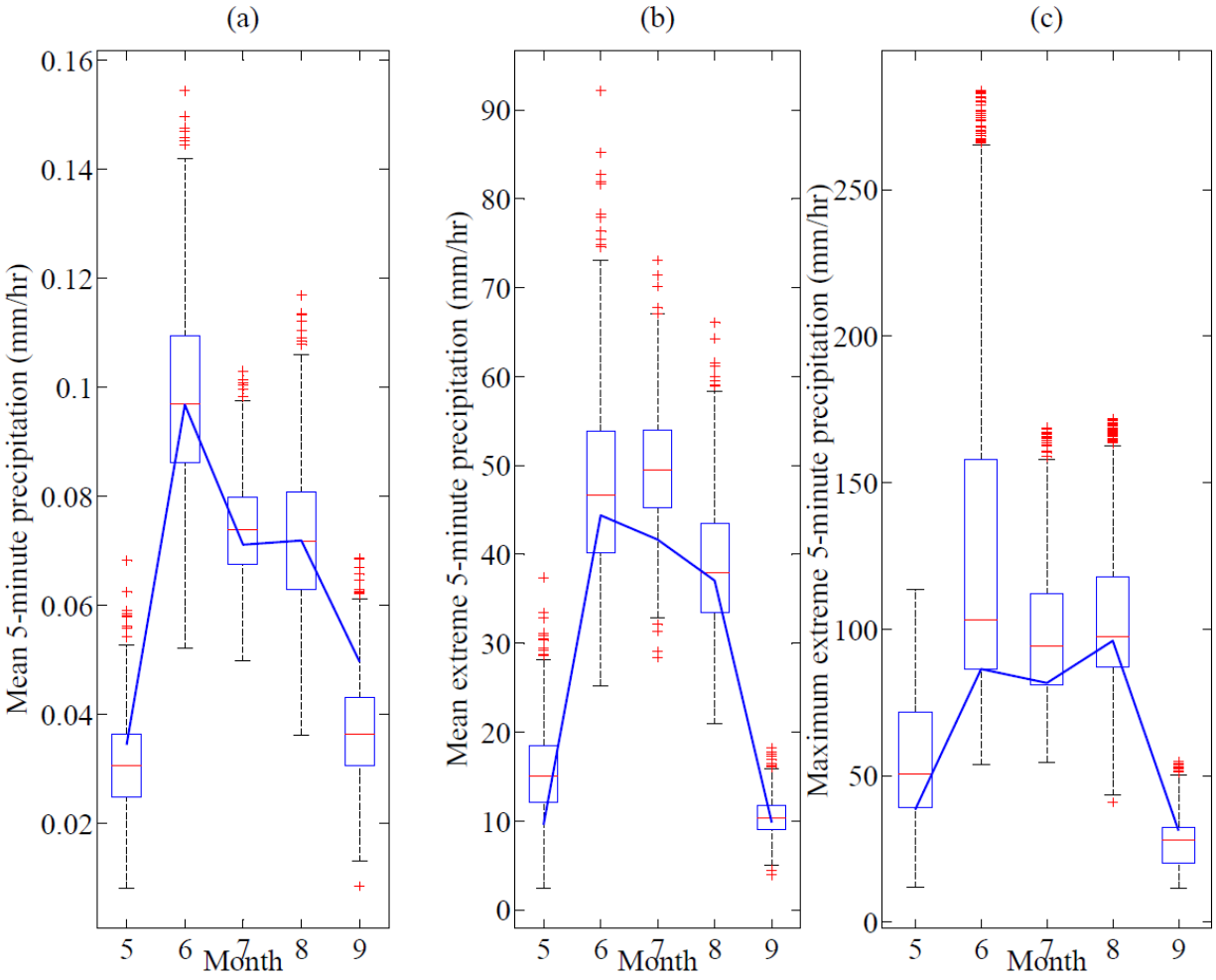

Figure 4.10: Performance of K-NN sub-hourly disaggregation model based on the observed monthly properties (solid lines) and 1000 realizations of disaggregated (box plots) sub-hourly (5-minute) precipitation time-series during 1992-2009.

After developing/calibrating the K-NN sub-hourly disaggregation model (Figure 4.10), the model was validated as shown in Figure 4.11. The K-NN sub-hourly disaggregation model was run using 1000 realizations of hourly precipitation obtained from the K-NN hourly disaggregation model during the baseline period (1961-1990) and the Saskatoon's observed 5-minute precipitation data during the period 1992-2009 (April-September) to obtain 1000 realizations of 5-minute precipitation during the baseline period. The simulated 5-minute precipitation was aggregated to obtain 1000 realizations of hourly precipitation series during the

baseline period. The performance of the validated model is shown in Figure 4.11 during the spring and summer months (April-September) of the baseline period.

Figure 4.11(a-c) shows that the hourly mean, mean extreme, and maximum extreme precipitation properties (obtained by aggregating 5-minute precipitation to an hourly time-scale) were reproduced well by the K-NN sub-hourly disaggregation model during the baseline period.

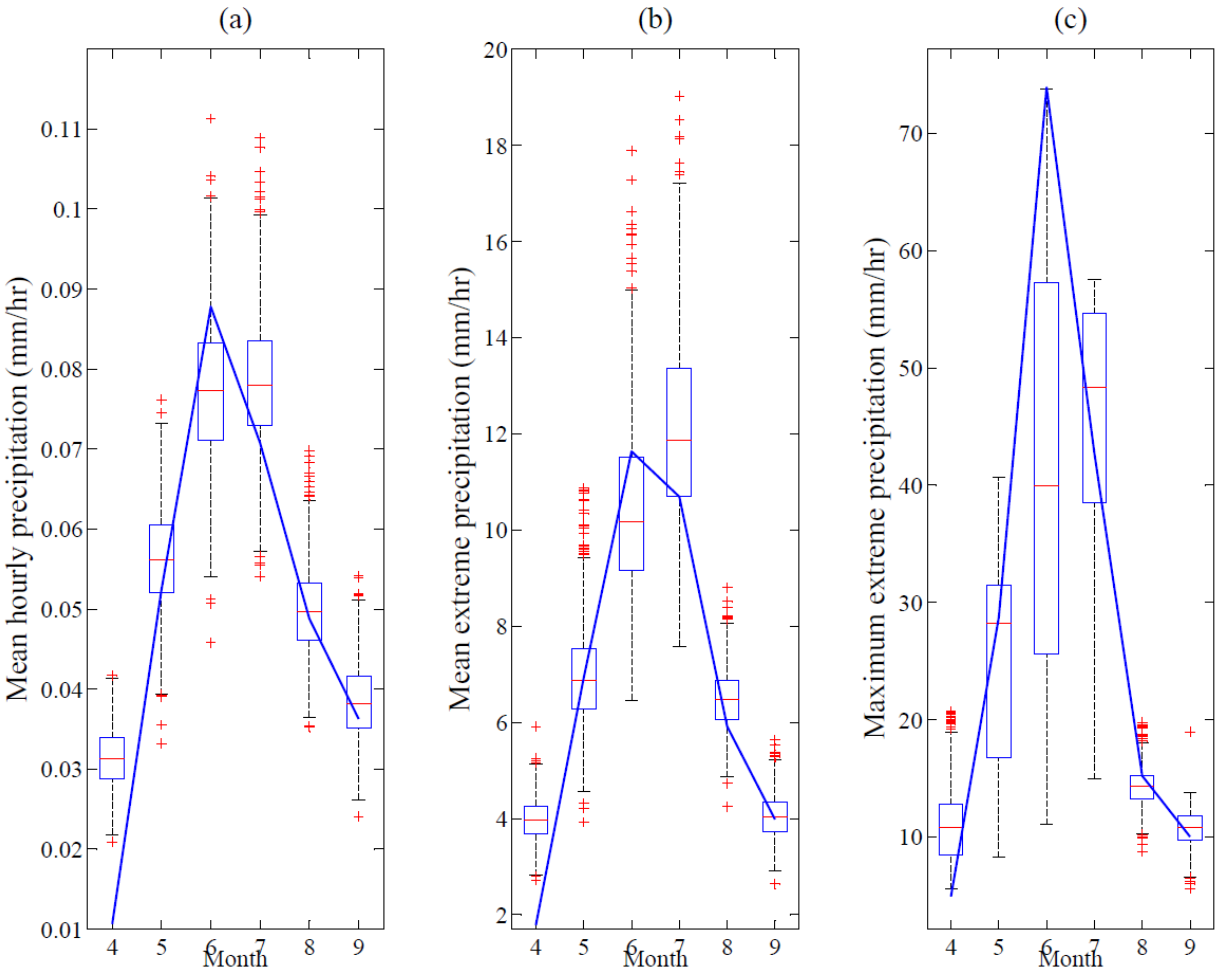

Figure 4.11: Performance of K-NN Sub-hourly Disaggregation Model based on the observed monthly properties (solid lines) of hourly precipitation time-series and 1000 realizations of disaggregated (box plots) 5-minute precipitation time-series (aggregated to produce hourly precipitation) during the baseline period (1961-1990).

The use of 5-minute precipitation distribution from a time period seems to be applicable in generating 5-minute precipitation distribution of other time periods. Hence, the 5-minute

precipitation distribution was used to generate future 5-minute precipitation distribution in order to create future IDF curves based on the performance of the K-NN hourly and sub-hourly disaggregation models.

4.4 Variations in the Future IDF Curves

4.4.1 Variations Obtained for CMIP5 Climate Models

Intensity-Duration-Frequency (IDF) curves for the City of Saskatoon were constructed using the GEV distribution for the baseline and the projection periods based on two GCMs (CanESM2 and HadGEM2-ES) and three RCPs (RCP2.6, RCP4.5, and RCP8.5) for nine selected durations (5-, 10-, 30-min, 1-, 2-, 3-, 6-, 18-, and 24-hour) and four different return periods (2-, 5-, 25-, and 100-year). The IDF curves for the 100-year return period are shown in Figure 4.12 (curves for all of the return periods are shown in Appendix E: Figures E.1, E.2, and E.3), and the design values (storms) during the baseline and projection periods are presented in Table 4.3 and Table 4.4, respectively. Design values for the two CMIP3 climate models (CGCM3.1 and HadCM3) are shown in Appendix F (Table F.1). The variations among the future precipitation quantiles, as represented by the IDF curves, are more significant at shorter durations and for longer return periods, which (the variations) seem to intensify toward the end of the 21st century. The significant variations in the quantiles emphasize the importance of disaggregation to fine temporal resolution; e.g., 5-minute precipitation as GCMs provide precipitation mostly in daily temporal scale. The sign and the magnitude of future variations in extreme precipitations at different durations and/or return periods are highly sensitive to the selection of GCMs and/or RCPs. The figures for CGCM3.1 and HadCM3 (CMIP3 climate models) based on A1B, A2, and B1 emission scenarios are shown in Appendix F (Figures F.4, F.5, F.6, and F.7).

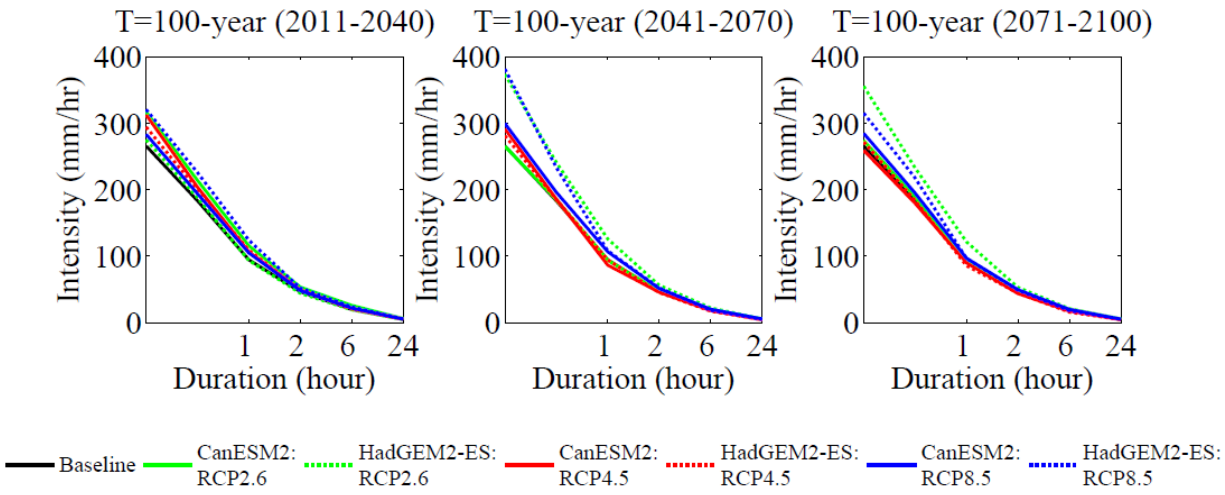

Figure 4.12: Variations in the future IDF curves for 100-year return period in the City of Saskatoon, according to CanESM2 and HadGEM2-ES based on three RCPs.

There are changes (increase/decrease) in future precipitation intensities compared to the baseline period (i.e., historical intensities) for all the return periods. The HadGEM2-ES: RCP8.5 IDF curve shows the greatest relative change (43.5%) in precipitation intensity for 5-minute duration and 100-year return period during 2041-2070, while CanESM2: RCP2.6 shows the greatest relative change (31.5%) in precipitation intensity for 6-hour duration and 100-year return period during 2011-2040. HadGEM2-ES: RCP4.5 shows the greatest relative decrease (20.8%) in precipitation intensity for 6-hour duration and 100-year return period during 2071-2100, while CanESM2: RCP4.5 shows the greatest relative decrease (15.6%) in precipitation intensity for 24-hour duration and 100-year return period during 2041-2070. The relative changes in precipitation intensities with respect to the historical intensities for the GCMs/RCPs is dependent on the duration, return period, and time periods during the 21st century.

The future IDF curves at sub-hourly (e.g., 5-minute and 15-minute) durations show increases in future precipitation intensities for most of the GCMs/RCPs during the 21st century with a maximum value of 43% (for HadGEM2-ES: RCP8.5 for 5-minute duration and 100-year

return period during 2041-2070) increase as compared to the historical intensities. The historical 5-minute precipitation intensity during the baseline period (1961-1990) for the 100-year return period in Saskatoon is 265 mm/hr (in Table 4.3), which is projected to increase to 320, 381, and 356 mm/hr (Table 4.4) according to the future IDF curves during 2011-2040, 2041-2070, and 2071-2100, respectively. The existing urban storm water collection systems are designed based on the historical IDF curves, so the projected increases in future sub-hourly precipitation intensities would make these urban systems more vulnerable in the future. However, the extent of the estimated vulnerability depends on the choice of GCMs/RCPs, return period, duration, and time slice.

Table 4.3: The precipitation intensity (mm/hr) during the baseline period (1961-1990) for selected return periods.

Duration	Return period (year)			
	2	5	25	100
5-min	57.2	87.2	159.6	265.5
15-min	36.5	57.2	107.6	183.1
1-hr	13.9	22.2	47.4	94.5
2-hr	9.2	14.0	26.5	46.3
6-hr	4.2	6.4	11.7	19.6
24-hr	1.4	2.1	3.4	4.9

Table 4.4: The expected precipitation intensity (mm/hr) for CanESM2 and HadGEM2-ES based on three RCPs obtained from CMIP5 during the 21st century for various return periods.

	(2011-2040)				(2041-2070)				(2071-2100)				(2011-2040)				(2041-2070)				(2071-2100)			
	Return period (year)																							
	2	5	25	100	2	5	25	100	2	5	25	100	2	5	25	100	2	5	25	100	2	5	25	100
	CanESM2: RCP2.6												HadGEM2-ES: RCP2.6											
5-min	59	92	178	317	57	87	160	265	56	87	162	274	56	87	162	275	61	97	199	373	61	97	194	356
15-min	37	60	119	214	37	57	108	185	36	57	109	189	35	56	108	189	39	64	130	241	39	64	128	233
1-hr	15	24	54	115	14	22	47	94	14	23	48	93	14	22	47	93	16	26	58	126	16	25	57	121
2-hr	10	15	29	53	9	14	27	47	10	15	27	46	9	14	26	44	11	16	32	56	11	16	31	53
6-hr	4	7	14	26	4	7	12	19	4	6	11	19	4	6	11	19	5	7	14	22	5	7	13	21
24-hr	1	2	4	6	1	2	3	5	1	2	3	5	2	2	3	4	2	2	4	5	2	2	4	5
	CanESM2: RCP4.5												HadGEM2-ES: RCP4.5											
5-min	59	91	177	312	57	89	170	291	56	86	156	259	58	91	172	294	57	89	166	281	55	86	161	272
15-min	37	59	116	204	36	57	109	186	36	56	105	179	37	59	114	199	37	58	109	185	35	56	106	184
1-hr	15	24	52	106	14	22	45	86	14	22	46	90	14	23	52	109	14	23	47	94	15	23	46	85
2-hr	10	15	28	49	9	14	27	46	9	14	26	44	10	15	28	49	10	15	27	45	10	15	27	44
6-hr	4	7	13	21	4	6	11	18	4	6	11	17	4	7	12	21	4	7	11	17	5	7	11	16
24-hr	2	2	4	5	2	2	3	4	1	2	3	4	1	2	4	5	2	2	3	4	2	2	3	4
	CanESM2: RCP8.5												HadGEM2-ES: RCP8.5											
5-min	56	87	165	283	58	90	171	299	56	87	165	285	59	93	180	320	60	97	202	381	55	88	175	315
15-min	36	57	111	194	37	59	113	196	35	56	110	195	38	61	123	226	39	63	128	233	35	58	117	218
1-hr	14	23	50	105	14	23	51	106	14	22	48	97	15	25	56	124	16	26	54	108	15	24	49	96
2-hr	9	14	27	48	10	15	29	51	9	14	28	49	10	15	30	52	11	17	31	52	10	15	29	49
6-hr	4	6	12	22	4	7	12	20	4	6	12	20	5	7	13	23	5	7	12	18	5	7	12	18
24-hr	1	2	3	5	2	2	4	5	1	2	3	5	2	2	4	5	2	3	4	5	2	2	4	5

4.4.2 Variations among the IDF Curves from the GP Method and the K-NN Hourly Disaggregation Model

The adopted downscaling/disaggregation (LARS-WG and K-NN) method and the GP method developed constructed future IDF curves using two GCMs and three RCPs for various return periods. As an example, a 2-year return period precipitation is shown in Figure 4.13. Plots for 100-year return period are shown in Appendix E: Figure E.4. Plots for CGCM3.1, based on various return periods, are shown in Appendix F (Figures F.8 and F.9). The IDF curves constructed using the two differing approaches produce similar historical IDF curves as shown in Table 4.5. The GP method seems to be more accurate for larger return periods (i.e. 100-year) and at shorter durations. For instance, the historical precipitation intensity of 1-hr duration and 100-year return period is 84.6 mm/hr, which was simulated as 88.4 mm/hr and 84.7 mm/hr by two sets of GP extracted equations (based on CanESM2 and HadGEM2-ES output during baseline period) while the same was simulated as 105.2 mm/hr by the K-NN hourly disaggregation model. Both GP methods reconstruct the historical IDF curves successfully during the baseline period (1961-1990) with less than 10% absolute error. Performance of GP extracted equations based on CGCM3.1 (CMIP3 climate model) are shown in Appendix F (Table F.3).

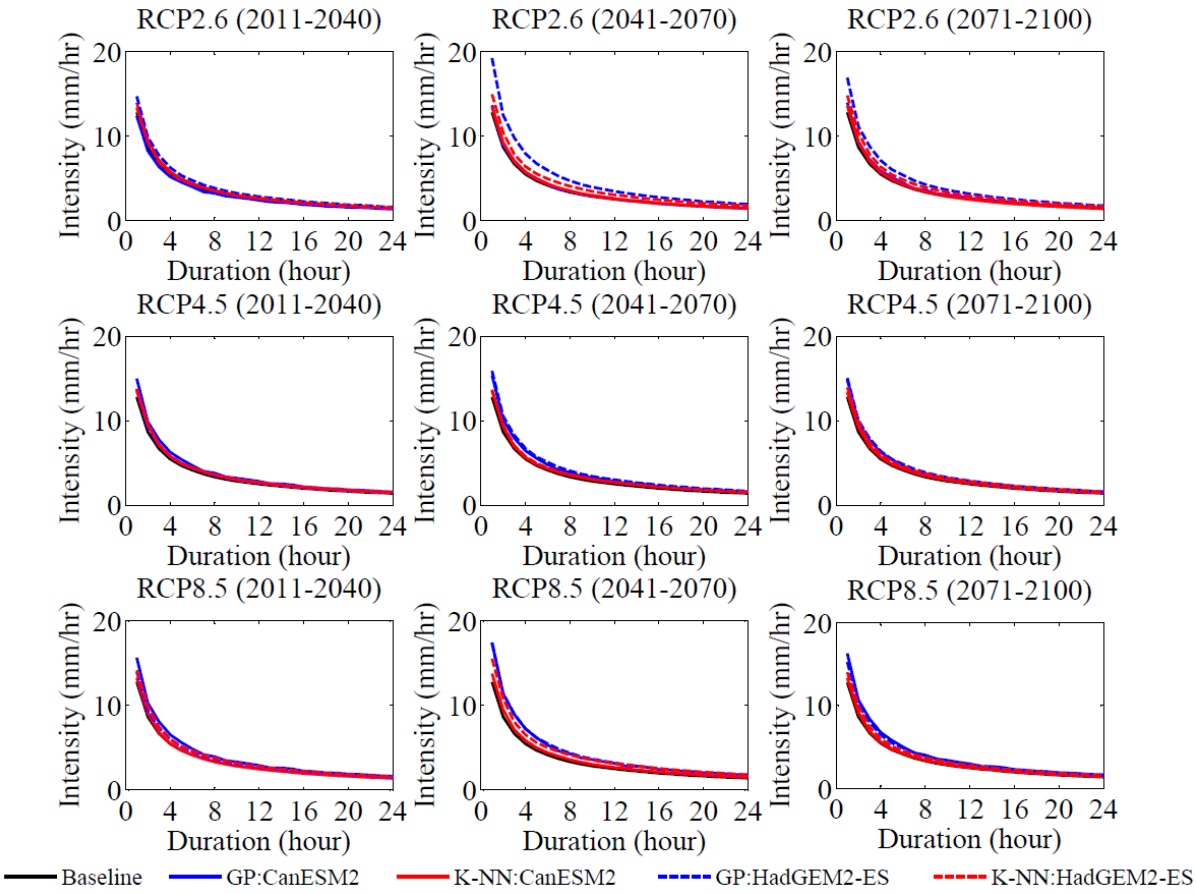

Figure 4.13: Comparison between the future IDF curves (2011-2100) according to CanESM2 (solid lines) and HadGEM2-ES (dashed lines) based on three RCPs and 2-year return period obtained using two different downscaling approaches, i.e. GP method and LARS-WG combined with K-NN Hourly Disaggregation Model.

Table 4.5: Comparison between the performance of K-NN hourly disaggregation model and GP method in simulating the expected precipitation intensity (mm/hr) during the baseline period (1961-1990) for various durations and return periods.

Duration	Return period (year)				Return period (year)			
	2	5	25	100	2	5	25	100
	Historical (observed) (1961-1990)				Simulated using K-NN Hourly Disaggregation Model (1961-1990)			
1-hr	12.8	21.0	44.9	84.6	13.2	21.5	48.6	105.2
2-hr	8.7	13.5	25.5	42.7	9.0	13.8	26.2	46.2
3-hr	6.7	10.4	18.7	29.3	6.8	10.4	20.2	36.8
4-hr	5.5	8.5	15.0	22.8	5.5	8.4	15.9	28.1
6-hr	4.2	6.3	10.3	14.7	4.2	6.3	11.7	19.7
12-hr	2.5	3.6	5.4	7.3	2.5	3.7	6.2	9.6
18-hr	1.8	2.5	3.9	5.3	1.8	2.6	4.4	6.5
24-hr	1.4	2.0	3.0	4.1	1.4	2.1	3.4	4.9
	Simulated using GP for CanESM2 (1961-1990)				Simulated using GP for HadGEM2-ES (1961-1990)			
1-hr	13.0	20.9	45.9	88.4	12.7	20.6	43.9	84.7
2-hr	8.6	13.3	25.0	41.7	8.7	13.2	25.6	43.5
3-hr	6.7	10.5	18.8	29.3	6.7	10.4	18.7	29.4
4-hr	5.4	8.4	14.9	22.9	5.5	8.4	14.9	23.0
6-hr	4.2	6.1	10.1	14.8	4.1	6.3	10.4	14.7
12-hr	2.5	3.5	5.3	7.1	2.5	3.6	5.5	7.2
18-hr	1.8	2.5	4.0	5.4	1.8	2.6	3.9	5.2
24-hr	1.4	2.0	3.1	4.1	1.4	2.0	3.1	4.2

The estimated changes in future precipitation intensities range from a minimum of -8.9% to a maximum of 81.7% using the GP Method, and from -0.6% to 75.6% using the K-NN hourly disaggregation model as shown in Table 4.6. The greatest precipitation intensity was 154 mm/hr from GP method for CanESM2: RCP4.5 of 1-hour duration and 100-year return period during 2071-2100, while the K-NN hourly disaggregation model shows the highest precipitation intensity of 126 mm/hr for CanESM2: RCP2.6 of 1-hour duration, and

100-year return period during 2011-2040. The simulated changes in the future precipitation intensities obtained from both methods depend on the selection of GCMs/RCPs, duration, return period, and time period. The results for HadGEM2-ES based on three RCPs, and for CGCM3.1 based on three AR4 emission scenarios, are shown in Appendix E (Table E.1) and Appendix F (Table F.4), respectively. The difference between the two methods in generating future precipitation intensities might be due to different approaches used for developing the disaggregation methodology, which contribute to the uncertainty in creating future IDF curves.

The IDF curves constructed using two different approaches (the GP-based method and the two-stage method adopted in this study) are similar. The AMP quantiles of the selected durations (1 to 24 hours) extracted from the K-NN and LARS-WG method are dependent on the downscaled daily precipitation series from the global to the local scale by LARS-WG. On the other hand, the performance of the GP method depends entirely on how perfectly the extreme precipitation quantiles at the global scale were mapped to the local scale by equations extracted from genetic programming (Hassanzadeh et al., 2014). So the differing approaches used in the two methods would contribute to quantifying the uncertainty in creating future (2011-2100) IDF curves, although the two methods reconstruct the historical IDF curves similarly during the baseline period (1961-1990). Using two sets of IDF curves that cover a wider range of risk (i.e., probability × cost) associated with the future designs of urban storm water collection systems under plausible climate change scenarios.

Table 4.6: Comparison between the K-NN hourly disaggregation model and the GP method in simulating the expected precipitation intensity (mm/hr) for CanESM2 based on three RCPs during the 21st century for various durations and return periods.

	GP Method												K-NN Hourly Disaggregation Model											
	(2011-2040)				(2041-2070)				(2071-2100)				(2011-2040)				(2041-2070)				(2071-2100)			
	Return period (year)												Return period (year)											
	2	5	25	100	2	5	25	100	2	5	25	100	2	5	25	100	2	5	25	100	2	5	25	100
CanESM2: RCP2.6																								
1-hr	12	18	34	60	14	22	46	82	14	23	43	67	14	23	55	126	13	22	48	103	14	22	49	101
2-hr	8	12	20	31	9	14	25	39	9	14	24	34	10	15	29	52	9	14	27	47	9	14	27	46
3-hr	6	9	15	23	7	11	19	28	7	11	18	24	7	11	23	44	7	11	20	36	7	11	20	36
4-hr	5	7	12	18	6	9	15	22	6	9	14	19	6	9	18	35	6	9	16	27	6	9	16	28
6-hr	4	5	8	12	4	6	10	14	4	6	10	13	4	7	14	26	4	6	12	19	4	6	11	19
12-hr	2	3	5	6	3	4	5	7	3	4	5	6	3	4	7	12	3	4	6	9	2	4	6	10
18-hr	2	2	3	5	2	3	4	5	2	3	4	5	2	3	5	8	2	3	4	7	2	3	4	7
24-hr	1	2	3	3	1	2	3	4	1	2	3	4	1	2	4	6	1	2	3	5	1	2	3	5
CanESM2: RCP4.5																								
1-hr	15	24	48	81	15	25	50	83	15	26	70	154	14	23	54	122	14	22	46	93	13	21	47	99
2-hr	10	15	26	39	10	15	26	40	10	16	35	66	10	15	28	49	9	14	26	45	9	14	26	44
3-hr	8	12	20	28	8	12	20	28	8	13	25	43	7	11	22	39	7	11	20	36	7	10	19	35
4-hr	6	9	15	22	6	10	16	22	6	10	20	33	6	9	17	31	6	8	16	27	6	8	15	25
6-hr	5	7	10	14	5	7	11	14	5	7	13	20	4	7	13	21	4	6	11	18	4	6	11	17
12-hr	3	4	5	7	3	4	5	7	3	4	6	9	3	4	7	10	3	4	6	8	3	4	6	8
18-hr	2	3	4	5	2	3	4	5	2	3	5	6	2	3	5	7	2	3	4	5	2	3	4	6
24-hr	2	2	3	4	2	2	3	4	2	2	4	5	2	2	4	5	2	2	3	4	1	2	3	4

Table 4.6 continued

	GP Method												K-NN Hourly Disaggregation Model											
	(2011-2040)				(2041-2070)				(2071-2100)				(2011-2040)				(2041-2070)				(2071-2100)			
	Return period (year)												Return period (year)											
	2	5	25	100	2	5	25	100	2	5	25	100	2	5	25	100	2	5	25	100	2	5	25	100
CanESM2: RCP8.5																								
1-hr	16	23	37	50	17	28	59	105	16	25	49	84	13	22	51	120	14	22	52	115	13	22	49	105
2-hr	10	15	21	27	11	17	30	48	11	16	26	40	9	14	26	47	10	15	29	52	9	14	27	50
3-hr	8	11	16	20	9	13	22	33	8	12	20	28	7	11	21	39	7	11	22	40	7	11	21	40
4-hr	7	9	13	16	7	11	18	26	7	10	16	22	5	8	17	30	6	9	17	30	6	9	17	30
6-hr	5	7	9	11	5	7	12	16	5	7	11	14	4	6	12	22	4	7	12	20	4	6	12	20
12-hr	3	4	5	5	3	4	6	8	3	4	5	7	2	4	7	10	3	4	7	10	3	4	6	10
18-hr	2	3	4	4	2	3	5	6	2	3	4	5	2	3	4	7	2	3	5	7	2	3	4	7
24-hr	2	2	3	3	2	2	3	4	2	2	3	4	1	2	3	5	2	2	4	5	1	2	3	5

4.5 Uncertainties in Constructing IDF Curves

4.5.1 Uncertainty due to Natural Weather Variability

The two-stage modeling scheme (downscaling-disaggregation) can be used to estimate various sources of uncertainty contributing to the projections of extreme precipitation quantiles represented by the IDF curves. One advantage of stochastic weather generators (e.g., LARS-WG) is their ability to generate multiple realizations of a variable such as precipitation. Such realizations can be considered representations of possible sequences of precipitation at the same location to represent the natural internal variability (caused due to the stochastic nature) of precipitation. The effects of such variability (uncertainty) on the IDF curves were quantified using AMP quantiles extracted from each of the 1000 realizations of daily precipitation obtained from LARS-WG during the baseline period for the selected return periods (2-, 5-, 25-, and 100-year) using the GEV distribution. The simulated AMP quantiles for various return periods were obtained by fitting GEV distribution to AMPs corresponding to the 1000 simulated realizations of daily precipitation, each realization having 30 years of daily precipitation. The mean of the AMP quantiles corresponding to the 1000 realizations represents the expected intensity, while 97.5^{th} and 2.5^{th} percentiles represent the upper and lower bounds of 95% confidence interval.

The values of the three parameters of GEV distribution with three values was used to obtain the expected intensity, upper, and lower bounds of the 95% confidence interval. Figure 4.11 shows the expected values and the 95% confidence intervals obtained from LARS-WG simulations, as compared to the corresponding theoretical quantiles derived for the observed daily AMPs. The simulated expected values overestimate the theoretical expected quantiles, while the simulated confidence intervals underestimate the theoretical 95% bounds, particularly at larger return periods. One observation is worth noting in Figure 4.14: the 95% confidence

intervals of the 1000 realizations simulated by LARS-WG slightly underestimate the historical confidence intervals of the GEV distribution. Therefore, such variability around projected future IDF curves should not be attributed to uncertainty due to climate change.

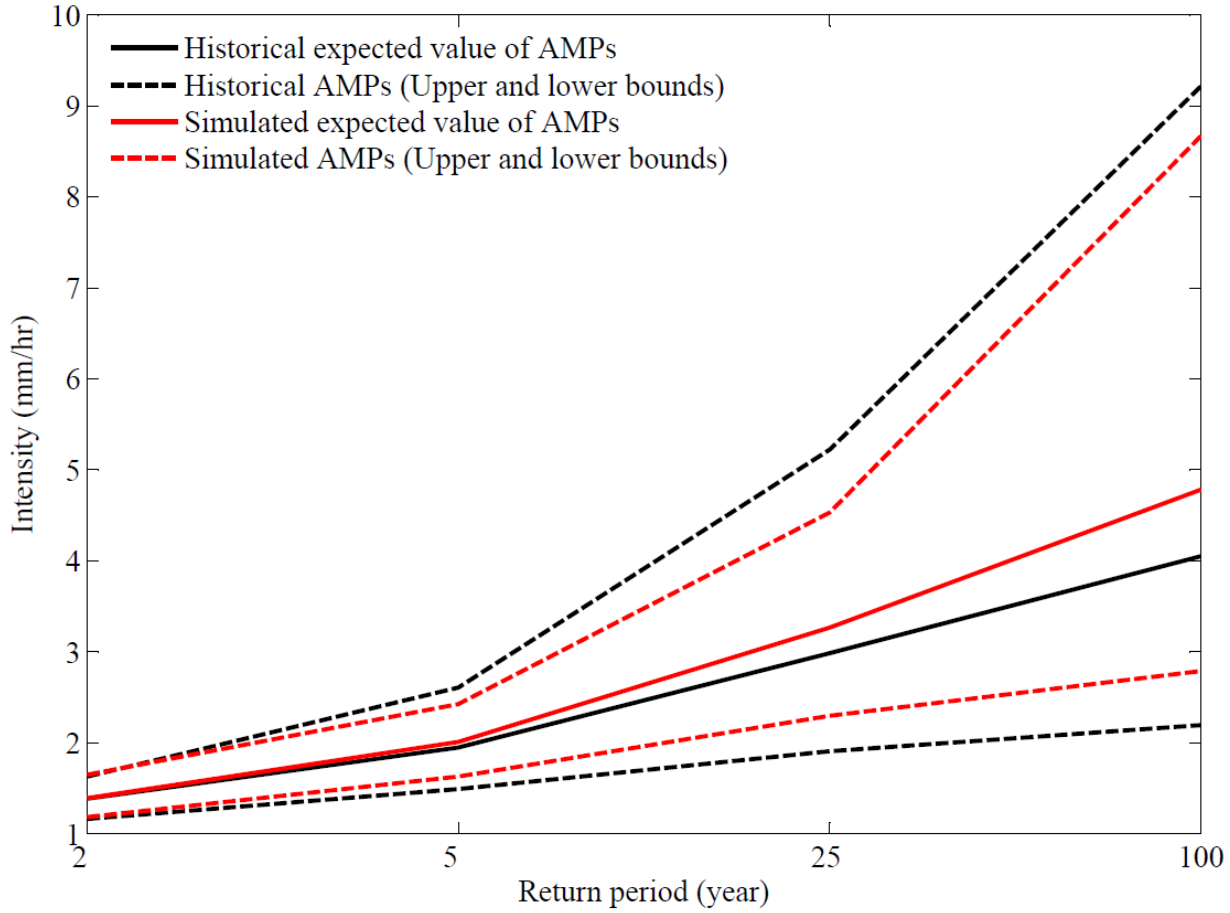

Figure 4.14: Theoretical GEV estimation of extreme quantiles based on the historical AMPs (black) and simulated AMPs obtained from 1000 realizations of daily precipitation time series during the baseline period using LARS-WG (red) with the corresponding 95% confidence intervals (dashed lines).

4.5.2 Uncertainty due to Natural Variability and Disaggregation Models

The K-NN hourly disaggregation model was run using 1000 realizations of daily precipitation values from LARS-WG to create 1000 realizations of hourly precipitation sequences during the baseline period. The simulated hourly AMP values were extracted from the

disaggregated series and GEV distributions were fitted to them. The mean and the 95% upper and lower bounds of 1000 realizations were obtained as discussed previously. Figure 4.15 plots the simulated hourly AMP quantiles (expected value and 95% confidence intervals) and the corresponding historical hourly quantiles. Similar to the daily values, the simulated expected values slightly overestimate the historical expected quantiles, while the simulated confidence intervals slightly underestimate the theoretical 95% bounds, particularly in larger return periods, with some exceptions (3-, 6-, 8-, and 12-hour durations).

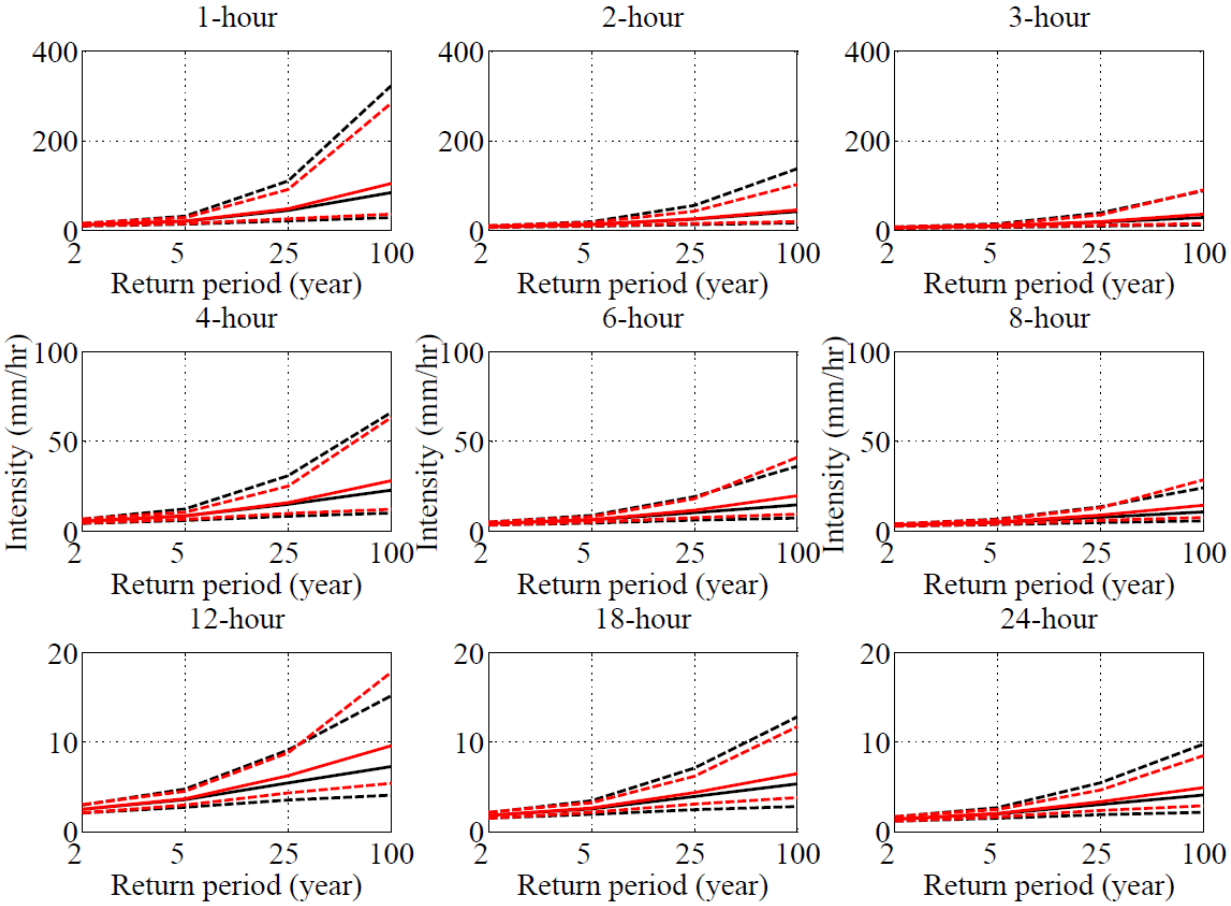

Figure 4.15: The IDF curves based on historical AMPs (black) as compared to the simulated values obtained from 1000 realizations of baseline time series from K-NN hourly disaggregation model and LARS-WG (red) with corresponding 95% confidence intervals (dashed lines).

The K-NN sub-hourly disaggregation model was run using 1000 realizations of hourly precipitation from the LARS-WG and K-NN hourly disaggregation model to create 1000 realizations of 5-minute precipitation sequences during the baseline period (1961-1990). The observed hourly precipitation was also used by the K-NN sub-hourly disaggregation model to generate 5-minute precipitation during the same baseline period (1961-1990), which was used to estimate the historical 5-minute quantiles. A similar process, mentioned above for the hourly precipitation quantiles, was repeated with the 30 years of 5-minute precipitation series, both for the simulated 1000 realizations and the observed precipitation. Figure 4.16 plots the simulated sub-hourly AMP quantiles and the corresponding sub-hourly quantiles for the gauged precipitation. The simulated expected values and the upper bounds underestimate the gauged precipitation expected quantiles and their upper bounds for almost all durations and return periods. However, the lower bounds of the simulated confidence intervals systematically overestimate the 95% lower bounds of the gauged precipitation for short durations and long return periods, while the lower bounds systematically underestimate the theoretical lower bounds in the larger durations. The underestimation of the expected values diminishes as the storm durations increase.

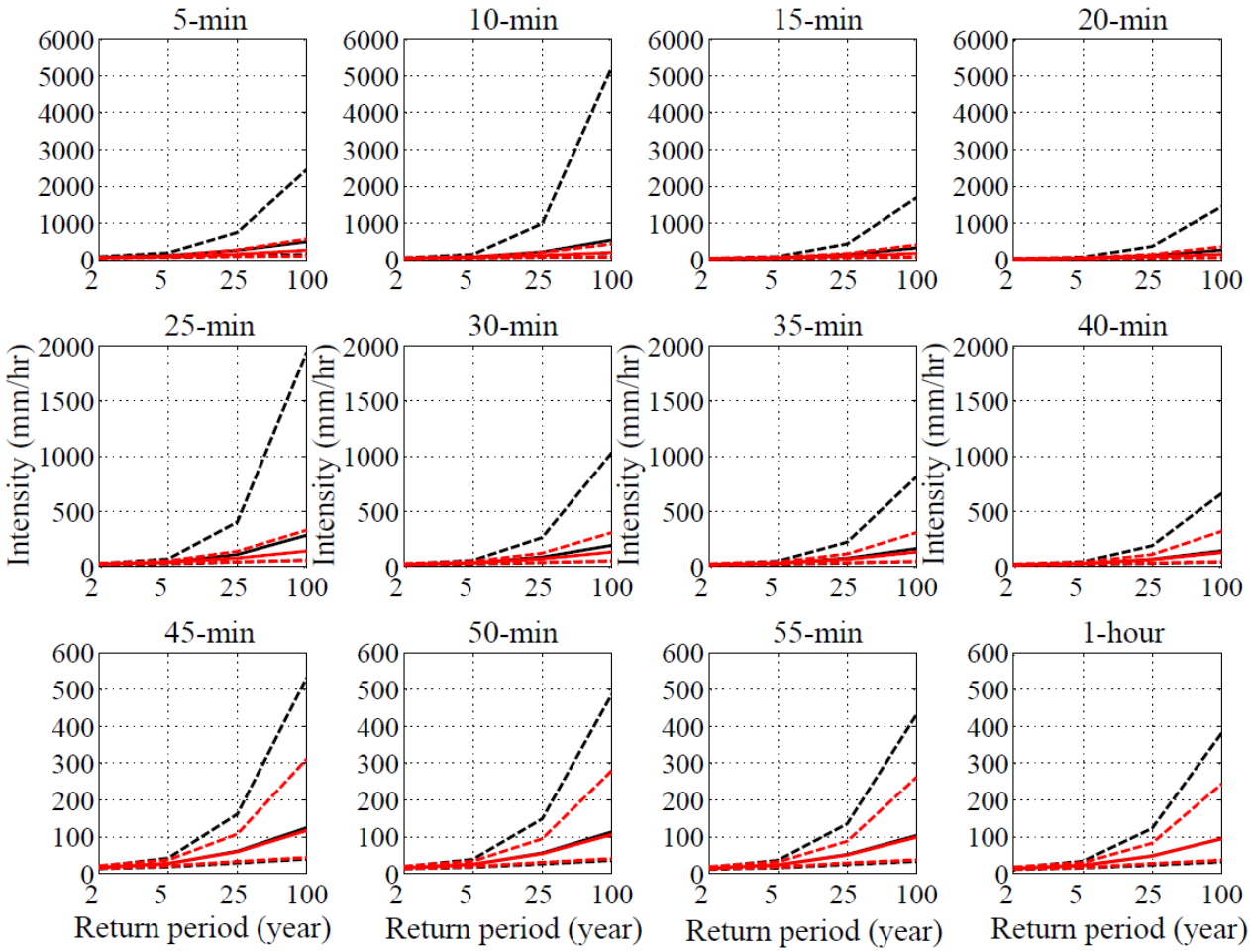

Figure 4.16: The sub-hourly IDF curves based on observed AMPs (black) as compared to the simulated values obtained from 1000 realizations of baseline time series from K-NN hourly and sub-hourly disaggregation models and LARS-WG (red) with corresponding 95% confidence intervals (dashed lines).

It is important to verify the results obtained from each downscaling method before using it to reduce the associated risks. In this study, the results of the adopted two-stage downscaling-disaggregation method using LARS-WG and K-NN were compared with results obtained from a published method based on GP. Comparing the results of GP and K-NN is considered a way to quantify uncertainty/variability due to disaggregation from daily to hourly precipitation. Hence, the expected hourly precipitation quantiles corresponding to 1000 realizations from the LARS-WG and K-NN hourly disaggregation model, and the expected hourly precipitation quantiles

from the GP method of a 2-year return period for CanESM2 (based on three RCPs during 2011-2040, 2041-2070, and 2071-2100) are compared in Figure 4.17. The results for a 100-year return period and HadGEM2-ES are provided in Appendix E (Figures E.5, E.6, and E.7). The internal variability of precipitation represented by 1000 realizations can be better explained by the box plots in Figure 4.17; the values within the whiskers of the box plots seem to contain the simulations of the GP method for almost all cases. This would provide more confidence in using the simulations from the adopted method of this study, as these are comparable to the results of the GP method. Similar results for the CMIP3 climate model (CGCM3.1) are shown in Appendix F (Figures F.10 and F.11).

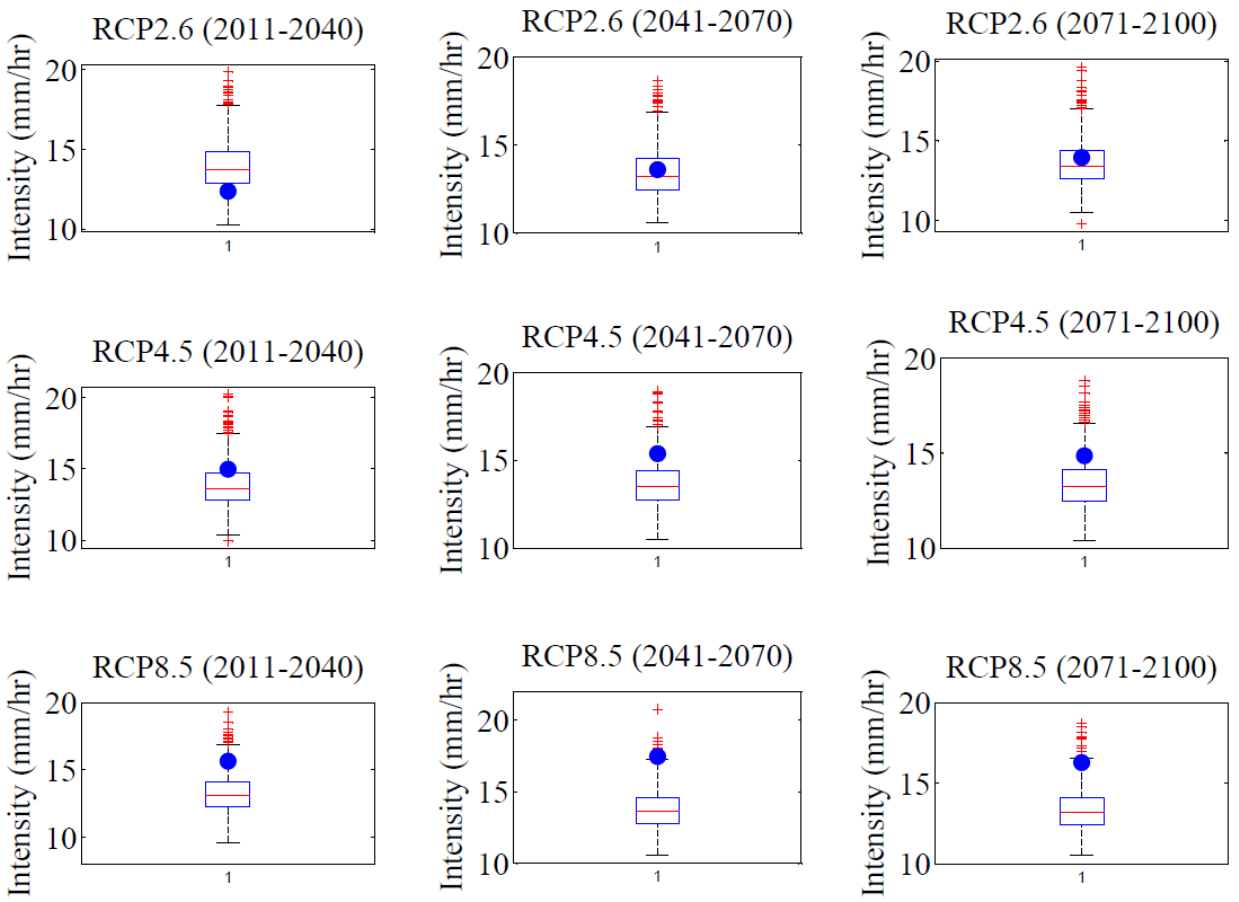

Figure 4.17: Expected 1-hr AMP corresponding to 1000 realizations from LARS-WG and K-NN hourly disaggregation model (boxplot), and the same from GP method (blue dots) of 2-year return period for CanESM2 based on three RCPs during the 21st century.

4.5.3 Uncertainty in the Projections of Future IDF Curves

The K-NN sub-hourly disaggregation model was run using 1000 realizations of hourly precipitation from LARS-WG and the K-NN hourly disaggregation model to create 1000 realizations of 5-minute precipitation sequences during the projection periods (2011-2040, 2041-2070, and 2071-2100) according to two GCMs (CanESM2 and HadGEM2-ES) and three RCPs. The simulated AMP quantiles were extracted from the disaggregated sub-hourly precipitation series related to selected return periods using the GEV distribution as explained earlier. Figure 4.18 plots the simulated sub-hourly AMP quantiles for both GCMs and three RCPs and the

corresponding quantiles obtained from the GEV distribution fitted to the observed (historical) AMPs for a 2-year return period. The graphs for other return periods and longer durations are plotted in Appendix E (Figures E.8 to E.14). The graphs for CMIP3 climate models (CGCM3.1 and HadCM3) are shown in Appendix F (Figures F.12 to F.19). In general, the uncertainty in the projections of future extreme precipitation quantiles increases for short durations and long return periods. The projections are highly sensitive to the choice of GCMs and/or RCPs, and include uncertainty in projecting both the sign and the magnitude of future variations (relative change) in extreme precipitation quantiles at different durations and/or return periods.

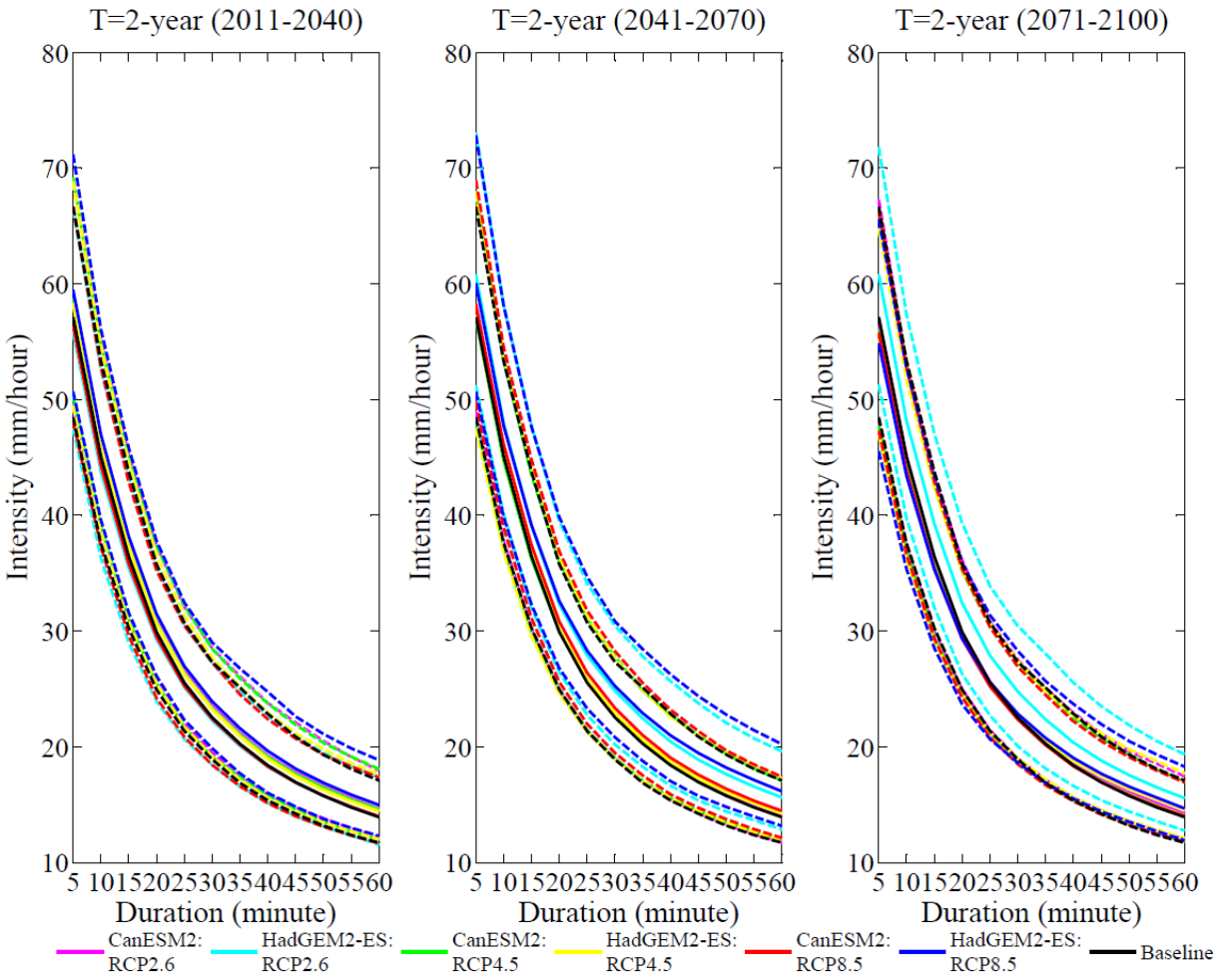

Figure 4.18: Uncertainty in the projections of future extreme precipitation quantiles for 2-year return period based on two GCMs and three RCPs obtained from CMIP5 and quantified by using GEV shown as 95% confidence intervals (dashed lines) with expected quantiles (solid lines).

4.5.4 Uncertainty due to GEV Fitting and Extrapolation

The K-NN sub-hourly disaggregation model was run using 1000 realizations of hourly precipitation from LARS-WG and the K-NN hourly disaggregation model to create 1000 realizations of 5-minute precipitation sequences during the projection period of 90 years (2011-2100) according to two GCMs (CanESM2 and HadGEM2-ES) and three RCPs. The simulated AMP quantiles were extracted from the disaggregated sub-hourly precipitation series related to various return periods using the GEV distribution as explained previously. Figure 4.19 plots the

expected values and 95% confidence intervals of the sub-hourly AMP quantiles for both GCMs, based on three RCPs obtained by fitting the GEV distribution to the future AMPs of 90 years (2011-2100) and the baseline sub-hourly AMP quantiles obtained by fitting the GEV distribution to the observed AMPs of 30 years (1961-1990) for 2-, 5-, 25-, and 100-year return periods. The graphs for CMIP3 climate models (CGCM3.1 and HadCM3) are shown in Appendix F (Figure F.20).

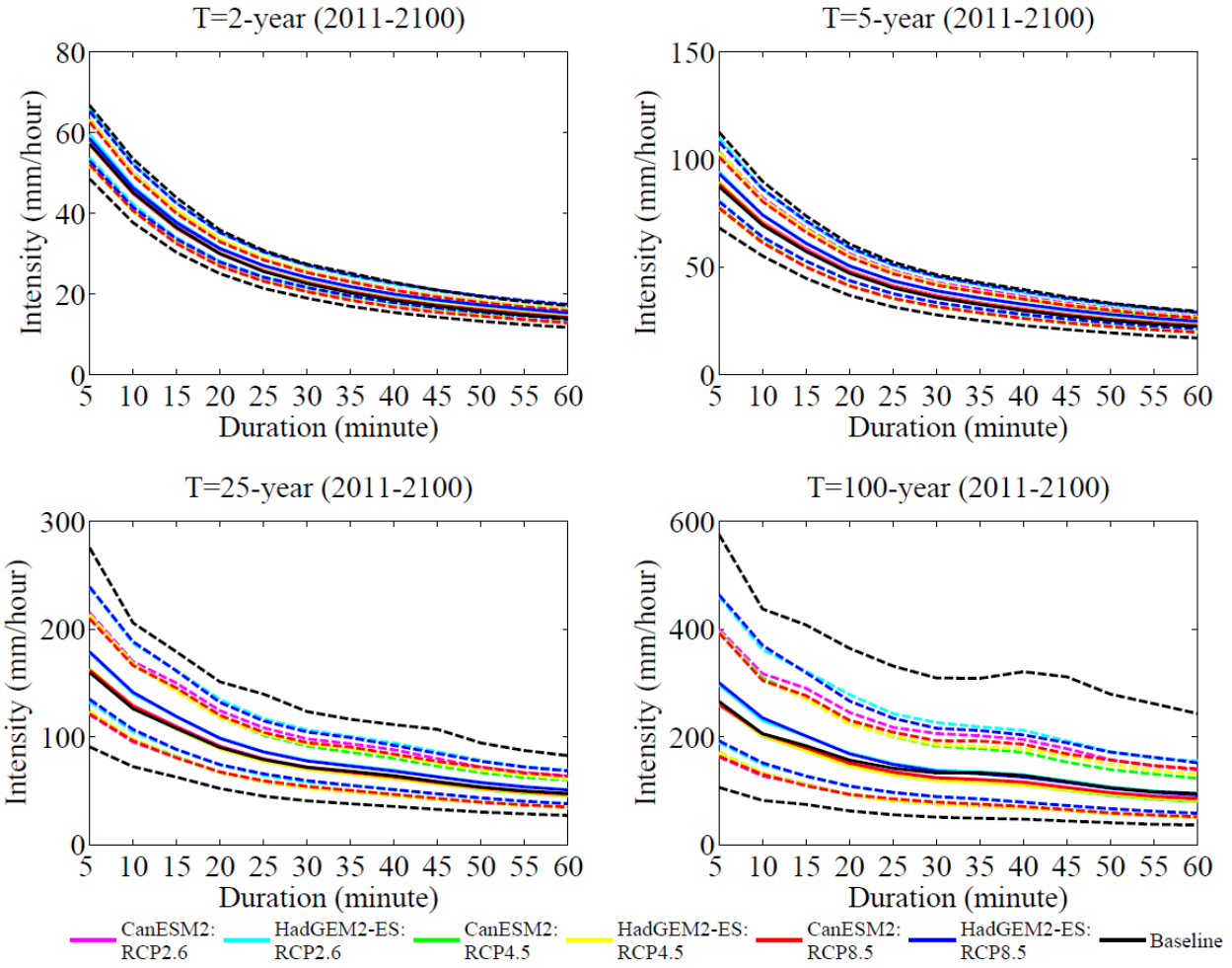

Figure 4.19: Uncertainty in the projections of future extreme precipitation quantiles for 2-, 5-, 25- and 100-year return periods based on two GCMs and three emission scenarios obtained from CMIP5 and quantified by using GEV shown as 95% confidence intervals (dashed lines) using 90 years of data (2011-2100) with expected quantiles (solid lines).

The uncertainty (represented by the 95% confidence intervals) in the projections of future extreme precipitation quantiles decreases when the GEV distribution is fitted to 90 years of AMP data, compared to the GEV fitted to 30 years of AMP data. This demonstrates the uncertainty due to the GEV fitting and extrapolation of the tail of the distribution beyond the available AMP data.

4.6 Discussion

It is found in this study that there are changes in future fine-resolution precipitation intensities compared to the precipitation intensities during the baseline period (i.e., historical intensities) for all return periods. The expected precipitation quantiles are compared and HadGEM2-ES: RCP8.5 shows the greatest relative change (43%) in precipitation intensity for 5-minute duration and 100-year return period during 2041-2070, while CanESM2: RCP2.6 shows the greatest relative change (25%) in precipitation intensity for 45-minute duration and 100-year return period during 2011-2040. HadGEM2-ES: RCP4.5 shows the biggest relative decrease (11%) in precipitation intensity for 35-minute duration and 100-year return period during 2071-2100, while CanESM2: RCP4.5 shows the greatest relative decrease (9%) in precipitation intensity for 35-minute duration and 100-year return period during 2071-2100.

The relative changes in precipitation intensity with respect to the historical intensities and the uncertainty bounds in the projections of future IDF curves for the GCMs/RCPs are dependent on the duration, return period, and time periods (2011-2040, 2041-2070, and 2071-2100). These dependencies may be important to consider when selecting the design values of storms for the design of urban storm water collection systems in the City of Saskatoon. Table 4.7 provides an overall summary of possible changes in design values of precipitation intensities in Saskatoon due to climate change. The projected increase in future precipitation intensities is greater at

shorter durations and longer return periods. Short duration storms are of significance to minor systems (e.g., street drainage inlets and storm sewers) and storms of longer return periods are of significance to major systems (e.g., storm detention ponds) (City of Saskatoon, 2012). A similar overall summary of possible changes in design values obtained for CMIP3 climate models (CGCM3.1 and HadCM3) is shown in Appendix F (Table F.5).

Table 4.7: Historical and projected precipitation intensities for selected durations and return periods of storms in Saskatoon. Base means historical values, Min means the lowest of future projection, and Max is the highest value of future projections. The **bold** values represent the greatest projected change.

Duration	Intensity (mm/hr)											
	2-year			5-year			25-year			100-year		
	Base	Min	Max	Base	Min	Max	Base	Min	Max	Base	Min	Max
5-min	57	56	61	87	86	97	160	156	**202**	265	259	**381**
15-min	37	35	39	57	56	64	108	105	130	183	179	**241**
1-hour	14	14	16	22	22	26	47	45	**58**	94	85	**126**
2-hour	9	9	11	14	14	17	27	26	32	46	44	**56**
6-hour	4	4	5	6	6	7	11	11	**14**	19	16	**26**
24-hour	1	1	**2**	2	2	**3**	3	3	**4**	5	4	**6**

CHAPTER 5: SUMMARY AND CONCLUSIONS

5. Overview

This chapter provides a summary of the modeling and analysis conducted in this study for constructing the Intensity-Duration-Frequency (IDF) curves in the city of Saskatoon under possible climate change. Subsequently, conclusions from the results and findings are presented, followed by an outline of the contributions and limitations of this study, and finally, recommendations for future work.

5.1 Summary of the Study

The research presented in this thesis followed a two-stage method for downscaling precipitation from a global scale to the local scale, which is the city of Saskatoon, Canada, and for disaggregating precipitation from daily, to hourly, and subsequently to sub-hourly time scales. In the first stage, a stochastic weather generator (i.e., LARS-WG) utilized the observed precipitation in Saskatoon and precipitation output from GCMs (CanESM2 and HadGEM2-ES) to generate local scale daily precipitation during the baseline period (1961-1990), as well as under projected climate change scenarios up to year 2100. In the second stage, K-nearest neighbor (K-NN)-based hourly and sub-hourly disaggregation models were developed and used to create continuous records of hourly and 5-minute precipitation series, respectively. The annual maximum precipitation (AMPs) of the disaggregated continuous records of hourly and 5-minute precipitation were used to construct the IDF curves during the baseline and the projection periods for different durations (i.e., 5-minute to 24-hour) and return periods (i.e., 2-, 5-, 25-, and 100-year). A comparison was made between the IDF curves constructed based on the K-NN hourly disaggregation model and those from the genetic programing (GP)-based downscaling method. Uncertainties due to the natural internal variability of precipitation, the downscaling methods (K-

NN hourly disaggregation model and GP-based downscaling method), two GCMs, and three Representative Concentration Pathways (RCPs) were quantified in this study.

5.1.1 Downscaling of Precipitation

LARS-WG was used to generate 1000 realizations of daily precipitation at the local scale in Saskatoon. The performance of the weather generator was evaluated based on the 1000 realizations of synthetic precipitation time series comparing to the observed data during the baseline period (1961-1990). A set of parameters of probability distributions of the observed precipitation for the given site was computed in LARS-WG; then 1000 synthetic precipitation time series of arbitrary length (30 years) were generated using the computed set of parameters by randomly sampling values from the probability distributions. Relative change factors (RCFs) were used in LARS-WG for each month to incorporate possible changes in the future daily precipitation scenarios. RCFs were calculated based on the GCMs' output at the coarse-grid resolution.

Mean wet and dry spell lengths for each month were also calculated during the baseline and projected to the future period. Monthly ratios of the average wet and dry spell lengths during the future period divided by those of the baseline period are the RCFs related to wet and dry spell lengths. The 1000 realizations of future daily precipitation time series for two GCMs (CanESM2 and HadGEM2-ES) and the corresponding three RCPs (RCP2.6, RCP4.5, and RCP8.5) using two sets of relative change factors (i.e., with and without wet/dry spell effects) were used to differentiate between the contributions of changes in mean monthly precipitation amounts and the changes in wet/dry spell lengths. The constructed probability distributions were updated using the RCFs and perturbed to generate 1000 realizations of future daily precipitation series in

Saskatoon. The LARS-WG was used as a "downscaling" method to produce future projections by employing RCFs to quantify the shift in precipitation from the baseline to the future period.

The annual maximum precipitation (AMPs) for the realizations of future daily precipitation projections, from the simulations using two GCMs both with and without consideration of wet/dry spell lengths, were used to estimate the expected values and 95% confidence intervals in comparison with the observed AMPs during the baseline period. The Generalized Extreme Value (GEV) distribution was used to fit probability distributions to the AMPs. The AMP quantiles of 1000 realizations of daily precipitation obtained from LARS-WG, based on the GCMs/RCPs using two sets of RCFs, were compared for selected return periods.

5.1.2 Disaggregation of Precipitation using K-NN Method

A method based on the K-nearest neighbor (K-NN) technique, originally developed by Sharif and Burn (2007), was used, with some modifications, for the disaggregation of precipitation from daily, to hourly, and to sub-hourly time scales for both the baseline and future precipitation. To develop an appropriate hourly disaggregation model, the optimal window size (i.e., the number of nearest neighbors to the current day of disaggregation) was searched and identified using the observed daily and hourly precipitation data during the baseline period (1961-1990). The performance of 30 window sizes was evaluated based on simulated AMPs of various durations (1- to 24-hour) which are compared to the corresponding observed AMPs. The window size that provided the lowest RMSE was considered to be the optimal.

An optimal window size for the sub-hourly disaggregation model was also selected in this study from a total of 120 different window sizes (3 hours to 241 hours), using the observed hourly and 5-minute precipitation data during 1992-2009 from the Acadia Reservoir rain gauge

in Saskatoon. The sub-hourly precipitation was aggregated to obtain hourly precipitation to conduct this part of the study.

The K-NN hourly disaggregation model was run using 1000 realizations of daily precipitation, obtained from LARS-WG, during the baseline period and also using the observed hourly precipitation data. The simulations produced 1000 realizations of hourly precipitation during the baseline period using the optimal window. The performance of the hourly disaggregation model was evaluated during the spring and summer months (April-September) only. The K-NN hourly disaggregation model was able to simulate properties (i.e., mean, mean of maximum, and maximum extreme) of the observed monthly precipitation quite well. The calibrated hourly disaggregation model was then used to disaggregate 1000 realizations of future daily precipitation into hourly precipitation for the future periods. Similarly, the K-NN sub-hourly disaggregation model was run using 1000 realizations of hourly precipitation during the baseline period, from LARS-WG, and the observed sub-hourly precipitation data; this resulted in obtaining 1000 realizations of sub-hourly precipitation during the baseline period (1992-2009) using the selected optimal window size. The performance of the sub-hourly disaggregation model was evaluated during the spring and summer months (May-September) only. The K-NN sub-hourly disaggregation model was able to simulate the observed monthly precipitation properties (i.e., mean, mean of maximum, and maximum extreme) at the Acadia Reservoir rain gauge quite well. The calibrated sub-hourly disaggregation model was then used to disaggregate 1000 realizations of future hourly precipitation into 1000 realizations of 5-minute precipitation for the future periods. Finally, the disaggregated hourly and sub-hourly precipitation time series were used to construct IDF curves during the baseline period and under the projections of climate change scenarios in Saskatoon.

5.1.3 Comparison of K-NN and GP Methods

The performance of the K-NN hourly disaggregation model was compared with that of the GP method, based on the constructed IDF curves during the baseline period and under the projections of climate change scenarios using these methods. The method was re-implemented in this study to construct the baseline and future IDF curves for two GCMs (CanESM2 and HadGEM2-ES) and corresponding three RCPs, following the same rationale and hypothesis assumed for CGCM3.1 and three AR4 emission scenarios (i.e., A1B, A2, and B1) by Hassanzadeh et al. (2014). A total of 24 mapping equations was extracted to describe the relationship between the GCM-scale daily AMP and the local-scale daily and sub-daily AMPs. The GCM-scale daily AMP quantiles were used as input in GPLAB, while the outputs were the daily and sub-daily AMP quantiles at the local scale (Saskatoon). Because the GP-based method for constructing IDF curves for the City of Saskatoon was published previously (Hassanzadeh et al., 2014), it was considered in this study to be a reference method for comparison with the developed two-stage downscaling-disaggregation approach.

5.1.4 Uncertainty Analysis

The two-stage modeling scheme (downscaling-disaggregation) was used to quantify the sources of uncertainty in the IDF curves. The uncertainty due to the natural internal variability of daily precipitation was quantified using AMP quantiles extracted from the 1000 realizations of daily precipitation obtained from LARS-WG during the baseline period for selected return periods (2-, 5-, 25-, and 100-year). The simulated AMP quantiles for various return periods were obtained by fitting GEV distribution to AMPs corresponding to the 1000 realizations of daily precipitation, each realization having 30 years of daily precipitation for both the baseline and the future projections. The mean of the quantiles from 1000 realizations represents the expected

intensity, while 97.5th and 2.5th percentiles represent the upper and lower bounds of a 95% confidence interval. The observed AMP quantiles for the selected return periods were obtained by fitting GEV distribution to AMPs from the observed daily precipitation series. The expected intensities, and upper and lower bounds of the 95% confidence intervals of the AMP quantiles were compared in order to estimate the uncertainty due to natural variability in the simulated daily precipitation. Similarly, the uncertainty due to natural variability of the simulated hourly and sub-hourly precipitation was quantified using the hourly and 5-minute precipitation series (1000 realizations) during the baseline and future projection periods, respectively.

In the case of observed AMP quantiles, each of the three parameters (location, scale, and shape) of the GEV distribution with three values were used to obtain the expected intensity, and upper and lower bounds of the 95% confidence interval. This represents the 95% confidence interval of the GEV fit.

The results of the two-stage downscaling-disaggregation method using the LARS-WG and the K-NN hourly disaggregation model were compared with results obtained from the GP-based method. To quantify the uncertainty/variability due to the method of disaggregation from daily to hourly precipitation. The expected hourly precipitation quantiles, from the 1000 realizations from LARS-WG and K-NN hourly disaggregation model, and the expected hourly precipitation quantiles from the GP method of various return periods for the GCMs/RCPs during 2011-2040, 2041-2070, and 2071-2100 periods, were compared to quantify the uncertainty due to the two downscaling methods.

5.2 Conclusions and Findings

The two-stage downscaling-disaggregation method is a promising tool for generating long records of hourly and sub-hourly precipitation and constructing a set of IDF curves for

hydraulic design purposes in Saskatoon. This method also enabled the quantification of uncertainties due to the natural internal variability of precipitation, and enabled a comparison with the GP method to quantify uncertainty in the disaggregation method.

LARS-WG performed well in reproducing the mean daily precipitation, mean extreme daily precipitation, and maximum extreme daily precipitation, underestimating variability of maximum extreme daily precipitation only in the month of June. Including the distributions of wet and dry spell lengths helped in widening the range of variabilities of extreme precipitation generated by LARS-WG. Compared to a historical (baseline) AMP value of 115 mm/day for a 100-year storm, a maximum value of 131 mm/day was projected for the 2011-2040 period with CanESM2 and RCP2.6.

For the K-NN method of disaggregation, optimal window sizes for hourly and sub-hourly disaggregation models were found to be 7 days and 113 hours, respectively. Based on the sub-hourly precipitation series, it was found that variations in the future extreme precipitation quantiles, as represented by the IDF curves, are more significant at shorter durations and for larger return periods when compared to historical IDF curves. The variations in future extreme precipitation quantiles seem to intensify toward the end of the 21st century. The sign and the magnitude of variations in future extreme precipitation quantiles at different durations and/or return periods are highly sensitive to the selection of GCMs and/or RCPs.

Storms of 15-minute duration having historical precipitation intensities of 37 mm/hr and 183 mm/hr for 2-year and 100-year return periods, respectively, are projected to intensify to 39 mm/hr and 241 mm/hr. Storms of 1-hour duration are projected to increase to 16 mm/hr and 126 mm/hr from historical values of 14 mm/hr and 94 mm/hr for the 2-year and 100-year return

periods, respectively. The intensification is greater for shorter durations and longer return period storms.

Uncertainty in the projections of future extreme precipitation quantiles increases for short durations and for long return periods. A 5-minute historical storm with a 100-year return period with an intensity of 265 mm/hr, an intensity of 317 mm/hr was projected for the 2011-2040 period with CanESM2 and RCP2.6, while an intensity of 275 mm/hr was projected for the same period with HadGEM2-ES and RCP2.6. During 2041-2070, the same return period event is projected to intensify to 281 mm/hr and 381 mm/hr by RCP4.5 and RCP8.5, respectively, based on HadGEM2-ES. A 1-hr storm with a historical precipitation intensity of 84 mm/hr for a 100-year return period, is projected to have an intensity of 84.6 mm/hr for 2071-2100 by HadGEM2-ES and RCP2.6 using a GP-based downscaling method, while an intensity of 140 mm/hr was projected for the same period with the same GCM/RCP using the LARS-WG and K-NN-based downscaling-disaggregation method.

The contribution of internal precipitation variability to the uncertainty of AMP values represented by 1000 realizations using LARS-WG should be taken into account and understood carefully. The realizations indicate a wider uncertainty in future projections than other sources of uncertainty. However, a similar wide range of variability in the constructed IDF curves was produced during the baseline (historical) period; therefore, the uncertainty cannot be attributed to possible climate change. If such variability was always present, and the historical IDF curves were successfully employed, it is logical to consider this source of projected future variability as a source of additional information. Thus, the mean of the realizations can be considered for representation of the IDF curves; this is the approach adopted in this study for assessing future values of AMPs.

5.3 Contribution of this Research

The main contribution of this thesis is to fill a knowledge gap. Sets of IDF curves under climate change were constructed, and long continuous precipitation records of 5-minute resolution for Saskatoon during both baseline and future periods were also generated. The fine resolution precipitation time series might be important to represent high resolution extreme precipitation quantiles in the prairie region where precipitation during the summer months occurs mostly in convective forms (Shook and Pomeroy, 2012). High-resolution continuous precipitation simulations during the baseline period, as well as those under the projections of climate change, might be valuable for understanding the dynamics of an urban hydrological system in Saskatoon and their impact on the city's storm water collection systems.

Another technical contribution can be described as follows: quantifying the effect of considering wet and dry spell lengths on the variability of the precipitation generated using a stochastic weather generator. Other investigations conducted in this study can be summarized as follows: (1) investigating the issue of optimal window size for the K-NN technique and emphasizing the importance of identifying a site-specific optimal window size and (2) showing the issue of uncertainty due to internal natural variability (due to randomness) of precipitation, quantifying it using the weather generator, and emphasizing that it is not a unique source of uncertainty that can be attributed to climate change.

5.4 Limitations of the Study

The assumptions and limitations of the current study are as follows.

- The development of the K-NN sub-hourly disaggregation model used only 14 years of 5-minute precipitation data, which might not be sufficient for model calibration and

validation. This was due to the data recorded over a limited time period (1992-2009 with some missing years).

- Out of eight rain gauges in Saskatoon, only sub-hourly precipitation from the Acadia Reservoir rain gauge was considered in this study. This might not adequately represent the spatial variability in precipitation throughout the city; thus caution should be exercised in deciding on design criteria for urban storm water collection systems based on the variations observed in the future IDF curves in this study. However, the precipitation, when available, from any rain gauge can easily be included in the two-stage downscaling-disaggregation method adopted in this research. The general method adopted in this study can be applied to any rain gauge in the city considering any other GCM/RCP for constructing multiple sets of future IDF curves in order to produce a wider range of variations for future extreme precipitation quantiles in Saskatoon.
- Two GCMs (the Canadian CanESM2 and the British HadGEM2-ES) were considered in this study, assuming that the two GCMs and the corresponding six RCPs (RCP2.6, RCP4.5, and RCP8.5) with multiple realizations would cover a wide range of variability, which was assumed to be sufficient to investigate the adopted two-stage modeling approach. However, the two-stage modeling approach adopted in this research can be implemented using other multiple GCMs.
- Only the K-NN method for temporal disaggregation of precipitation was used in this study and was compared with the GP method. However, there are other techniques available in the literature that can be used for better quantification of uncertainties due to the disaggregation process. Similarly, only LARS-WG was adopted as a downscaling

technique. Other downscaling approaches, as presented in chapter 2, can be used for better quantification of uncertainty due to the downscaling process.

5.5 Future Work

For improving the results of the research conducted in this study and for gaining more confidence in its recommendations, it is recommended that the current study be extended in the following ways:

- Inclusion of several other Global Climate Models (GCMs) available through PCMDI under CMIP5 to better understand the impact of climate change on the IDF curves in the City of Saskatoon, with better estimation of uncertainty due to GCMs using a multi-model ensemble. This is not difficult, given the framework already developed in this thesis.
- Improvement in the collection fine-resolution precipitation data at various gauges of the city should be done by performing quality check of the data, followed by spatial analysis to construct a representative precipitation record of fine temporal resolution.
- The study may consider dynamical downscaling methods using multiple RCMs, and comparing the results with the statistical downscaling methods adopted in this study.
- There is a body of literature (Westra et al., 2014) suggesting that intensification of sub-daily extreme rainfall intensities occurs as a result of an increase in atmospheric temperature. With global warming in the northern hemisphere, it is recommended to investigate the rate of temperature increase in the Canadian prairies under climate change, and the empirical evidence of a relationship between increasing temperatures and extreme sub-daily rainfall intensities.

References

Abdellatif, M., Atherton, W., & Alkhaddar, R. (2013). Application of the stochastic model for temporal rainfall disaggregation for hydrological studies in north western England. Journal of Hydroinformatics, 15(2), pp. 555-567. doi:10.2166/hydro.2012.090.

Adamowski, J., Adamowski, K., and Bougadis, J. (2009). Influence of Trend on Short Duration Design Storms. Water Resources Management, 24(3), pp. 401–413.

Anandhi, A., Frei, A., Pierson, D. C., Schneiderman, E. M., Zion, M. S., Lounsbury, D., & Matonse, A. H. (2011). Examination of change factor methodologies for climate change impact assessment. Water Resources Research, 47(3), pp. 1-10. doi:10.1029/2010WR009104

Alzahrani, F. (2013). An Approach to Quantifying Uncertainty in Estimates of Intensity Duration Frequency (IDF) Curves. PhD thesis, University of Waterloo, Waterloo, Ontario, Canada.

Arnbjerg-Nielsen, K. (2012). Quantification of climate change effects on extreme precipitation used for high resolution hydrologic design. Urban Water Journal, 9(2), pp. 57–65. doi:10.1080/1573062X.2011.630091

Artlert, K., Chaleeraktrakoon, C., & Nguyen, V.-T.-V. (2013). Modeling and analysis of rainfall processes in the context of climate change for Mekong, Chi, and Mun River Basins (Thailand). Journal of Hydro-environment Research, 7(1), pp. 2–17. doi:10.1016/j.jher.2013.01.001.

Babovic, V., and Keijzer, M. (2000). Genetic programming as model induction engine. J. Hydroinf., 2(1), pp. 35–60.

Barrow, E. (2002). Scenarios of climate change, In Proceeding of Climate Change and Water Resources in South Saskatchewan River Basin, Saskatoon, Saskatchewan, Canada, April 2002, pp. 22-45.

Beniston, M., et al. (2007). Future extreme events in European climate: an exploration of regional climate model projections. Clim. Change, 81(1), pp. 71–95.

Bo, Z., Islam, S., and Eltahir, E. A. B. (1994). Aggregation-disaggregation properties of a stochastic precipitation model, Water Resour. Res., 30 (12), pp. 3423-3435.

Buishand, T. A. and Brandsma, T. (2001). Multisite simulation of daily precipitation and temperature in the Rhine basin by nearest-neighbor resampling. Water Resour. Res., 37(11), pp. 2761–2776.

Burian, B. S. J., Durrans, S. R., Nix, S. J., and Pitt, R. E. (2001). Training of Artificial Neural Networks to Perform Precipitation Disaggregation, J. Hydrol. Eng. 6, pp. 43-51.

Burian, B. S. J., Durrans, S. R., Tomic, S., Pimmel, R. L., & Wai, C. N. (2000). Rainfall disaggregation using Artificial Neural Networks. Journal of Hydrologic Engineering, 5, pp. 299–307.

Burn, D. H., & Taleghani, A. (2013). Estimates of changes in design rainfall values for Canada. Hydrological Processes, 27(11), 1590–1599. doi:10.1002/hyp.9238

Busuioc, A., Tomozeiu, R., & Cacciamani, C. (2008). Statistical downscaling model based on canonical correlation analysis for winter extreme precipitation events in the Emilia-Romagna region, 464 (July 2007), pp. 449–464. doi:10.1002/joc

Cameron, D., Beven, K., and Tawn, J. (2001). Modelling extreme precipitations using a modified random pulse Bartlett-Lewis stochastic precipitation model (with uncertainty). Adv. Water Resour., 24(2), pp. 203–211.

Chadwick, R., Coppola, E., & Giorgi, F. (2011). An artificial neural network technique for downscaling GCM outputs to RCM spatial scale. Nonlinear Processes in Geophysics, 18(6), pp. 1013–1028. doi:10.5194/npg-18-1013-2011

Chandler, R. E., and Wheater, H. S. (2002). Analysis of rainfall variability using generalized linear models: A case study from the west of Ireland. Water Resour. Res., 38(10), 1192, pp. 10-1-10-11. doi:10.1029/2001WR000906.

Chun, K. P., Wheater, H. S., Nazemi, a., & Khaliq, M. N. (2013). Precipitation downscaling in Canadian Prairie Provinces using the LARS-WG and GLM approaches. Canadian Water Resources Journal, 38(4), 311–332. doi:10.1080/07011784.2013.830368.

City of Saskatoon. (2012). New Neighborhood Design and Development Standards Manual, Storm Water Drainage System, Section six.

CMIP5 (2013). CMIP5 Coupled Model Intercomparison Project, Data Access, Availability. Available at: http://cmip-pcmdi.llnl.gov/cmip5/availability.html. Accessed on 12 December 2014.

Coe, R. and Stern, R. D. (1982). Fitting Models to Daily Rainfall Data. Journal of Applied Meteorology, 21 (7), pp. 1024–1031.

Denault, C., Millar, R. G., & Lence, B. J. (2002). Climate change and drainage infrastructure capacity in an urban catchment. In Proc. Annual Conference of the Canadian Society for Civil Engineering, pp. 5-6. [http://pedago.cegepoutaouais.qc.ca/media/0260309/0378334/SCGC-BON/Documents/GE110-Denault.pdf]

Dibike Y.B., Coulibaly, P. (2005). Hydrologic impact of climate change in the Saguenay watershed: comparison of downscaling methods and hydrologic models. J Hydrol., 307, pp. 145–163.

Elshorbagy, A., Panu, U., and Simonovic, S. (2000). Group-based estimation of missing hydrological data: I. Approach and general methodology. Hydrological Sciences Journal, 45(6), 849 – 866.

Ehret, U., Zehe, E., Wulfmeyer, V., Warrach-Sagi, K., & Liebert, J. (2012). Should we apply bias correction to global and regional climate model data? Hydrology and Earth System Sciences, 16(9), pp. 3391–3404. doi:10.5194/hess-16-3391-2012

Franczyk, J. and Chang, H. (2009). The effects of climate change and urbanization on the runoff of the Rock Creek basin in the Portland metropolitan area, Oregon, USA. Hydrological Processes, 23 (6), pp. 805–815.

Fowler, H. J. and Kilsby, C. G. (2007). Using regional climate model data to simulate historical and future river flows in northwest England. Climatic Change, 80(3-4), pp. 337–367. doi:10.1007/s10584-006-9117-3

Gabriel, K. R. and Neumann, J. (1962). A markov chain model for daily rainfall occurrence at Tel Aviv. Quarterly Journal of the Royal Meteorological Society, 88, pp. 90–95.

Gan, T. Y. (2000). Reducing vulnerability of water resources of Canadian prairies to potential droughts and possible climatic warming. Water Resources Management, 14(2), pp. 111-135.

Giorgi, I. F. and Mearns, L. O. (1999). Introduction to special section- Regional climate modeling revisited in the issue illustrate a wide range of applications. Journal of Geophysical Research, 104(D6), pp. 6335–6352.

Hashmi, M. Z., Shamseldin, A. Y., and Melville, B. W. (2011). Comparison of SDSM and LARS-WG for simulation and downscaling of extreme precipitation events in a watershed. Stochastic Environmental Research and Risk Assessment, 25(4), pp. 475–484. doi:10.1007/s00477-010-0416-x

Hassanzadeh, E., Nazemi, A., and Elshorbagy, A. (2014). Quantile-Based Downscaling of Precipitation using Genetic Programming: Application to IDF Curves in the City of Saskatoon. J. Hydrol. Eng., pp. 943-955. doi:10.1061/(ASCE)HE.1943-5584.0000854

Hay, L. E., Wilby, R. J. L., and Leavesley, G. H. (2000). A comparison of delta change and downscaled GCM scenarios for three mountainous basins in the United States. J. Am. Water Resour. Assoc., 36, pp. 387–397, doi:10.1111/j.1752-1688.2000.tb04276.x

Hu, S. (1987). Determination of confidence intervals for design floods. Journal of Hydrology, 96, pp. 201--213

Hewitson, B. C. and Crane, R. G. (1996). Climate downscaling: techniques and application. Climate Research, 7, pp. 85-95.

Hundecha, Y. and Bardossy, A. (2008). Statistical downscaling of extremes of daily precipitation and, Int. J. Climatology, (28), 589–610. doi: 10.1002/joc.1563.

Intergovernmental Panel on Climate Change (IPCC). (2013). Climate change 2013: the physical science basis. Contribution of Working Group I to the Fifth Assessment Report of the Intergovernmental Panel on Climate Change. Stocker et al., eds., Cambridge University Press, Cambridge, United Kingdom and New York, NY, USA, pp. 1535.

Intergovernmental Panel on Climate Change (IPCC). (2012). Managing the risks of extreme events and disasters to advance climate change adap- tation. A special report of working groups I

and II of the Intergovernmental Panel on Climate Change, C. B. Field, et al., eds., Cambridge University Press, New York.

Intergovernmental Panel on Climate Change (IPCC). (2007). Climate change (2007) synthesis report, contribution of working groups I, II and III to the fourth assessment report of the Intergovernmental Panel on Climate Change, Geneva, Switzerland.

Irwin, S. E., Sarwar, R, King, L. M., and Simonovic, S.P. (2012). Assessment of climatic vulnerability in the Upper Thames River basin: Downscaling with LARS-WG. Department of Civil and Environmental Engineering, The University of Western Ontario, London, Ontario, Canada, Report 081, April 2012.

Jeong, D. I., St-Hilaire, a., Ouarda, T. B. M. J., & Gachon, P. (2012). Multisite statistical downscaling model for daily precipitation combined by multivariate multiple linear regression and stochastic weather generator. Climatic Change, 114(3-4), pp. 567–591. doi:10.1007/s10584-012-0451-3

Katz, R. (2012). Statistical methods for nonstationary extremes. Extremes in a changing climate: Detection, analysis and uncertainty, A. AghaKouchak, D. Easterling, K. Hsu, S. Schubert, and S. Sorooshian, eds., Springer, Dordrecht, Netherlands.

Kelly, D.L. and Kolstad, C.D. (1998). Integrated assessment models for climate change control. Retrieved from http://www.econ.ucsb.edu/papers/wp31-98.pdf on September 7, 2014.

Khaliq, M. N., & Cunnane, C. (1996). Modelling point rainfall occurrences with the modified Bartlett-Lewis rectangular pulses model. Journal of Hydrology, 180(1-4), pp. 109–138. doi:10.1016/0022-1694(95)02894-3.

Kharin, V. V., and Zwiers, F. W. (2005). Estimating extremes in transient climate change simulations. J. Clim., 18(8), pp. 1156–1173.

King, L. M., McLeod, a. I., & Simonovic, S. P. (2014). Simulation of historical temperatures using a multi-site, multivariate block resampling algorithm with perturbation. Hydrological Processes, 28(3), 905–912. doi:10.1002/hyp.9596.

King, L. M., Irwin, S., Sarwar, R., McLeod, A. I., & Simonovic, S. P. (2012). The Effects of Climate Change on Extreme Precipitation Events in the Upper Thames River Basin: A Comparison of Downscaling Approaches. Canadian Water Resources Journal, 37(3), 253–274. doi:10.4296/cwrj2011-938.

Koza, J. R. (1992). Genetic programming: On the programming of computers by means of natural selection, MIT Press, Cambridge, MA.

Kuo, C.-C., Gan, T. Y., & Hanrahan, J. L. (2014). Precipitation frequency analysis based on regional climate simulations in Central Alberta. Journal of Hydrology, 510, 436–446. doi:10.1016/j.jhydrol.2013.12.051

Kuo, C., Gan, T. Y., & Chan, S. (2013). Regional Intensity-Duration-Frequency Curves Derived from Ensemble Empirical Mode Decomposition and Scaling Property. Journal of Hydrologic Engineering, 18, pp. 66-74. doi:10.1061/(ASCE)HE.1943-5584.0000612

Koutsoyiannis, D., Onof, C., & Wheater, H. S. (2003). Multivariate rainfall disaggregation at a fine timescale. Water Resources Research, 39(7), SWC 1, 1-18. doi:10.1029/2002WR001600

Lall, U., and Sharma A. (1996). A nearest neighbor bootstrap for resampling hydrologic time series, Water Resour. Res., 32(3), pp. 679– 693.

Landau, D. P., and Binder, K. (2009). A guide to Monte Carlo simulations in statistical physics. Cambridge university press. Retrieved on September 22, 2014 from http://books.google.ca/books?hl=en&lr=&id=hrIhAwAAQBAJ&oi=fnd&pg=PR1&dq=monte+carlo+simulations&ots=piAWcTEbPC&sig=OlFSGRCgTgUC6N1rbKS0EfJtL2Q#v=onepage&q=monte%20carlo%20simulations&f=false.

Lapp, S., Sauchyn, D., & Wheaton, E. (2008). Institutional Adaptations to Climate Change Project : Future Climate Change Scenarios for the South Saskatchewan River Basin, (November).

Lavellee, D. (1991). Multifractal analysis and simulation techniques and turbulent fields. PhD thesis, McGill University, Montreal, Canada.

Liew, S. C., Raghavan, S. V., & Liong, S.-Y. (2014). How to construct future IDF curves, under changing climate, for sites with scarce rainfall records? Hydrological Processes, 28(8), pp. 3276–3287. doi:10.1002/hyp.9839

Liu, T. (2006). Fast Nonparametric Machine Learning Algorithms for High-dimensional Massive Data and Applications. Doctoral thesis, Carnegie Mellon University, Pittsburgh, PA 15213, USA.

Lu, Y., & Qin, X. S. (2014). Multisite rainfall downscaling and disaggregation in a tropical urban area, Journal of Hydrology (509), 55–65.

Lu, L.-H. and Stedinger, J. R. (1992). Sampling variance of normalized GEV/PWM quantile estimators and a regional homogeneity test. Journal of Hydrology, 138(1-2), pp. 223–245. doi:10.1016/0022-1694(92)90166-S

Mailhot A., Duchesne S. (2010). Design Criteria of Urban Drainage Infrastructures under Climate Change, Journal of Water Resources Planning and Management, 136(2), pp. 201-208. doi: 10.1061/(ASCE)WR.1943-5452.0000023

Mailhot, A., Duchesne, S., Caya, D., & Talbot, G. (2007). Assessment of future change in intensity–duration–frequency (IDF) curves for Southern Quebec using the Canadian Regional Climate Model (CRCM). Journal of Hydrology, 347(1-2), pp. 197–210.

Martz, L., Bruneau, J., and Rolfe, J. T. (2007). Climate change and water: SSRB, final technical report. [http://www.parc.ca/ssrb/] (Jun. 11, 2014).

Massie, M. and Reed, M.G. (2012). Cumberland House in the Saskatchewan River Delta: Flood memory and the municipal response, 2005 and 2011. In Keskitalo (ed.) 2012. Adaptive Capacity and Response to Flooding: International Lessons for Sweden. Edward Elgar Publishers.

McGuffie, K. and Henderson-Sellers, A. (2014). The Climate Modelling Primer, Fourth Edition, John Wiley & Sons, Ltd. Retrieved on August 20, 2014 from http://books.google.ca/books?hl=en&lr=&id=_dXFAgAAQBAJ&oi=fnd&pg=PR3&dq=The+Climate+Modelling+Primer&ots=Oh_jH0pdZ&sig=lXRcZiLUKqLaRqJxOeCMkh9PYvk#v=onepage&q=The%20Climate%20Modelling%20Primer&f=false

Mooney, C. Z. (ed.) (1997). Monte Carlo simulation. No. 116. Sage University Paper. Retrieved on September 22, 2014 from http://books.google.ca/books?hl=en&lr=&id=xQRgh4z_5acC&oi=fnd&pg=PR7&dq=monte+carlo+simulations&ots=hgHCHRzqIM&sig=4mu2ZAfR5MIDBiYdwFTk4y8LMQc#v=onepage&q=monte%20carlo%20simulations&f=false.

Mladjic, B., Sushama, L., Khaliq, M. N., Laprise, R., Caya, D., & Roy, R. (2011). Canadian RCM Projected Changes to Extreme Precipitation Characteristics over Canada. Journal of Climate, 24(10), pp. 2565–2584. doi:10.1175/2010JCLI3937.1

Moss, R. H., Edmonds, J. A, Hibbard, K. A, Manning, M. R., Rose, S. K., van Vuuren, D. P., Wilbanks, T. J. (2010). The next generation of scenarios for climate change research and assessment. Nature, 463(7282), pp. 747–56. doi:10.1038/nature08823

Nakicenovic, N., and Davidson, O., eds. (2000). Summary for Policymakers (Emission Scenarios): A Special Report of Working Group III of the Intergovernmental Panel on Climate Change (IPCC).

Nazemi, A., Elshorbagy, A. and Pingale, S. (2011). Uncertainties in the estimation of future annual extreme daily rainfall for the city of Saskatoon under climate change effects. In proceedings of the 20th annual Hydrotechnical Conference, Canadian Society of Civil Engineering Conference, 14-17 June 2011, Ottawa, Canada.

Nguyen, V.T.V., Desramaut, N., & Nguyen, T.D. (2008). Estimation of Design Storms in Consideration of Climate Variability and Change. 11th International Conference on Urban Drainage, Edinburgh, Scotland, UK, 2008, pp. 1–10.

Olsson, J., Gidhagen, L., Gamerith, V., Gruber, G., Hoppe, H., & Kutschera, P. (2012a). Downscaling of Short-Term Precipitation from Regional Climate Models for Sustainable Urban Planning. Sustainability, 4(12), 866–887. doi:10.3390/su4050866

Olsson, J., Willén, U., & Kawamura, A. (2012b). Downscaling extreme short-term regional climate model precipitation for urban hydrological applications. Hydrology Research, 43(4), pp. 341-351. doi:10.2166/nh.2012.135

Olsson, J., Berggren, K., Olofsson, M., & Viklander, M. (2009). Applying climate model precipitation scenarios for urban hydrological assessment: A case study in Kalmar City, Sweden. Atmospheric Research, 92, pp. 364–375.

Olsson, J. (1998). Evaluation of a scaling cascade model for temporal rainfall disaggregation. Hydrology and Earth System Sciences, 2(1), pp. 19–30.

Ormsbee, L. E. (1989). Rainfall disaggregation model for continuous hydrologic modeling. Journal of Hydraulic Engineering, 115(4), pp. 507–525.

Overeem, A., Buishand, A., & Holleman, I. (2008). Rainfall depth-duration-frequency curves and their uncertainties. Journal of Hydrology, 348(1-2), pp. 124–134. doi:10.1016/j.jhydrol.2007.09.044

Peck, A., Prodanovic, P., & Simonovic, S. P. P. (2012). Rainfall Intensity Duration Frequency Curves Under Climate Change: City of London, Ontario, Canada. Canadian Water Resources Journal, 37(3), 177–189. doi:10.4296/cwrj2011-935

Prodanovic, P. and Simonovic, S. P. (2007). Development of rainfall intensity duration frequency curves for the City of London under the changing climate. Department of Civil and Environmental Engineering, The University of Western Ontario, London, Ontario, Canada, Report 058, November 2007.

Prudhomme, C., Jakob, D., and Svensson, C. (2003). Uncertainty and climate change impact on the flood regime of small UK catchments. Journal of Hydrology, 277 (1), pp. 1-23.

Prudhomme, C., Reynard, N., & Crooks, S. (2002). Downscaling of global climate models for flood frequency analysis : where are we now? Hydrological Processes, 16, pp. 1137–1150.

Qian, B., Gameda, S., and Hayhoe, H. (2008). Performance of stochastic weather generators LARS-WG and AAFC-WG for reproducing daily extremes of diverse Canadian climates. Climate Research, 37 (September), pp. 17–33. doi:10.3354/cr00755

Qian, B., Gameda, S., Hayhoe, H., Jong, R. De, & Bootsma, A. (2004). Comparison of LARS-WG and AAFC-WG stochastic weather generators for diverse Canadian climates, Climate Research, 26, pp. 175–191.

Racsko, P., Szeidl, L., and Semenov, M. (1991) A serial approach to local stochastic weather models. Ecol Model, 57, pp. 27–41.

Rajagopalan, B. and Lall, U. (1999). A k-nearest-neighbor simulator for daily precipitation and other weather variables. Water resources research, 35 (10), pp. 3089-3101.

Richardson, C. W. (1981). Stochastic Simulation of Daily Precipitation, Temperature and Solar Radiation. Water Resources Research, 17, pp. 182–190.

Rodríguez, R., Navarro, X., Casas, M. C., Ribalaygua, J., Russo, B., Pouget, L., & Redaño, A. (2014). Influence of climate change on IDF curves for the metropolitan area of Barcelona (Spain). International Journal of Climatology, 34(3), 643–654. doi:10.1002/joc.3712

Rodriguez-Iturbe, I., Cox, D. R., and Isham, V. (1988). A point process model for rainfall: Further developments. Proc. R. Soc. London, Ser. A , 417, pp. 283-298.

Rodriguez-Iturbe, I., Cox, D. R., and Isham, V. (1987). Some models for rainfall based on stochastic point processes. Proc. R. Soc. London, Ser. A, 410, pp. 269-288.

Rogelj, J., Meinshausen, M., & Knutti, R. (2012). Global warming under old and new scenarios using IPCC climate sensitivity range estimates. Nature Climate Change, 2(4), pp. 248–253. doi:10.1038/nclimate1385

Rupp, D. E., Keim, R. F., Ossiander, M., Brugnach, M., & Selker, J. S. (2009). Time scale and intensity dependency in multiplicative cascades for temporal rainfall disaggregation. Water Resources Research, 45(7), pp. W07409 (1-14). doi:10.1029/2008WR007321

Savic, D. A., Walters, G. A., and Davidson, J. W. (1999). A genetic programming approach to rainfall-runoff modeling. Water Resour. Manage., 13(3), pp. 219–231.

Schilling, W. (1991). Rainfall data for urban hydrology: what do we need? Atmospheric Research, 27(1), pp. 5-21. doi:10.1016/0169-8095(91)90003-F

Schoof, J. T., & Pryor, S. C. (2001). Downscaling temperature and precipitation: a comparison of regression-based methods and artificial neural networks. International Journal of Climatology, 21(7), pp. 773–790. doi:10.1002/joc.655

Segond, M.-L., Neokleous, N., Makropoulos, C., Onof, C., & Maksimovic, C. (2007). Simulation and spatio-temporal disaggregation of multi-site rainfall data for urban drainage applications. Hydrological Sciences Journal, 52(5), pp. 917–935. doi:10.1623/hysj.52.5.917

Segond, M.-L., Onof, C., and Wheater, H. S. (2006). Spatial–temporal disaggregation of daily rainfall from a generalized linear model. Journal of Hydrology, 331, pp. 674– 689.

Semenov, M. A., Stratonovitch, P. (2010). Use of multi-model ensembles from global climate models for assessment of climate change impacts, Climate Research, 41, pp. 1-14.

Semenov M. A., Barrow, E. M. (2002) LARS-WG: A Stochastic Weather Generator for Use in Climate Impact Studies, User Manual for Version 3.0, August 2002, [http://www.rothamsted.ac.uk/mas-models/download/LARS-WG-Manual.pdf].

Semenov, M. A., Brooks, R. J., Barrow, E. M., and Richardson, C. W. (1998). Comparison of the WGEN and LARS-WG stochastic weather generators for diverse climates, Climate Research, 10, pp. 95–107.

Semenov, M. A., & Barrow, E. M. (1997). Use of a stochastic weather generator in the development of climate change scenarios, Climate Change, 35, pp. 397–414.

Sharif, M. and Burn, D. H. (2007). Improved K-nearest neighbor weather generating model. Journal of Hydrologic Engineering, 12, pp. 42-51.

Sharma, M., Coulibaly, P., and Dibike, Y. (2011). Assessing the Need for Downscaling RCM Data for Hydrologic Impact Study. Journal of Hydrologic Engineering, 16 (6), pp. 534–539. doi:10.1061/(ASCE)HE.1943-5584

Shook, K., & Pomeroy, J. (2012). Changes in the hydrological character of rainfall on the Canadian prairies. Hydrological Processes, 26(12), pp. 1752–1766. doi:10.1002/hyp.9383

Shook, K. and Pomeroy, J. W. (2010). Hydrological effects of the temporal variability of the multiscaling of snowfall, Hydrol. Earth Syst. Sci., 14, pp. 1195–1203.

Silva, S. (2007). GPLAB- A genetic programming toolbox for MATLAB. ⟨http://gplab.sourceforge.net⟩ (August 22, 2014).

Sivakumar, B., Sorooshian, S., Gupta, H. V., and Gao, X. (2001) A chaotic approach to rainfall disaggregation, Water Resources Research, 37 (1), pp. 61-72.

Solaiman, T. A. (2011). Uncertainty estimation of extreme precipitations under climate change: A non-parametric approach. PhD thesis, University of Western Ontario, London, Ontario, Canada.

Solaiman, T. and Simonovic, S. P. (2011). Development of probability based intensity duration frequency curves under climate change. Department of Civil and Environmental Engineering, The University of Western Ontario, London, Ontario, Canada, Report 072, March 2011.

Solomon, S., Qin, D., Manning, M., Marquis, M., and others (eds) (2007). Climate Change 2007: the physical science basis. Contribution of Working Group I to the Fourth Assessment Report of the Intergovernmental Panel on Climate Change. Cambridge University Press, Cambridge.

Srikanthan, R., McMahon, T.A. (2001) Stochastic generation of annual, monthly and daily climate data: A review. Hydrology and Earth System Sciences, 5(4), pp. 653–670.

Srivastav, R. K., Schardong, A., & Simonovic, S. P. (2014). Equidistance Quantile Matching Method for Updating IDF Curves under Climate Change. Water Resources Management. doi:10.1007/s11269-014-0626-y

Sun, F., Roderick, M. L., Lim, W. H., & Farquhar, G. D. (2011). Hydroclimatic projections for the Murray-Darling Basin based on an ensemble derived from Intergovernmental Panel on Climate Change AR4 climate models. Water Resources Research, 47(12), pp. 1-14. doi:10.1029/2010WR009829

Taylor, K. E., Stouffer, R. J., & Meehl, G. A. (2012). An Overview of CMIP5 and the Experiment Design. Bulletin of the American Meteorological Society, 93(4), pp. 485–498. doi:10.1175/BAMS-D-11-00094.1

Todorovic, P. and Woolhiser, D. A. (1975). A stochastic model of n-day precipitation. J. Appl. Meteorol., 14(1), pp. 17-24.

Trenberth, K. E., Dai, A., Rasmussen, R. M., & Parsons, D. B. (2003). The Changing Character of Precipitation. Bulletin of the American Meteorological Society, 84(9), 1205–1217.

von Storch, H., Zorita, E., and Cubasch, U. (1993). Downscaling of global climate change estimates to regional scale: An application to Iberian precipitation in wintertime. Journal of Climate, 6, pp. 1161–1171.

Waters, D., Watt, W. E., Marsalek, J., & Anderson, B. C. (2003). Adaptation of a storm drainage system to accommodate increased rainfall resulting from climate change. Journal of Environmental Planning and Management, 46(5), pp. 755–770. doi:10.1080/0964056032000138472

Watt, E., & Marsalek, J. (2013). Critical review of the evolution of the design storm event concept. Canadian Journal of Civil Engineering, 40(2), pp. 105-113.

Watt, W.E., Waters, D., and McLean, R. (2003). Climate change and urban stormwater infrastructure in Canada: Context and case studies. Toronto-Niagara Region Study Report and Working Paper Series, Report 2003-1. Meteorological Service of Canada, Waterloo, Ontario.

Weyant, et. al. (1996). Integrated assessment of climate change: An overview and comparison of approaches and results, pp. 367-439 in J. P. Bruce, et. al. (eds), Climate Change 1995: Economic and Social Dimensions of Climate Change, Cambridge University Press, Cambridge. Retrieved on October 12, 2014 from http://books.google.ca/books?hl=en&lr=&id=1BEjH8IPF8cC&oi=fnd&pg=PA367&dq=Integrated+assessment+of+climate+change:+An+overview+and+comparison+of+approaches+and+results&ots=RAU3U_dVwa&sig=HeMckgRYQRnylmINgZZF5D5tDCQ#v=onepage&q=Integrated%20assessment%20of%20climate%20change%3A%20An%20overview%20and%20comparison%20of%20approaches%20and%20results&f=false.

Wheater, H. S., Chandler, R. E., Onof, C. J., Isham, V. S., Bellone, E., Yang, C., Lekkas, D., Lourmas, G., and Segond, M.-L. (2005). Spatial-temporal precipitation modelling for flood risk estimation. Stochastic Environmental Research and Risk Assessment, 19(6), pp. 403–416. doi:10.1007/s00477-005-0011-8

Wilby, R. L. and Dawson, C. W. (2007). SDSM 4 .2-A decision support tool for the assessment of regional climate change impacts, Version 4.2 user manual, pp. 1–94.

Wilby, R. L. and Dawson, C. W. (2004). Using SDSM Version 3.1-A decision support tool for the assessment of regional climate change impacts, User Manual, pp. 1–67.

Wilby, R., Dawson, C., & Barrow, E. (2002). SDSM — a Decision Support Tool for the Assessment of Regional Climate Change Impacts. Environmental Modelling & Software, 17(2), pp. 145–157. doi:10.1016/S1364-8152(01)00060-3

Wilby, R. L., Wigley, T. M. L., Conway, D., Jones, P. D., Hewitson, B. C., Main, J., & Wilks, D. S. (1998). Statistical downscaling of general circulation model output: A comparison of methods. Water Resources Research, 34(11), pp. 2995–3008. doi:10.1029/98WR02577

Wilby, R. L., & Wigley, T. M. L. (1997). Downscaling general circulation model output: a review of methods and limitations. Progress in Physical Geography, 21(4), pp. 530–548. doi:10.1177/030913339702100403

Wilks, D. S. (1999). Multisite downscaling of daily precipitation with a stochastic weather generator. Climate Research, 11(2), 125-136.

Wilks, D.S. (1992) Adapting stochastic weather generation algorithms for climate changes studies. Clim Change, 22, pp. 67–84.

Wilks, D. S., & Wilby, R. L. (1999). The weather generation game: a review of stochastic weather models. Progress in Physical Geography, 23(3), 329–357. doi:10.1177/030913339902300302

Willems, P., Arnbjerg-Nielsen, K., Olsson, J., & Nguyen, V. T. V. (2012). Climate change impact assessment on urban rainfall extremes and urban drainage: Methods and shortcomings. Atmospheric Research, 103, pp. 106–118. doi:10.1016/j.atmosres.2011.04.003.

Willems, P., & Vrac, M. (2011). Statistical precipitation downscaling for small-scale hydrological impact investigations of climate change. Journal of Hydrology, 402(3-4), pp. 193–205. doi:10.1016/j.jhydrol.2011.02.030

Wood, A.W., Leung, L. R., Sridhar, V., and Lettenmaier, D. P. (2004) Hydrologic implications of dynamical and statistical approaches to downscaling climate model outputs. Climatic Change, 62, pp. 189–216.

Xu, Y.-P., Booij, M., and Tong, Y.-B. (2010). Uncertainty analysis in statistical modeling of extreme hydrological events. Stochastic Environmental Research and Risk Assessment, 24(5), pp. 567-578.

Xue, Y., Janjic, Z., Dudhia, J., Vasic, R., & De Sales, F. (2014). A review on regional dynamical downscaling in intraseasonal to seasonal simulation/prediction and major factors that affect downscaling ability. Atmospheric Research, 147-148, 68–85. doi:10.1016/j.atmosres.2014.05.001

Yang, C., Chandler, R. E., Isham, V. S., & Wheater, H. S. (2005). Spatial-temporal rainfall simulation using generalized linear models. Water Resources Research, 41(11), pp. W11415 (1-13). doi:10.1029/2004WR003739

Yates, D., Gangopadhyay, S., Rajagopalan, B., Strzepek, K. (2003). A technique for generating regional climate scenarios using a nearest-neighbor algorithm. Water Resources Research 39 (7), pp. SWC 7-1–SWC 7-14.

Yilmaz, A. G., and Perera, B. J. C. (2014). Extreme rainfall Nonstationarity Investigation and Intensity – Frequency – Duration Relationship. J. Hydrol. Eng., 19 (6), pp. 1160–1172. doi:10.1061/(ASCE)HE.1943-5584.0000878

Yusop, Z., Nasir, H., & Yusof, F. (2013). Disaggregation of daily rainfall data using Bartlett Lewis Rectangular Pulse model: a case study in central Peninsular Malaysia. Environmental Earth Sciences. doi:10.1007/s12665-013-2755-7

Zhang, H., Huang, G. H., Wang, D., & Zhang, X. (2011). Uncertainty assessment of climate change impacts on the hydrology of small prairie wetlands. Journal of Hydrology, 396(1-2), 94–103. doi:10.1016/j.jhydrol.2010.10.037

Appendix A

With reference to section 2.1, the relative projections due to AR4 and AR5 emission scenarios/RCPs are shown below.

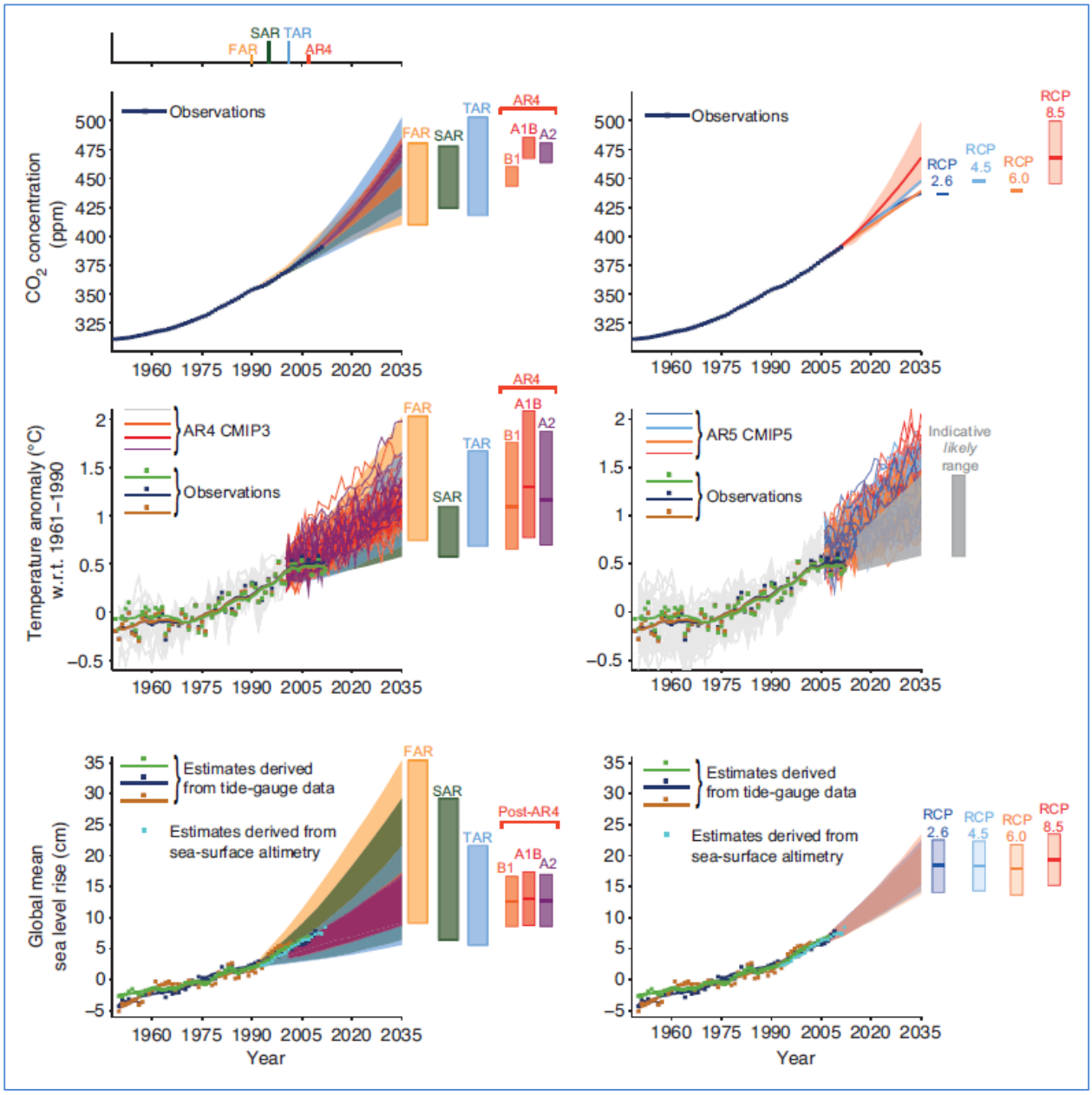

Figure A.1: Comparison of the observed globally and annually averaged CO2 concentration, temperature anomaly, and mean sea level rise and those under the projections of climate change scenarios obtained from various IPCC assessment reports (e.g., AR4, AR5) (Source: IPCC, 2013, printed with the permission from WG I).

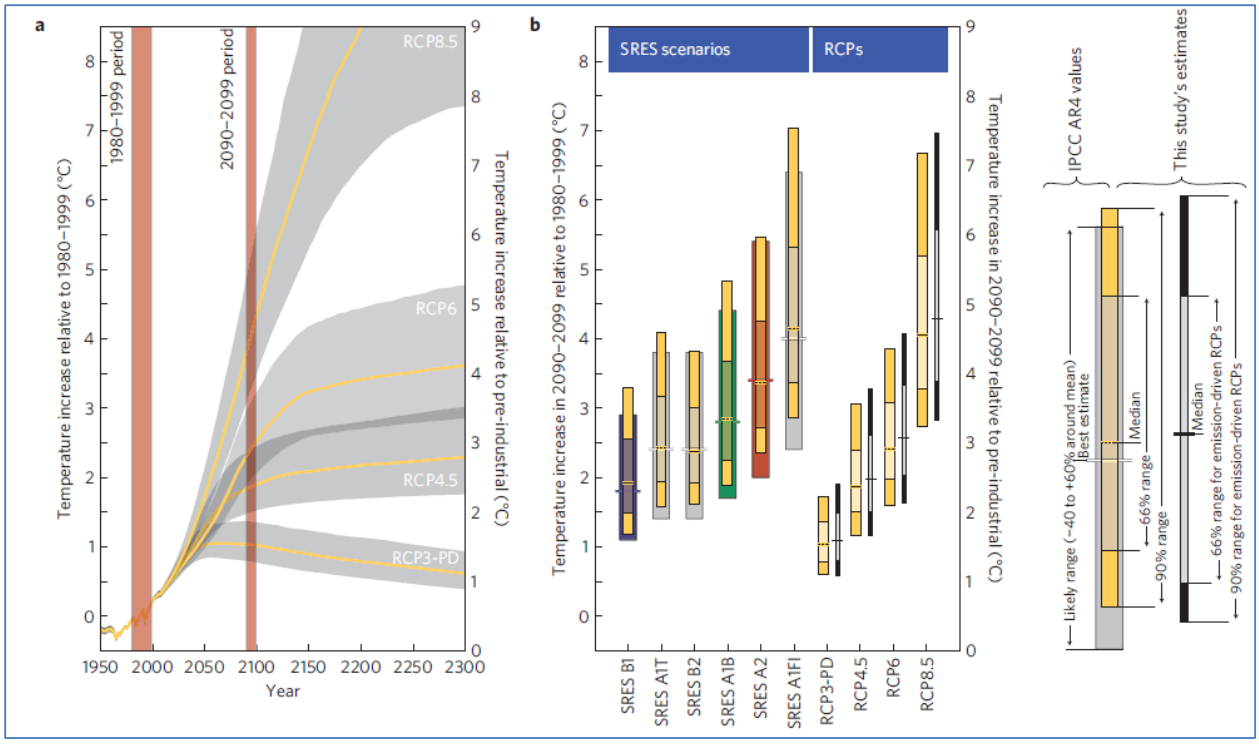

Figure A.2: Temperature increase obtained for SRES emission scenarios and RCPs based on CMIP3 and CMIP5 climate model simulations, respectively (Source: Rogelj et al., 2012, printed with the permission from Nature Publishing Group).

Appendix B

B.1 Steps involved in LARS-WG

Simulation of multiple realizations of daily precipitation using LARS-WG involves a number of steps as briefly described below with reference to section 2.2.2 (iii).

(i) Site Analysis

The stochastic weather generation process in LARS-WG starts with *Site Analysis* in order to generate daily precipitation time series. It is necessary to update the information for Saskatoon in Site Analysis by specifying the local station name (e.g., Saskatoon), latitude, longitude, altitude, path of the folder where precipitation files are located, and format of the precipitation data files (as shown in Figure B.1).

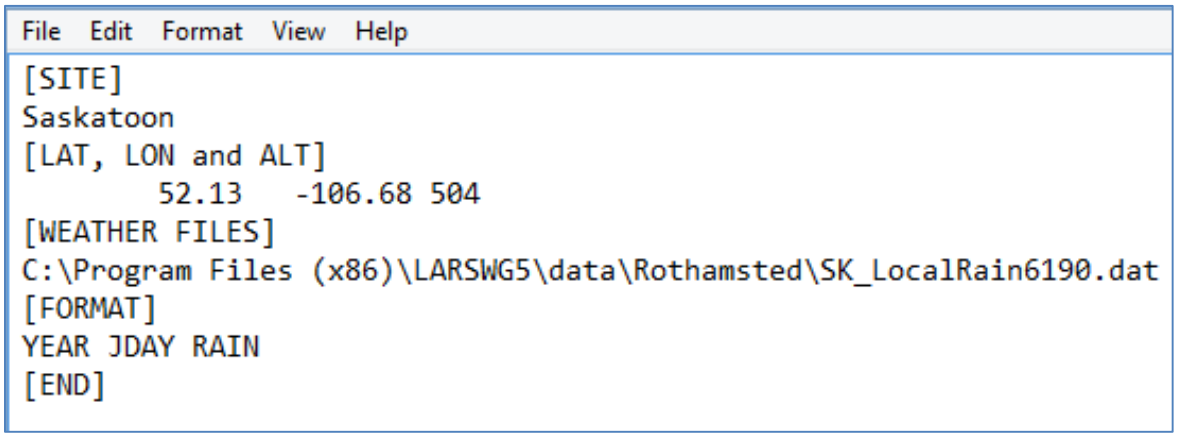

Figure B.1: Updated Site Analysis file for Saskatoon

Site Analysis is performed when the file is updated using the Site Analysis option in LARS-WG, which produces three files namely a parameter file (Saskatoon.wgx), a statistics file (Saskatoon.stx), and a test file (Saskatoon.tst). LARS-WG uses the parameters located in the parameter file for generating synthetic precipitation time series, while the seasonal frequency distributions for wet/dry spell lengths and precipitation series are located in the statistics file. The statistical characteristics of the observed data and simulated data are compared and the results of comparison are located in the test file (Table B.1), where the simulated data are generated using the parameter files of the observed data. Among the important statistics, the test file contains test statistics (KS-, t-, and f-statistics) with the corresponding p-values, average wet/dry spell lengths for each month, and mean monthly precipitation amounts for each month. The statistics are used

to assess the performance of LARS-WG by evaluating the corresponding p-values – evaluating if the observed and simulated data belong to the same distribution, i.e., the simulated precipitation is not significantly different from the observed data.

(ii) Generation of scenario files

Scenario files are required in LARS-WG for determining the perturbation rule of the weather generator parameters located in the parameter files. In case of generating synthetic precipitation series based on the parameters calculated from the observed precipitation data, no perturbation of the parameter values is applied so that the statistical characteristics of the simulated and observed precipitation series remain the same. However, relative change factors (RCFs) are calculated corresponding to the mean monthly precipitation amounts, and wet and dry spell lengths for each month, which are then included in the scenario file for generating future precipitation time series of arbitrary length under climate change scenarios by perturbing the parameter values obtained from the observed data. An example of a scenario file of LARS-WG is shown in Figure B.2. For detailed explanation of LARS-WG weather generation procedures, please refer to Semenov and Barrow (2002).

```
// LARS-WG5.5
//      Columns are:
//      [1]     month
//      [2]     relative change in monthly mean rainfall
//      [3]     relative change in duration of wet spell
//      [4]     relative change in duration of dry spell
//      [5]     absolute changes in monthly mean min temperature
//      [6]     absolute changes in monthly mean max temperature
//      [7]     relative changes in daily temperature variability
//      [8]     relative changes in mean monthly radiation
[VERSION]
LARS-WG5.5
[NAME]
Saskatoon_CGCM_RCP85_2071-2100
[BASELINE]
1975
[FUTURE]
2085
[GCM PREDICTIONS]
        Jan     1.29    1.28    0.92    0.00    0.00    1.00    1.00
        Feb     1.23    1.25    0.78    0.00    0.00    1.00    1.00
        Mar     2.12    1.81    0.79    0.00    0.00    1.00    1.00
        Apr     1.64    1.10    0.73    0.00    0.00    1.00    1.00
        May     1.50    0.99    0.71    0.00    0.00    1.00    1.00
        Jun     0.87    0.77    1.14    0.00    0.00    1.00    1.00
        Jul     0.69    0.84    1.49    0.00    0.00    1.00    1.00
        Aug     1.29    1.09    0.78    0.00    0.00    1.00    1.00
        Sep     0.94    1.05    0.91    0.00    0.00    1.00    1.00
        Oct     2.45    1.95    0.85    0.00    0.00    1.00    1.00
        Nov     1.39    1.30    0.79    0.00    0.00    1.00    1.00
        Dec     1.02    1.25    0.90    0.00    0.00    1.00    1.00
```

Figure B.2: Scenario file used in LARS-WG for the perturbation of parameter values obtained from the observed data

Table B. 1: Test statistics (KS-, t-, and f-statistics) with the corresponding p-values for the calibration of LARS-WG using observed daily precipitation during the baseline period (1961-1990) (printout from LARS-WG result output of the site analysis).

[VERSION]
LARS-WG5.5
[NAME]
Saskatoon
[LAT, LON and ALT]
52.13 -106.68 504.00
[KS-test for seasonal wet/dry SERIES distributions: Effective N, KS statistic and p-value]
DJF wet 12 0.106 0.9989
DJF dry 12 0.192 0.7436
MAM wet 12 0.288 0.2486
MAM dry 12 0.062 1.0000

JJA wet 12 0.031 1.0000
JJA dry 12 0.057 1.0000
SON wet 12 0.015 1.0000
SON dry 12 0.034 1.0000
[KS-test for daily RAIN distributions: Effective N, KS statistic and p-value]
J 12 0.424 0.0219
F 12 0.518 0.0024
M 12 0.398 0.0374
A 12 0.032 1.0000
M 12 0.224 0.5543
J 12 0.181 0.8052
J 12 0.183 0.7944
A 12 0.252 0.4025
S 12 0.270 0.3192
O 12 0.308 0.1845
N 12 0.046 1.0000
D 12 0.054 1.0000
[RAIN monthly mean & sd: obs mean & sd, gen mean & sd, t- and f- statistics with p-values]
15.93 12.87 15.99 19.69 43.46 63.47 58.33 36.84 32.13 16.50 13.87 17.56
8.794 8.956 9.921 14.772 32.319 35.682 31.723 23.830 17.909 15.760 10.210 7.378
15.81 14.42 17.65 23.30 42.83 53.25 63.18 36.15 28.65 17.47 16.87 15.41
6.946 8.999 10.229 14.389 26.221 34.993 41.769 22.633 19.596 16.305 12.123 7.528
0.063 -0.712 -0.677 -1.026 0.090 1.198 -0.532 0.123 0.764 -0.250 -1.095 1.193
0.950 0.479 0.501 0.308 0.929 0.235 0.597 0.902 0.447 0.803 0.278 0.237
1.603 1.010 1.063 1.054 1.519 1.040 1.734 1.109 1.197 1.070 1.410 1.041
0.168 0.992 0.875 0.867 0.222 0.898 0.127 0.754 0.620 0.859 0.339 0.922
[RAIN paired t-test for monthly means to detect bias: bias, t-statistic and p-value]
0.138 0.126 0.902
[RAIN daily maxima: obs and gen median, 95 percentile and maximum]
4.10 3.60 4.60 6.70 14.00 20.10 14.80 10.10 11.90 5.60 4.40 5.60
10.40 14.50 9.90 16.80 36.30 39.10 57.40 36.60 24.40 35.80 15.20 10.70
14.20 30.00 22.10 22.60 43.20 96.60 70.90 43.70 27.70 41.70 15.70 10.70
3.80 4.00 5.80 8.80 18.00 15.40 20.70 10.70 8.90 5.70 4.50 4.50
12.20 25.70 21.40 20.10 33.90 86.50 60.00 34.70 26.00 32.70 22.30 8.80
17.60 29.40 24.70 27.60 61.90 96.00 71.60 44.10 30.10 37.50 25.80 12.20

The following results are presented here with reference to section 4.2 of the thesis.

Table B. 2: Relative change factors for CanESM2 during 2041-2070.

	Mean monthly precipitation			Wet spell length			Dry spell length		
Month	RCP2.6	RCP4.5	RCP8.5	RCP2.6	RCP4.5	RCP8.5	RCP2.6	RCP4.5	RCP8.5
Jan	1.13	1.09	1.29	1.05	1.01	0.99	0.80	0.91	0.94
Feb	0.96	0.84	1.13	1.01	1.12	1.11	0.86	0.99	0.84
Mar	1.61	1.55	2.02	1.34	1.30	1.54	0.97	0.88	0.77
Apr	1.64	1.90	1.38	1.11	1.27	1.21	0.78	0.81	0.90
May	1.01	1.40	1.37	0.95	0.93	1.00	0.97	1.01	0.82
Jun	1.00	0.78	1.14	0.93	0.94	0.89	1.07	1.00	0.88
Jul	0.98	0.84	0.81	1.14	0.93	0.96	0.99	1.23	1.15
Aug	1.22	0.98	1.30	1.07	0.92	0.96	0.90	0.93	0.79
Sep	0.80	1.12	0.99	1.07	1.03	1.07	0.94	0.90	0.87
Oct	1.48	1.58	1.84	1.33	1.23	1.40	0.78	0.78	0.91
Nov	0.90	1.22	1.38	1.27	1.28	1.27	1.01	0.98	0.91
Dec	1.37	1.47	1.20	1.29	1.27	1.45	0.95	0.80	0.91

Table B. 3: Relative change factors for CanESM2 during 2071-2100.

	Mean monthly precipitation			Wet spell length			Dry spell length		
Month	RCP2.6	RCP4.5	RCP8.5	RCP2.6	RCP4.5	RCP8.5	RCP2.6	RCP4.5	RCP8.5
Jan	0.93	1.03	1.29	1.05	1.10	1.28	0.91	1.01	0.92
Feb	0.96	1.16	1.23	0.99	1.04	1.25	0.93	0.87	0.78
Mar	1.99	2.13	2.12	1.41	1.43	1.81	0.92	0.91	0.79
Apr	1.89	1.87	1.64	1.06	1.21	1.10	0.79	0.81	0.73
May	0.97	1.21	1.50	0.94	0.96	0.99	0.86	1.00	0.71
Jun	1.22	1.04	0.87	1.07	0.96	0.77	0.92	0.93	1.14
Jul	0.90	0.78	0.69	1.18	0.89	0.84	1.13	1.23	1.49
Aug	0.94	1.05	1.29	1.08	0.99	1.09	0.82	0.91	0.78
Sep	0.98	0.97	0.94	1.10	1.04	1.05	0.97	0.88	0.91
Oct	1.26	1.61	2.45	1.31	1.37	1.95	0.82	0.81	0.85
Nov	0.81	1.37	1.39	1.27	1.37	1.30	1.00	0.95	0.79
Dec	1.31	1.51	1.02	1.09	1.11	1.25	0.92	0.91	0.90

Table B. 4: Relative change factors for HadGEM2-ES during 2011-2040.

	Mean monthly precipitation			Wet spell length			Dry spell length		
Month	RCP2.6	RCP4.5	RCP8.5	RCP2.6	RCP4.5	RCP8.5	RCP2.6	RCP4.5	RCP8.5
Jan	1.24	1.01	1.37	1.05	0.72	1.04	1.10	0.90	0.88
Feb	1.17	1.06	1.13	0.76	1.06	0.94	0.90	0.87	0.94
Mar	1.17	1.00	1.09	0.90	0.58	0.81	1.18	1.20	1.29
Apr	1.48	1.05	1.36	0.96	0.85	0.88	0.93	1.17	1.07
May	0.97	1.03	0.79	0.82	0.89	0.91	1.28	1.22	1.40
Jun	0.74	0.98	1.00	0.76	0.88	0.78	1.01	0.93	0.74
Jul	0.91	0.92	1.24	0.81	0.81	1.00	1.01	1.04	0.94
Aug	0.82	0.90	1.00	0.94	1.20	1.20	1.13	1.20	1.11
Sep	1.46	1.26	1.68	0.97	0.97	1.11	1.08	0.88	1.03
Oct	1.48	1.02	1.29	1.01	0.79	1.07	0.98	1.04	1.30
Nov	1.01	0.83	1.08	1.02	0.82	1.07	0.98	1.03	1.10
Dec	1.08	1.11	1.14	1.00	1.19	0.88	0.94	1.17	1.01

Table B. 5: Relative change factors for HadGEM2-ES during 2041-2070.

	Mean monthly precipitation			Wet spell length			Dry spell length		
Month	RCP2.6	RCP4.5	RCP8.5	RCP2.6	RCP4.5	RCP8.5	RCP2.6	RCP4.5	RCP8.5
Jan	1.11	1.07	1.13	0.94	1.13	0.97	0.86	0.81	1.06
Feb	0.96	1.04	1.37	0.82	1.20	1.39	0.98	0.94	0.89
Mar	1.37	1.47	1.62	0.80	0.95	0.86	1.17	1.27	1.57
Apr	1.31	1.47	1.66	1.06	1.18	1.18	0.95	0.98	1.14
May	1.19	1.19	1.47	0.83	0.95	0.87	1.26	1.12	1.17
Jun	0.96	0.98	1.10	0.78	0.81	0.77	0.99	0.83	0.93
Jul	1.06	0.84	0.76	0.84	0.79	0.75	1.03	1.03	1.05
Aug	1.00	0.78	0.85	0.95	0.93	0.94	1.05	1.20	1.27
Sep	1.48	1.08	1.63	0.89	0.80	0.99	1.00	1.29	1.11
Oct	1.46	1.57	1.05	1.08	1.13	0.89	1.09	1.04	1.19
Nov	1.19	1.35	1.21	0.93	0.81	1.13	1.06	0.94	0.84
Dec	1.13	1.05	1.18	1.31	0.97	1.51	0.84	1.08	0.86

Table B. 6: Relative change factors for HadGEM2-ES during 2071-2100.

	Mean monthly precipitation			Wet spell length			Dry spell length		
Month	RCP2.6	RCP4.5	RCP8.5	RCP2.6	RCP4.5	RCP8.5	RCP2.6	RCP4.5	RCP8.5
Jan	1.24	1.33	1.06	1.04	0.87	0.76	0.87	1.10	0.75
Feb	1.12	1.21	1.36	0.87	1.09	0.61	0.90	0.96	0.94
Mar	1.00	1.22	1.59	0.98	0.55	0.59	1.11	1.49	1.19
Apr	1.40	1.55	1.63	0.84	0.82	1.07	1.13	1.22	1.07
May	1.14	1.21	0.84	0.90	0.75	0.52	1.12	1.07	1.38
Jun	1.17	0.89	0.94	0.85	0.70	0.62	0.83	1.01	0.96
Jul	1.01	0.68	0.60	0.73	0.80	0.64	0.89	1.01	1.11
Aug	0.76	0.95	0.63	1.07	1.00	0.89	1.15	1.08	1.19
Sep	1.62	0.99	1.12	1.09	0.78	0.93	0.96	1.13	0.98
Oct	1.47	1.22	1.74	0.99	0.81	0.86	1.13	1.21	1.06
Nov	1.05	1.45	1.41	1.26	1.13	1.17	0.90	0.96	0.90
Dec	1.08	1.22	1.30	1.08	1.11	1.18	0.86	1.02	1.10

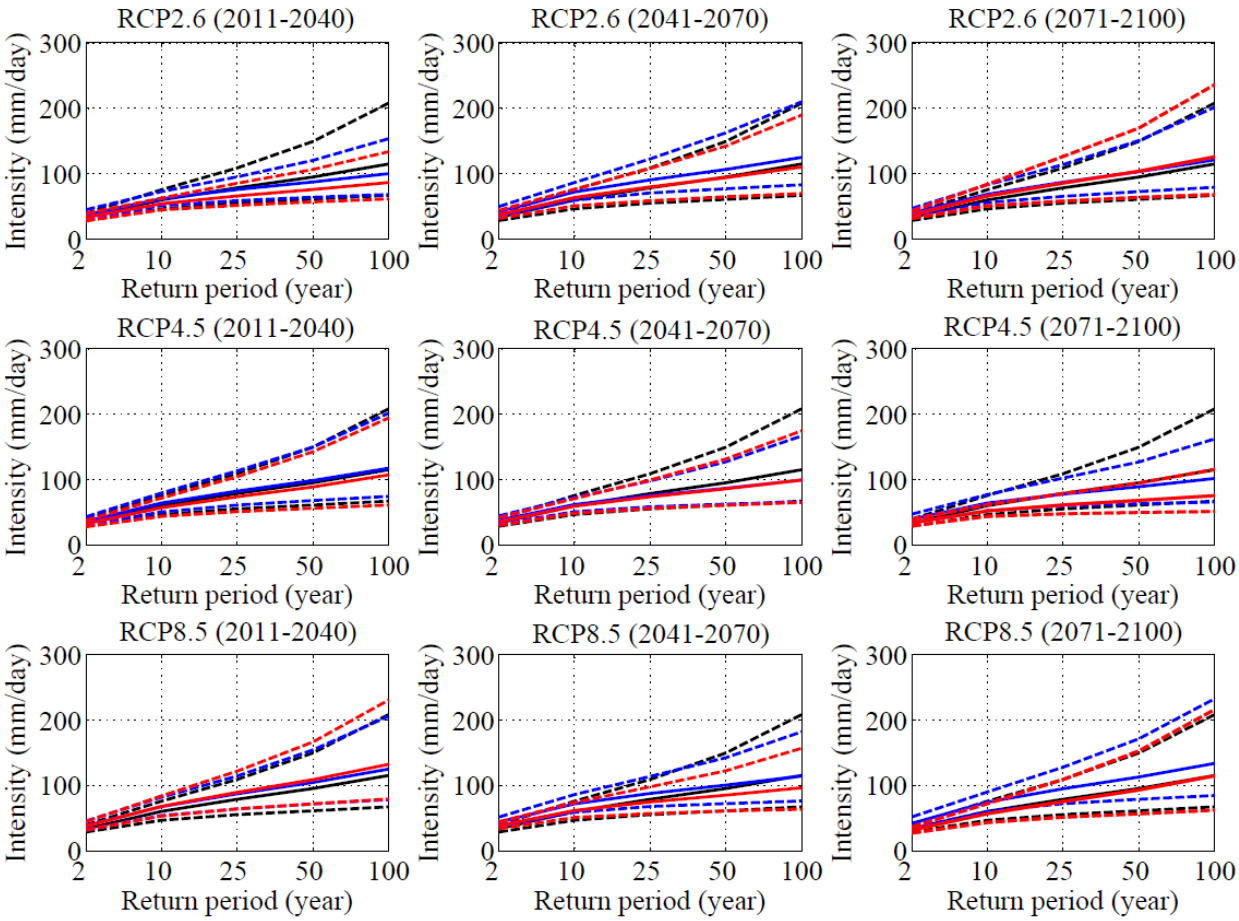

Figure B.3: Variations in the future projections of daily AMP quantiles in the City of Saskatoon according to HadGEM2-ES forced with three RCPs using two sets of change factors: with wet/dry spell (blue) and without wet/dry spell (red) effects. The expected quantiles (solid lines) and their 95% confidence intervals (dashed lines) are shown with the corresponding quantiles during the baseline period (black).

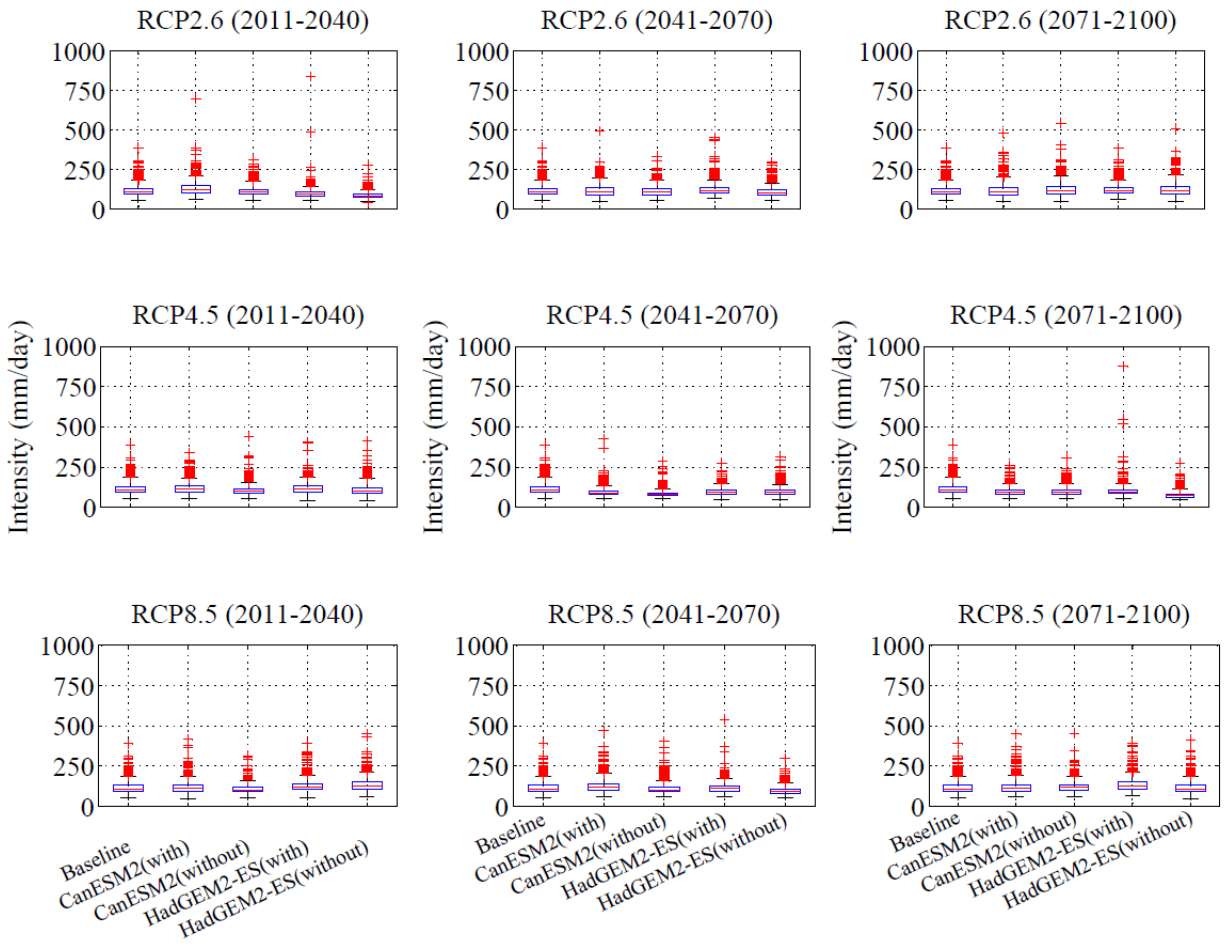

Figure B.4: Variations in the future projections of daily expected quantiles for **100-year** return period in the City of Saskatoon according to CanESM2 and HadGEM2-ES forced with three RCPs using two sets of change factors, i.e. with wet/dry spell and without wet/dry spell effects along with the corresponding daily expected quantiles during the baseline.

Appendix C

An attempt was made in this study to investigate the homogeneity of sub-hourly precipitation data recorded at four rain-gauges in the City of Saskatoon during the period 1992-2009 with missing records during 2002-2004. An attempt was also made to identify the representative rain gauge for the City of Saskatoon by evaluating the consistency between the rain gauges with comparison to the Environment Canada (EC) daily precipitation data during the same period. Please refer to section 3.1 of this thesis.

C.1 Double mass curve analysis

Analysis of double mass curves was conducted for each of the four rain gauges to investigate the homogeneity of precipitation records over the period of operation. The double mass curves of the four rain gauges against EC measurement station show some fluctuations in the corresponding slopes. There are more fluctuations in slopes of the City Hall, the Diefenbaker Fire Hall (i.e., Diefenbaker), and the Warman Fire Hall (i.e., Warman) stations than that of the Acadia Reservoir rain gauge (i.e., Acadia). The slope of the Acadia record suggests that this gauge record might be more consistent with the EC data and thus, it might represent a reliable sub-hourly data series for the City of Saskatoon. Other rain gauges, i.e., City Hall, Diefenbaker, and Warman contain substantial missing data in their records, which is approximately 19% each, whereas Acadia gauge has 11% missing data during the period of sub-hourly precipitation record. The amount of missing data seems to affect the fluctuations in the slopes of the corresponding rain gauges. The comparison of double mass curves among the rain gauges in Figure C.1 shows that Diefenbaker and Warman gauges might be consistent in recording sub-hourly precipitation, while no other two rain gauges seem to demonstrate such consistency. Examination of Figure C.1 reveals that the Acadia gauge seems to keep consistency with EC precipitation record in the early few years, and later deviated from that trend during the last few years due to underestimation. On the other hand, the remaining three rain gauges seem to underestimate the EC precipitation values except in 1992 and part of 1993.

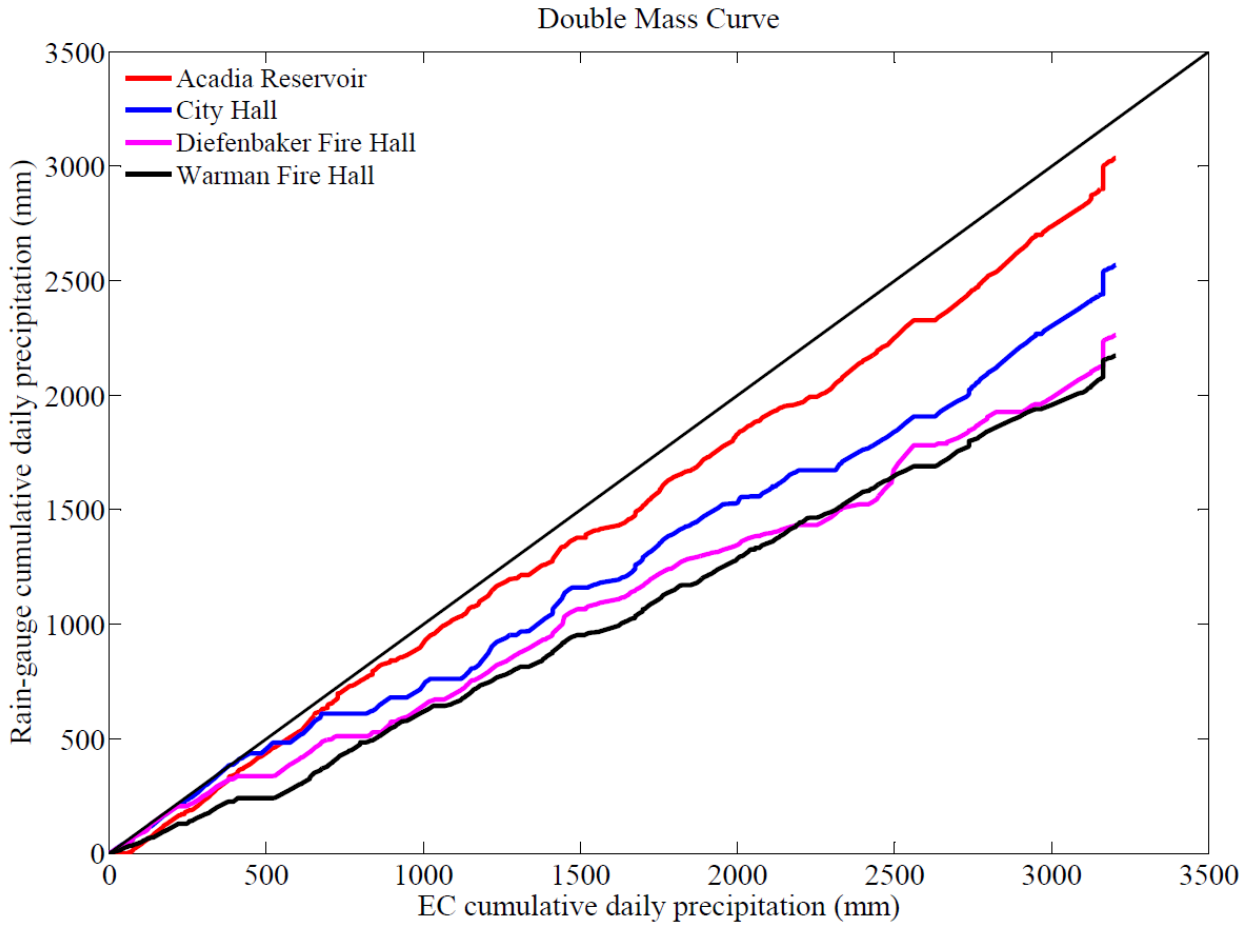

Figure C.1: Double mass curve of cumulative precipitation (mm)

C.2 Efficiency of rain-gauges as compared to EC records

The rain gauges seem to underestimate the annual total precipitation of EC in most of the years except in 1993, 1994, 2006 and 2007 where Acadia overestimated the EC annual total precipitation (Figure C.2). Overall, Acadia seems to estimate the annual total EC values better than the other rain gauges in most of the years, although some of the rain gauges estimate EC annual total precipitation quite closely in some years.

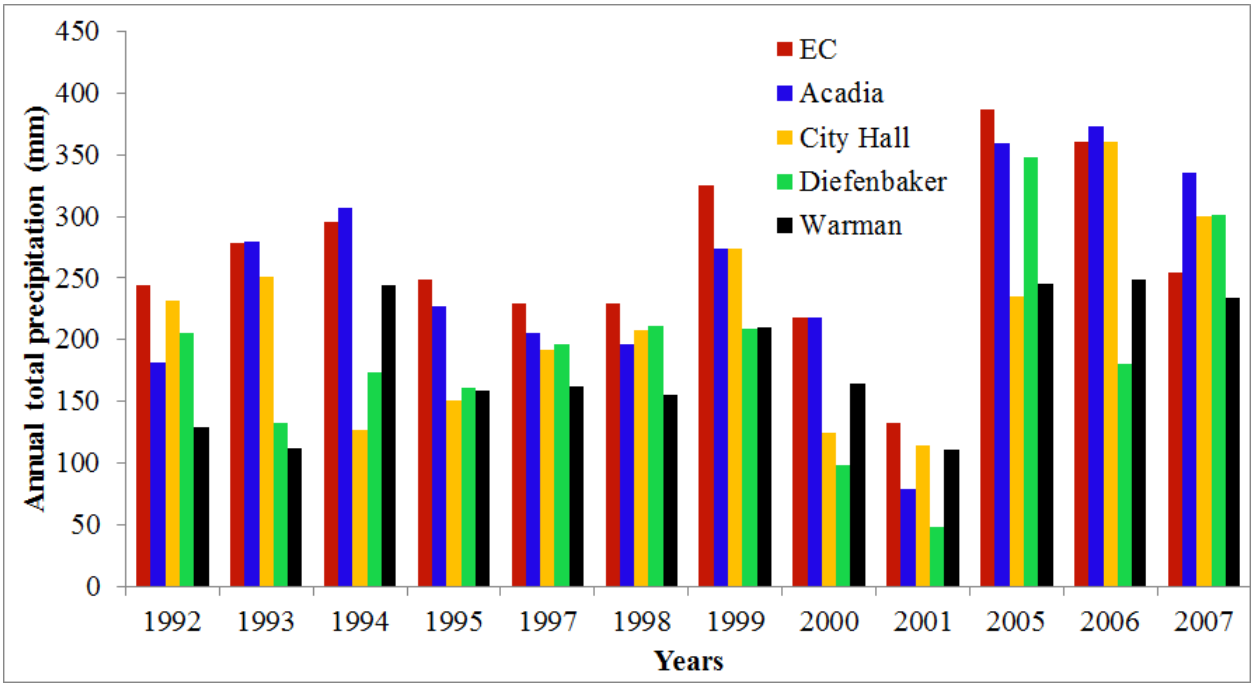

Figure C.2: Annual precipitation obtained from EC daily and Saskatoon's rain gauge sub-hourly precipitation data.

C.3 Tukey's multiple comparison test

The differences of mean between Diefenbaker-Acadia (D-A) and Warman-Acadia (W-A) rain-gauges are significant at 10% significance level, since the p-values are less than 0.10. Also the differences of mean between Environment Canada-Diefenbaker (E-D) and Warman-Environment Canada (W-E) are significant at 10% significance level since the p-values are less than 0.10 in Table C.1. Figure C.3 shows that the differences in mean levels for C-A, E-C, D-C, W-C and W-D rain gauges includes the zero-line within their intervals and so, the differences may become zero anytime leading to a non-significant difference between two means at 10% significance level. But the differences in the results between Diefenbaker and Acadia; and Warman and Acadia are comparatively large with the highest difference between Warman and Acadia (W and A) rain gauges. As compared to EC data, the differences in the mean between EC and Diefenbaker; and EC and Warman are comparatively large with the highest difference occurs between Warman and EC (W and EC) rain gauges. Overall, Acadia has the lowest difference in the mean in comparison to EC, which is also suggested by the corresponding p-value (i.e. p-value>>0.10).

Table C.1: Results of Tukey's test for comparison between differences in multiple means

Stations	Difference in mean	Lower limit	Upper limit	p-value
City Hall-Acadia	-0.209	-0.542	0.123	0.529
Diefenbaker-Acadia	-0.346	-0.678	-0.014	0.077
Environment Canada-Acadia	0.075	-0.257	0.408	0.981
Warman-Acadia	-0.386	-0.719	-0.054	0.034
Diefenbaker-City Hall	-0.137	-0.469	0.195	0.850
Environment Canada -City Hall	0.285	-0.047	0.617	0.216
Warman-City Hall	-0.177	-0.509	0.155	0.685
Environment Canada-Diefenbaker	0.422	0.089	0.754	0.016
Warman-Diefenbaker	-0.040	-0.372	0.292	0.100
Warman- Environment Canada	-0.462	-0.794	-0.129	0.006

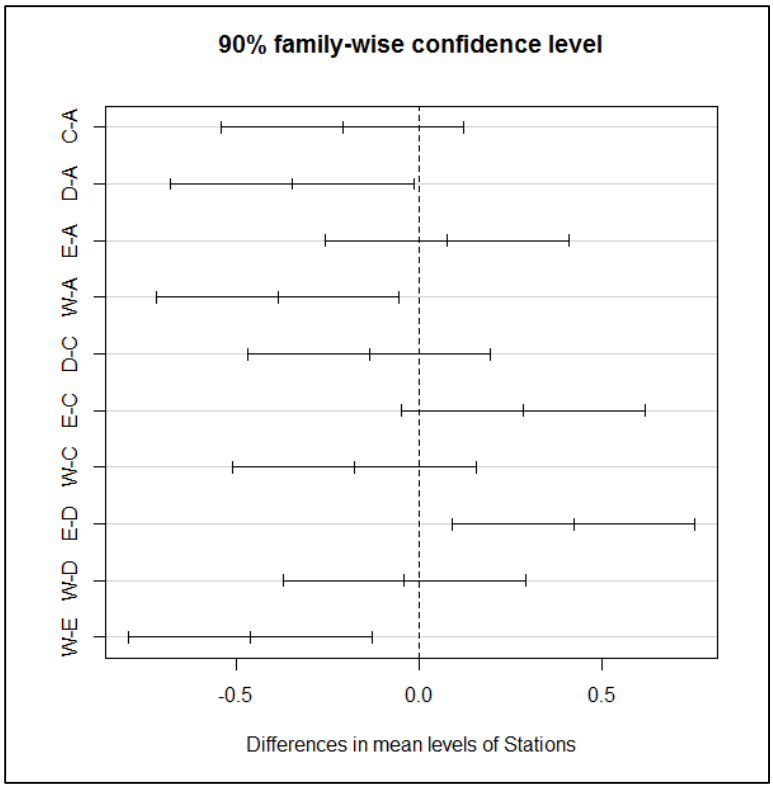

Figure C.3: Differences in mean precipitation between the rain-gauges and EC station

C.4 Extreme precipitation of the City rain gauges

The extreme precipitation can be analyzed by the identification of annual maximum precipitation of various temporal resolutions at the four rain gauges in Saskatoon. The annual maximum precipitation of different temporal resolutions (i.e., daily, 1-hour, 15-min, and 5-min) at each of the four rain gauges and the EC's daily precipitation at Diefenbaker Airport Station were used to compare the variability in the extreme precipitation (Figure C.4). It is apparent from the previous results shown in Figures C.1 to C.3 that Acadia rain gauge is more consistent with the EC daily precipitation data than other rain gauges in the city. However, the remaining three rain gauges seem to perform quite similar to Acadia in terms of median and inter-quartile ranges of the corresponding extreme precipitation values. The median and inter-quartile ranges of the rain gauges fall within the inter-quartile range of the EC station in case of daily precipitation. The medians of extreme precipitation values at the rain gauges were not significantly different from each other in cases of other temporal resolutions. The annual maximum precipitation of 5-minute resolution at Acadia rain gauge shows quite similar variability as that of other rain gauges. However, the annual maximum precipitation of other temporal resolutions at Acadia rain gauge shows more variability than those of other rain gauges.

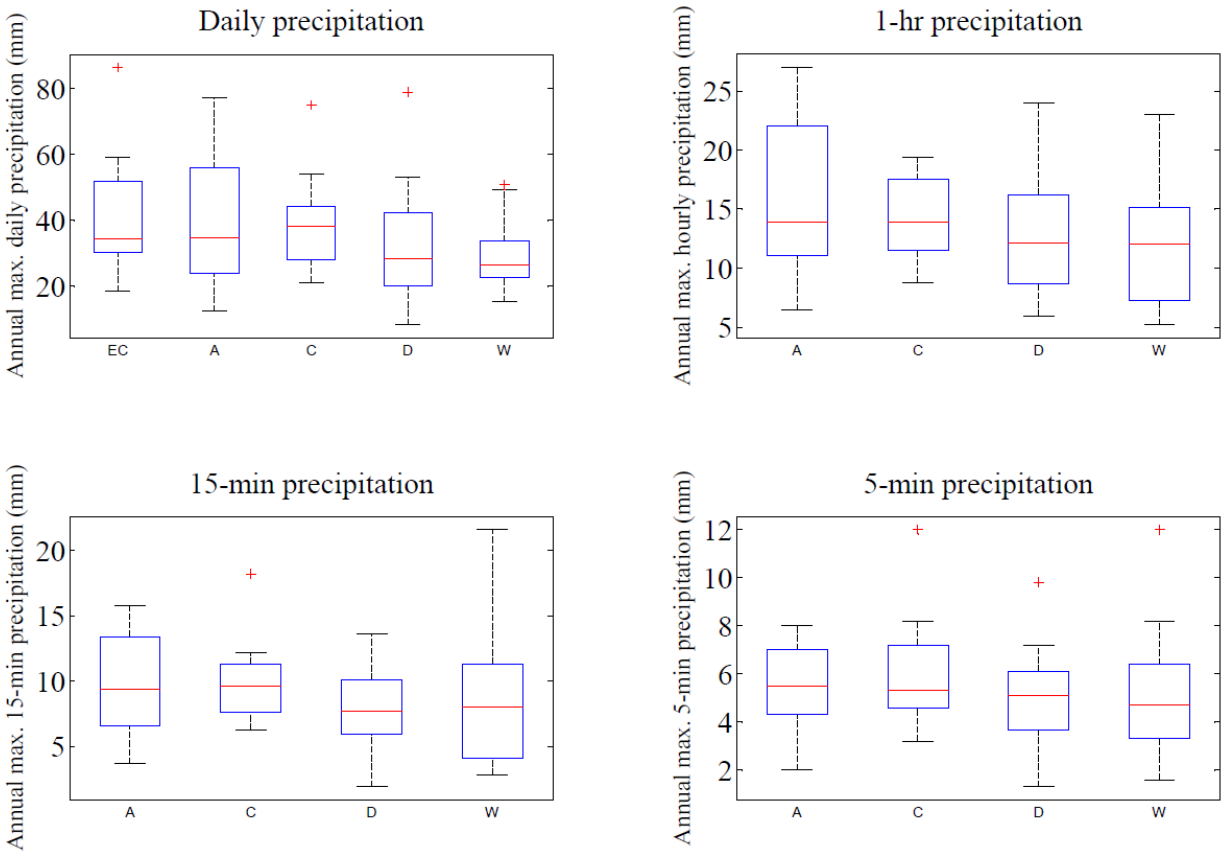

Figure C.4: Annual maximum precipitation of different temporal resolutions at the city rain gauges; A: Acadia, EC: Environment Canada, C: City hall, D: Diefenbaker, and W: Warman

The analysis of double mass curve and other performance evaluation criteria show that the Acadia rain gauge might be more reliable showing higher consistency with EC data having mean value, which is not significantly different from the EC mean precipitation value. Therefore, the sub-hourly precipitation data from Acadia rain gauge was considered for the hydrological study in the City of Saskatoon.

Appendix D

A detailed explanation of the GP method implementation with setting internal parameters of the model is provided below with reference to section 3.2.5.

Table D.1: Internal parameters used in the GP search for extracting equations representing the relationships between the AMPs at the GCM (CanESM2 and HadGEM2) and the local scales

GP parameter	Type of parameter	Value
Inicmaxlevel	Variable parameters (internal settings)	19, 20
Dynamiclevel		24, 25, 26
Realmaxlevel		30, 32, 35
Minprob		0.025, 0.08
Mathematical operations	Fixed parameters	{+, -, x, /, exp(x), x^2}
Terminal		24

Table D.2: Internal parameters used in the GP search for extracting equations representing the relationships between the AMPs at the GCM (CGCM3.1) and the local scales

GP parameter	Type of parameter	Value
Inicmaxlevel	Variable parameters (internal settings)	17, 18
Dynamiclevel		23, 24
Realmaxlevel		29, 30
Minprob		0.025, 0.08
Mathematical operations	Fixed parameters	{+, -, x, /, exp(x), x^2}
Terminal		24

Table D.3: Equations extracted from GP based on CanESM2 and their performance statistics for training, validation and testing data sets

Duration (h)	Equations	Training				Validation				Testing			
		RMSE	R	MB	MARE	RMSE	R	MB	MARE	RMSE	R	MB	MARE
1	$Q_{Local}(x)=(Q_{GCM}(x)-24/Q_{GCM}(x)^2-2)(23-Q_{GCM}(x)/\exp(Q_{GCM}(x)/24)+Q_{GCM}(x)/8)$	1.02	1.00	-0.24	0.02	0.67	1.00	-0.28	0.02	4.32	0.96	0.33	0.07
2	$Q_{Local}(x)=Q_{GCM}(x)^2/24+(36Q_{GCM}(x)+11Q_{GCM}(x)^2)/(Q_{GCM}(x)+12)+24$	0.39	1.00	0.07	0.01	0.22	1.00	0.08	0.01	2.20	0.97	0.34	0.07
3	$Q_{Local}(x)=10Q_{GCM}(x)+\exp(24/Q_{GCM}(x))-48$	0.14	1.00	-0.03	0.01	0.11	1.00	-0.03	0.01	1.29	0.97	0.09	0.07
4	$Q_{Local}(x)=119Q_{GCM}(x)/24+2.7183Q_{GCM}(x)-\exp(24/Q_{GCM}(x))-24$	0.14	1.00	0.02	0.01	0.10	1.00	0.02	0.01	1.00	0.98	0.12	0.08
5	$Q_{Local}(x)=145Q_{GCM}(x)/24-Q_{GCM}(x)^2/288-\exp(24/Q_{GCM}(x)+1)$	0.13	1.00	-0.01	0.02	0.12	1.00	-0.01	0.02	0.87	0.97	0.06	0.08
6	$Q_{Local}(x)=31Q_{GCM}(x)/6-Q_{GCM}(x)^2/192-\exp(24/Q_{GCM}(x))-1)$	0.19	1.00	-0.02	0.04	0.19	1.00	-0.03	0.04	0.74	0.97	0.04	0.09
7	$Q_{Local(x)}=4Q_{GCM}(x)-\exp(Q_{GCM}(x)/24)/Q_{GCM}(x)+576/Q_{GCM}(x)\exp(24/(\exp(\exp(Q_{GCM}(x)/24))))$	0.27	0.99	0.05	0.05	0.26	0.99	0.04	0.05	0.66	0.97	0.09	0.10
8	$Q_{Local}(x)=576/Q_{GCM}(x)^2+3Q_{GCM}(x)-576/Q_{GCM}(x)-\exp(Q_{GCM}(x)/24)/Q_{GCM}(x)+46$	0.16	1.00	0.01	0.01	0.14	1.00	0.00	0.02	0.60	0.96	0.05	0.10
9	$Q_{Local}(x)=3Q_{GCM}(x)+24Q_{GCM}(x)^2/(Q_{GCM}(x)^2+576)+(24Q_{GCM}(x)-Q_{GCM}(x)^2)/(576-Q_{GCM}(x))$	0.14	1.00	0.04	0.03	0.13	1.00	0.04	0.03	0.57	0.96	0.08	0.09
10	$Q_{Local}(x)=3Q_{GCM}(x)+Q_{GCM}(x)^2/24\exp(Q_{GCM}(x)/24)+Q_{GCM}(x)/24-Q_{GCM}(x)^2/288$	0.10	1.00	-0.04	0.03	0.10	1.00	-0.04	0.03	0.51	0.96	-0.01	0.08
11	$Q_{Local}(x)=25Q_{GCM}(x)/12-Q_{GCM}(x)^2/576+\exp(24/Q_{GCM}(x))-576/Q_{GCM}(x)+47$	0.09	1.00	0.03	0.02	0.08	1.00	0.03	0.02	0.50	0.95	0.06	0.08
12	$Q_{Local}(x)=2Q_{GCM}(x)-Q_{GCM}(x)^2/288-552/Q_{GCM}(x)+47$	0.11	1.00	0.07	0.04	0.11	1.00	0.07	0.04	0.47	0.94	0.09	0.10
13	$Q_{Local}(x)=29Q_{GCM}(x)/24+(Q_{GCM}(x)^2+48Q_{GCM}(x))/(Q_{GCM}(x)+24+\exp(Q_{GCM}(x)/24))$	0.14	0.99	0.04	0.05	0.14	0.99	0.03	0.06	0.39	0.96	0.05	0.08
14	$Q_{Local}(x)=Q_{GCM}(x)+24\exp(1-24/Q_{GCM}(x))+24Q_{GCM}(x)^2/(576+Q_{GCM}(x)^2)+2.7183$	0.05	1.00	0.00	0.01	0.04	1.00	0.00	0.01	0.37	0.94	0.01	0.09
15	$Q_{Local}(x)=(576-Q_{GCM}(x)^2/12-3Q_{GCM}(x))/(\exp(\exp(24/Q_{GCM}(x)))+24)+2Q_{GCM}(x)$	0.06	1.00	0.03	0.02	0.07	1.00	0.03	0.03	0.38	0.94	0.05	0.10
16	$Q_{Local}(x)=(Q_{GCM}(x)-8)(48-Q_{GCM}(x)+1152/Q_{GCM}(x))/192+2Q_{GCM}(x)$	0.08	1.00	0.02	0.03	0.08	1.00	0.02	0.03	0.33	0.95	0.03	0.08
17	$Q_{Local}(x)=(48-Q_{GCM}(x)+24/Q_{GCM}(x))/\exp(48/Q_{GCM}(x))+24/(\exp(24/Q_{GCM}(x))+Q_{GCM}(x))+2Q_{GCM}(x)$	0.04	1.00	0.00	0.01	0.03	1.00	0.00	0.01	0.30	0.95	0.01	0.07
18	$Q_{Local}(x)=(24Q_{GCM}(x)-576)/(\exp(Q_{GCM}(x)/24)+24)+25Q_{GCM}(x)/24-24/Q_{GCM}(x)+25$	0.06	1.00	0.02	0.02	0.06	1.00	0.03	0.02	0.27	0.96	0.03	0.02
19	$Q_{Local}(x)=((6912+48Q_{GCM}(x)^3)/Q_{GCM}(x))/(Q_{GCM}(x)^2+576)+Q_{GCM}(x)$	0.03	1.00	0.00	0.01	0.03	1.00	0.00	0.01	0.28	0.95	0.01	0.07
20	$Q_{Local}(x)=23Q_{GCM}(x)/24+331776Q_{GCM}(x)/(25Q_{GCM}(x)^2+576Q_{GCM}(x)+331776)$	0.03	1.00	0.00	0.02	0.03	1.00	0.00	0.02	0.25	0.96	0.01	0.07
21	$Q_{Local}(x)=48/\exp(24/Q_{GCM}(x))+\exp(1-Q_{GCM}(x)^4\exp(Q_{GCM}(x)/24-24))+Q_{GCM}(x)$	0.03	1.00	-0.01	0.01	0.02	1.00	-0.01	0.01	0.26	0.95	0.00	0.07
22	$Q_{Local}(x)=Q_{GCM}(x)-\exp(24/Q_{GCM}(x))-\exp(2Q_{GCM}(x)/(Q_{GCM}(x)+24))+(24Q_{GCM}(x)-576)/(24+Q_{GCM}(x))+24$	0.06	1.00	0.00	0.02	0.05	1.00	0.00	0.02	0.25	0.95	0.02	0.06
23	$Q_{Local}(x)=(48-(96Q_{GCM}(x)-576)/(576-Q_{GCM}(x)))/\exp(24/Q_{GCM}(x))+Q_{GCM}(x)$	0.02	1.00	0.02	0.01	0.02	1.00	0.02	0.01	0.24	0.95	0.03	0.07
24	$Q_{Local}(x)=24Q_{GCM}(x)/(\exp(\exp(Q_{GCM}(x)/576))(\exp(Q_{GCM}(x)/24+1)+24))+Q_{GCM}(x)+24/\exp(24/Q_{GCM}(x))$	0.05	1.00	-0.01	0.01	0.03	1.00	-0.01	0.01	0.22	0.95	0.00	0.07

Units of RMSE and MB are mm/hr.

Table D.4: Equations extracted from GP based on HadGEM2-ES and their performance statistics for training, validation and testing data sets

Duration (h)	Equations	Training				Validation				Testing			
		RMSE	R	MB	MARE	RMSE	R	MB	MARE	RMSE	R	MB	MARE
1	$Q_{Local}(x)=3Q_{GCM}(x)+Q_{GCM}(x)\exp(1+Q_{GCM}(x)/24)-\exp(49Q_{GCM}(x)/576)+73$	1.20	1.00	0.16	0.01	1.02	1.00	0.15	0.01	46.35	0.94	0.49	0.07
2	$Q_{Local}(x)=Q_{GCM}(x)^3/288+4Q_{GCM}(x)-48/Q_{GCM}(x)+72$	0.39	1.00	-0.07	0.03	0.27	1.00	-0.09	0.03	1.94	0.97	0.04	0.08
3	$Q_{Local}(x)=71Q_{GCM}(x)/12+23Q_{GCM}(x)^3/13824+1$	0.06	1.00	0.02	0.01	0.06	1.00	0.02	0.01	1.17	0.97	0.08	0.06
4	$Q_{Local}(x)=48Q_{GCM}(x)^2/(552-2Q_{GCM}(x)-7.3891)+2Q_{GCM}(x)+31.3891$	0.17	1.00	-0.04	0.03	0.17	1.00	-0.05	0.03	0.70	0.98	-0.01	0.06
5	$Q_{Local}(x)=Q_{GCM}(x)^2/12+(Q_{GCM}(x)-24)/\exp(Q_{GCM}(x)/12)+Q_{GCM}(x)/\exp(8/(Q_{GCM}(x)+8))+Q_{GCM}(x)+24$	0.08	1.00	0.04	0.01	0.06	1.00	0.03	0.01	0.60	0.98	0.05	0.06
6	$Q_{Local}(x)=(27Q_{GCM}(x)+\exp(Q_{GCM}(x)/24)+600)(Q_{GCM}(x)+1)./576+2Q_{GCM}(x)$	0.05	1.00	0.01	0.01	0.04	1.00	0.01	0.01	0.58	0.98	0.02	0.08
7	$Q_{Local(x)}=(21Q_{GCM}(x)^2+1632Q_{GCM}(x)+1152)./576$	0.02	1.00	0.01	0.00	0.02	1.00	0.01	0.00	0.53	0.97	0.02	0.08
8	$Q_{Local}(x)=Q_{GCM}(x)2/(48-Q_{GCM}(x)^2/(1152-Q_{GCM}(x)))+71Q_{GCM}(x)/24$	0.03	1.00	-0.01	0.01	0.03	1.00	-0.01	0.01	0.49	0.97	0.01	0.08
9	$Q_{Local}(x)=Q_{GCM}(x)^2/48+2.5Q_{GCM}(x)+\exp(1-Q_{GCM}(x)/24)+\exp(Q_{GCM}(x)/24)/24+\exp(Q_{GCM}(x)/24)$	0.01	1.00	0.00	0.00	0.01	1.00	0.00	0.00	0.43	0.97	0.01	0.08
10	$Q_{Local}(x)=(Q_{GCM}(x)-2.7138)(Q_{GCM}(x)-24)/48+70Q_{GCM}(x)/24$	0.05	1.00	0.02	0.01	0.04	1.00	0.02	0.01	0.38	0.97	0.02	0.07
11	$Q_{Local}(x)=3Q_{GCM}(x)+(23Q_{GCM}(x)^2+Q_{GCM}(x)3)/13824-24/\exp(\exp(24/Q_{GCM}(x)^2))$	0.06	1.00	0.03	0.02	0.06	1.00	0.03	0.02	0.37	0.97	0.03	0.08
12	$Q_{Local}(x)=3Q_{GCM}(x)-24Q_{GCM}(x)/(\exp(Q_{GCM}(x)/12)+2Q_{GCM}(x)-24+576/Q_{GCM}(x))$	0.05	1.00	-0.01	0.01	0.05	1.00	0.00	0.01	0.33	0.97	0.00	0.07
13	$Q_{Local}(x)=(Q_{GCM}(x)^2-Q_{GCM}(x)\exp(1/(24-\exp(Q_{GCM}(x)/24))))/(Q_{GCM}(x)+24)+45Q_{GCM}(x)/23$	0.03	1.00	0.00	0.01	0.03	1.00	0.00	0.01	0.32	0.97	0.00	0.07
14	$Q_{Local}(x)=69Q_{GCM}(x)/24+24/\exp(Q_{GCM}(x)/24)-23$	0.03	1.00	0.01	0.01	0.03	1.00	0.01	0.01	0.28	0.97	0.01	0.07
15	$Q_{Local}(x)=Q_{GCM}(x)2/144+2Q_{GCM}(x)+1/\exp(Q_{GCM}(x)/12)$	0.01	1.00	0.00	0.00	0.01	1.00	0.00	0.00	0.30	0.96	0.00	0.07
16	$Q_{Local}(x)=1-((5Q_{GCM}(x)-24)(24-Q_{GCM}(x)))/576+\exp(Q_{GCM}(x)/24)/24+2Q_{GCM}(x)$	0.01	1.00	0.00	0.00	0.01	1.00	0.01	0.00	0.29	0.96	0.01	0.07
17	$Q_{Local}(x)=((3Q_{GCM}(x)-96)(\exp(Q_{GCM}(x)/24)+2Q_{GCM}(x)-24))/576+2Q_{GCM}(x)$	0.02	1.00	-0.01	0.01	0.01	1.00	-0.01	0.01	0.25	0.97	0.00	0.06
18	$Q_{Local}(x)=45Q_{GCM}(x)/24-Q_{GCM}(x)(24-Q_{GCM}(x))(24+Q_{GCM}(x))/13824$	0.04	1.00	0.00	0.01	0.04	1.00	0.00	0.01	0.24	0.97	0.00	0.05
19	$Q_{Local}(x)=727.4067Q_{GCM}(x)/(387.7032-Q_{GCM}(x))-121Q_{GCM}(x)/576$	0.05	1.00	-0.01	0.02	0.05	1.00	-0.01	0.02	0.23	0.96	-0.01	0.06
20	$Q_{Local}(x)=25Q_{GCM}(x)/24+Q_{GCM}(x)^2/1152+(Q_{GCM}(x)^3/72+24Q_{GCM}(x))/(Q_{GCM}(x)+24)-1$	0.02	1.00	0.01	0.01	0.02	1.00	0.01	0.10	0.22	0.97	0.01	0.06
21	$Q_{Local}(x)=(Q_{GCM}(x)\exp(Q_{GCM}(x)/24)-24Q_{GCM}(x))/(0.5Q_{GCM}(x)+47.9765)+2Q_{GCM}(x)$	0.04	1.00	-0.01	0.02	0.05	1.00	0.00	0.02	0.23	0.96	-0.04	0.06
22	$Q_{Local}(x)=0.5\exp(1+Q_{GCM}(x)/24-576/(Q_{GCM}(x)^2+24Q_{GCM}(x)))+1.5Q_{GCM}(x)-0.25$	0.04	1.00	0.00	0.02	0.04	1.00	0.00	0.02	0.22	0.96	0.00	0.06
23	$Q_{Local}(x)=2Q_{GCM}(x)-(Q_{GCM}(x)-21.28)/(\exp(Q_{GCM}(x)/24)+24/Q_{GCM}(x))-$	0.03	1.00	0.00	0.00	0.03	1.00	0.00	0.00	0.20	0.96	0.00	0.06
24	$Q_{Local}(x)=(2Q_{GCM}(x)^3-4Q_{GCM}(x)^2+192Q_{GCM}(x))/(Q_{GCM}(x)^2+120Q_{GCM}(x)-576)+Q_{GCM}(x)$	0.04	1.00	0.00	0.02	0.04	1.00	0.00	0.02	0.19	0.96	0.00	0.06

Units of RMSE and MB are mm/hr.

Table D.5: Equations extracted from GP based on CGCM3.1 and their performance statistics for training, validation and testing data sets

Duration (h)	Equations	Training				Validation				Testing			
		RMSE	R	MB	MARE	RMSE	R	MB	MARE	RMSE	R	MB	MARE
1	$Q_{Local}(x)=0.31482Q_{GCM}(x)^2+0.31482Q_{GCM}(x)\exp(Q_{GCM}(x)/24-\exp(24/Q_{GCM}(x)))+96$	2.39	0.99	-0.20	0.10	2.29	1.00	-0.11	0.10	3.14	0.97	0.07	0.16
2	$Q_{Local}(x)=Q_{GCM}(x)^2/6+0.90558/\exp(-0.03773(24+Q_{GCM}(x)))+83.36069$	0.97	0.99	0.13	0.07	0.91	1.00	0.13	0.07	1.78	0.97	0.29	0.12
3	$Q_{Local}(x)=Q_{GCM}(x)^2/12+2Q_{GCM}(x)+24/Q_{GCM}(x)+\exp(Q_{GCM}(x)/24)+50$	0.23	1.00	0.04	0.02	0.21	1.00	0.04	0.02	1.44	0.96	0.13	0.11
4	$Q_{Local}(x)=(Q_{GCM}(x)+24)^2/24+Q_{GCM}(x)+Q_{GCM}(x)/8+\exp(Q_{GCM}(x)/24)$	0.14	1.00	0.01	0.00	0.09	1.00	0.01	0.00	1.30	0.95	0.06	0.11
5	$Q_{Local}(x)=24/(Q_{GCM}(x)/24+24/Q_{GCM}(x))+25Q_{GCM}(x)/24+24+Q_{GCM}(x)(24+Q_{GCM}(x))/24$	0.11	1.00	-0.04	0.02	0.12	1.00	-0.05	0.02	1.05	0.95	0.01	0.11
6	$Q_{Local}(x)=4Q_{GCM}(x)+(576/Q_{GCM}(x)+Q_{GCM}(x))/\exp(24/\exp(Q_{GCM}(x)/24))+\exp(Q_{GCM}(x)-24)/24))$	0.12	1.00	0.01	0.03	0.12	1.00	0.01	0.03	0.90	0.94	0.04	0.12
7	$Q_{Local(x)}=3Q_{GCM}(x)+(Q_{GCM}(x)^2-Q_{GCM}(x)+24)/(48+Q_{GCM}(x))+48\exp(Q_{GCM}(x)/24)/Q_{GCM}(x)$	0.10	1.00	-0.01	0.02	0.11	1.00	0.00	0.02	0.76	0.94	0.01	0.13
8	$Q_{Local}(x)=Q_{GCM}(x)^2/288+3Q_{GCM}(x)+72/Q_{GCM}(x)$	0.12	1.00	0.01	0.02	0.11	1.00	0.01	0.02	0.69	0.94	0.03	0.13
9	$Q_{Local}(x)=3Q_{GCM}(x)+72/Q_{GCM}(x)+(\exp(Q_{GCM}(x)/24)-72)Q_{GCM}(x)/576$	0.13	1.00	-0.03	0.02	0.14	1.00	-0.02	0.02	0.67	0.93	-0.01	0.13
10	$Q_{Local}(x)=3Q_{GCM}(x)+24Q_{GCM}(x)/(72+2\exp(24-Q_{GCM}(x))+\exp(Q_{GCM}(x)/24))$	0.12	1.00	0.02	0.03	0.11	1.00	0.02	0.03	0.57	0.94	0.02	0.11
11	$Q_{Local}(x)=2Q_{GCM}(x)+72/Q_{GCM}(x)+7Q_{GCM}(x)/16$	0.09	1.00	0.00	0.02	0.09	1.00	0.00	0.02	0.54	0.93	0.01	0.12
12	$Q_{Local}(x)=2Q_{GCM}(x)-\exp(2.5417+1/Q_{GCM}(x)-1/Q_{GCM}(x)^2)+24$	0.09	1.00	0.00	0.01	0.09	1.00	0.00	0.01	0.50	0.93	0.01	0.11
13	$Q_{Local}(x)=2Q_{GCM}(x)-Q_{GCM}(x)/(24+\exp(24-Q_{GCM}(x))+Q_{GCM}(x))+6+24/Q_{GCM}(x)$	0.02	1.00	0.00	0.01	0.02	1.00	0.00	0.01	0.45	0.93	0.00	0.11
14	$Q_{Local}(x)=2Q_{GCM}(x)+12/Q_{GCM}(x)-Q_{GCM}(x)/24+(3Q_{GCM}(x)+24)/Q_{GCM}(x)$	0.07	1.00	-0.01	0.02	0.08	1.00	-0.01	0.02	0.40	0.93	-0.01	0.12
15	$Q_{Local}(x)=23Q_{GCM}(x)/12+48/Q_{GCM}(x)-Q_{GCM}(x)/16.611+2$	0.05	1.00	0.00	0.02	0.05	1.00	0.00	0.02	0.39	0.93	0.01	0.11
16	$Q_{Local}(x)=1.5972Q_{GCM}(x)+Q_{GCM}(x)^2/864+8$	0.05	1.00	-0.03	0.02	0.05	1.00	-0.02	0.02	0.37	0.93	-0.02	0.10
17	$Q_{Local}(x)=1081Q_{GCM}(x)/576+48/Q_{GCM}(x)-24/\exp(48/Q_{GCM}(x))$	0.06	1.00	0.01	0.02	0.05	1.00	0.01	0.02	0.32	0.94	0.01	0.10
18	$Q_{Local}(x)=Q_{GCM}(x)^2/192+25Q_{GCM}(x)/24+14$	0.04	1.00	0.00	0.02	0.04	1.00	0.00	0.02	0.29	0.95	0.01	0.08
19	$Q_{Local}(x)=1.5Q_{GCM}(x)+Q_{GCM}(x)\exp(Q_{GCM}(x)/24)/1152+12/\exp(Q_{GCM}(x)/24)$	0.04	1.00	-0.01	0.01	0.04	1.00	-0.01	0.01	0.28	0.95	-0.01	0.09
20	$Q_{Local}(x)=4Q_{GCM}(x)/3-Q_{GCM}(x)(48-Q_{GCM}(x))/300+8$	0.04	1.00	0.00	0.02	0.04	1.00	0.00	0.02	0.26	0.95	0.01	0.09
21	$Q_{Local}(x)=Q_{GCM}(x)^2/192+11Q_{GCM}(x)/12+12$	0.02	1.00	-0.02	0.01	0.02	1.00	-0.02	0.01	0.25	0.95	-0.01	0.08
22	$Q_{Local}(x)=Q_{GCM}(x)^2/576+13Q_{GCM}(x)/12+9$	0.06	1.00	-0.02	0.02	0.06	1.00	-0.02	0.02	0.25	0.95	-0.01	0.09
23	$Q_{Local}(x)=(144+4Q_{GCM}(x)+\exp((Q_{GCM}(x)+24))/24+Q_{GCM}(x)$	0.04	1.00	0.00	0.02	0.04	1.00	0.00	0.02	0.24	0.94	0.00	0.09
24	$Q_{Local}(x)=Q_{GCM}(x)^2/576+25Q_{GCM}(x)/24+8/Q_{GCM}(x)+6.389$	0.02	1.00	0.00	0.01	0.02	1.00	0.00	0.01	0.22	0.95	0.00	0.09

Units of RMSE and MB are mm/hr.

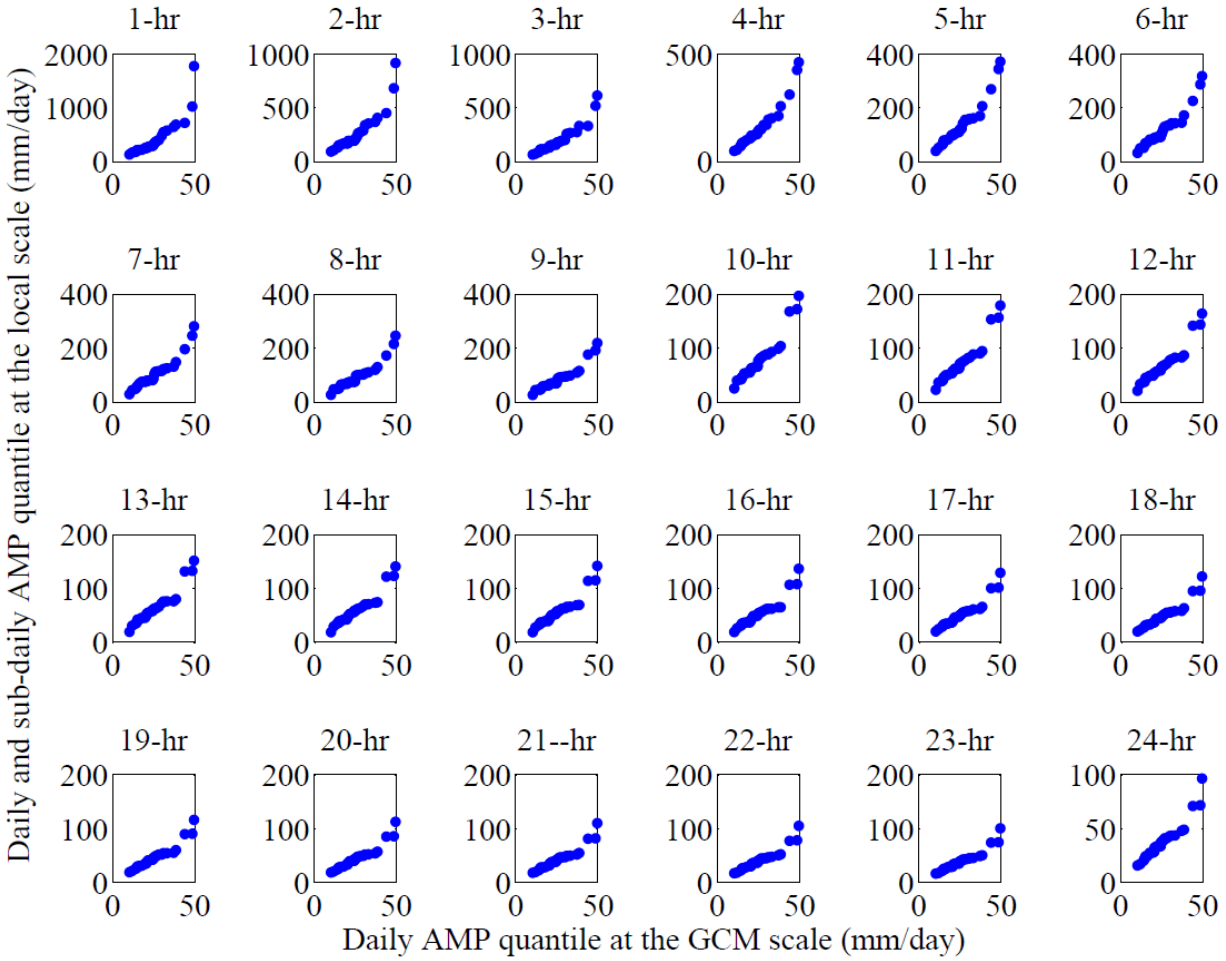

Figure D.1: Comparison between the GCM-scale (using output of HadGEM2-ES) daily AMP quantiles and the corresponding local-scale daily and sub-daily AMP quantiles during the baseline (1961-1990) period in Saskatoon.

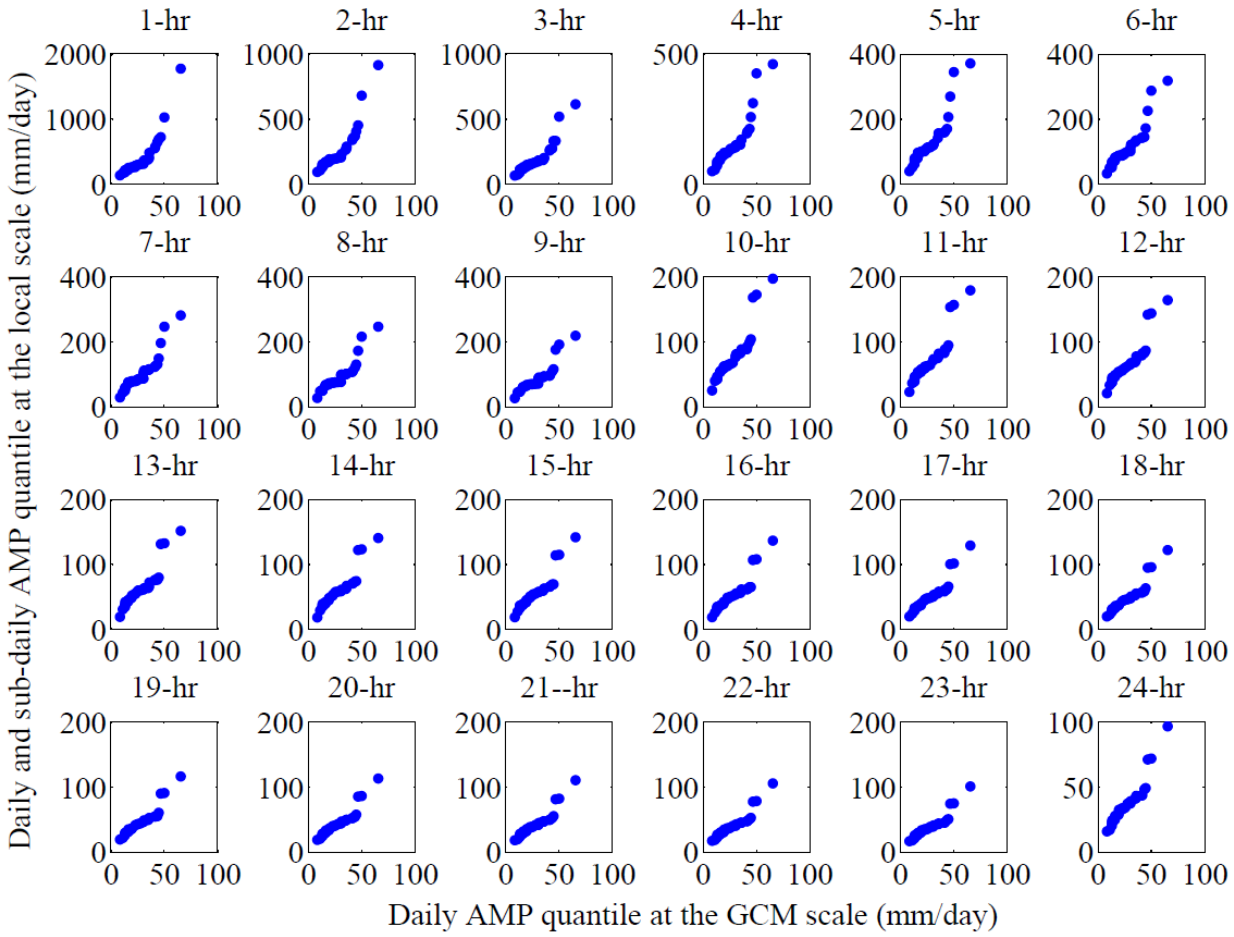

Figure D.2: Comparison between the GCM-scale (using output of CGCM3.1) daily AMP quantiles and the corresponding local-scale daily and sub-daily AMP quantiles during the baseline (1961-1990) period in Saskatoon.

Appendix E

The following results are presented here with reference to section 4.4.1.

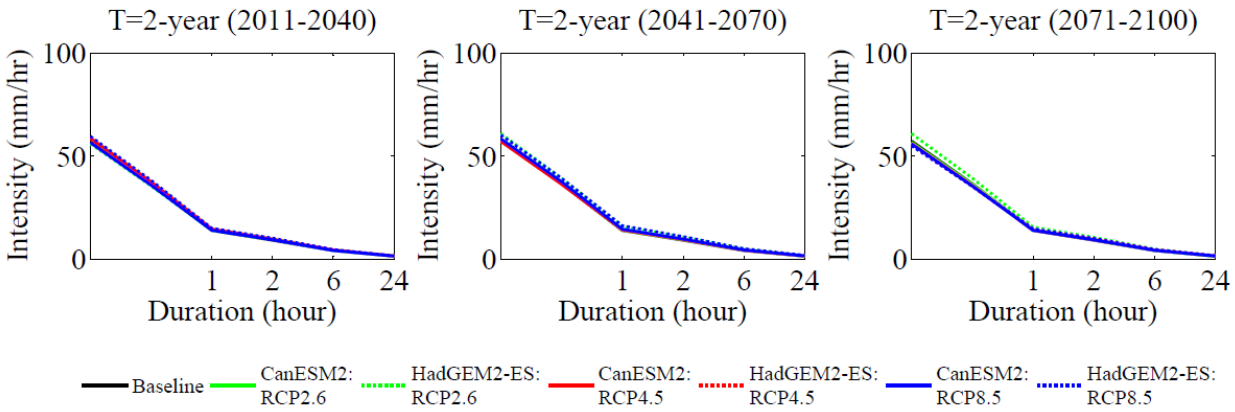

Figure E.1: Variations in the future IDF curves for 2-year return period in the City of Saskatoon according to CanESM2 and HadGEM2-ES based on three RCPs.

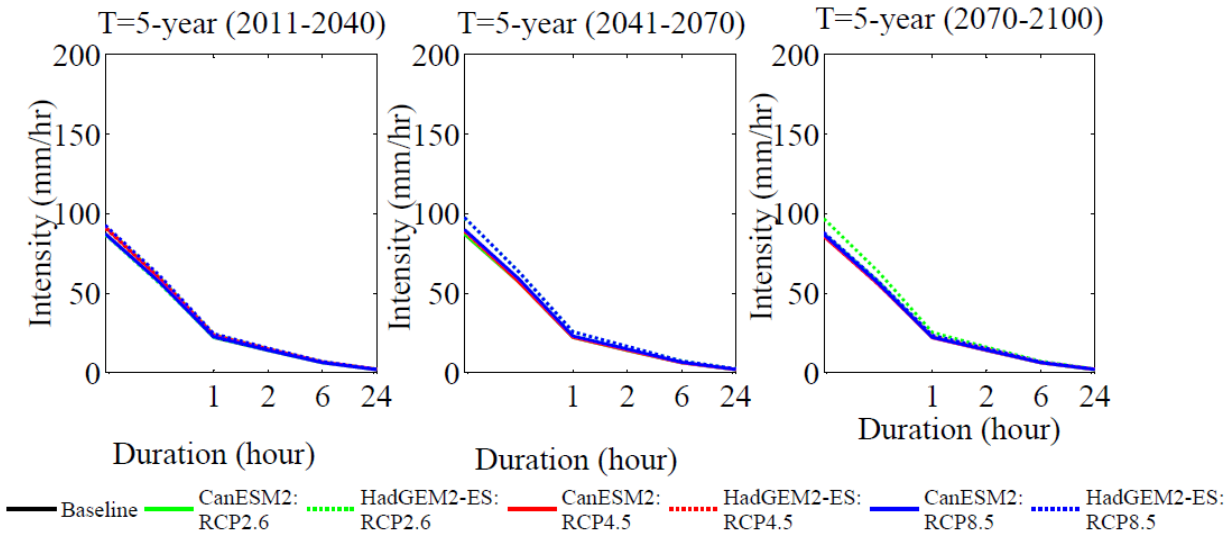

Figure E.2: Variations in the future IDF curves for 5-year return period in the City of Saskatoon according to CanESM2 and HadGEM2-ES based on three RCPs.

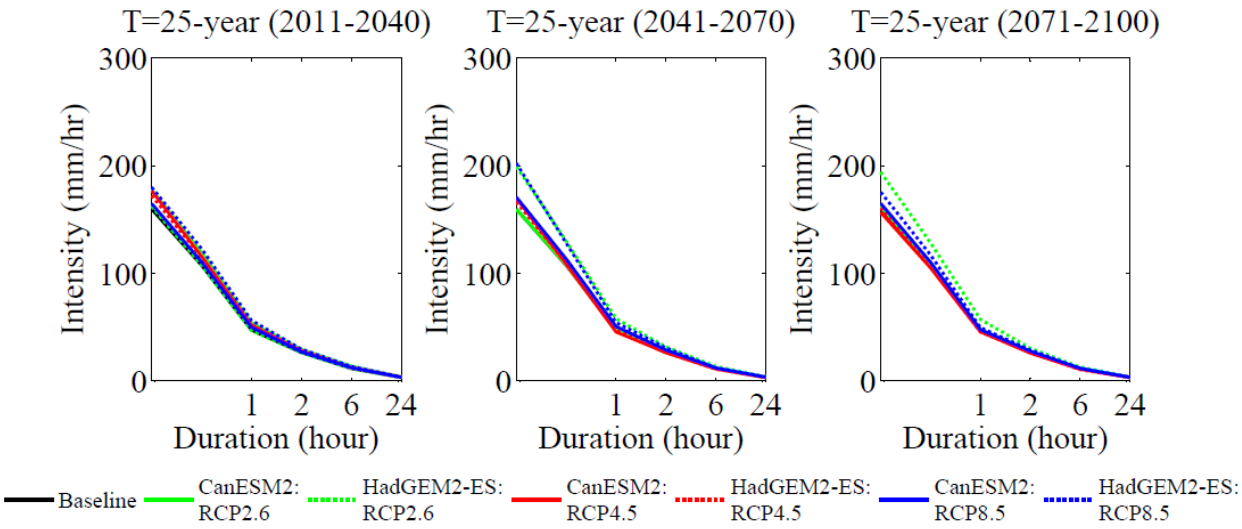

Figure E.3: Variations in the future IDF curves for 25-year return period in the City of Saskatoon according to CanESM2 and HadGEM2-ES based on three RCPs.

The following results are presented here with reference to section 4.4.2.

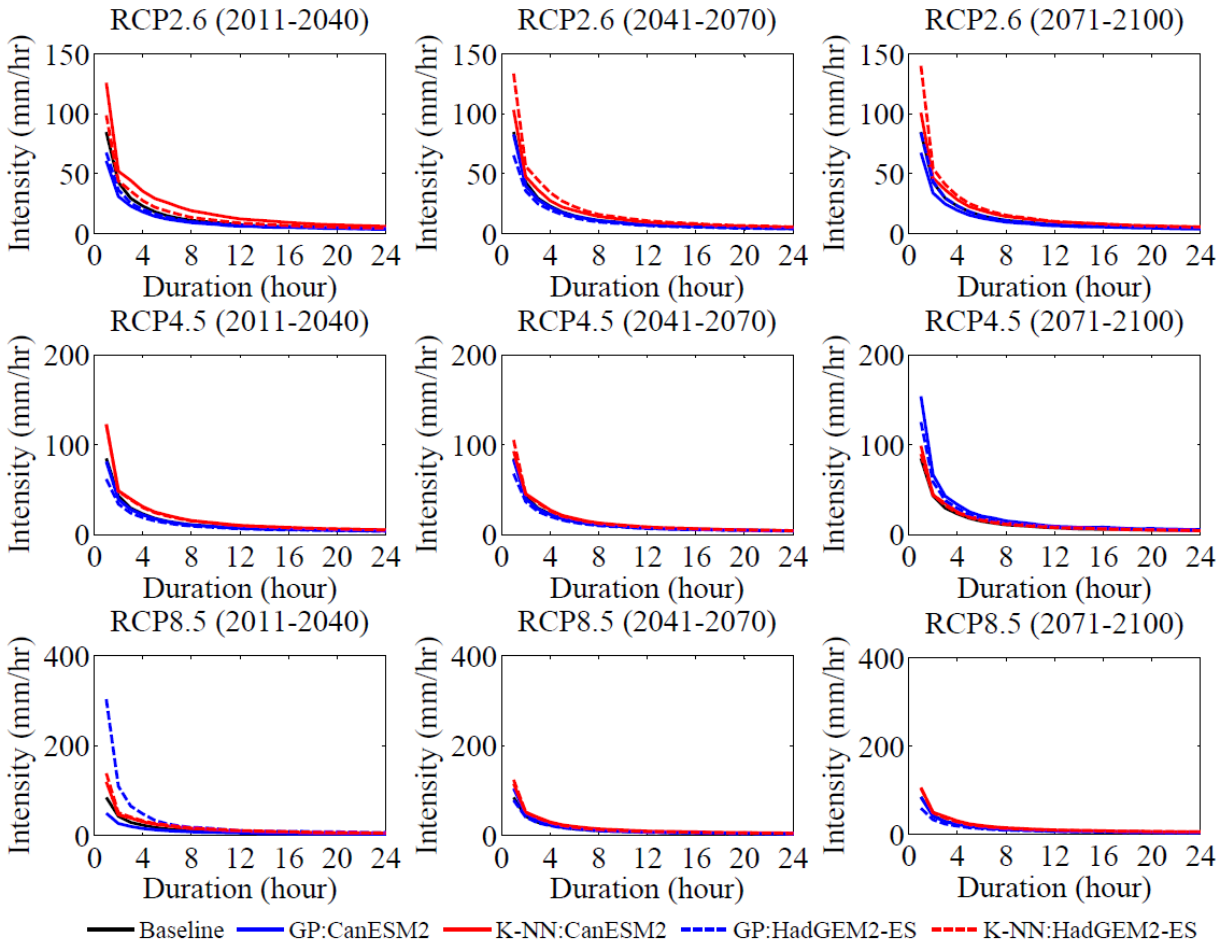

Figure E.4: Comparison between the future IDF curves (2011-2100) according to CanESM2 (solid lines) and HadGEM2-ES (dashed lines) based on three RCPs and 100-year return period obtained using two different downscaling approaches, i.e. GP method and LARS-WG combined with K-NN Hourly Disaggregation Model.

Table E.1: Comparison between the K-NN hourly disaggregation model and the GP method in simulating the expected precipitation intensity (mm/hr) for HadGEM2-ES based on three RCPs during the 21st century for various durations and return periods.

	GP Method												K-NN Hourly Disaggregation Model											
	(2011-2040)				(2041-2070)				(2071-2100)				(2011-2040)				(2041-2070)				(2071-2100)			
	Return period (year)												Return period (year)											
	2	5	25	100	2	5	25	100	2	5	25	100	2	5	25	100	2	5	25	100	2	5	25	100
HadGEM2-ES: RCP2.6																								
1-hr	15	22	39	68	19	29	48	65	17	27	51	84	13	22	48	99	15	25	59	133	15	25	60	140
2-hr	10	14	23	36	12	18	27	35	11	17	29	43	9	14	26	44	10	16	31	56	10	16	30	54
3-hr	8	11	17	25	10	14	20	25	9	13	21	29	7	11	20	35	8	12	24	44	8	12	23	41
4-hr	6	9	14	20	8	11	16	19	7	10	16	23	6	8	16	27	6	10	19	34	6	10	18	31
6-hr	5	6	10	13	6	8	11	13	5	8	11	15	4	6	11	19	5	7	14	22	5	7	13	21
12-hr	3	4	5	7	3	4	6	7	3	4	6	7	3	4	6	9	3	4	7	11	3	4	7	10
18-hr	2	3	4	5	2	3	4	5	2	3	4	5	2	3	4	6	2	3	5	7	2	3	5	7
24-hr	2	2	3	4	2	3	3	4	2	2	3	4	2	2	3	4	2	2	4	5	2	2	4	5
HadGEM2-ES: RCP4.5																								
1-hr	14	21	38	62	16	26	46	68	15	25	59	125	14	23	54	122	14	22	49	105	14	22	46	90
2-hr	9	13	23	34	11	16	27	36	10	16	33	58	10	15	28	48	9	14	26	45	10	15	27	44
3-hr	7	10	17	24	8	12	19	25	8	12	23	38	7	11	21	39	7	11	20	35	7	11	20	32
4-hr	6	8	13	19	7	10	15	20	6	10	18	29	6	9	17	30	6	9	16	26	6	9	15	24
6-hr	4	6	9	13	5	7	11	13	5	7	12	18	4	7	12	20	4	6	11	17	5	7	11	16
12-hr	3	4	5	6	3	4	6	7	3	4	6	8	3	4	7	10	3	4	6	8	3	4	6	8
18-hr	2	3	4	5	2	3	4	5	2	3	4	6	2	3	5	7	2	3	4	6	2	3	4	5
24-hr	1	2	3	4	2	2	3	4	2	2	4	5	1	2	4	5	2	2	3	4	2	2	3	4

Table E.1 continued

	GP Method												K-NN Hourly Disaggregation Model											
	(2011-2040)				(2041-2070)				(2071-2100)				(2011-2040)				(2041-2070)				(2071-2100)			
	Return period (year)												Return period (year)											
	2	5	25	100	2	5	25	100	2	5	25	100	2	5	25	100	2	5	25	100	2	5	25	100
HadGEM2-ES: RCP8.5																								
1-hr	14	26	89	303	17	28	51	78	15	25	42	59	14	24	58	139	16	25	56	124	14	23	51	104
2-hr	9	17	45	110	11	17	29	41	10	16	25	33	10	15	29	51	11	16	31	52	10	15	29	49
3-hr	7	13	30	66	9	13	21	28	8	12	18	23	7	12	23	41	8	12	23	39	7	11	21	37
4-hr	6	10	24	48	7	11	16	22	6	10	15	18	6	9	18	33	7	10	18	29	6	9	17	28
6-hr	5	8	15	26	5	8	11	14	5	7	10	12	5	7	13	23	5	7	12	19	5	7	12	18
12-hr	3	4	7	11	3	4	6	7	3	4	5	6	3	4	7	11	3	4	7	9	3	4	6	9
18-hr	2	3	5	9	2	3	4	5	2	3	4	4	2	3	5	7	2	3	5	6	2	3	5	7
24-hr	2	2	4	7	2	2	3	4	2	2	3	4	2	2	4	5	2	3	4	5	2	2	4	5

The following results are presented here with reference to section 4.5.2.

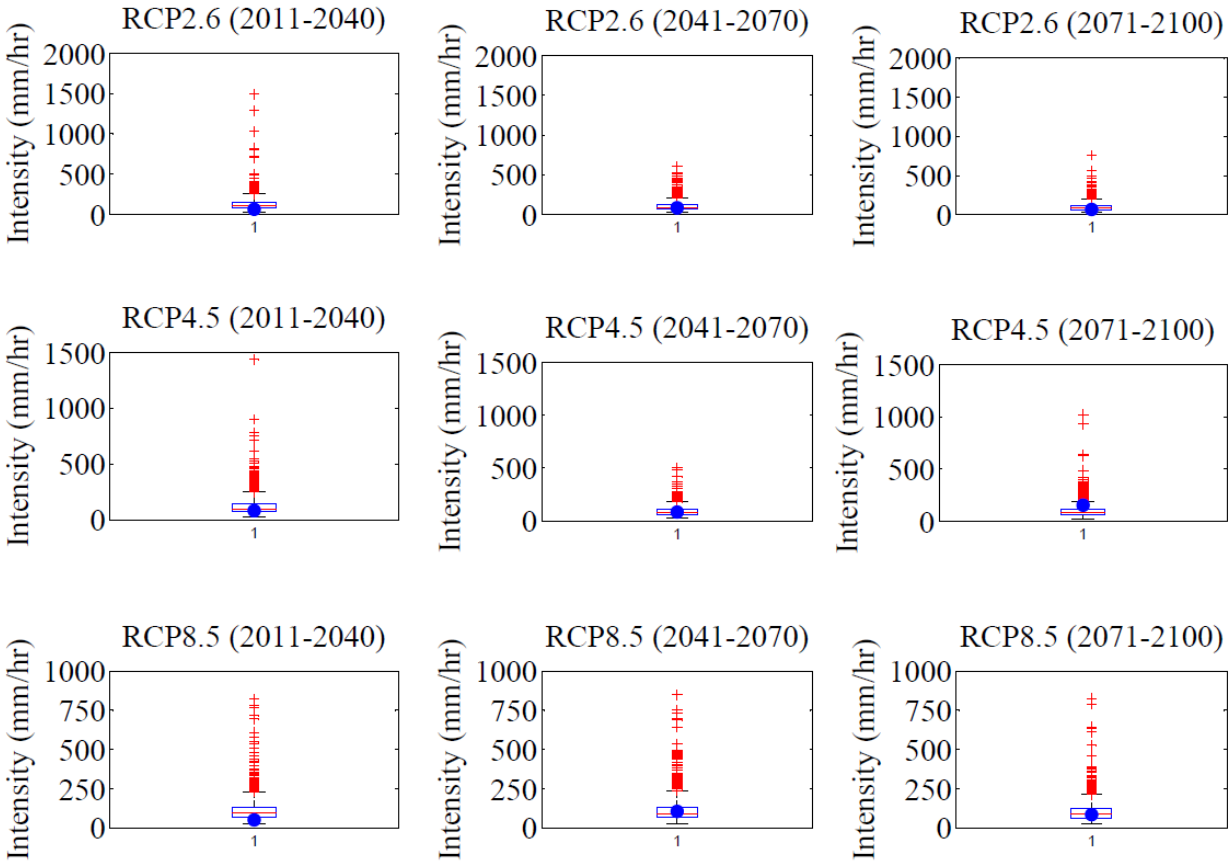

Figure E.5: Expected 1-hr AMP corresponding to 1000 realizations from LARS-WG and K-NN hourly disaggregation model (boxplot), and the same from GP method (blue dots) of **100-year** return period for **CanESM2** based on three RCPs during the 21st century.

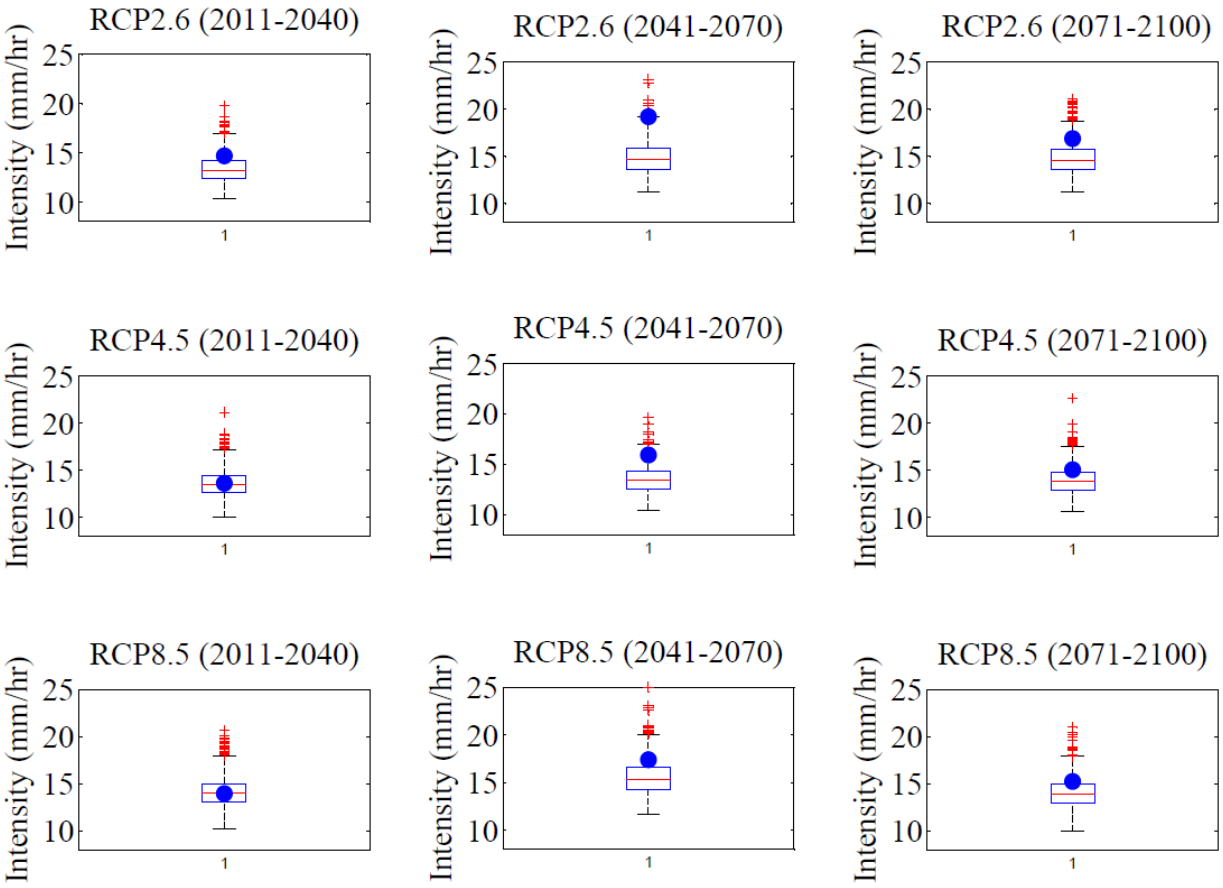

Figure E.6: Expected 1-hr AMP corresponding to 1000 realizations from LARS-WG and K-NN hourly disaggregation model (boxplot), and the same from GP method (blue dots) of **2-year** return period for **HadGEM2-ES** based on three RCPs during the 21st century.

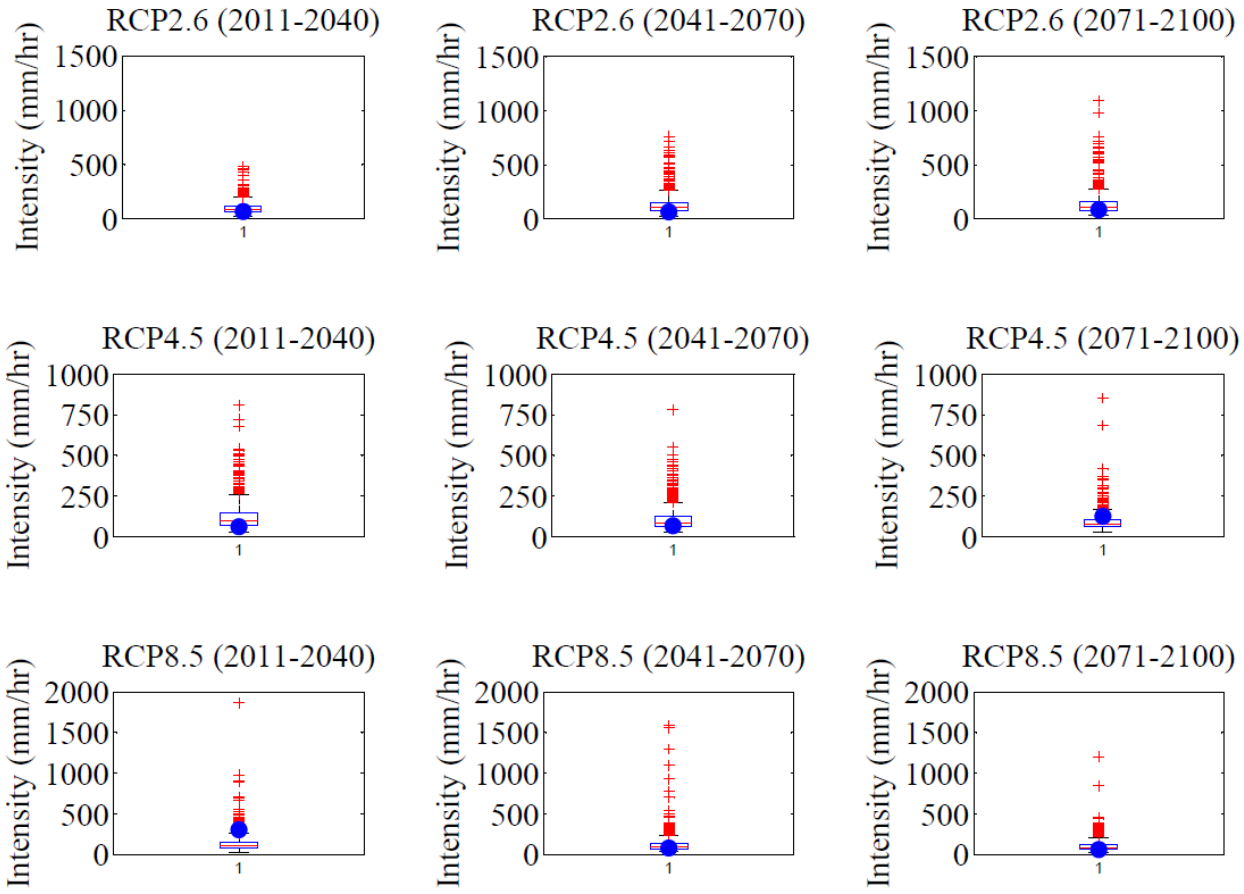

Figure E.7: Expected 1-hr AMP corresponding to 1000 realizations from LARS-WG and K-NN hourly disaggregation model (boxplot), and the same from GP method (blue dots) of **100-year** return period for **HadGEM2-ES** based on three RCPs during the 21st century.

The following results are presented here with reference to section 4.5.3.

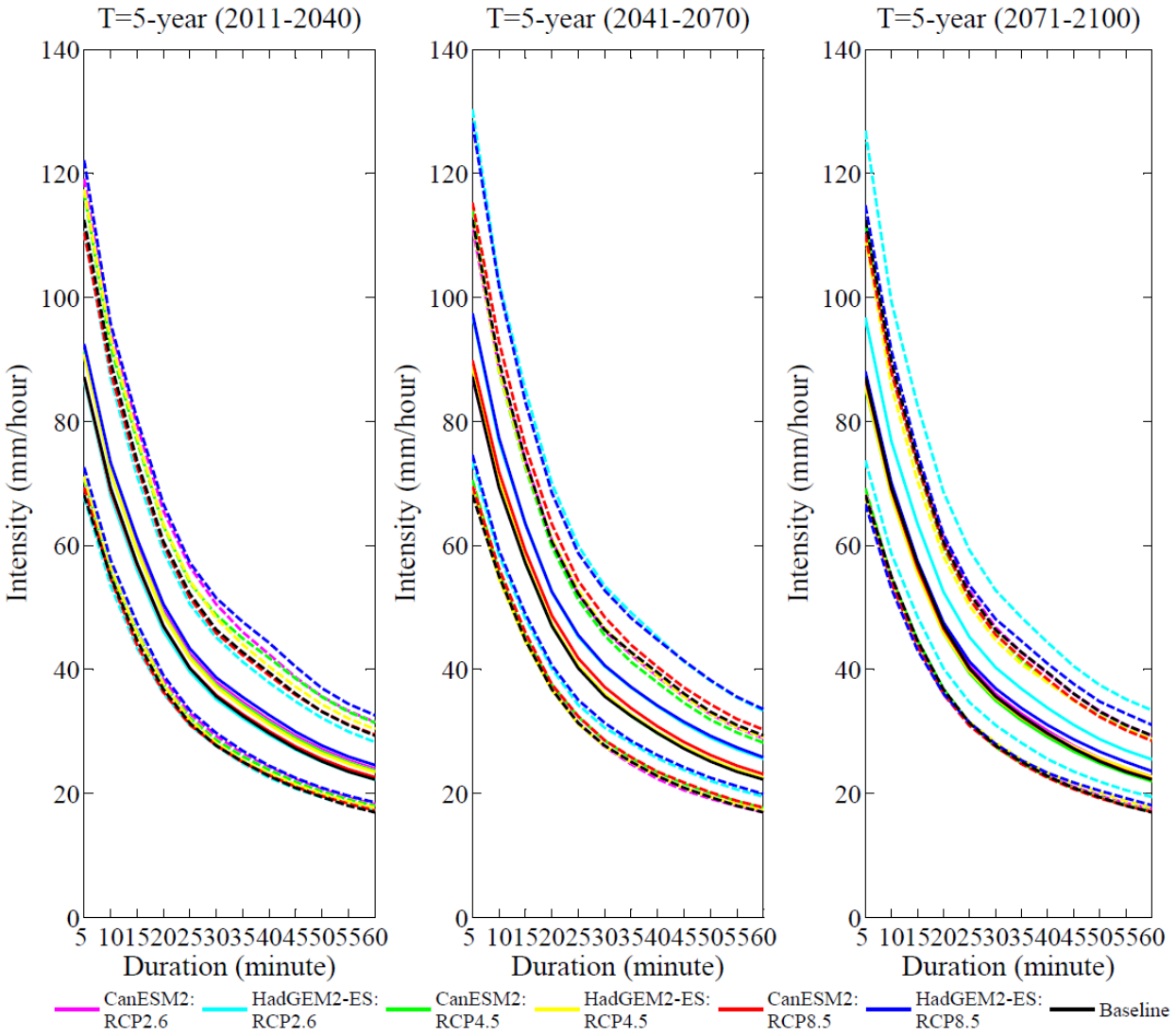

Figure E.8: Uncertainty in the projections of future extreme precipitation quantiles for 5-year return period based on two GCMs and three RCPs obtained from CMIP5 and quantified by using GEV shown as 95% confidence intervals (dashed lines).

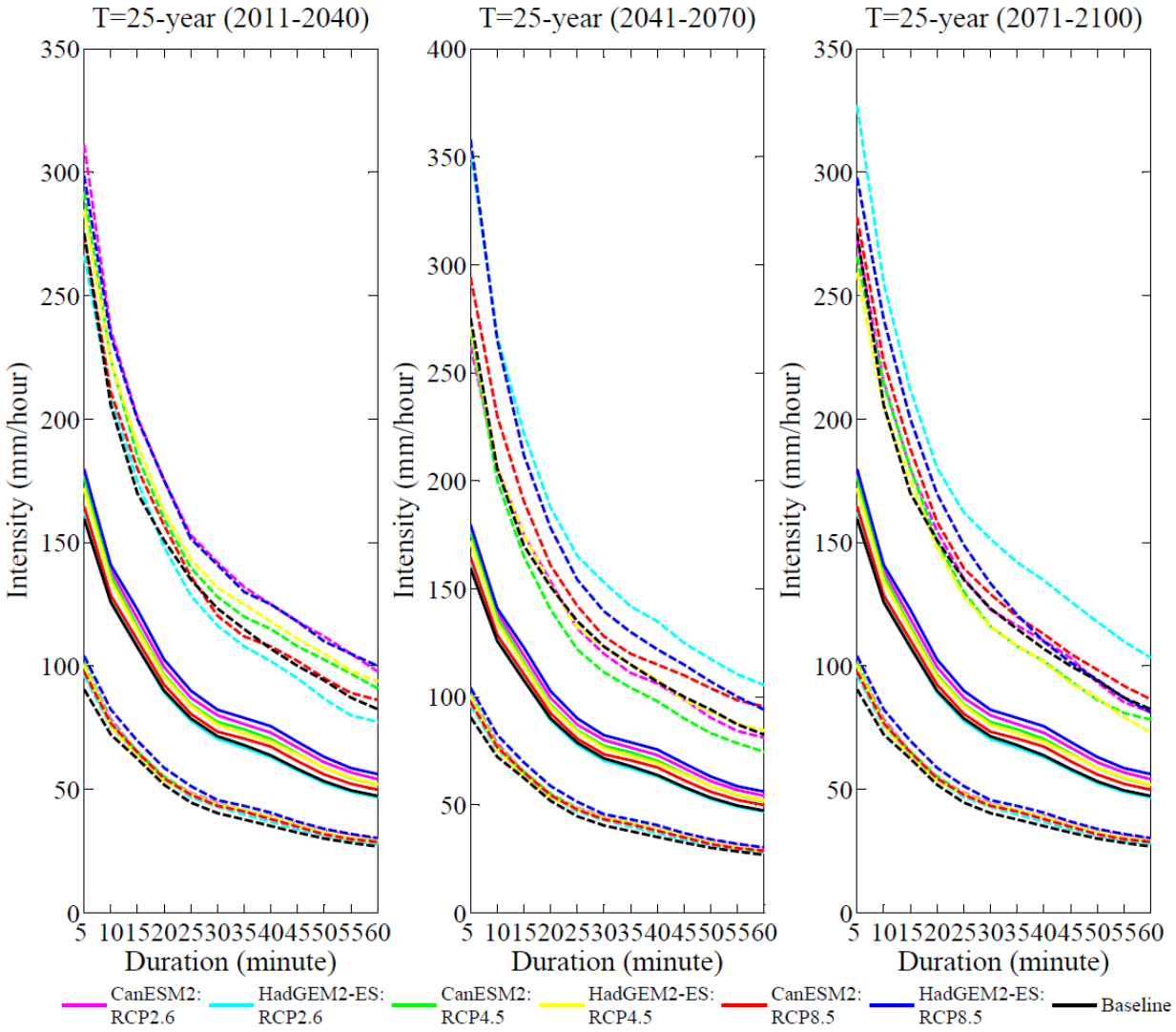

Figure E.9: Uncertainty in the projections of future extreme precipitation quantiles for 25-year return period based on two GCMs and three RCPs obtained from CMIP5 and quantified by using GEV shown as 95% confidence intervals (dashed lines).

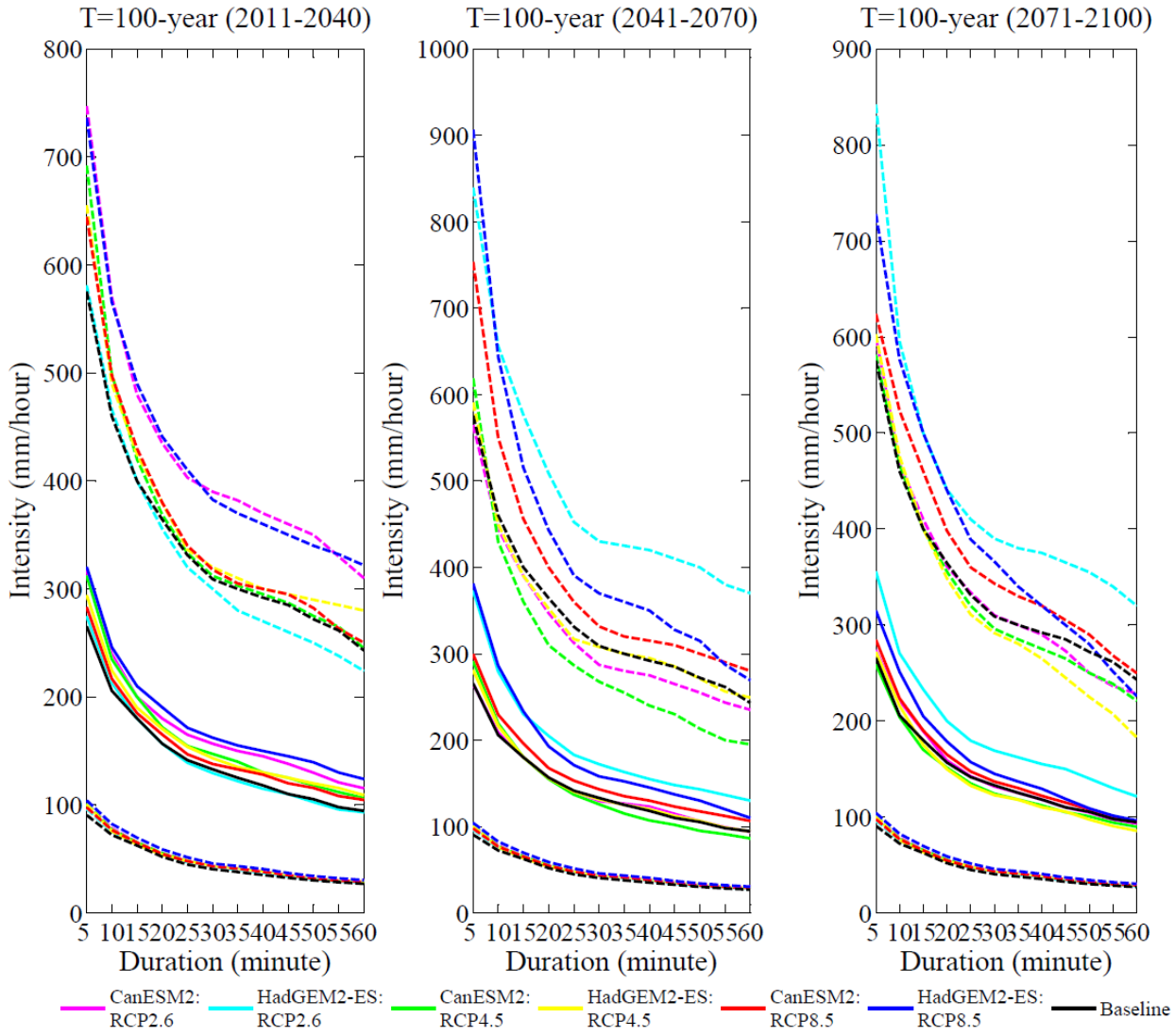

Figure E.10: Uncertainty in the projections of future extreme precipitation quantiles for 100-year return period based on two GCMs and three RCPs obtained from CMIP5 and quantified by using GEV shown as 95% confidence intervals (dashed lines).

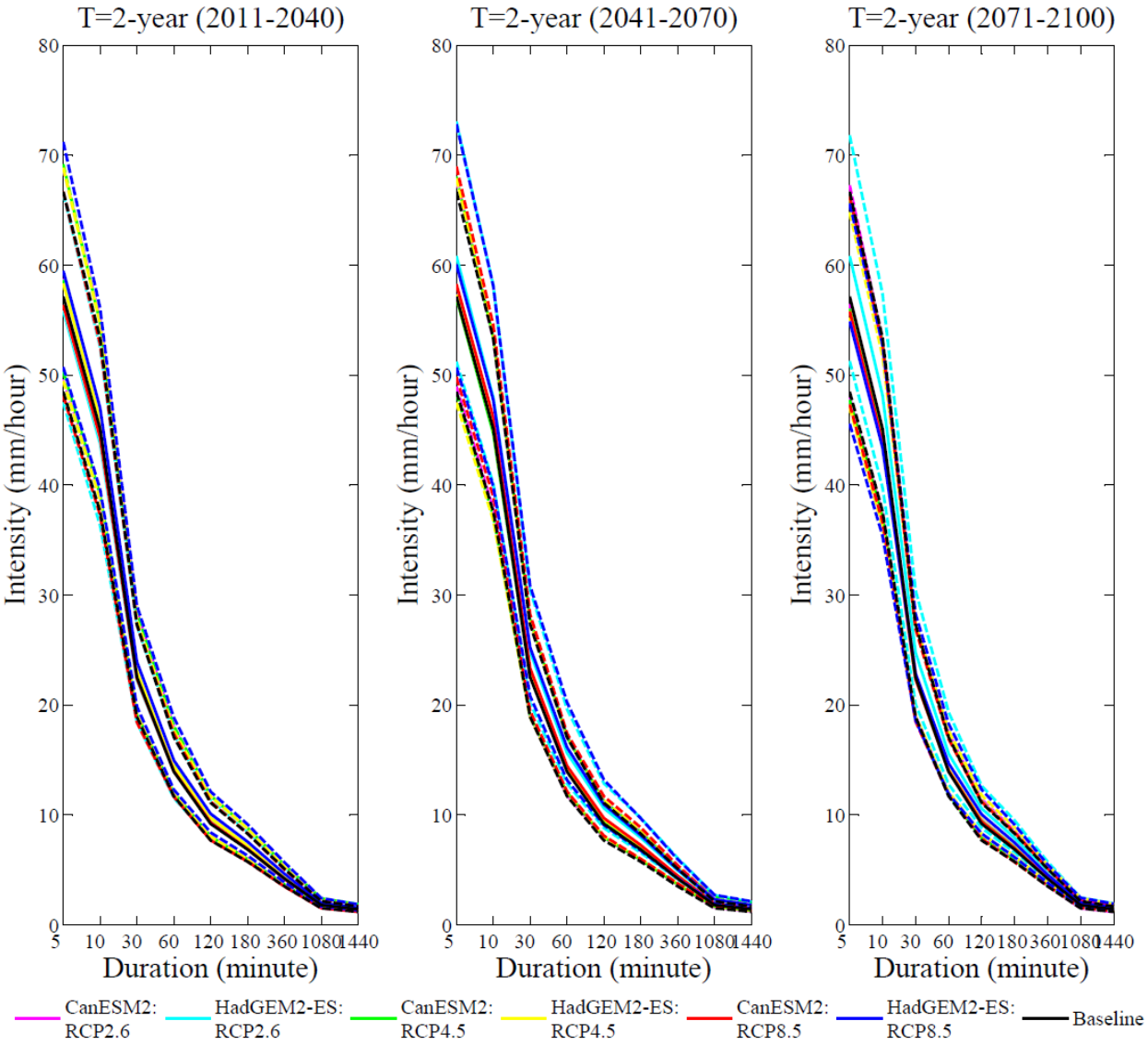

Figure E.11: Uncertainty in the projections of future extreme precipitation quantiles of durations from 5-min to 24-hour for 2-year return period based on two GCMs and three RCPs obtained from CMIP5 and quantified by using GEV shown as 95% confidence intervals (dashed lines).

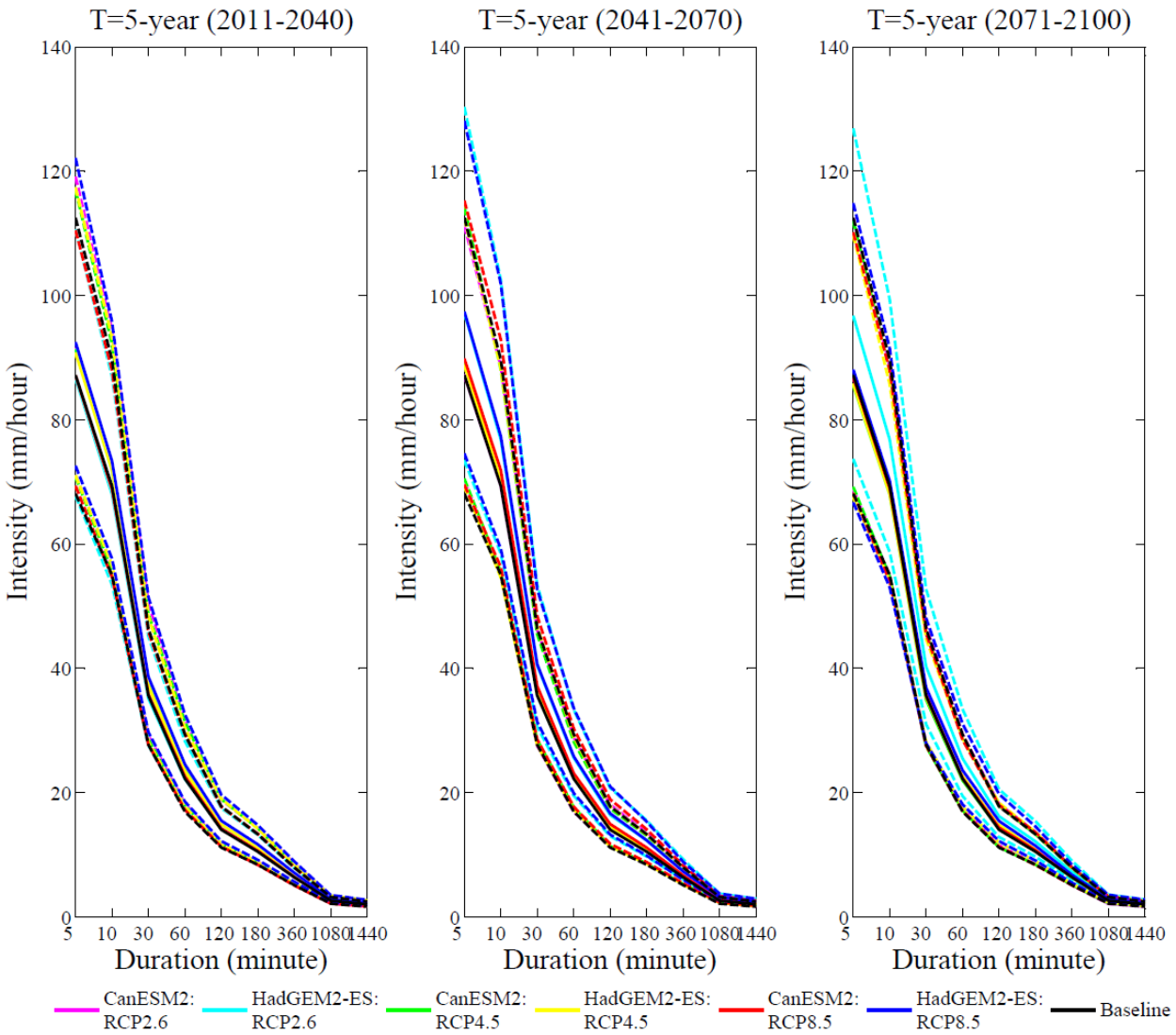

Figure E.12: Uncertainty in the projections of future extreme precipitation quantiles of durations from 5-min to 24-hour for 5-year return period based on two GCMs and three RCPs obtained from CMIP5 and quantified by using GEV shown as 95% confidence intervals (dashed lines).

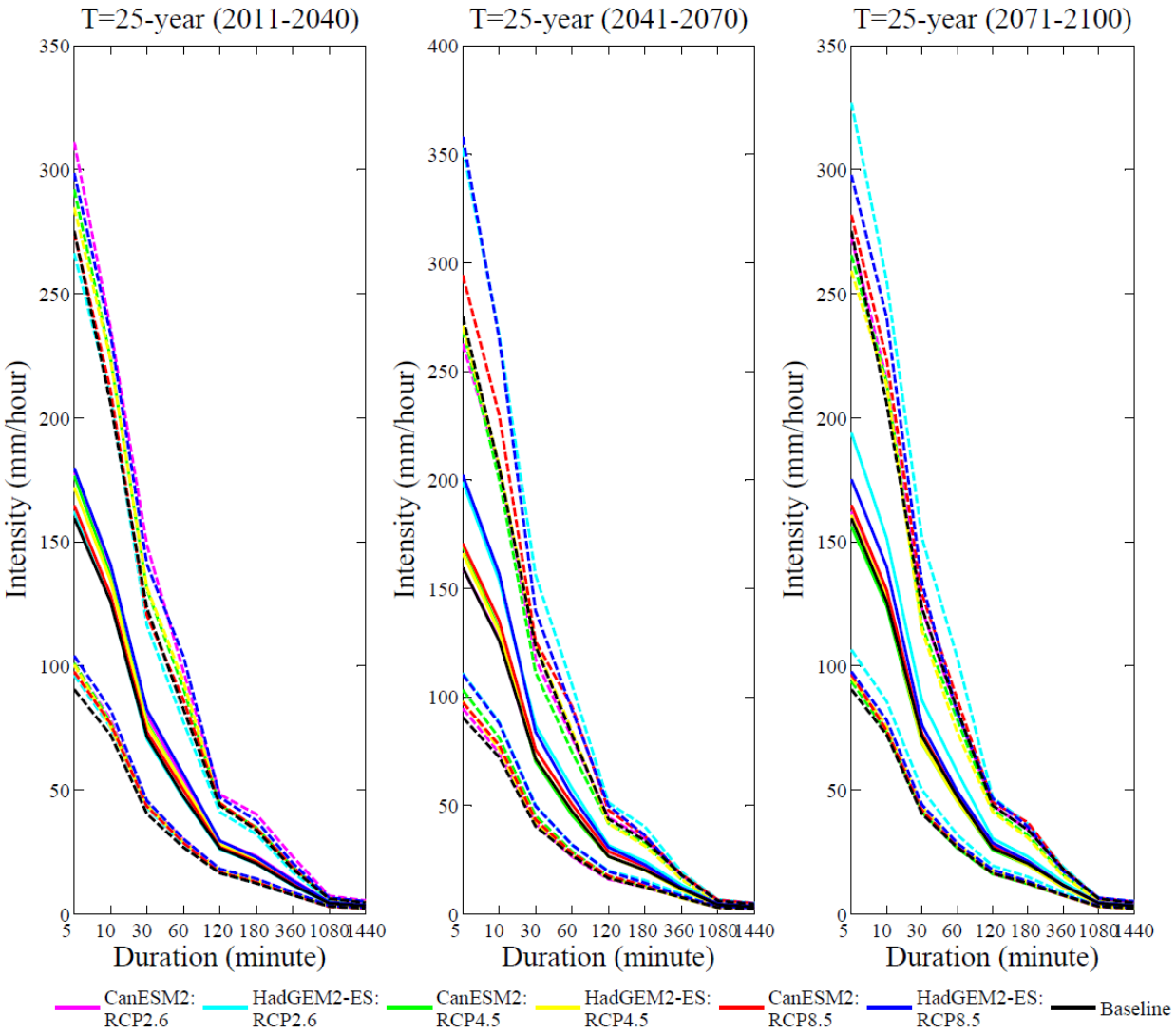

Figure E.13: Uncertainty in the projections of future extreme precipitation quantiles of durations from 5-min to 24-hour for 25-year return period based on two GCMs and three RCPs obtained from CMIP5 and quantified by using GEV shown as 95% confidence intervals (dashed lines).

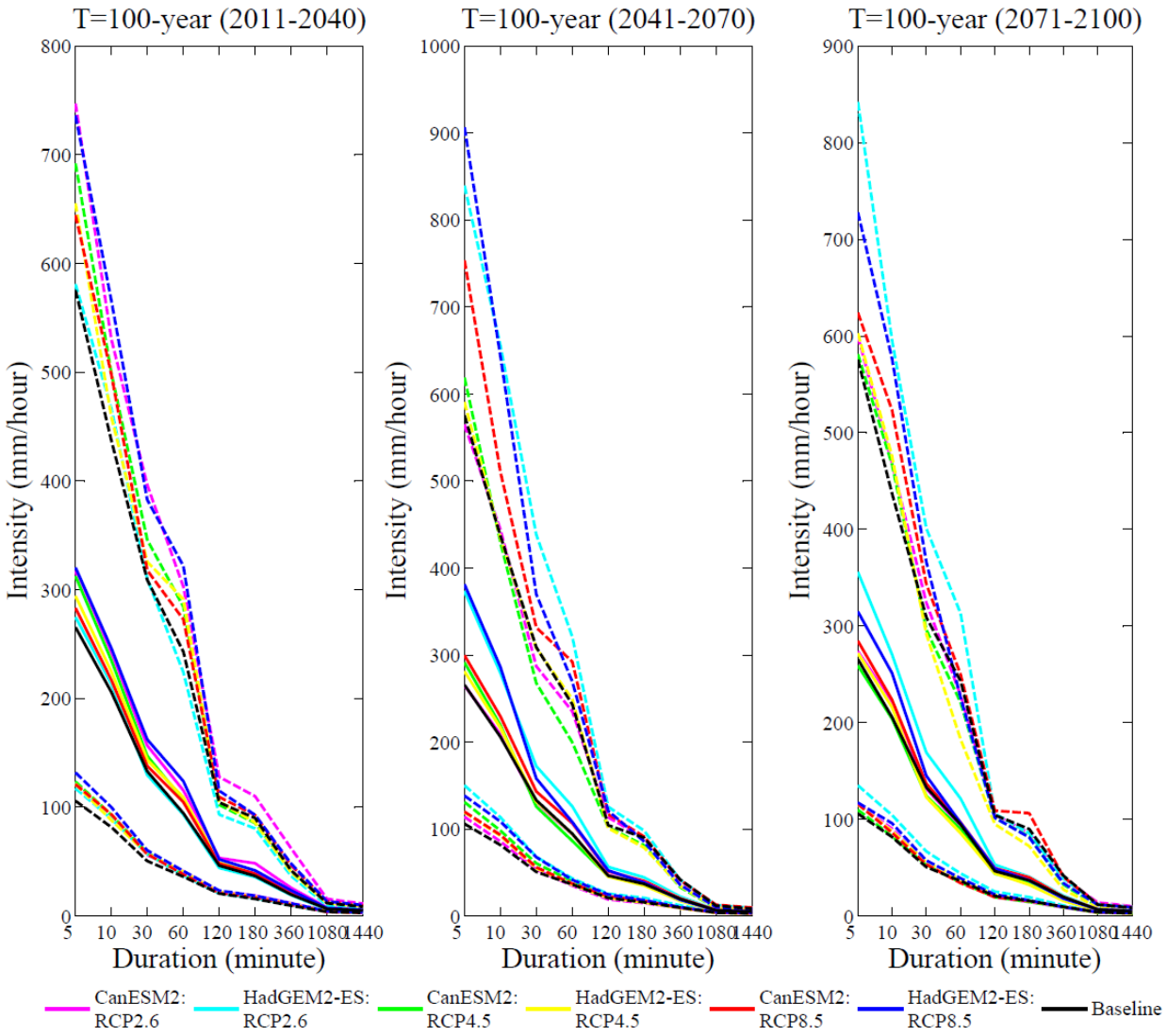

Figure E.14: Uncertainty in the projections of future extreme precipitation quantiles of durations from 5-min to 24-hour for 100-year return period based on two GCMs and three RCPs obtained from CMIP5 and quantified by using GEV shown as 95% confidence intervals (dashed lines).

Appendix F

F.1 Effect of wet and dry spell lengths

The following results are presented here with reference to section 4.2 of the thesis.

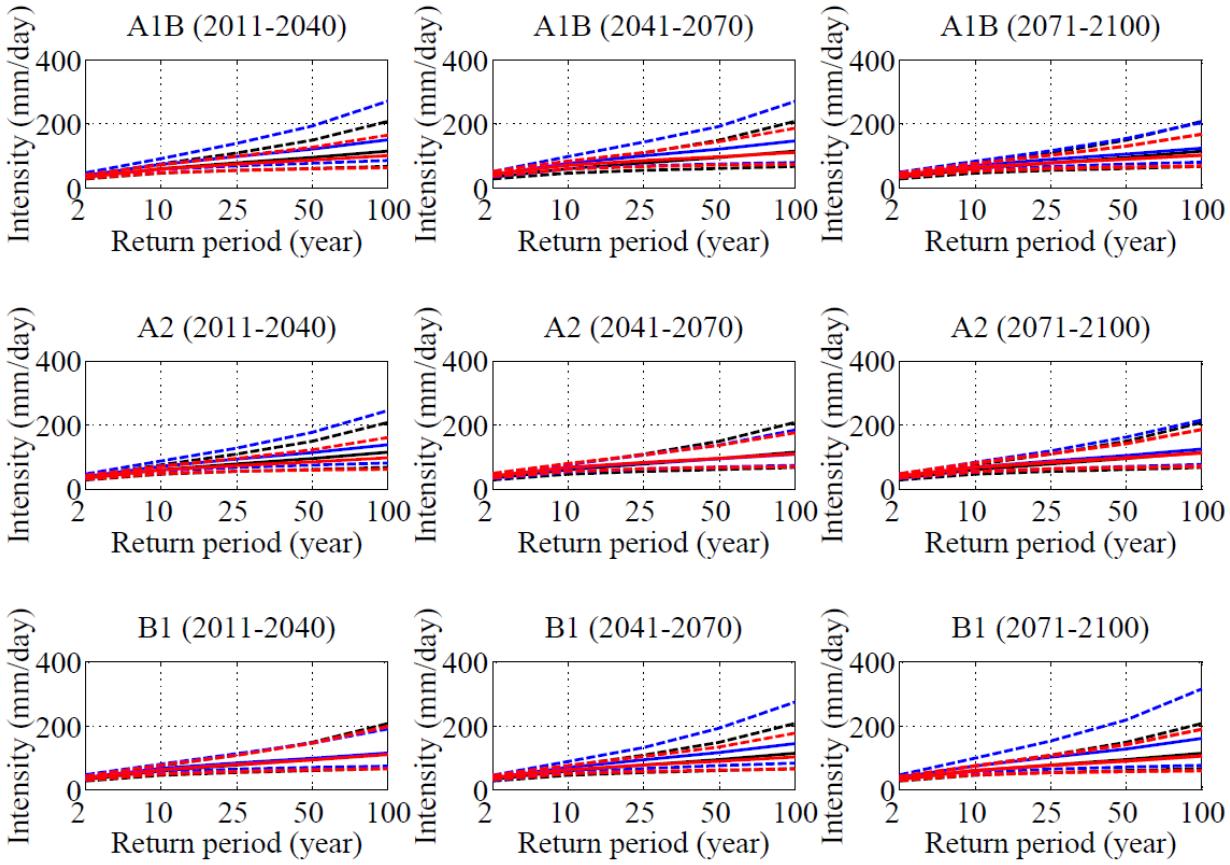

Figure F.1: Variations in the future projections of daily AMP quantiles in the City of Saskatoon according to CGCM3.1 forced with three emission scenarios using two sets of change factors: with wet/dry spell (blue) and without wet/dry spell (red) effects. The expected quantiles (solid lines) and their 95% confidence intervals (dashed lines) are shown with the corresponding quantiles during the baseline period (black).

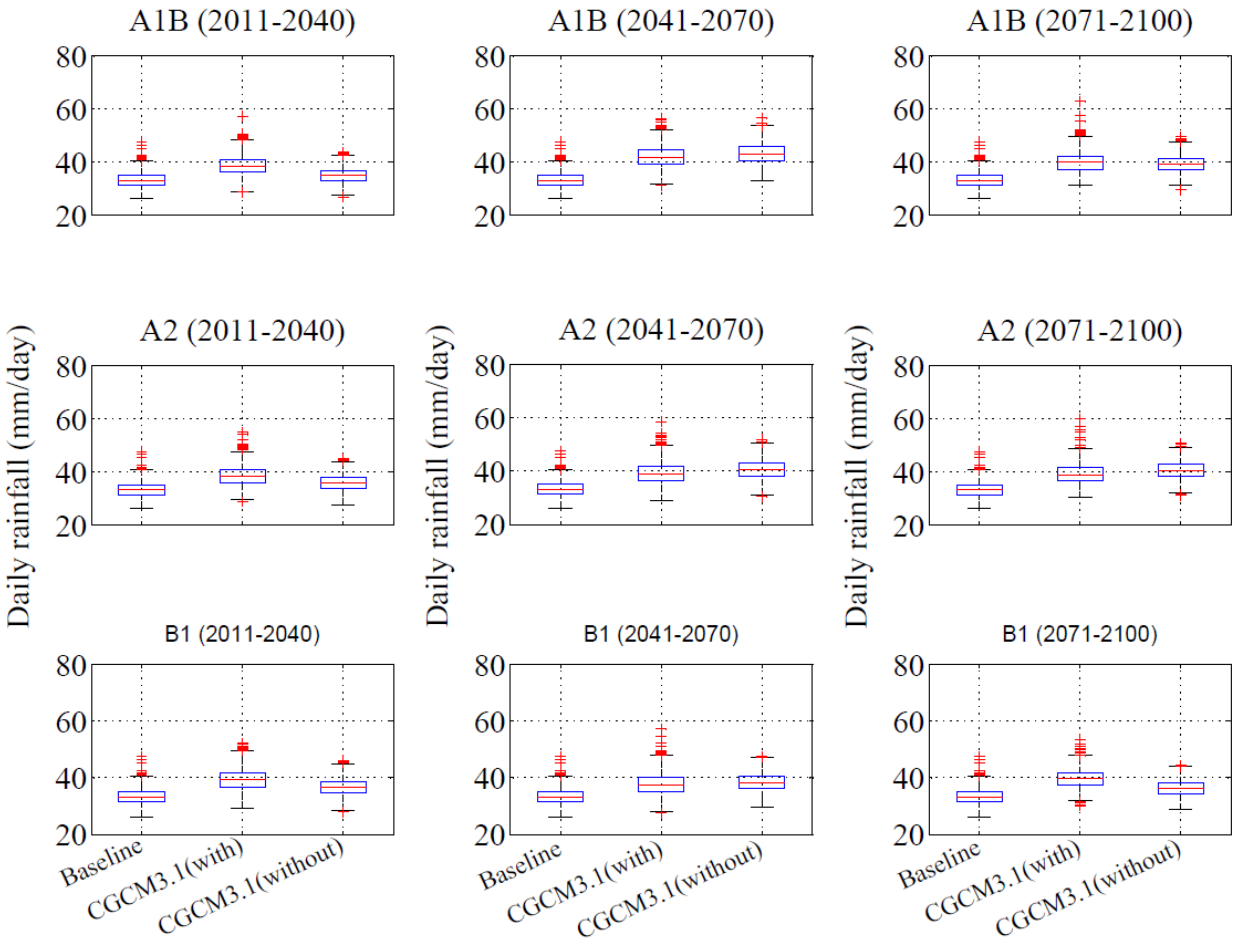

Figure F.2: Variations in the future projections of daily expected quantiles for 2-year return period in the City of Saskatoon according to CGCM3.1 forced with three emission scenarios using two sets of change factors, i.e. with wet/dry spell and without wet/dry spell effects along with the corresponding daily expected quantiles during the baseline.

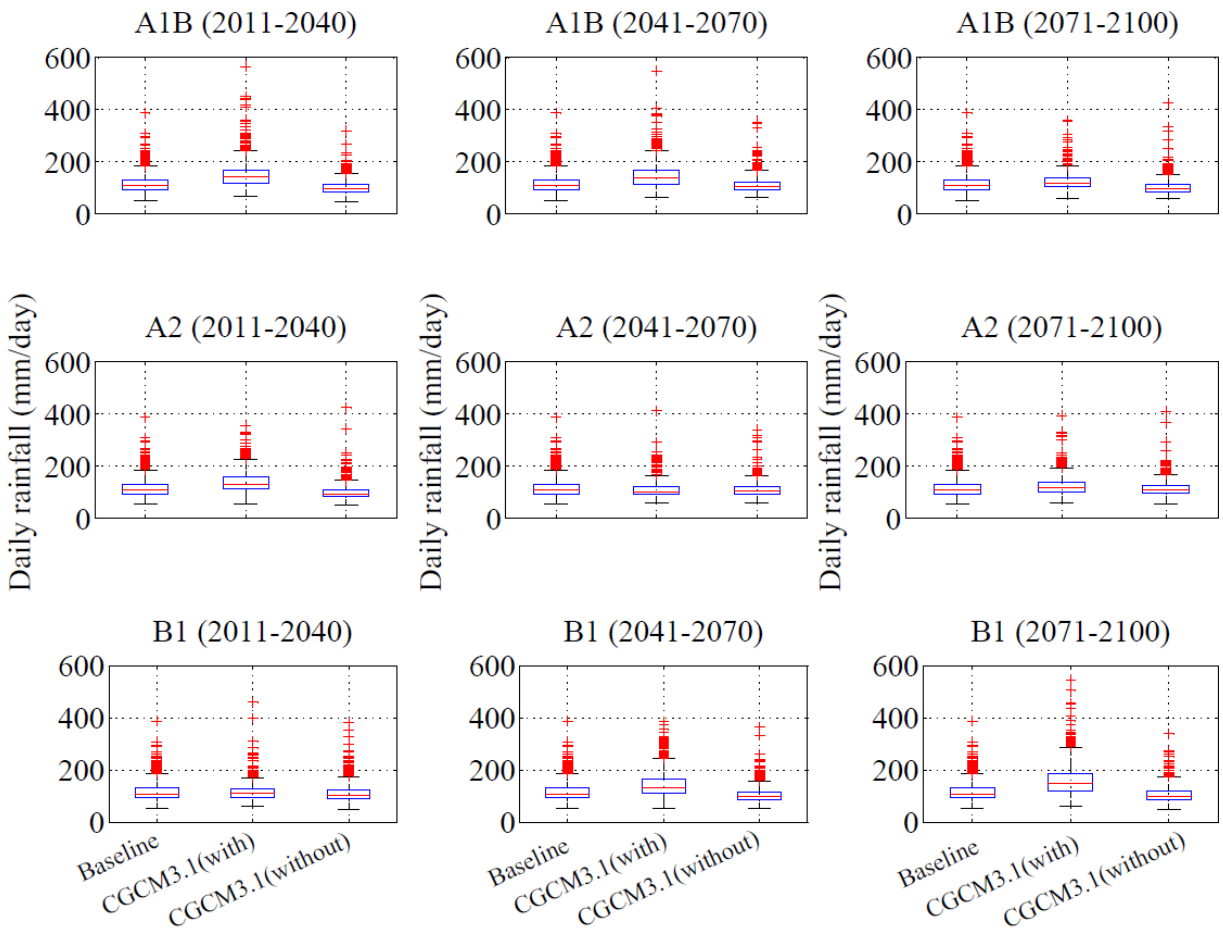

Figure F.3: Variations in the future projections of daily expected quantiles for 100-year return period in the City of Saskatoon according to CGCM3.1 forced with three emission scenarios using two sets of change factors, i.e. with wet/dry spell and without wet/dry spell effects along with the corresponding daily expected quantiles during the baseline.

F.2 Variations in the future IDF curves obtained for CMIP3 climate models

The following results are presented here with reference to section 4.4.1 of the thesis.

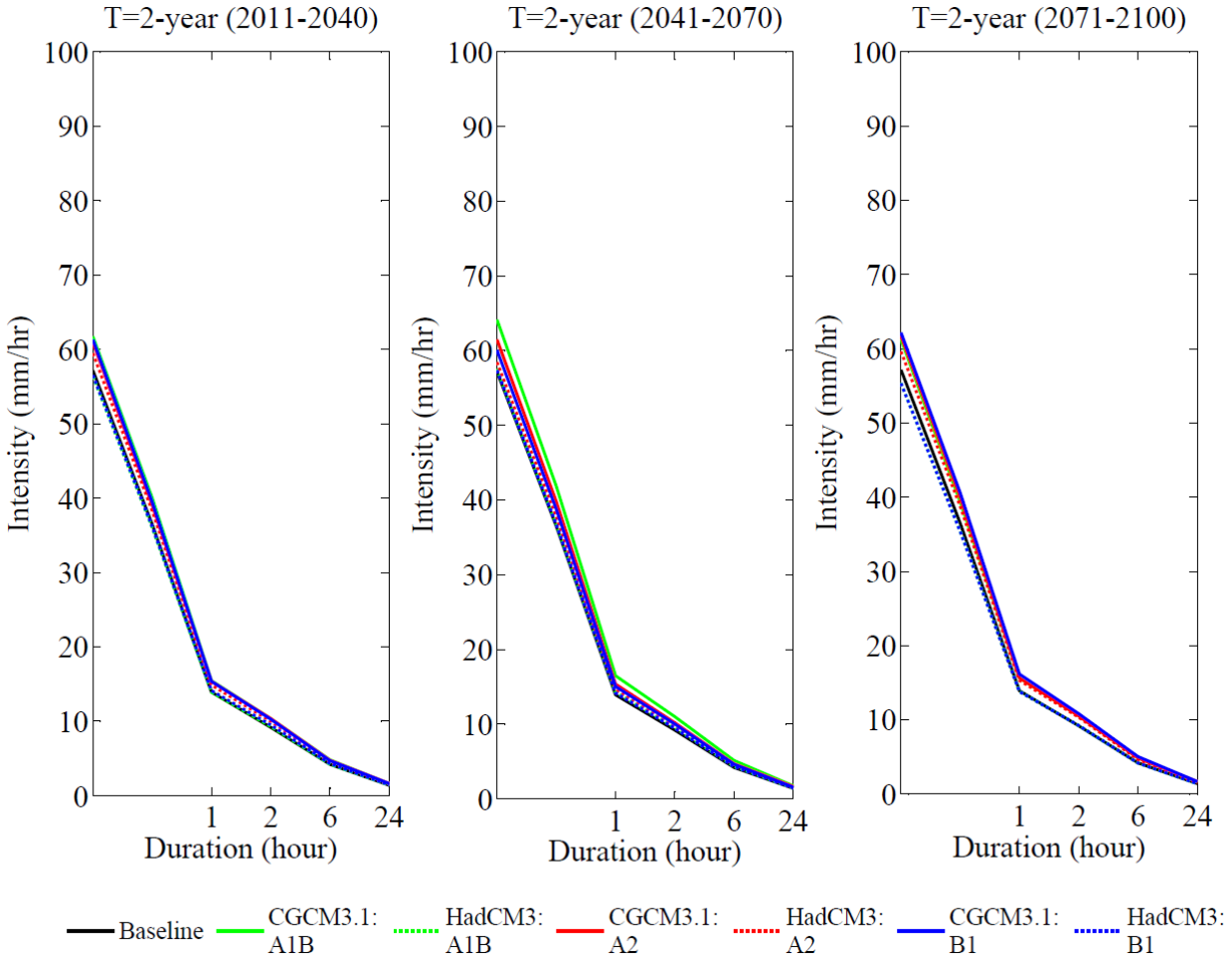

Figure F.4: Variations in the future IDF curves for 2-year return period in the City of Saskatoon according to CGCM3.1 and HadCM3 based on three AR4 emission scenarios.

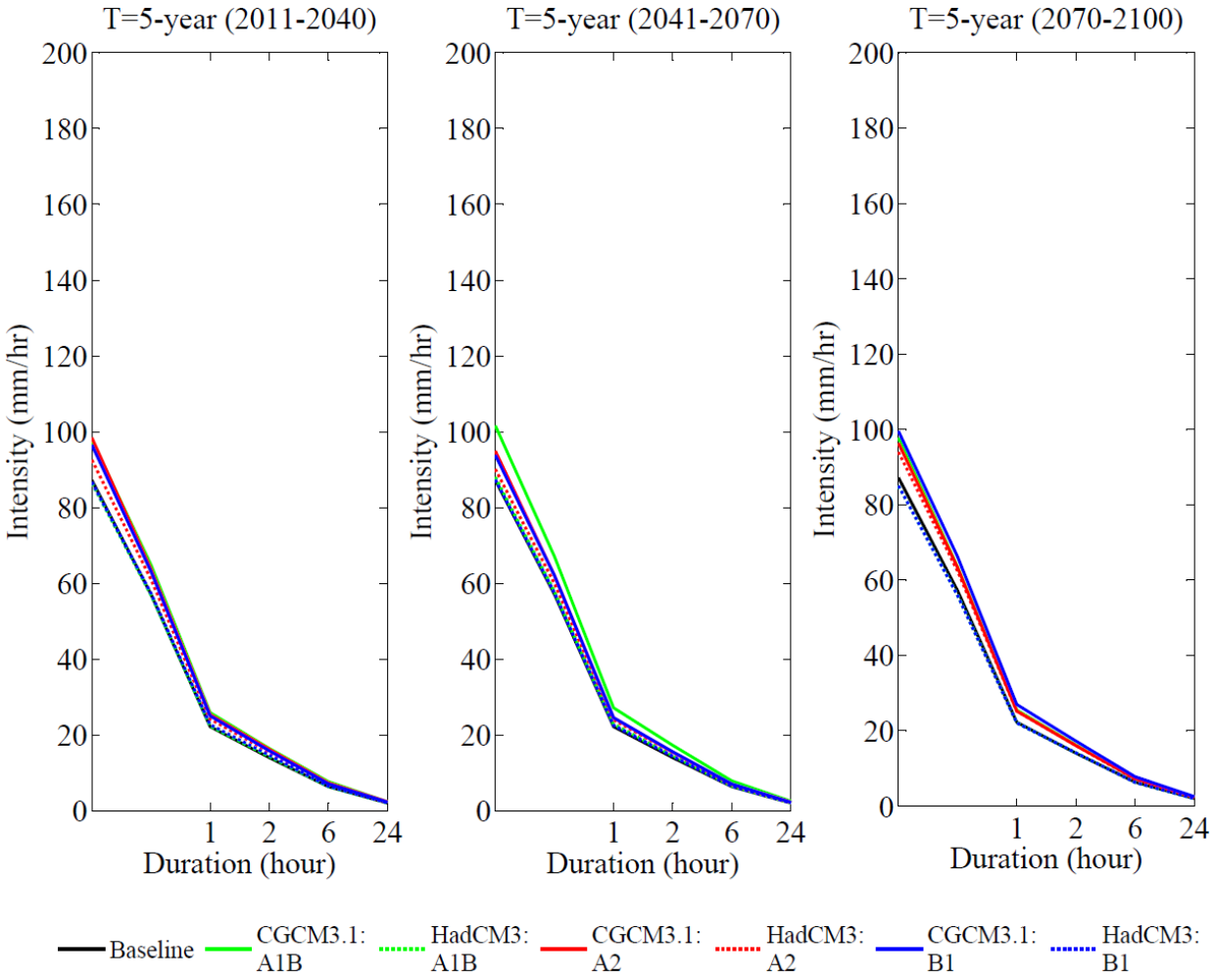

Figure F.5: Variations in the future IDF curves for 5-year return period in the City of Saskatoon according to CGCM3.1 and HadCM3 based on three AR4 emission scenarios.

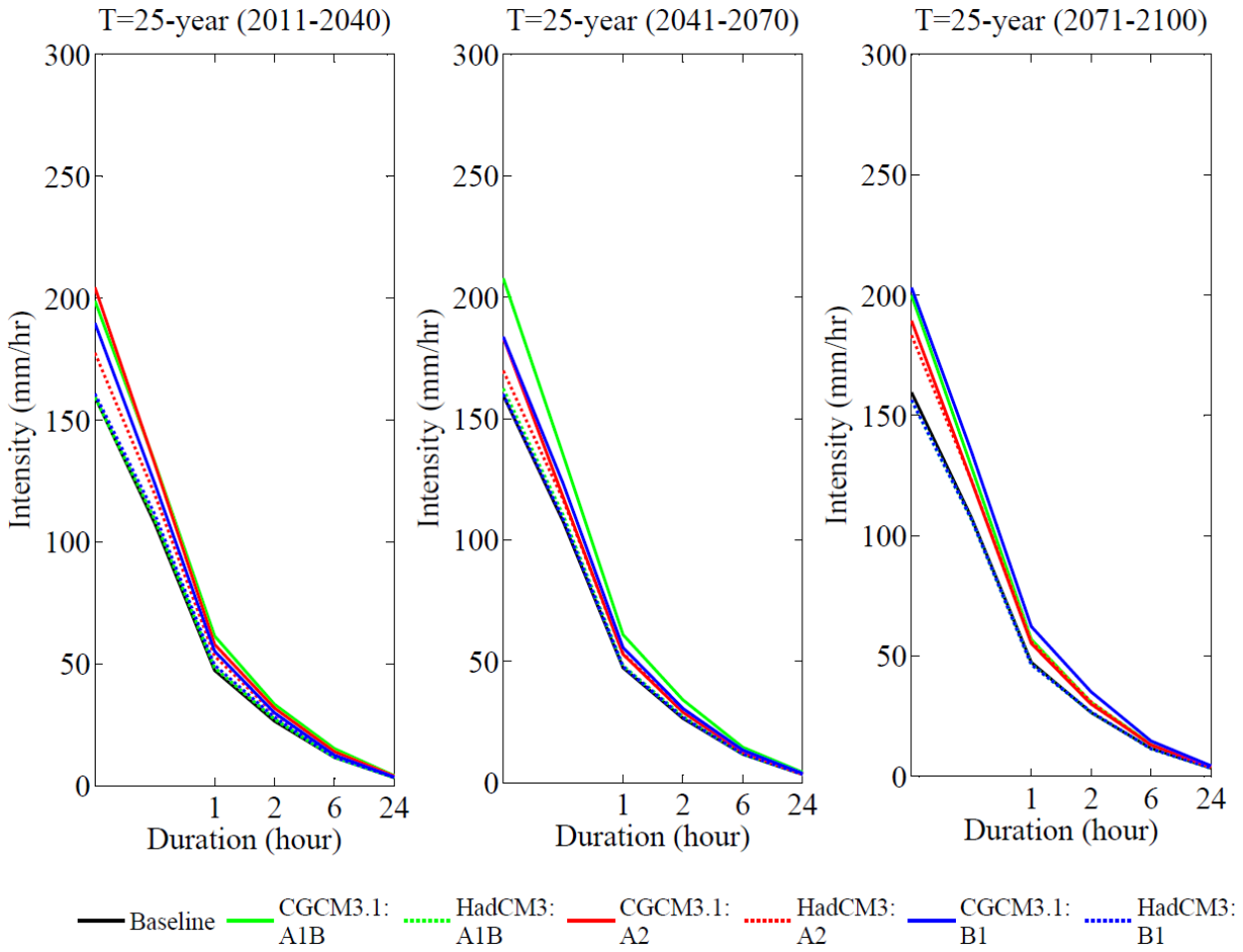

Figure F.6: Variations in the future IDF curves for 25-year return period in the City of Saskatoon according to CGCM3.1 and HadCM3 based on three AR4 emission scenarios.

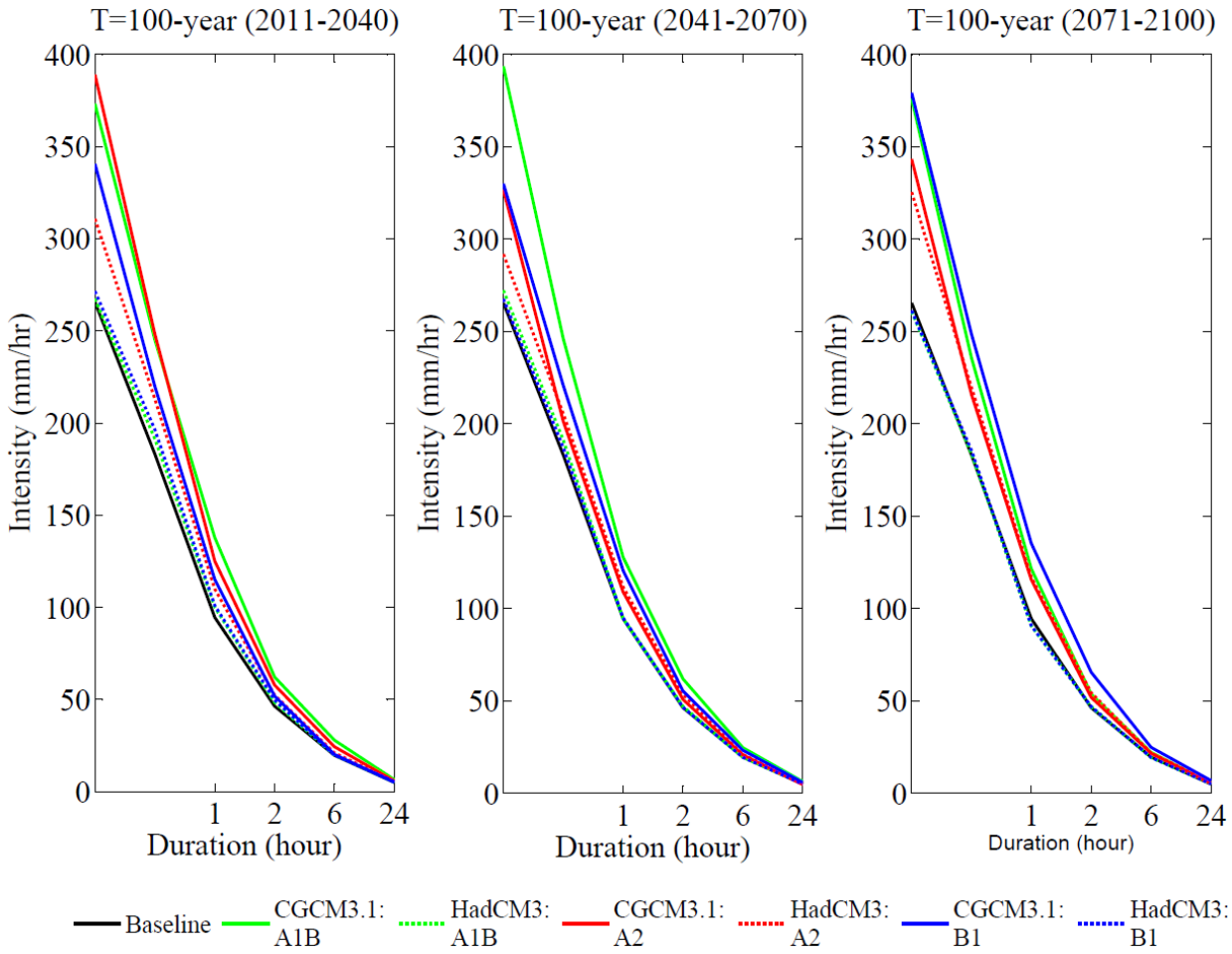

Figure F.7: Variations in the future IDF curves for 100-year return period in the City of Saskatoon according to CGCM3.1 and HadCM3 based on three AR4 emission scenarios.

Table F.1: The expected precipitation intensity (mm/hr) for CGCM3.1 and HadCM3 based on three AR4 emission scenarios obtained from CMIP3 during the 21st century for various return periods.

	(2011-2040)				(2041-2070)				(2071-2100)				(2011-2040)				(2041-2070)				(2071-2100)			
	Return period (year)																							
	2	5	25	100	2	5	25	100	2	5	25	100	2	5	25	100	2	5	25	100	2	5	25	100
	CGCM3.1: A1B																HadCM3: A1B							
5-min	62	98	199	373	64	102	208	394	61	98	200	376	56	86	159	267	58	88	162	272	55	85	156	261
15-min	40	65	133	245	42	67	135	246	39	63	129	236	36	57	109	191	37	58	110	191	35	56	107	184
1-hr	15	26	61	138	16	27	61	128	16	25	57	121	14	22	49	100	14	23	48	94	14	22	46	91
2-hr	10	16	33	62	11	17	34	62	11	16	31	54	9	14	27	48	10	15	27	47	9	14	27	47
6-hr	5	8	15	28	5	8	15	25	5	7	13	22	4	6	12	20	4	7	12	19	4	6	11	19
24-hr	2	2	4	6	2	3	4	6	2	2	4	6	1	2	3	5	1	2	3	5	1	2	3	5
	CGCM3.1: A2																HadCM3: A2							
5-min	61	98	204	389	61	95	183	327	62	96	189	343	59	93	178	311	58	90	170	292	60	94	183	326
15-min	39	64	132	248	40	62	118	201	40	63	123	216	38	61	120	213	38	60	117	205	39	62	123	220
1-hr	15	25	58	125	15	25	53	109	16	25	55	116	15	24	53	110	15	24	53	112	15	25	56	117
2-hr	10	16	32	58	10	16	29	51	11	16	30	52	10	15	30	52	10	15	30	53	10	16	31	54
6-hr	5	7	14	24	5	7	13	21	5	7	13	22	5	7	13	21	5	7	13	21	5	7	13	22
24-hr	2	2	4	6	2	2	3	5	2	2	4	5	2	2	4	6	2	2	4	6	2	2	4	6
	CGCM3.1: B1																HadCM3: B1							
5-min	61	97	190	341	60	94	184	330	62	100	203	379	56	87	161	271	57	87	160	268	55	85	156	261
15-min	40	63	124	220	39	62	123	221	41	66	135	249	36	57	111	196	37	58	109	187	35	56	107	186
1-hr	15	25	55	115	15	25	56	121	16	27	62	135	14	23	49	101	14	23	48	95	14	22	46	91
2-hr	10	16	30	52	10	16	31	55	11	17	35	66	10	15	28	50	9	14	27	46	9	14	27	47
6-hr	5	7	13	20	5	7	13	23	5	8	15	25	4	7	12	20	4	7	12	19	4	6	11	19
24-hr	2	2	4	5	2	2	4	6	2	3	4	7	1	2	4	5	1	2	3	5	1	2	3	5

With the advent of CMIP5 climate models and their corresponding simulations, the previously available simulations for CMIP3 climate models have become outdated. However, temperature projections of RCP4.5 show similarities with those of B1 emission scenario with similar mean temperature scenarios at the global scale by the end of 2100 (Rogelj et al., 2012). In this study, an attempt was made to investigate variations in the future extreme precipitation quantiles using the same GCM, i.e., CGCM3.1 and CanESM2 and the corresponding equivalent (based on temperature projections) emission scenarios, i.e., B1 and RCP4.5 obtained from CMIP3 and CMIP5, respectively (Table F.2). Both CGCM3.1: B1 and CanESM2: RCP4.5 show that the precipitation intensities increase in shorter durations and longer return periods. CGCM3.1: B1 shows the highest precipitation intensity of 379 mm/hr for 5-min duration and 100-year return period during 2071-2100, while CanESM2: RCP4.5 shows the highest precipitation intensity of 312 mm/hr for 5-min duration and 100-year return period during 2011-2040. The percentage change in precipitation intensity for the GCMs/RCPs is dependent on the duration, return period, and time slice. Generally, the percentage change in precipitation intensities with respect to the historical intensities for CanESM2: RCP4.5 is less than those for CGCM3.1: B1, which might be due to the inclusion of climate policies (i.e., adaptation and mitigation) in CMIP5 climate models.

Table F.2: Comparison between the expected rainfall intensity (mm/hr) for CGCM3.1: B1 and CanESM2: RCP4.5 obtained from CMIP3 and CMIP5, respectively, during the 21st century for various return periods.

	Rainfall intensity (mm/hr)												% Change in rainfall intensity											
	(2011-2040)				(2041-2070)				(2071-2100)				(2011-2040)				(2041-2070)				(2071-2100)			
	Return period (year)																							
	2	5	25	100	2	5	25	100	2	5	25	100	2	5	25	100	2	5	25	100	2	5	25	100
CGCM3.1: B1																								
5-min	61	97	190	341	60	94	184	330	62	100	203	379	7	11	19	28	5	8	15	24	9	14	27	43
15-min	40	63	124	220	39	62	123	221	41	66	135	249	8	10	15	20	6	9	14	21	11	16	25	36
1-hr	15	25	55	115	15	25	56	121	16	27	62	135	10	13	17	22	8	11	18	28	16	21	31	43
2-hr	10	16	30	52	10	16	31	55	11	17	35	66	12	13	13	12	9	11	15	20	18	23	33	42
6-hr	5	7	13	20	5	7	13	23	5	8	15	25	12	11	7	3	10	11	14	18	20	23	25	27
24-hr	2	2	4	5	2	2	4	6	2	3	4	7	16	14	7	1	10	11	14	18	20	23	30	40
CanESM2: RCP4.5																								
5-min	59	91	177	312	57	89	170	291	56	86	156	259	3	5	11	18	0	2	6	10	-2	-2	-2	-3
15-min	37	59	116	204	36	57	109	186	36	56	105	179	2	4	8	11	-1	0	1	1	-2	-3	-2	-2
1-hr	15	24	52	106	14	22	45	86	14	22	46	90	5	6	9	13	3	0	-4	-9	1	-1	-4	-5
2-hr	10	15	28	49	9	14	27	46	9	14	26	44	6	7	7	7	3	2	0	-1	3	1	-2	-6
6-hr	4	7	13	21	4	6	11	18	4	6	11	17	6	7	8	9	3	1	-4	-9	3	-1	-7	-14
24-hr	2	2	4	5	2	2	3	4	1	2	3	4	8	8	6	4	12	6	-5	-16	6	2	-6	-13

F.3 Variations obtained with the GP method and the K-NN hourly disaggregation model

The following results are presented here with reference to section 4.4.2 of the thesis.

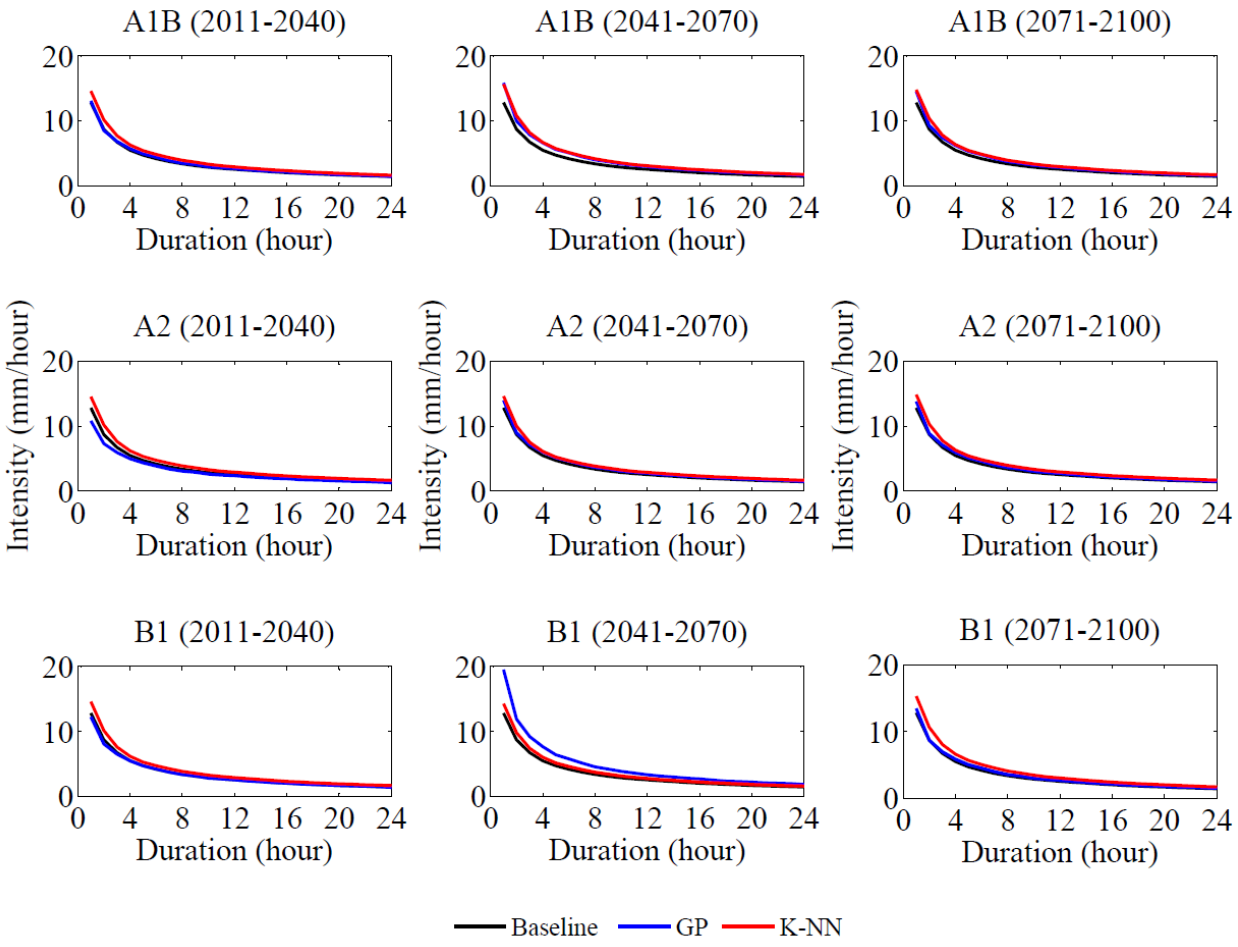

Figure F.8: Comparison between the future IDF curves (2011-2100) according to CGCM3.1 based on three AR4 emission scenarios and 2-year return period obtained using two different downscaling approaches, i.e. GP method and LARS-WG combined with K-NN Hourly Disaggregation Model.

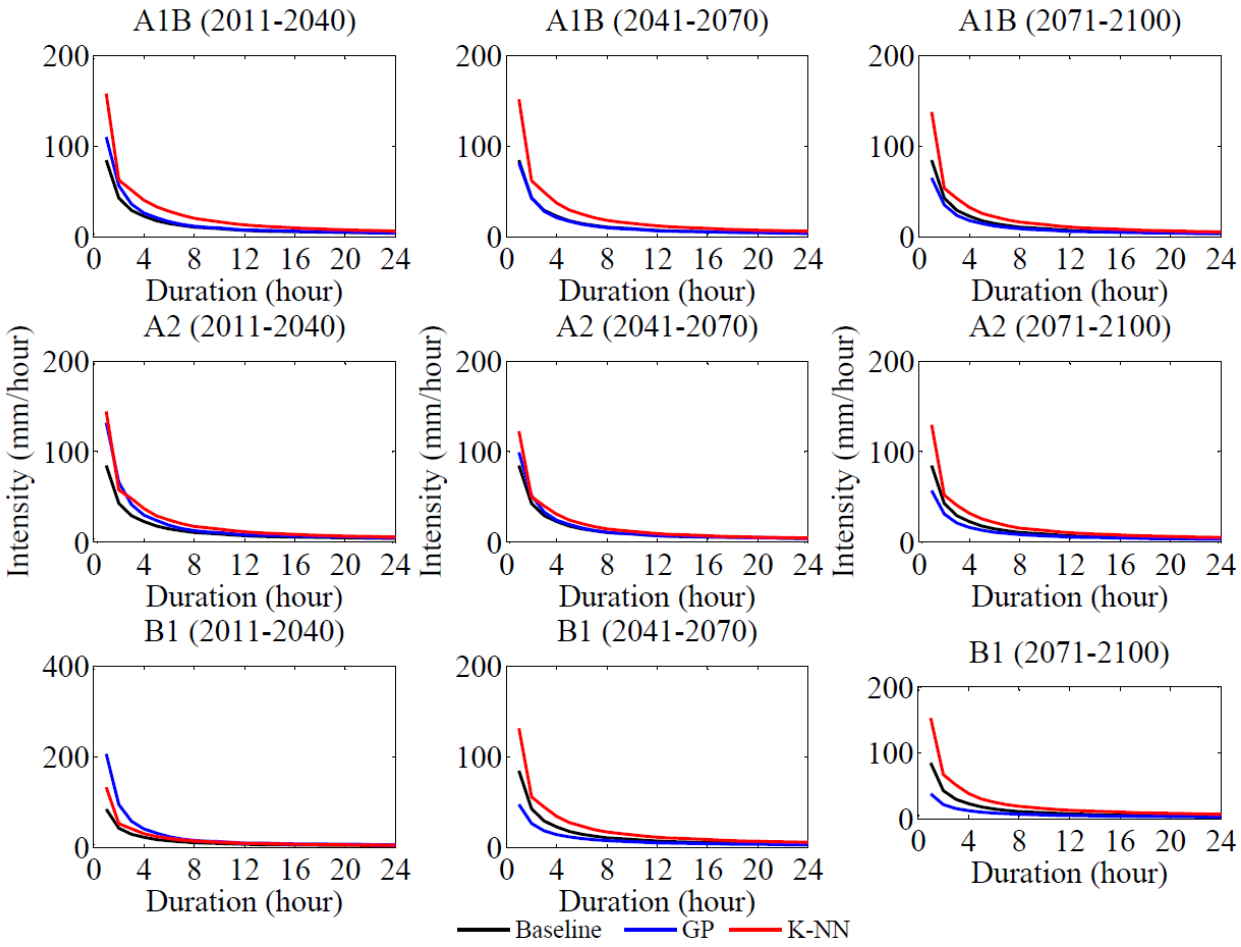

Figure F.9: Comparison between the future IDF curves (2011-2100) according to CGCM3.1 based on three AR4 emission scenarios and 100-year return period obtained using two different downscaling approaches, i.e. GP method and LARS-WG combined with K-NN Hourly Disaggregation Model.

Table F.3: Performance of the GP method based on CGCM3.1 in simulating the expected precipitation intensity (mm/hr) during the baseline period (1961-1990) for various durations and return periods.

Duration	Return period (year)				Return period (year)			
	2	5	25	100	2	5	25	100
	Historical (observed) hourly precipitation (1961-1990)				Simulated hourly precipitation (Using GP for CGCM3.1) (1961-1990)			
1-hr	12.8	21.0	44.9	84.6	12.3	22.8	50.2	88.4
2-hr	8.7	13.5	25.5	42.7	8.1	13.6	27.8	46.5
3-hr	6.7	10.4	18.7	29.3	6.5	10.3	19.2	30.2
4-hr	5.5	8.5	15.0	22.8	5.5	8.5	14.9	22.4
6-hr	4.2	6.3	10.3	14.7	4.2	6.3	10.2	14.6
12-hr	2.5	3.6	5.4	7.3	2.5	3.6	5.3	6.9
18-hr	1.8	2.5	3.9	5.3	1.8	2.5	3.8	5.2
24-hr	1.4	2.0	3.0	4.1	1.4	2.0	3.0	4.0

Table F.4: Comparison between the K-NN hourly disaggregation model and the GP method in simulating the expected precipitation intensity (mm/hr) for CGCM3.1 based on three AR4 emission scenarios during the 21st century for various durations and return periods.

	GP Method												K-NN Hourly Disaggregation Model											
	(2011-2040)				(2041-2070)				(2071-2100)				(2011-2040)				(2041-2070)				(2071-2100)			
	Return period (year)												Return period (year)											
	2	5	25	100	2	5	25	100	2	5	25	100	2	5	25	100	2	5	25	100	2	5	25	100
CGCM3.1: A1B																								
1-hr	13	25	58	110	16	28	53	81	15	24	44	65	15	25	64	158	16	27	64	152	15	25	59	138
2-hr	8	15	32	57	10	16	29	43	9	14	24	35	10	16	33	63	11	17	34	62	10	16	30	54
3-hr	7	11	21	36	8	12	20	28	7	11	17	24	8	12	26	52	8	13	26	49	8	12	23	42
4-hr	6	9	16	26	7	10	15	21	6	9	13	18	6	10	21	41	7	10	21	37	6	10	19	33
6-hr	4	7	11	17	5	7	11	14	5	7	9	12	5	8	15	28	5	8	15	25	5	7	13	22
12-hr	3	4	6	8	3	4	5	7	3	4	5	6	3	4	8	13	3	5	8	12	3	4	7	11
18-hr	2	3	4	6	2	3	4	5	2	3	4	4	2	3	5	9	2	3	5	8	2	3	5	7
24-hr	1	2	3	4	2	2	3	4	2	2	3	3	2	2	4	6	2	3	4	6	2	2	4	6
CGCM3.1: A2																								
1-hr	11	19	53	132	14	25	55	99	14	23	40	57	15	25	61	144	15	24	55	123	15	24	57	129
2-hr	7	12	29	66	9	15	30	52	9	14	23	31	10	16	31	58	10	15	29	50	10	16	30	52
3-hr	6	9	20	41	7	11	20	33	7	10	16	21	8	12	25	48	7	12	22	40	8	12	23	41
4-hr	5	8	15	30	6	9	16	24	6	9	13	16	6	10	20	37	6	9	18	31	6	10	18	32
6-hr	4	6	11	19	5	7	11	16	5	6	9	11	5	7	14	24	5	7	13	20	5	7	13	22
12-hr	2	3	5	8	3	4	6	7	3	4	5	6	3	4	7	11	3	4	7	10	3	4	7	10
18-hr	2	2	4	6	2	3	4	6	2	3	3	4	2	3	5	8	2	3	5	6	2	3	5	7
24-hr	1	2	3	5	1	2	3	4	1	2	3	3	2	2	4	6	2	2	3	5	2	2	4	5

Table F.4 continued

	GP Method												K-NN Hourly Disaggregation Model											
	(2011-2040)				(2041-2070)				(2071-2100)				(2011-2040)				(2041-2070)				(2071-2100)			
	Return period (year)												Return period (year)											
	2	5	25	100	2	5	25	100	2	5	25	100	2	5	25	100	2	5	25	100	2	5	25	100
CGCM3.1: B1																								
1-hr	12	21	64	207	19	30	41	48	13	20	30	38	15	24	58	133	14	24	57	132	15	26	65	153
2-hr	8	13	35	95	12	17	23	26	9	12	17	21	10	16	30	53	10	15	30	56	11	17	35	67
3-hr	6	10	23	58	9	13	16	18	7	9	13	15	8	12	23	41	7	12	24	45	8	13	27	51
4-hr	5	8	18	41	8	10	13	14	6	8	10	12	6	9	18	31	6	9	19	34	7	10	21	38
6-hr	4	6	12	24	6	7	9	10	4	6	7	9	5	7	13	20	5	7	13	24	5	8	15	25
12-hr	3	3	6	10	3	4	5	5	3	3	4	5	3	4	7	10	3	4	7	11	3	5	8	13
18-hr	2	2	4	8	2	3	3	4	2	2	3	3	2	3	5	7	2	3	5	8	2	3	6	9
24-hr	1	2	3	6	2	2	3	3	1	2	2	3	2	2	4	5	2	2	4	6	2	3	4	7

The following results are presented here with reference to section 4.5.2 of the thesis.

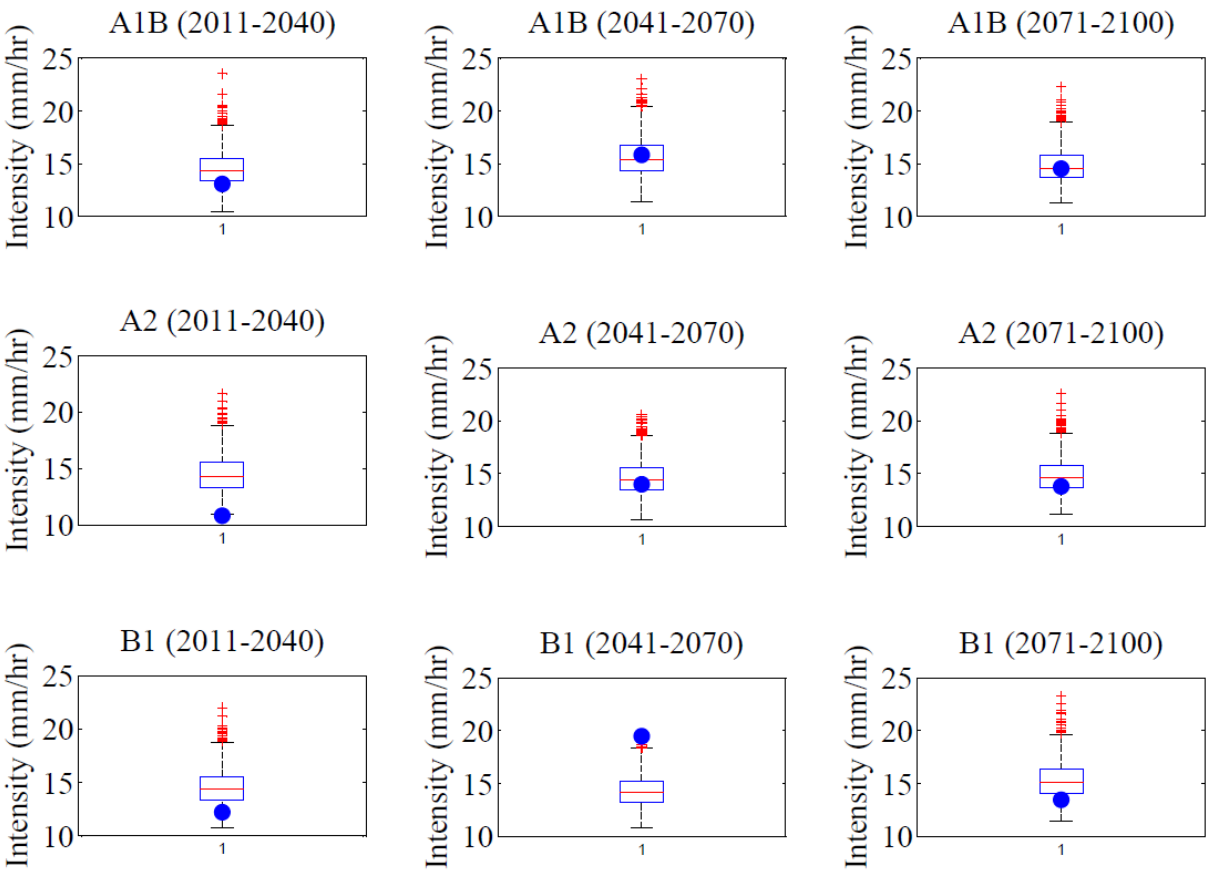

Figure F.10: Expected 1-hr AMP corresponding to 1000 realizations from LARS-WG and K-NN hourly disaggregation model (boxplot), and the same from GP method (blue dots) of 2-year return period for CGCM3.1 based on three emission scenarios during the 21st century.

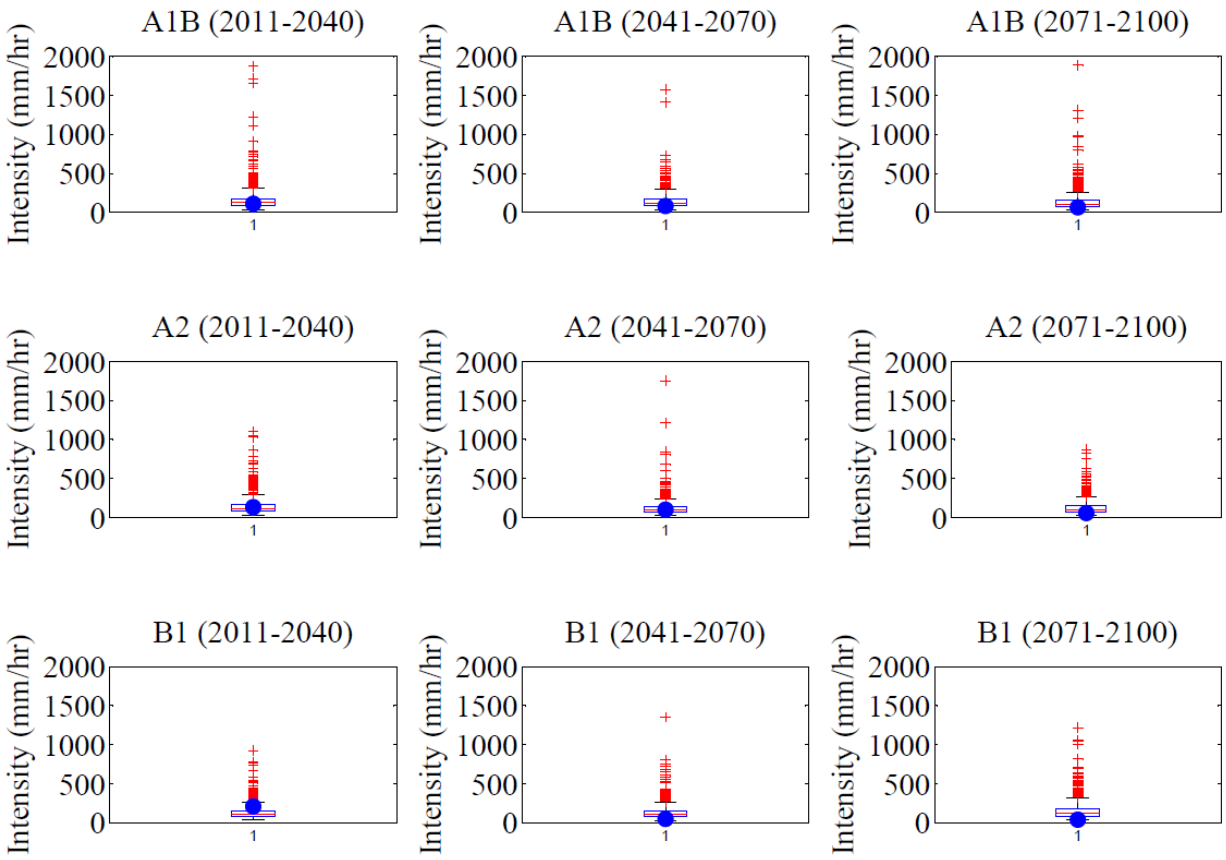

Figure F.11: Expected 1-hr AMP corresponding to 1000 realizations from LARS-WG and K-NN hourly disaggregation model (boxplot), and the same from GP method (blue dots) of 100-year return period for CGCM3.1 based on three emission scenarios during the 21st century.

F.4 Uncertainty in the projections of future IDF curves

The following results are presented here with reference to section 4.5.3 of the thesis.

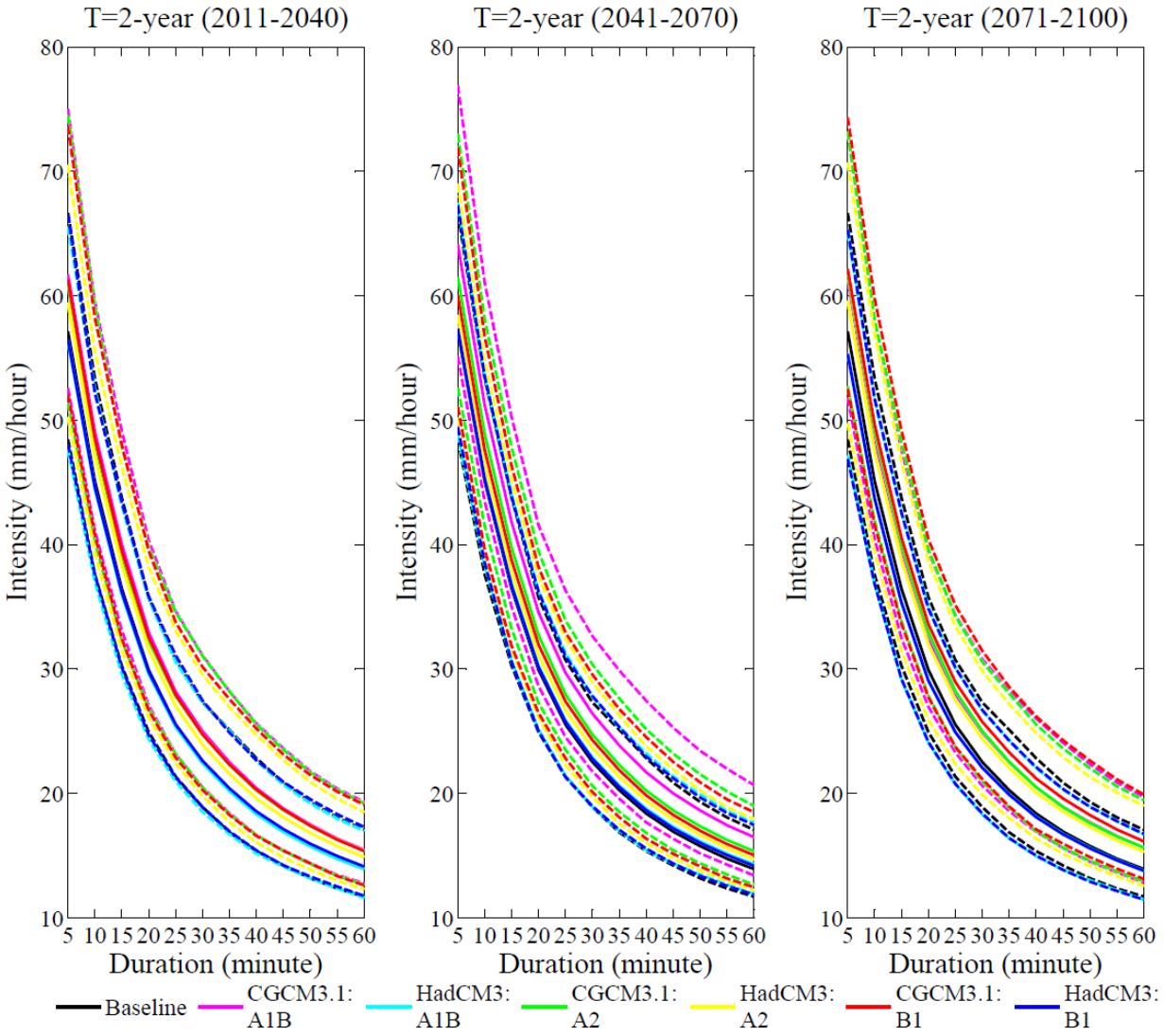

Figure F.12: Uncertainty in the projections of future extreme precipitation quantiles for 2-year return period based on two GCMs and three emission scenarios obtained from CMIP3 and quantified by using GEV shown as 95% confidence intervals (dashed lines).

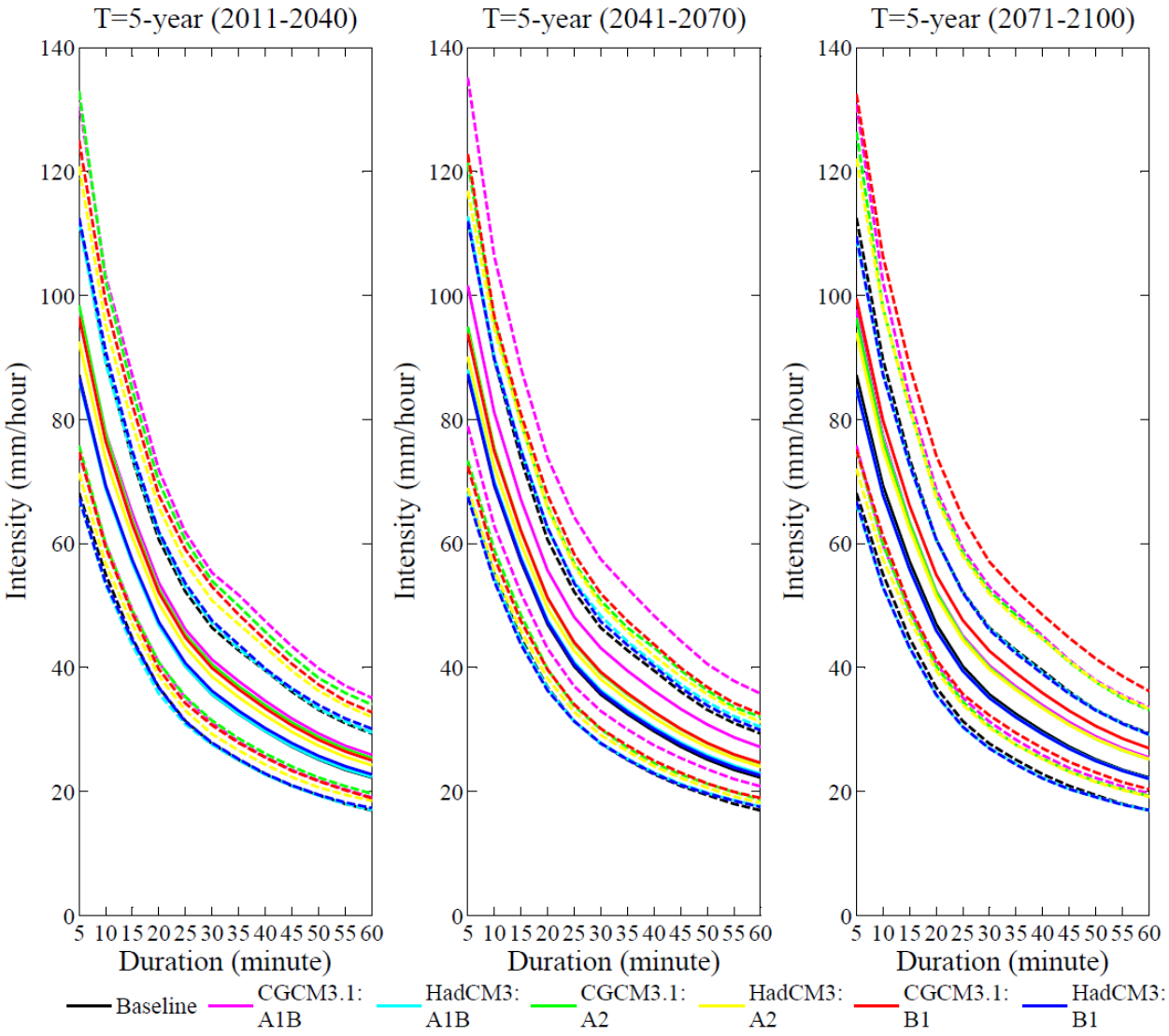

Figure F.13: Uncertainty in the projections of future extreme precipitation quantiles for 5-year return period based on two GCMs and three emission scenarios obtained from CMIP3 and quantified by using GEV shown as 95% confidence intervals (dashed lines).

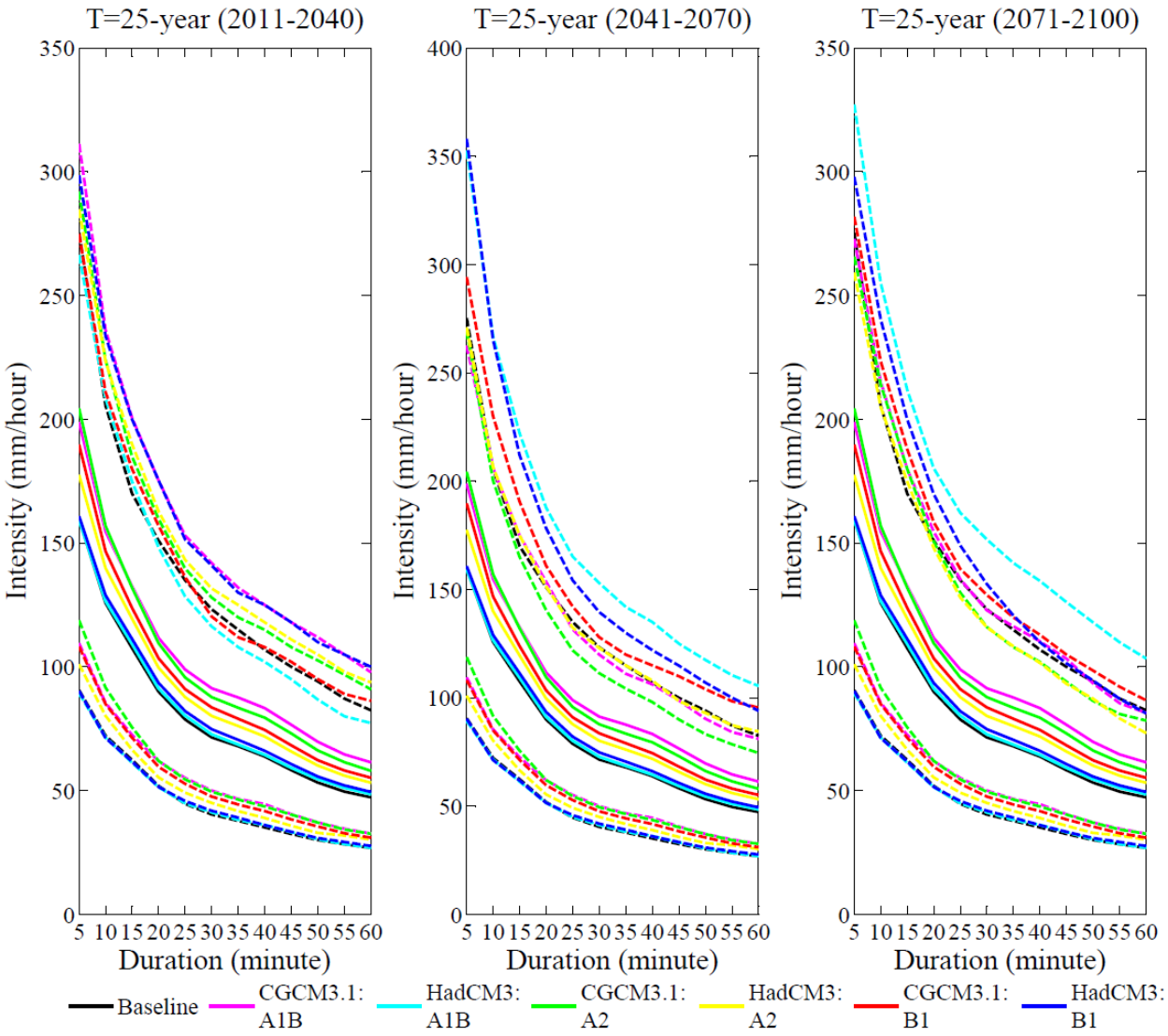

Figure F.14: Uncertainty in the projections of future extreme precipitation quantiles for 25-year return period based on two GCMs and three emission scenarios obtained from CMIP3 and quantified by using GEV shown as 95% confidence intervals (dashed lines).

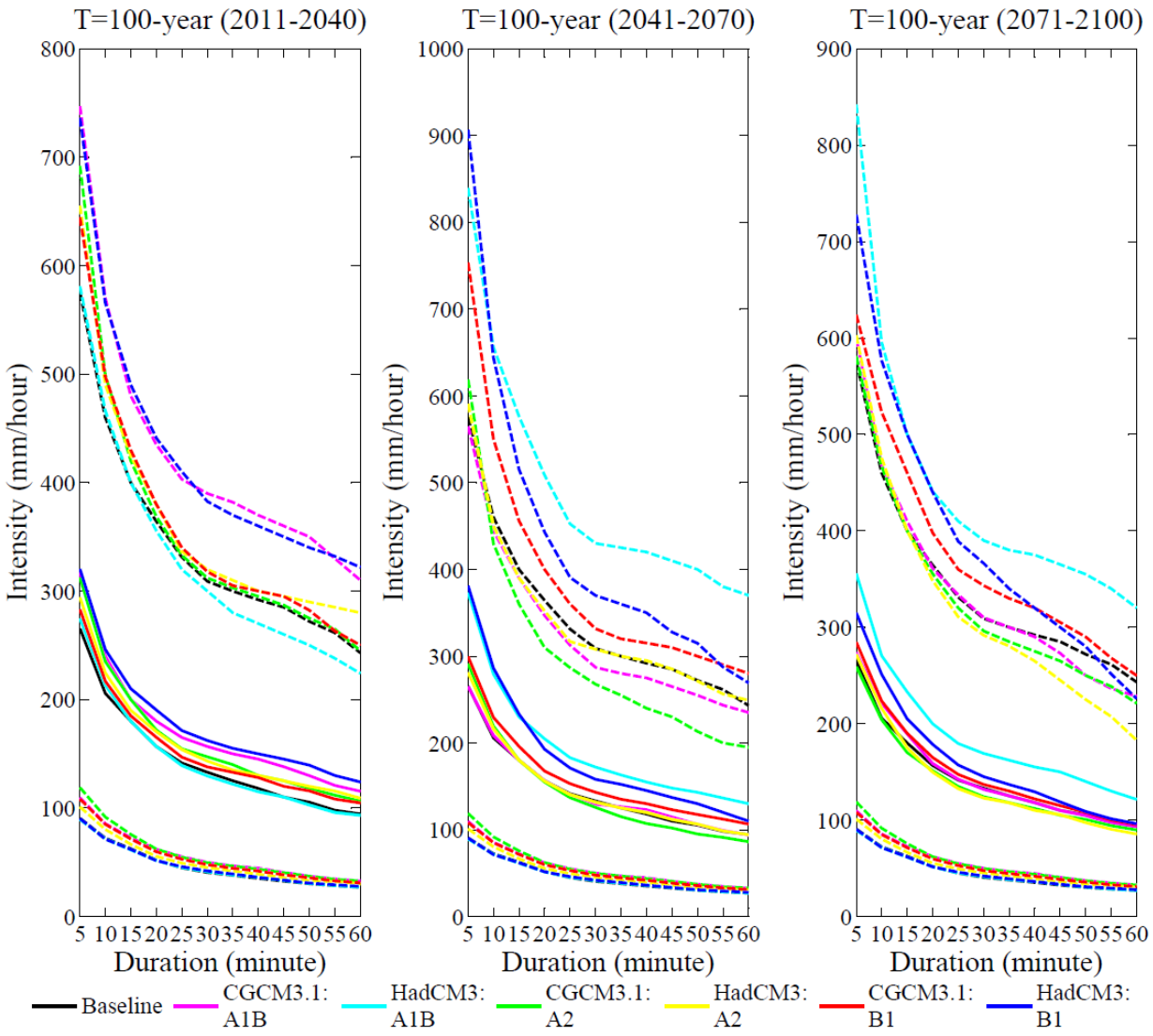

Figure F.15: Uncertainty in the projections of future extreme precipitation quantiles for 100-year return period based on two GCMs and three emission scenarios obtained from CMIP3 and quantified by using GEV shown as 95% confidence intervals (dashed lines).

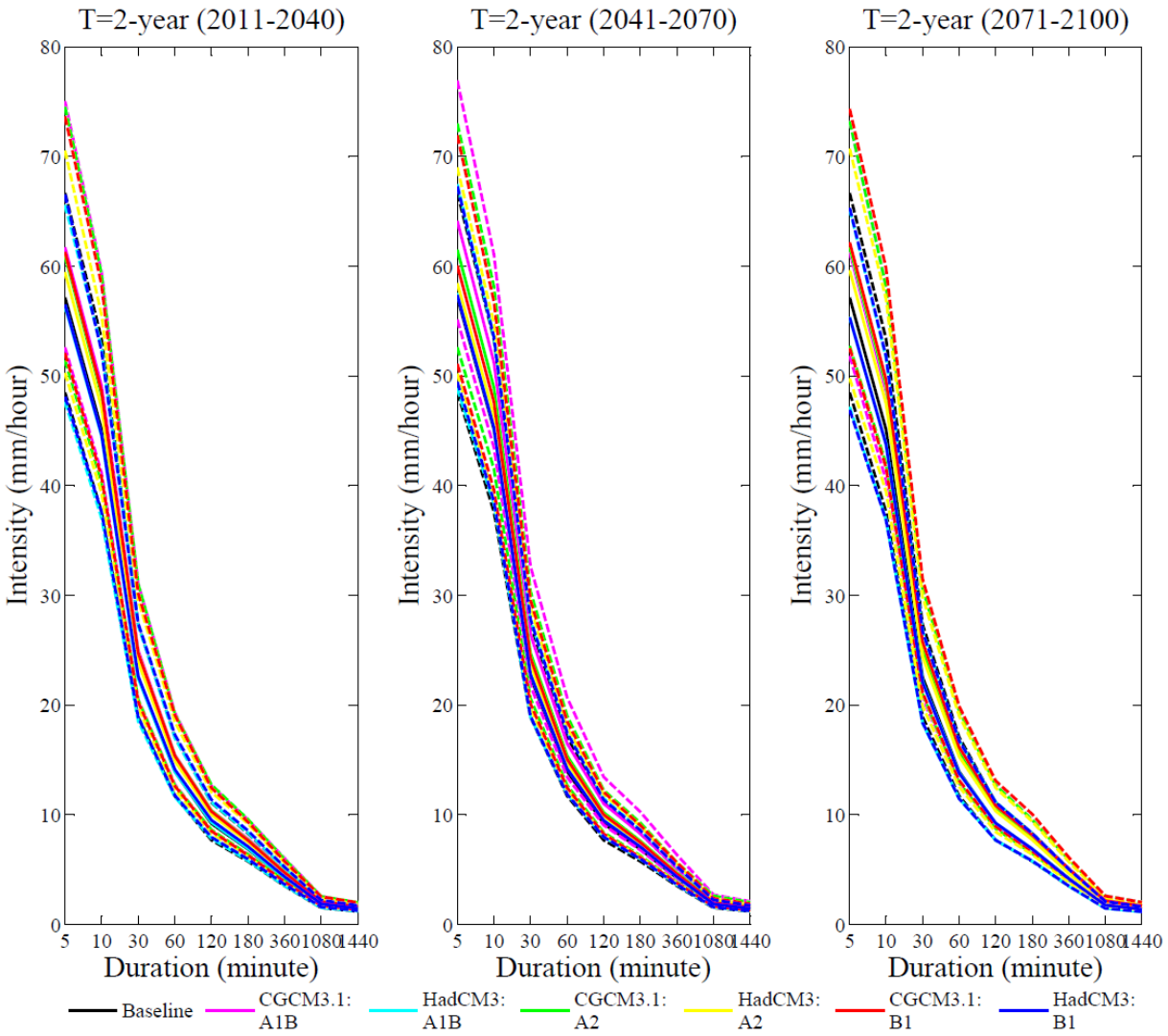

Figure F.16: Uncertainty in the projections of future extreme precipitation quantiles of durations from 5-min to 24-hour for 2-year return period based on two GCMs and three emission scenarios obtained from CMIP3 and quantified by using GEV shown as 95% confidence intervals (dashed lines).

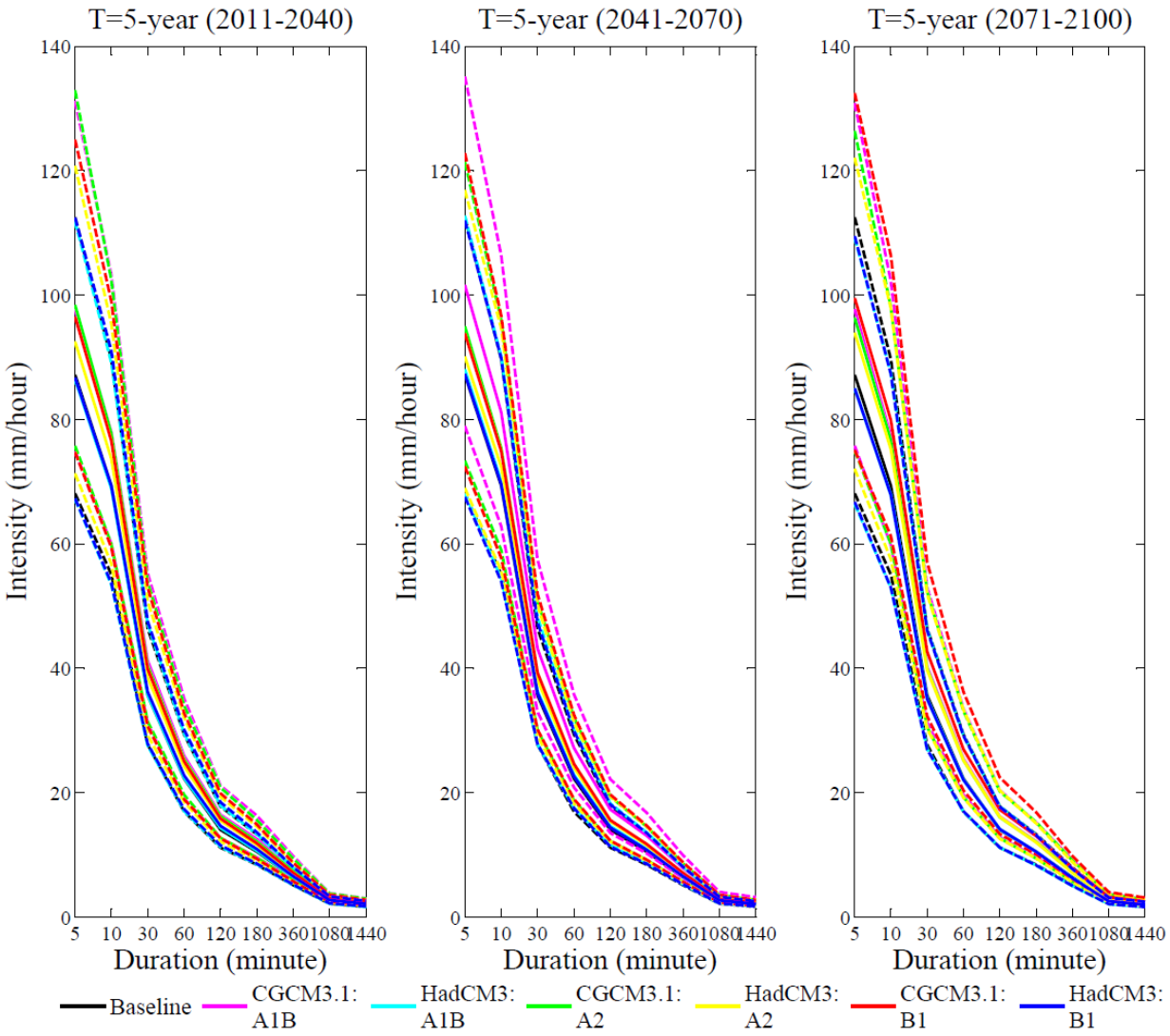

Figure F.17: Uncertainty in the projections of future extreme precipitation quantiles of durations from 5-min to 24-hour for 5-year return period based on two GCMs and three emission scenarios obtained from CMIP3 and quantified by using GEV shown as 95% confidence intervals (dashed lines).

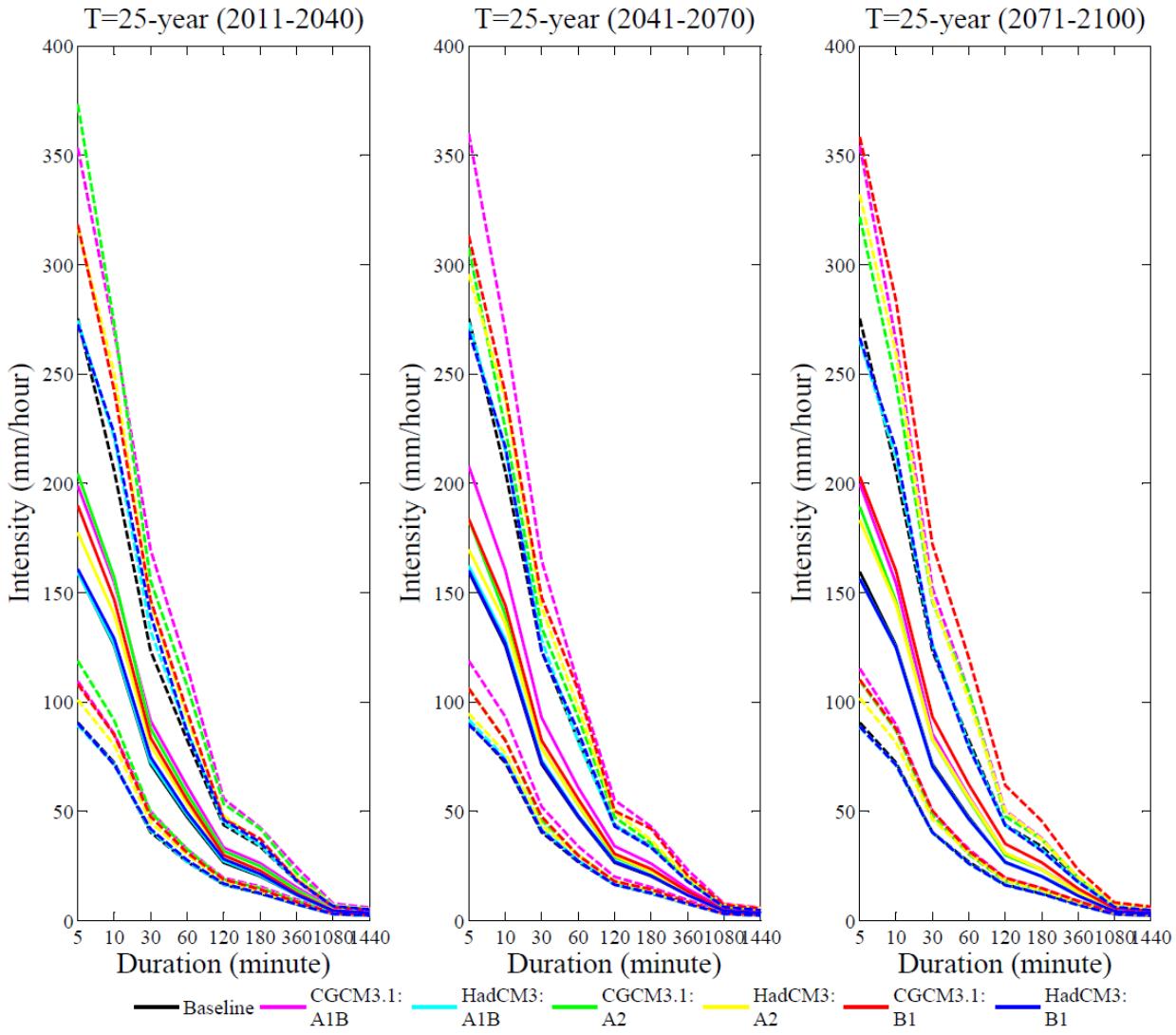

Figure F.18: Uncertainty in the projections of future extreme precipitation quantiles of durations from 5-min to 24-hour for 25-year return period based on two GCMs and three emission scenarios obtained from CMIP3 and quantified by using GEV shown as 95% confidence intervals (dashed lines).

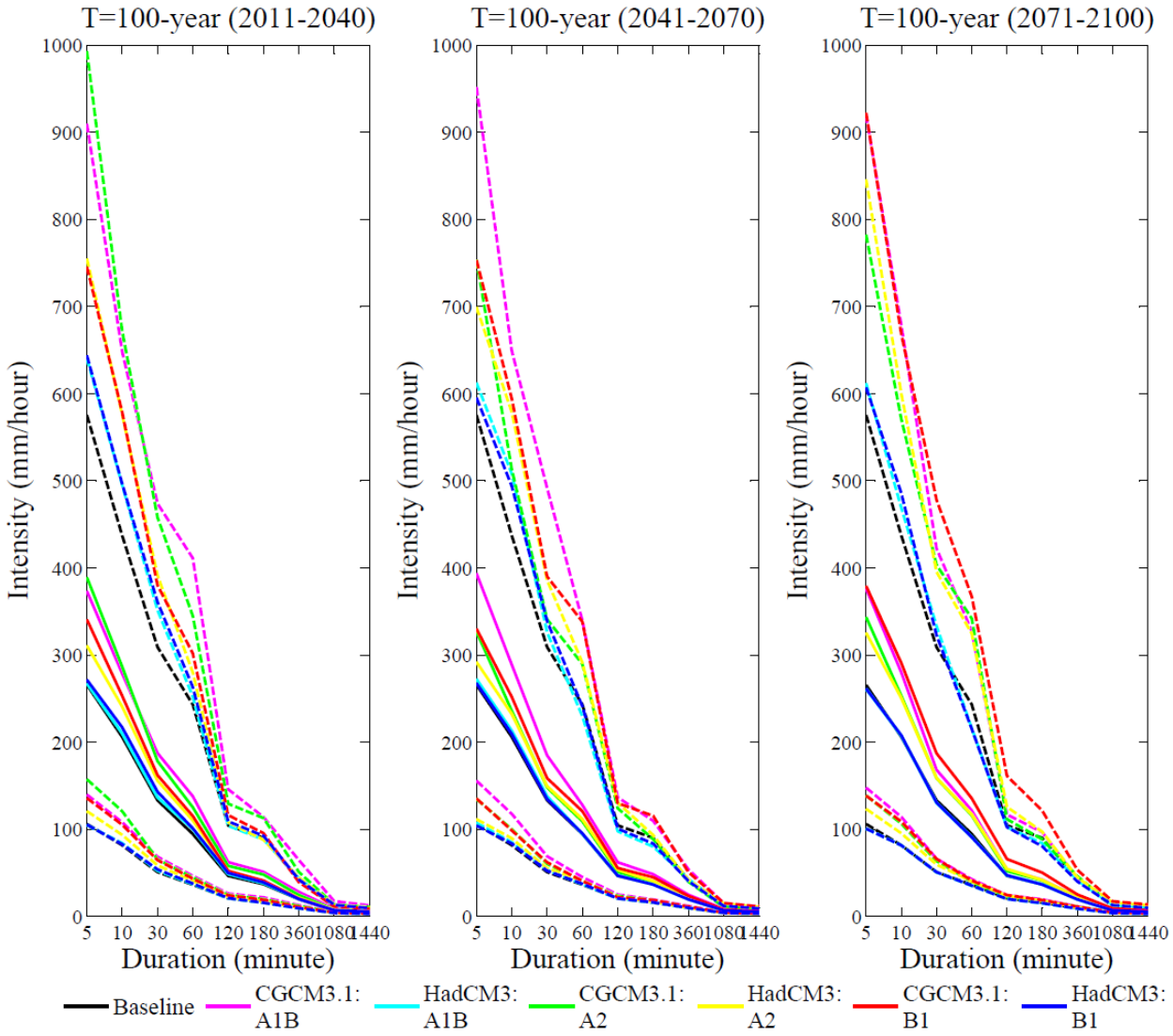

Figure F.19: Uncertainty in the projections of future extreme precipitation quantiles of durations from 5-min to 24-hour for 100-year return period based on two GCMs and three emission scenarios obtained from CMIP3 and quantified by using GEV shown as 95% confidence intervals (dashed lines).

F.6 Uncertainty due to GEV fit and extrapolation

The following results are presented here with reference to section 4.5.4 of the thesis.

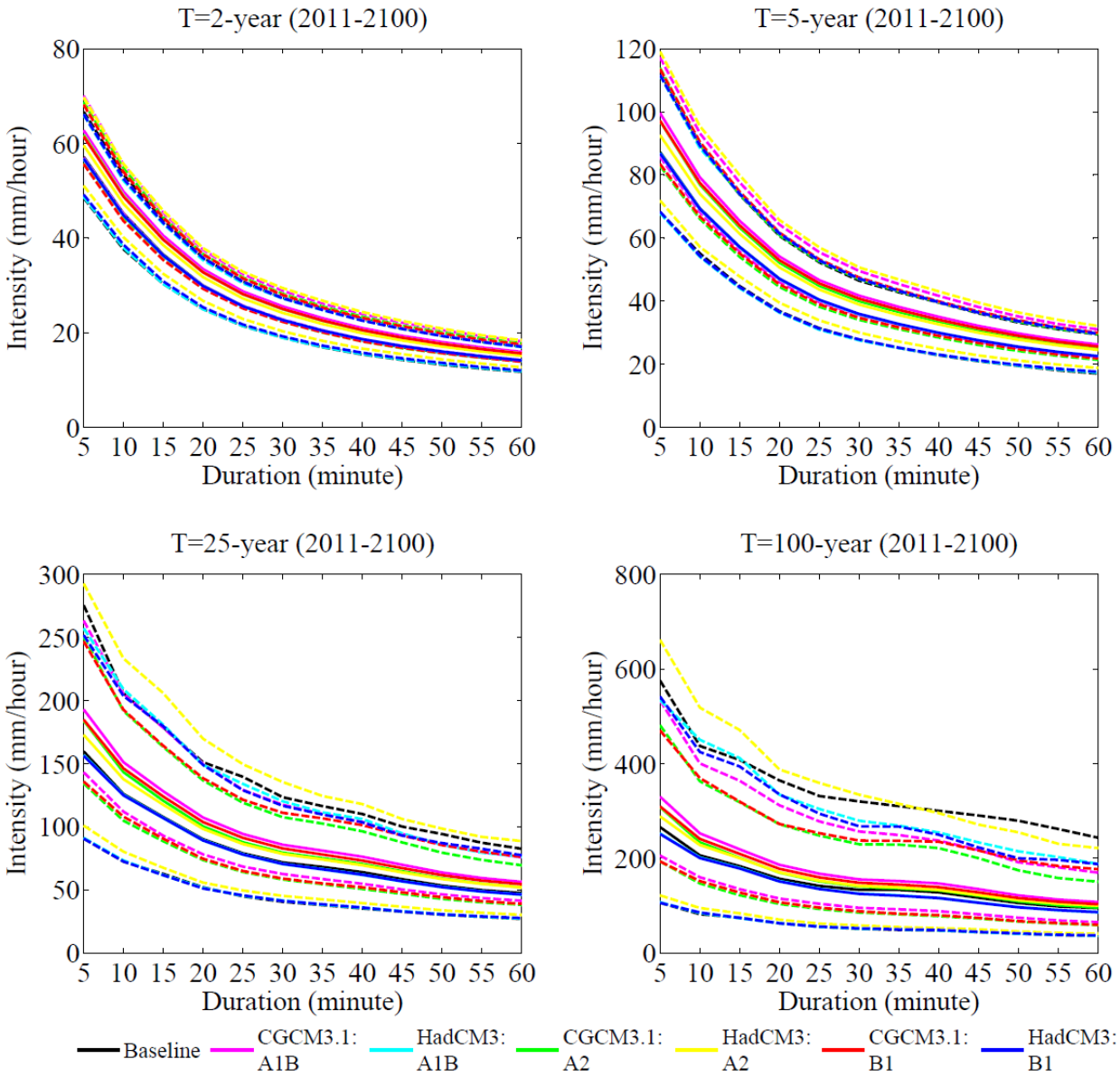

Figure F.20: Uncertainty in the projections of future extreme precipitation quantiles for 2-, 5-, 25- and 100-year return periods based on two GCMs and three emission scenarios obtained from CMIP3 and quantified by using GEV shown as 95% confidence intervals (dashed lines) using 90 years of data (2011-2100).

F.5 Overall changes in the future IDF curves obtained from CMIP3 climate models

Table F.5: Historical and projected rainfall intensities based on two CMIP3 climate models (CGCM3.1 and HadCM3) and three emission scenarios for selected durations and return periods of storms in Saskatoon. Base means historical values, Min means the lowest of future projection, and Max is the highest value of future projections. The **"bold"** values represent the greatest projected change (refer to section 4.6 in the thesis).

Duration	Intensity (mm/hr)											
	2-year			5-year			25-year			100-year		
	Base	Min	Max	Base	Min	Max	Base	Min	Max	Base	Min	Max
5-min	57	55	64	87	85	102	160	156	**208**	265	261	**394**
15-min	37	35	42	57	56	67	108	107	**135**	183	184	**249**
1-hour	14	14	16	22	22	**27**	47	46	**62**	94	91	**138**
2-hour	9	9	**11**	14	14	**17**	27	27	**35**	46	46	**66**
6-hour	4	4	**5**	6	6	**8**	11	11	**15**	19	19	**28**
24-hour	1	1	**2**	2	2	**3**	3	3	**4**	5	5	**7**